

University of Alberta

**Behaviour of Steel Plate Shear Walls Fabricated with Partially Encased
Composite Columns**

by

Xiaoyan Deng

A thesis submitted to the Faculty of Graduate Studies and Research
in partial fulfillment of the requirements for the degree of

Doctor of Philosophy

in

Structural Engineering

Department of Civil and Environmental Engineering

©Xiaoyan Deng

Spring 2012

Edmonton, Alberta

Permission is hereby granted to the University of Alberta Libraries to reproduce single copies of this thesis and to lend or sell such copies for private, scholarly or scientific research purposes only. Where the thesis is converted to, or otherwise made available in digital form, the University of Alberta will advise potential users of the thesis of these terms.

The author reserves all other publication and other rights in association with the copyright in the thesis and, except as herein before provided, neither the thesis nor any substantial portion thereof may be printed or otherwise reproduced in any material form whatsoever without the author's prior written permission.

Abstract

Partially encased composite columns consist of thin-walled built-up H-shaped steel sections with links welded near the flange tips and concrete cast between the flanges. The use of PEC columns under concentric axial load only was incorporated into the Canadian steel design standard, CAN/CSA S16-01, in 2001 and the use of PEC columns as beam-columns is permitted in the current edition, CSA S16-09 (CSA 2009). A half-size two-storey one-bay steel plate shear wall specimen, with PEC columns as the boundary elements, was tested under vertical and cyclic lateral loads to study its behaviour, and good ductility and performance was observed. A finite element model of the specimen was also developed and loaded in a push-over analysis with a dynamic explicit solution strategy to help study the behaviour of PEC columns and the whole system.

The failure mode of the test specimen was the initiation of tears at the outside column flange tips at the bottom of the columns during the formation of plastic hinges. The specimen behaved in a ductile manner with no rapid drop of the specimen strength after the ultimate capacity was reached. Compared with steel plate shear walls with a steel frame, more nonlinear behaviours were observed in the specimen due to the existence of the concrete, which led to severely pinched hysteresis curves without a clear yield portion. Although the energy dissipation capacity did not keep increasing until the end of the test, it did increase beyond the value observed when the ultimate capacity was reached. Based on the test data, strain hardening occurred in the first floor infill panel and the corresponding finite element material curve was modified accordingly. In general, the model gave good predictions of the overall specimen behaviour and internal frame forces.

Acknowledgements

This research project was partially funded by the Canam Group, who patented PEC columns. This research project was also funded by the Natural Sciences and Engineering Research Council of Canada (NSERC).

Sincere thanks go to my supervisor, Dr. Robert G. Driver, who always had time for fruitful discussions and was a constant source and inspiration throughout my program. I would like also to thank all individuals who made significant contributions to help me complete this research, Dr. Elwi, Dr. Adeeb, R. Helfrich, A. Neilson, and M. Begum.

I would like to thank my husband Yuhong for the patience he has had with me during my whole program. I also want to thank my parents for always supporting me and believing my success.

Table of Contents

1.	INTRODUCTION	1
1.1	Background	1
1.2	Objectives and Scope	3
1.3	Report Organization	3
2.	LITERATURE REVIEW	8
2.1	Introduction.....	8
2.2	PEC Columns Fabricated with Thin-Walled Built-up Sections	8
2.2.1	Tremblay et al. (1998)	8
2.2.2	Chicoine et al. (2002a).....	10
2.2.3	Chicoine et al. (2003).....	13
2.2.4	Chicoine et al. (2002b).....	14
2.2.5	Bouchereau and Toupin (2003).....	16
2.2.6	Begum et al. (2005).....	17
2.2.7	Prickett and Driver (2006)	18
2.3	Steel Plate Shear Walls.....	19
2.3.1	Mimura and Akiyama (1977)	20
2.3.2	Thorburn et al. (1983)	21
2.3.3	Timler and Kulak (1983).....	22
2.3.4	Tromposch and Kulak (1987).....	23
2.3.5	Driver et al. (1997; 1998a,b)	24
2.3.6	Behbahanifard et al. (2003).....	25
2.3.7	Choi, I and Park, H. (2008)	25
3.	DESCRIPTION OF TEST SPECIMEN	32
3.1	Objectives.....	32
3.2	Specimen Design Details and Considerations	32
3.2.1	Overall Design.....	33
3.2.2	PEC Columns.....	33

3.2.3	Fully Plastic Moment Beam-to-Column Connections.....	34
3.2.4	Infill Panels and Beams.....	36
3.2.5	Column Cap Plates and Base Plate.....	36
3.3	Fabrication Procedures.....	37
3.4	As-built Measurements.....	38
3.5	Imperfections.....	39
3.6	Summary.....	40
4.	TEST PROCEDURES AND SPECIMEN BEHAVIOUR.....	53
4.1	Introduction.....	53
4.2	Test Set-up.....	53
4.2.1	Vertical Loading.....	53
4.2.2	Lateral Loading.....	54
4.2.3	Sliding and Out-of-Plane Bracing.....	55
4.3	Instrumentation and Data Acquisition.....	56
4.4	Ancillary Tests.....	58
4.4.1	Steel Tension Coupon Tests.....	58
4.4.2	Concrete Cylinder Tests.....	59
4.5	Load and Deflection History.....	60
4.5.1	Gravity load.....	60
4.5.2	Lateral load.....	60
4.6	Specimen Behaviour During Test.....	62
4.6.1	Gravity Load Application.....	62
4.6.2	Lateral Load Application.....	62
5.	TEST RESULTS.....	91
5.1	Introduction.....	91
5.2	Hysteretic Behaviour.....	91
5.3	Energy Dissipation.....	94
5.4	Failure Mode.....	95
5.5	Discussion.....	96

5.5.1	Infill Panels	96
5.5.1.1	General Observations	96
5.5.1.2	Stress Results	97
5.5.2	Partially Encased Composite Columns	98
5.5.2.1	General Observations	98
5.5.2.2	Concrete Shrinkage.....	99
5.5.2.3	Internal Force Distribution	101
5.5.3	Beam	102
5.5.4	Ductility-Related Force Modification Factor, R_d (NBCC).....	103
6.	FINITE ELEMENT MODEL	122
6.1	Introduction.....	122
6.2	Model Properties	122
6.2.1	Element Selection	122
6.2.2	Mesh Description and Imperfections.....	125
6.2.3	Modelling of Steel–Concrete Interactions	128
6.2.4	Boundary Conditions.....	129
6.2.5	Material Properties	130
6.3	Loading application and solution strategy.....	133
7.	DISCUSSION OF MODEL RESULTS	145
7.1	Introduction.....	145
7.2	Overall Behaviour.....	145
7.3	Infill Panels	146
7.4	PEC Columns.....	149
7.4.1	Internal Force Distribution	149
7.4.2	P-M Diagram	151
7.4.3	Yield Deflection.....	153
7.5	Internal Force Distribution in the Bottom Beam	153
7.6	Summary	154
8.	SUMMARY AND CONCLUSIONS	174

8.1	Summary	174
8.2	Conclusions	175
8.3	Recommendations	177
8.3.1	Design and Fabrication	177
8.3.2	Future Research.....	178
	Reference List	180
	Appendix A - Shop Drawings.....	188
	Appendix B - Steel Tension Coupons.....	197
	Appendix C - Steel Tension Coupon Design.....	202
	Appendix D - Steel Tension Coupon Test Results	205
	Appendix E - Concrete Cylinder Test Results	212

List of Tables

Table 4-1: Steel Strength and Elastic Modulus	68
Table 4-2: Concrete Strength and Elastic Modulus.....	68
Table 4-3: Load and Deflection History	68
Table 5-1: Displacement Ductility	107

List of Figures

Figure 1-1: Partially Encased Composite Column	6
Figure 1-2: Tension Field in Infill Panel	7
Figure 2-1: Hysteresis Model (Mimura and Akiyama 1977).....	27
Figure 2-2: Strip Model (Thorburn et al. 1983).....	27
Figure 2-3: Equivalent Brace Model (Thorburn et al. 1983).....	28
Figure 2-4: One-storey Test Specimen (Timler and Kulak 1983).....	29
Figure 2-5: Hysteresis Model (Tromposch and Kulak 1987).....	30
Figure 2-6: Four-storey Test Specimen (Driver et al. 1997; 1998a).....	31
Figure 3-1: Overall Test Specimen (East Elevation)	42
Figure 3-2: Partially Encased Composite Columns (East Elevation).....	43
Figure 3-3: Typical Moment Connection for Steel Frame	44
Figure 3-4: Moment Connection for PEC Column	45
Figure 3-5: Steel Portion of Specimen	46
Figure 3-6: Concrete Casting and Formwork Arrangement	47
Figure 3-7: Gap Left at Top of Columns for Grouting.....	48
Figure 3-8: Formwork Clamp	49
Figure 3-9: Mock Column.....	50
Figure 3-10: Local Imperfection in South Flange of South Column (East Side).....	51
Figure 3-11: Link Initial Imperfections in South Column (East Side).....	52
Figure 4-1: Test Set-up (East Elevation)	69
Figure 4-2: Test Set-up (North Elevation).....	70
Figure 4-3: Overview of Test Set-up.....	71
Figure 4-4: Lateral Load Transition System (Schematic).....	72
Figure 4-5: Lateral Load Transition System (Photos)	73
Figure 4-6: Lateral Loading Facilities	74
Figure 4-7: Connection Tab.....	75
Figure 4-8: Test Set-up at Base (Plan View).....	76
Figure 4-9: Watt Brace	77
Figure 4-10: Data Acquisition Devices (East Elevation)	78
Figure 4-11: Buckled Panel in Cycle 30 (East View).....	79
Figure 4-12: Buckled South-East Flange of South Column in Cycle 19	80
Figure 4-13: Torn South Flange of South Column in Cycle 21	81
Figure 4-14: Link Exposed in West Side of North Column in Cycle 24.....	82
Figure 4-15: Opening in South Flange of South Column in Cycle 25.....	83
Figure 4-16: Tear at Crest of Buckled North Flange in North Column in Cycle 26	84

Figure 4-17: Link Torn from Column Flanges in Cycle 26.....	85
Figure 4-18: “S” Shaped Tear in Infill Panel in Cycle 25	86
Figure 4-19: Weld Tear in Column at Beam Bottom Flange in Cycle 26	87
Figure 4-20: South Column Base in Cycle 27.....	88
Figure 4-21: Flange Tear at Top of Columns in Cycle 29.....	89
Figure 4-22: Flange Tear in Columns in Cycle 30.....	90
Figure 5-1: First Floor Hysteretic Curves	108
Figure 5-2: First Floor Hysteretic Curve – Cycle 20.....	109
Figure 5-3: Second Floor Hysteretic Curves.....	110
Figure 5-4: Dissipated Energy in First Cycle at Each Ductility Ratio	111
Figure 5-5: Dissipated Energy in Each Cycle	112
Figure 5-6: Stress Results from Strain Rosettes in Infill Panel	113
Figure 5-7: Stress Results from Camera System Data for Infill Panel.....	114
Figure 5-8: Individual Stress Results from Camera System Data for Infill Panel	115
Figure 5-9: Axial Forces in First Storey Columns (Push to North).....	116
Figure 5-10: Bending Moments in Bottom Columns (Push to North).....	117
Figure 5-11: Axial Forces in Bottom Beam (Push to North).....	118
Figure 5-12: Bending Moments in Bottom Beam (Push to North)	119
Figure 5-13: Structure Base Shear vs. Deflection Responses	120
Figure 5-14: Base Shear vs. First Storey Deflection.....	121
Figure 6-1: Deformation of a First-Order Element with Reduced Integration under Bending	135
Figure 6-2: Lateral Loading System in Model	135
Figure 6-3: Mesh in Columns	136
Figure 6-4: Specimen Mesh.....	137
Figure 6-5: Mesh of Columns without Concrete.....	137
Figure 6-6: Meshes of Infill Panels (Out-of-Plane Scale 20).....	138
Figure 6-7: Meshes of Frame Beams	139
Figure 6-8: Strain Hardening Rules	140
Figure 6-9: Material Curves under Unidirectional and Cyclic Loading.....	141
Figure 6-10: Material Curves for First Storey Infill Panel	142
Figure 6-11: History of First Floor Applied Displacement.....	143
Figure 6-12: Energy History	144
Figure 7-1: Base Shear vs. First Storey Deflection.....	156
Figure 7-2: Deformation of Model (P = 1690 kN).....	157
Figure 7-3: Residual Deformed Shape of Test Specimen.....	158
Figure 7-4: Average Value of Von Mises Stresses in North Bottom Corner (West Side) of	

First Storey Infill Panel.....	159
Figure 7-5: Differential of von Mises Stresses in North Bottom Corner (West Side) of First Storey Infill Panel.....	160
Figure 7-6: Average Stresses in First Storey Infill Panel Near Columns	161
Figure 7-7: Vertical Anchorage Stresses into Top Beam.....	162
Figure 7-8: Axial Forces in South Column	163
Figure 7-9: Axial Forces in North Column	164
Figure 7-10: Bending Moments in South Column.....	165
Figure 7-11: Bending Moments in North Column.....	166
Figure 7-12: Flange Bending between Links due to Concrete Expansion under Compression.....	167
Figure 7-13: Calculation of P-M Diagram of PEC Column.....	167
Figure 7-14: Internal Forces at Top and Bottom of Columns in P-M Diagram	168
Figure 7-15: Internal Forces at Levels of Strain Gauges in P-M Diagram	169
Figure 7-16: Yielding in Critical Column Flanges	170
Figure 7-17: Determination of Yield Displacement.....	171
Figure 7-18: Axial Forces in Bottom Beam	172
Figure 7-19: Bending Moments in Bottom Beam	173

List of Symbols

A	Cross-sectional areas of equivalent brace
A_b	Cross-sectional areas of beam
A_c	Cross-sectional area of concrete
A_{cl}	Cross-sectional areas of column
A_r	Cross-sectional area of additional reinforcing steel bars
A_s	Cross-sectional area of steel shape
A_{se}	Effective cross-sectional area of steel shape
b	Unsupported flange width
b_e	Effective flange width
b_f	Full flange width (equals $2b$)
C_c	Axial compressive capacity of concrete
C_{ec}	Euler buckling load for PEC column
C_f	Total axial load on the column
C_{fs}	Sustained axial load on the column
C_r	Axial compressive capacity of PEC column
C_s	Axial compressive capacity of steel shape
C_u	Design capacity for PEC column
d	Column depth
E_c	Modulus of elasticity for concrete
E_s	Modulus of elasticity for steel
$(EI)_e$	Effective stiffness for PEC column
f	load rate scaling factor
f'_c	Maximum measured concrete strength; Design concrete stress
F_y	Yield strength for steel

F_{yr}	Yield strength for additional reinforcing steel bars
h	Storey height
I_b	moment of inertia of the beam about an axis perpendicular to the panel
I_c	Moment of inertia for concrete section
I_{cl}	moment of inertia of the column about an axis perpendicular to the panel
I_s	Moment of inertia for steel section
k	Plate buckling coefficient
KL'	Effective column length
L	Centre-to-centre distance of columns
L'	Column length
M	Moment force
n	Empirical factor use to relate effective flange width to actual flange width
P	Load
Q_y	Yield base shear
Q_y^*	Control yield base shear used in the test
R	Displacement Ductility
R_d	Ductility-related force modification factor
R_o	Overstrength-related force modification factor
s	Centre-to-centre link spacing
t	Column plate thickness
V	Design base shear
V_e	Elastic base shear
V_y	Yield base shear
w	Infill panel thickness
α	Empirical factor to account for initial imperfections and residual stresses in PEC column
α'	Inclined angle of the strips from the vertical

α_1	Ratio of average stress in rectangular compression block to the specified concrete strength (CSA 2004 - R2010)
δ	Storey deformation
δ_e	Elastic storey deformation
δ_{max}	Maximum storey deformation
δ_y	Yield storey deformation
δ_y^*	Control yield storey deformation used in the test
ε_{cu}	Maximum strain at the extreme concrete compression fibre at ultimate
ε_f	Failure strain of steel
ε_{nom}	nominal or engineering strain
ε_{SH}	Strength hardening strain of steel
ε_y	Yield strain of steel
ε_u	Ultimate strain of steel
ε_{ln}^{pl}	logarithmic plastic strain
λ	Column slenderness parameter
λ_p	Column plate slenderness
ν	Possion's ratio
σ_f	Failure strength of steel
σ_{nom}	nominal or engineering stress
σ_{true}	true stress
σ_y	Yield strength of steel
σ_u	Ultimate strength of steel
ψ	Parameter to account for size effects on PEC columns
\emptyset	angle of the single diagonal brace

1. INTRODUCTION

1.1 Background

In the mid-1990s, a new type of partially encased composite column (PEC column) was developed and patented by the Canam Group to be used in the mid- and high-rise building market. At first, the behaviour of PEC columns under axial compressive loading was studied experimentally and numerically. The design equation and corresponding design rules for PEC columns were developed and then incorporated into the Canadian Standards Association (CSA) standard S16-01 (CSA 2001). The behaviour of PEC columns under bending moments in addition to axial compressive forces was further studied and their use as beam-columns was permitted in CSA S16-09 (CSA 2009).

PEC columns consist of a thin-walled, H-shaped, built-up steel column with concrete cast between the flanges (see Figure 1-1), with transverse links welded near the flange tips at intervals along the column height. Unlike partially encased composite columns fabricated with standard rolled steel sections (Hunaiti and Fattah, 1994; Elnashai and Broderick, 1994; Plumier et al. 1995), the size of the PEC column is flexible, without limitations associated with the use of standard sections. The plates in the bare steel section are slender, making them prone to local buckling, but the larger fraction of the compressive load is sustained by concrete. Concrete is filled between the flanges to resist part of the axial loading and to prevent the local buckling of the web. The concrete also prevents the inward local buckling of the flanges, while the links help increase the local buckling of the flanges by preventing out-of-plane movement at the link positions. The lateral expansion of the concrete under load is partially confined by the flanges and web at three sides and by the links at the free side. An additional benefit of the concrete is that it increases the fire resistance of the column.

Regarding construction, PEC columns take advantage of the erection speed of the bare steel section and then the concrete is cast and cured later in the construction sequence. The steel section supports the dead and live loads during construction and the in-service loads are resisted by composite action of the column. At each floor level, side plates (shown in Figure 1-1) are welded to the flange tips to provide a means for connecting the beams framing into the weak axis of the column. Simple formwork is needed at the flange tips only for the construction of the concrete and the existence of the side plates typically makes the forms reusable at every floor. Less crane capacity is needed because of the relatively light weight of the thin plates used in the steel section, and it is frequently the column size at the base that governs the crane capacity requirements for high-rise steel buildings. Moreover, the steel section uses the same thickness plate for both the web and flanges to facilitate fabrication procedures. All these characteristics lead to cost efficiency.

PEC columns are allowed to be used as beam-columns as well as columns sustaining concentric compressive loads by CSA S16-09 (CSA 2009). The objective of this research project is to investigate the behaviour of PEC columns in steel plate shear walls, which are used as primary elements to resist lateral loads in buildings. Numerous experimental and numerical studies have been conducted on steel plates shear walls with rolled wide-flange columns, and their performance under severe seismic-type loading has been shown to be excellent if properly designed. A key feature of the behaviour of steel plate shear walls is that the thin infill plate connected to the beams and columns tends to buckle under lateral loading, and the lateral forces on the system are resisted largely via a tension field that develops in the plate, as shown in Figure 1-2. Because of the need to anchor this tension field at the surrounding frame, the relatively high flexural stiffness of PEC columns is beneficial for use as boundary elements in steel plate shear walls. However, research is needed to investigate the behaviour and the failure mechanism of PEC columns in steel plate shear walls, and the potential local buckling in PEC column flanges must be assessed. The task of this research project is to study, both analytically and

experimentally, the behaviour of PEC columns subject to axial, shear and bending forces as applied by frame action in steel plate shear walls.

1.2 Objectives and Scope

The research is aimed at extending the applicability of PEC columns and developing a new efficient type of lateral-load resisting system for structures, particularly suitable for seismic regions. The primary interests are:

- to determine the moment and axial forces in the columns when the system is under cyclic lateral loading;
- to determine the capability of the columns to provide appropriate anchorage after the infill plates buckle and the tension field is developed;
- to evaluate the failure mode of the columns under frame action and anchorage forces from the infill panels;
- to investigate the tension field development and distribution after the steel plate shear wall infill plates buckle;
- to evaluate the ultimate capacity and the post-ultimate strength of the system under cyclic lateral loading;
- to evaluate the ductility of the columns and the whole system;
- to evaluate the anchoring stress near the top beam of the steel plate shear wall; and
- to make recommendations for the design of steel plate shear walls with PEC columns.

A two-storey steel plate shear wall with PEC columns was constructed and tested, and a detailed finite element model of the specimen was developed, to achieve the above objectives.

1.3 Report Organization

This report includes eight chapters and an overview of the report structure is as follows:

Chapter 1 is the introduction of the PEC column and system of steel plate shear walls with PEC columns. The objectives and scope of the research is included, as well as the organization of the report.

Chapter 2 reviews previous experimental and numerical research work related to PEC columns and steel plate shear walls. The scopes and conclusions of the research work are presented.

Chapter 3 describes the test program, including additional details about the objectives of this part of the research, the specimen design details and considerations, fabrication procedures, as-built measurements and imperfections of the fabricated specimen.

Chapter 4 describes the test set-up, instrumentation and data acquisition, as well as the ancillary tests to determine mechanical properties of all the materials used in the specimen. Considerations in the determination of the load and deflection history used for the test are included, while the specimen behaviour during the test is described in detail.

Chapter 5 presents the test results, including hysteretic behaviour, energy dissipation and failure mode of the test specimen, as well as the results from the strain gauges, strain rosettes and camera system. Discussions about the strain hardening in the first floor infill panel, the concrete shrinkage in the PEC columns prior to the test and the ductility-related force modification factor, R_d , are included.

Chapter 6 presents the development of the finite element model, including the element selection, mesh description incorporating the as-built dimensions, steel–concrete interaction modelling, boundary condition simulation, measured material properties and the modified material curve for the first floor infill panel. Loading application and solution strategy used in the model are included.

Chapter 7 presents the behaviour of the model of the test specimen. Internal force distributions in the PEC columns, the P-M diagram of the PEC columns and the determination of the yield deflection based on the yielding in the columns are presented as well.

Chapter 8 presents a summary of the research work, including the test and the model. Conclusions are drawn and recommendations for the design, fabrication and future work are presented.

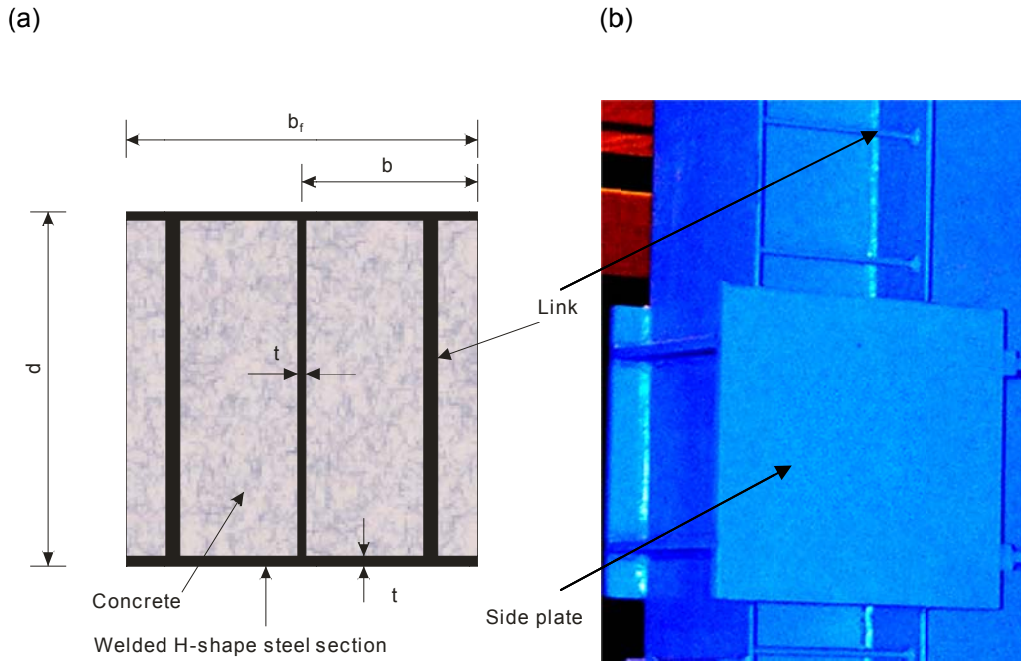


Figure 1-1: Partially Encased Composite Column
 (a) Column Cross-Section; (b) 3D View of the Steel Configuration

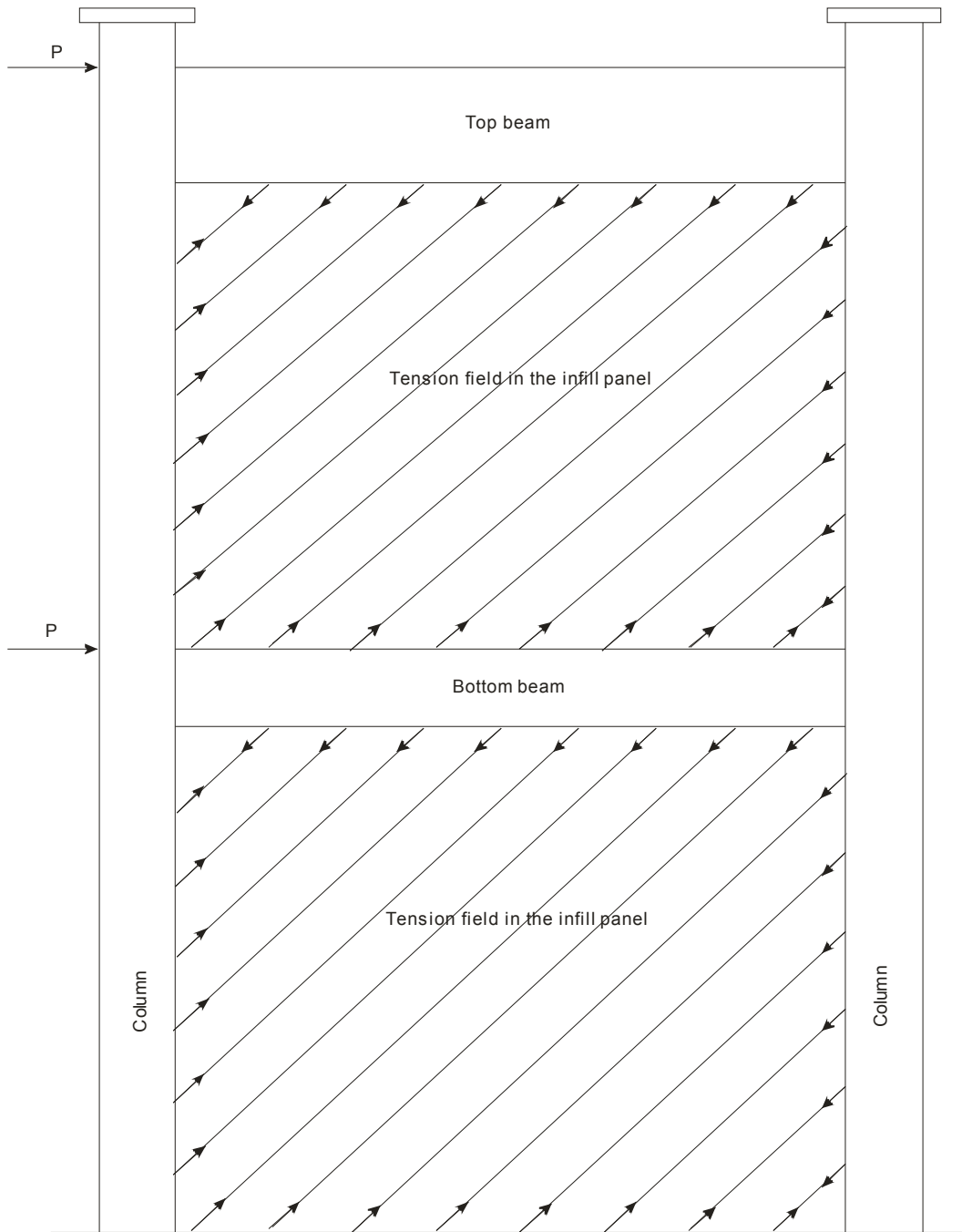


Figure 1-2: Tension Field in Infill Panel

2. LITERATURE REVIEW

2.1 Introduction

After years of research, the theory of the steel plate shear wall system is quite mature and the system is used to resist lateral loads, especially seismic loads. Although the PEC column is still a relatively new concept, research was conducted on the behaviour of PEC columns sustaining concentric and eccentric loading. Considering its large stiffness, the PEC column could be used as a boundary element in steel plate shear walls due to its potential anchorage capacity. This chapter provides a summary of previous research on the steel plate shear wall system and the PEC column.

2.2 PEC Columns Fabricated with Thin-Walled Built-up Sections

In 1996, a new type of partially encased composite column (PEC column) was developed by the Canam Group that consists of a thin-walled H-shaped steel section built-up from hot-rolled plates, with transverse links welded between the flanges to inhibit local buckling and with concrete cast between the flanges. Sections fabricated from thin plates are used rather than the standard sections used in Europe (Hunaiti and Fattah, 1994; Elnashai and Broderick, 1994; Plumier et al. 1995), which leads to lighter weight of the steel section without any size limitation, and structural efficiency because concrete sustains a greater portion of the compressive load in the column. Since then, the behaviour of PEC columns has been studied both experimentally and numerically.

2.2.1 Tremblay et al. (1998)

In 1998, an experimental study on the behaviour of PEC columns under compressive axial load was undertaken by Tremblay et al. (1998). Six stub PEC columns with a length-to-depth (L/d) ratio of 5, fabricated with CSA-G40.21-350W grade steel and normal strength concrete, were tested under axial compression, and the study focused on the failure mode, the ultimate capacity and the post-peak behaviour. For all the specimens,

the concrete crushed while local buckling of the steel flange occurred near the crushed concrete at the failure.

To calculate the capacity of the steel section with slender flanges, the plate slenderness, λ_p , was defined to account for the effect of the slenderness of the steel flanges, considering the support from the existing transverse links and encased concrete, which also appears relevant to the post-peak behaviour in the test.

$$\lambda_p = \frac{b}{t} \sqrt{\frac{12(1 - \nu^2)F_y}{\pi^2 E k}} \quad (2.1)$$

$$k = \frac{4}{(s/b)^2} + \frac{15}{\pi^4} (s/b)^2 + \frac{20}{3\pi^2} (2 - 3\nu) \quad (2.2)$$

In Equation (2.1), b is the half-flange width, t is the thickness of the steel plate, ν and E are Poisson's ratio and Young's modulus for the steel, F_y is the yield strength of the steel and k is the plate buckling coefficient calculated in Equation (2.2), in which s is the centre-to-centre link spacing along the length of the column.

After the plate slenderness, λ_p , is obtained, the capacity of the steel section for compression, C_s , is calculated using an effective area for the steel section corresponding to an effective width of the column flanges. The effective width concept by Yu (1985) was adopted to account for the reduced width of the column flanges under local buckling due to large slenderness. Two analytical methods for the effective width calculation were used to compare the predicted value with the test value, and von Karman's formula was recommended for a better match with the test results.

$$C_s = A_{se} F_y \quad (2.3)$$

$$A_{se} = t(d - 2t + 4b_e) \quad (2.4)$$

$$b_e = \alpha \cdot \frac{1}{\lambda_p} \cdot b \leq 1.0 \quad (2.5)$$

In Equation (2.3), C_s is the axial compressive capacity of the steel section and A_{se} is the effective area of the steel section, which is the sum of the web area and the reduced flange area calculated using Equation (2.4), while b_e is the effective width for the steel flanges. In Equation (2.5), α is an empirical factor to account for initial imperfections and residual stresses, taken as 0.6 by Tremblay et al. (1998).

For the ultimate capacity of the PEC column, contributions from both the steel section and the concrete were superimposed.

$$C_r = C_c + C_s \quad (2.6)$$

$$C_c = 0.85A_c f'_c \quad (2.7)$$

In Equation (2.6), C_r is the overall axial compressive capacity of the PEC column, while C_c is the axial compressive capacity of the concrete portion. In Equation (2.7), A_c is the cross-sectional area of the concrete, and f'_c is the concrete cylinder strength.

Although the mathematical model proposed by Tremblay et al. (1998) provides results within 3% of the experimental ultimate capacity for the columns, more tests on larger specimens were recommended to validate the mathematic model under the size effect.

2.2.2 Chicoine et al. (2002a)

Following previous research on PEC columns, five more large-scale stub PEC columns, with the size of 600 mm x 600 mm x 3000 mm, were tested under axial compressive load by Chicoine et al. (2002a). Residual stresses were measured, as well as out-of-straightness of the flange edges at the mid-distance between transverse links, in which inward imperfection governs due to the fabrication procedure.

The load vs. axial strain curves clearly show that a smaller s/d ratio (d is the depth of the column) leads to more ductile response, since in the test, larger deformations at the peak and larger residual capacities were detected in the specimens with a link spacing of $d/2$ than those with a link spacing of d . As well, larger deformation differences before and after the peak at a load level of 95% of the peak load were observed. This result is because more confinement of the encased concrete near the flange tip is provided by more closely-spaced transverse links.

The tests also showed that the ductility and post-peak capacity of PEC columns are influenced mainly by the b/t ratio, the link spacing and the presence of steel reinforcement (rebar) due to their effects on the confinement of the concrete at the column face and the delay of local buckling of the steel flanges. To avoid brittle failure and to obtain enough post-peak ductility, Chicoine et al. (2002a) recommended that the maximum link spacing should be $d/2$ and the maximum b/t ratio should be 30.

Small transverse stresses were measured in the loaded steel section, although they had a negligible effect on the axial capacity of the PEC columns. However, large axial stresses in the transverse links were also measured, caused by concrete expansion and the tendency of the steel flange to buckle. Due to the importance of the links, recommendations were given that the cross-sectional area of a transverse link should be the greater of $0.025dt$ and 100 mm^2 , and the welds at the ends of the transverse links must be designed to develop the full yield capacity of the links.

The size effect was studied by comparing these tests on five 600 mm x 600 mm stub PEC columns with previous tests on six stub PEC columns with sizes of 450 mm x 450 mm and 300 mm x 300 mm (Tremblay et al. 1998). With the same b/t ratio and s/d ratio, there is no significant size effect either on the failure mode or on post-peak behaviour. The latter appears to be improved by a smaller link spacing, larger link diameter and additional steel reinforcement.

The equations proposed by Tremblay et al. (1998) for axial compressive capacity of PEC columns were examined by Tremblay et al. (2000a) to check the size effect on column strength. A new expression for the effective flange width based on a column equation by Loov (1996) was recommended, since a large size column could make the prediction based on the previous equation non-conservative.

$$b_e = b(1 + \lambda_p^{2n})^{(-1/n)} \leq b \quad (2.8)$$

In Equation (2.8), n was taken as 1.0.

Chicoine et al. (2002a) conducted a further detailed analysis on the size effect on column strength and determined that concrete strength drops in larger size columns. In Equation (2.7), 0.85 is a reduction factor to consider the difference between the strength of a standard 152 mm diameter cylinder and the strength of concrete in a PEC column. To better explain the size effect on concrete strength, 0.85 in Equation (2.7) was then replaced by a new factor, ψ , while $n = 0.8$ instead of 1.0 was used in Equation (2.8) for a more conservative prediction.

$$0.97 \geq \psi = 0.85 \left(0.96 + \frac{22}{b} \right) \geq 0.85 \quad (2.9)$$

With the use of ψ and including the contribution from the additional reinforcement, Equation (2.6) became:

$$C_r = \psi A_c f'_c + A_{se} F_y + A_r F_{yr} \quad (2.10)$$

In Equation (2.10), A_r and F_{yr} are the cross-sectional area and the yield strength of the longitudinal reinforcement.

2.2.3 Chicoine et al. (2003)

The long-term behaviour of PEC columns was studied by Chicoine et al. (2003) through five PEC columns with dimensions of 300 mm x 300 mm x 1500 mm and two PEC columns with a cross section of 450 mm x 450 mm and lengths of 2350 mm or 900 mm. The entire loading procedure was designed to simulate the loading sequence in PEC columns based on the construction procedure, including loading in the bare steel section, loading in the whole column 14 days after concrete casting, and loading to failure 150 days after concrete casting. The amount of loading in the first two stages was determined according to the stresses expected in PEC columns for a 36-storey office building (Chicoine et al. 2000). Five out of seven columns were loaded to failure with different loading sequences chosen for the columns to extract individual results from the overall behaviour. Strains were measured throughout the 150 days after concrete casting in all the columns and the axial load loss due to long-term shortening was compensated by adjusting long-term load continually.

Based on the test data, the average value of the restrained shrinkage strains was 35 $\mu\epsilon$, with a corresponding compressive stress of 7 MPa in the steel section. Since a low water-to-cement ratio was used in the cast concrete, with a slump of only 5 mm, the low shrinkage strain was considered reasonable. The strains due to creep in the columns were obtained by subtracting the shrinkage strain and the values were close to the result of the ACI (1992) prediction model. The test data showed neither the loading sequence nor the concrete shrinkage and creep had a significant influence on the ultimate capacity of the columns. The research suggested that Equation (2.10) (Chicoine et al. 2002a) for determining short-term axial compressive capacity of PEC columns could also be used for long-term axial capacity.

2.2.4 Chicoine et al. (2002b)

A finite element model was developed by Chicoine et al. (2002b) to study the behaviour of PEC columns under axial compression, including the long-term behaviour. The long-term stresses were applied on the columns by removing the concrete elements from the model first, applying load to the bare steel section only, and putting back the concrete elements so the stresses in the steel section and concrete after redistribution would match the long-term stresses measured in the tests. The columns were then loaded so the stress distribution in the steel section and concrete in the model would be identical to the test result at the end of the long term loading. Hence, the model was able to predict the long-term behaviour of PEC columns without built-in creep models in the program. The long-term effects on PEC columns were further studied by the model to consider greater creep and shrinkage under more severe conditions in real structures, such as lower humidity and longer loading time. The result showed negligible influence of either the loading sequence or the long term effects on the capacity of PEC columns.

The model was not able to simulate the rapid lateral expansion of the concrete near failure, which forced the steel flanges to buckle outwards in the test (Chicoine et al. 2002a). As a result, a different buckling mode was observed in the model than in the test. Therefore, initial outward imperfections were introduced into the model to trigger the outward local buckling in the flanges. The inability of modelling the rapid lateral expansion of the concrete also resulted in the inability of the model to trace the post-peak behaviour of PEC columns.

Besides the factor ψ in Equation (2.10), which is used to consider the size effect on the concrete strength, a factor of 0.92 was also used to further reduce the concrete strength, mainly to account for the lower quality of the concrete in PEC columns compared with the concrete in cylinders. About the capacity of PEC columns, the research also suggested that $n = 1.5$ should be used in the calculation of the effective flange width, b_e , as shown

in Equation (2.8), to give a sufficient margin in case of more severe imperfections in PEC columns than in the test. Moreover, based on the analysis results of the elastic buckling of the steel column flanges in the model, the plate stiffness coefficient, k , given in Equation (2.2), was modified as shown in Equation (2.11), assuming a Poisson's ratio of 0.3.

$$k = \frac{3.6}{(s/b)^2} + 0.05(s/b)^2 + 0.75, \quad (1 \leq s/b \leq 2) \quad (2.11)$$

Design equations for PEC columns under concentric axial loads, with corresponding design rules and recommendations, were proposed and incorporated into CSA S16-01 (CSA 2001), with a conservative value of 0.8 used instead of 0.92ψ for determining the concrete capacity. Global buckling was accounted for in the same way as for steel columns. The design equations for PEC columns, excluding resistance factors, adopted by CSA S16-01 (CSA 2001) are summarized below:

$$C_u = C_r(1 + \lambda^{2.68})^{-1/1.34} \quad (2.12)$$

$$C_r = A_{se}F_y + 0.8A_c f'_c + A_r F_{yr} \quad (2.13)$$

$$\lambda = \sqrt{\frac{C_r}{C_{ec}}} \quad (2.14)$$

$$C_{ec} = \frac{\pi^2 EI_e}{(KL)^2} \quad (2.15)$$

$$EI_e = EI_s + \frac{0.6E_c I_c}{1 + C_{fs}/C_f} \quad (2.16)$$

where λ is the slenderness parameter, C_r is the cross-sectional capacity, C_{ec} is the Euler buckling load for the column, EI_e is the effective stiffness of the column, KL is the column effective length, I_s and I_c are the moments of inertia of the steel and concrete

areas, respectively, E and E_c are the moduli of elasticity of steel and concrete, respectively, C_{fs} is the sustained axial load on the column, and C_f is the total axial load on the column. Equations (2.1), (2.4), (2.8), with $n = 1.5$, and (2.11) were also adopted into S16-01 for determining A_{se} . The design equations in S16-01 all remain in the current standard, S16-09, except that in Equation (2.13), the coefficient 0.8 was changed to $0.95\alpha_1$ mainly to unify the format with that of the CSA concrete design standard, A23.3, as follows:

$$C_r = A_{se}F_y + 0.95\alpha_1 A_c f'_c + A_r F_{yr} \quad (2.17)$$

where

$$\alpha_1 = 0.85 - 0.0015f'_c \geq 0.67 \quad (2.18)$$

and f'_c is the nominal strength of the concrete. While this change makes the value of the coefficient dependent upon the strength of the concrete, for typical concrete strengths there is little change in the predicted column capacity.

2.2.5 Bouchereau and Toupin (2003)

To study the behaviour of PEC columns in bending and under cyclic loading, Bouchereau and Toupin (2003) tested 22 PEC columns with dimensions of 450 mm x 450 mm x 2250 mm and two PEC beams with dimensions of 450 mm x 450 mm x 5000 mm. Four 20M reinforcing bars tied with 10M stirrups were added in eleven columns and one beam to study the effect of the additional strength and concrete confinement. The columns were designed to sustain either axial compressive loading alone or the combination of axial compressive loading and bending moment, while pure bending moments were applied on the beams. Moreover, the applied bending moments were either bending about the strong axis or weak axis of the columns. Static

loading was applied on eleven columns and two beams, while cyclic loading was applied on eleven columns, including columns with or without additional reinforcement.

The test results showed that the capacities of the columns under static and cyclic loading were similar and even the difference in the post-peak strengths was not significant. When subjected to cyclic loading, the columns always failed in a ductile manner, but the additional reinforcement further improved the ductility of the columns. Moreover, the additional reinforcement also increased the capacity of the columns a small amount, except the columns subjected to relatively large weak axis bending moments, in which there was a relatively large increase in capacity.

A linear strain distribution assumption was adopted to construct the P-M diagram of the PEC columns. The strain at one extreme fibre was the concrete crushing strain ($\epsilon_u = 3500\mu\epsilon$), while the strain at the other extreme fibre varied for different points on the P-M diagram. The test results were shown in the corresponding P-M diagrams and matched the PEC column interaction diagram quite well except for two columns without additional reinforcement and subjected to relatively large weak axis bending moments.

Bouchereau and Toupin (2003) also performed seismic dynamic analyses on 16- and 24-storey braced frame buildings with PEC columns. The analyses showed the gravity columns were subjected to limited bending moments and acceptable amounts of axial compression, while significantly higher demands for axial compression and bending moments were found in the columns of the bracing bents.

2.2.6 Begum et al. (2005)

To simulate numerically the complete behavioural history of PEC columns, a finite element model using ABAQUS/Explicit (Hibbitt et al. 2003) was developed by Begum et al. (2005). A concrete damage plasticity model and dynamic explicit solution strategy were used to predict the rapid volumetric expansion of the concrete under low confinement pressures

and improve the results around and after the peak load. A contact-pair algorithm was used to simulate the interaction between the steel flanges and concrete. By comparing the previous test results and the model results, the model was proved to give good predictions for the behaviour of PEC columns subjected to axial compression as well as both axial compression and flexure. The model predicted the average load vs. strain curves of PEC columns subjected to axial compression well, including the peak load and axial strain before, at, and after the peak load. The model also predicted the load vs. moment curves for eccentrically loaded PEC columns well. Moreover, the failure mode and post-peak behaviour of the PEC columns observed in the tests were accurately simulated by the model.

2.2.7 Prickett and Driver (2006)

Prickett and Driver (2006) conducted an experimental and analytical research program on PEC columns made with high performance concrete. The behaviour of PEC columns under concentric axial loading was studied by the testing of seven PEC columns, in which normal-strength, high-strength, and steel-fibre reinforced high-strength concrete were used. The normal-strength concrete was used as a control to compare with previous research and the steel fibres were used to study their effect on the behaviour of PEC columns with high-strength concrete. The behaviour of PEC columns with high strength concrete under eccentric axial loading was studied by the test of four identical PEC columns. The amount of initial eccentricity of the load was varied and the eccentricities were orientated so the PEC columns bent either about their strong or weak axis.

Concrete crushing combined with the steel flange buckling at the failure was observed in all the concentric tests, except for one with atypical outward local imperfections in the steel flanges between the links, in which local buckling occurred prior to the peak load. The steel fibres increased the ductility of the high-strength concrete and the PEC columns, indicating that the properties of the infill concrete affected the failure mode of the PEC

columns. Uniform longitudinal strains were found in the steel section when subjected to concentric compression, except in the flanges at the links due to the link welds. It was also found that transverse strains had no effect on the column capacity and low confinement of the concrete was provided by the steel section. The current design requirements for links were proved satisfactory based on the stresses measured in the links. However, it was recommended that 0.9 instead of 0.8 could be used for the concrete strength modifier, while the unreduced steel section could be used in the design equations in CSA S16-01 (CSA 2001) based on the test data and the observation in the test that flange buckling did not occur before the peak load.

Concrete crushing combined with steel flange buckling during the formation of a plastic hinge was observed as the failure mode in the eccentric loading tests. Local buckling occurred simultaneously with concrete crushing in three columns, while local buckling occurred prior to the peak load in one column that was bent about the weak axis. Columns bending about the strong axis failed in a more ductile manner than the columns bending about the weak axis. A linear gradient for the longitudinal strains was confirmed in the cross-sections of the PEC columns under eccentric loading. On that basis, axial load vs. moment interaction diagrams were developed to predict the capacities of the columns. The effective area was used for the flanges in compression, according to the equation in CSA S16-01 (CSA 2001). The theoretical strength was compared with the test results and proved to be conservative. The use of PEC columns as beam-columns is permitted in CSA S16-09 (CSA 2009), but the full area instead of the effective area is used for the flange in compression when determining the moment capacity of the cross-section.

2.3 Steel Plate Shear Walls

Research on steel plate shear walls started at the early 1970s experimentally and analytically. The steel plate shear wall system was proved to be both effective and economical in resisting lateral load, especially severe seismic loading, if properly

designed. An early design concept was to prevent buckling in the panel and the post-buckling strength of the panel was not considered. Takahashi et al. (1973) conducted the first extensive research program on the behaviour of steel plate shear walls. The test results demonstrated that stiffened steel panels performed better than unstiffened panels under cyclic loading and the use of stiffened steel panels to prevent buckling was recommended. Due to the high cost of adding multiple stiffeners to the infill plates, the behaviour of unstiffened steel plate shear walls was studied through a series of experimental and analytical projects, and the primary research developments are described in the following sections.

2.3.1 Mimura and Akiyama (1977)

Mimura and Akiyama (1997) developed a method for predicting the monotonic and hysteretic behaviour of steel plate shear walls. The monotonic loading curve consists of contributions from both the panel and the surrounding frame. The panels buckle elastically first and then the panel shear is resisted by a diagonal tension field. The yield and ultimate shear strength of the panel can be determined by the pure diagonal tension in the panel.

The hysteresis model proposed by Mimura and Akiyama (1977) and depicted in Figure 2-1 describes the hysteretic behaviour of a panel based on the monotonic behaviour. Under monotonic loading, the steel plate shear wall panel behaves linearly until yielding occurs at point A, and the panel behaves inelastically afterwards through point B to point H. Under cyclic loading, the steel plate shear wall panel follows the same path as under monotonic loading to point B, at which point the panel is unloaded to point C' and then reloaded in a reversed direction to point C. At point C', there is only inelastic deformation left in the panel with zero loading and elastic buckling in the panel occurs at point C, which prevents the load in the panel from increasing. The panel regains stiffness at point D when the tension field in the panel is redeveloped in the opposite direction. If unloaded at point D, the panel will reach point D' and D' is the middle point of OC' since

Poisson's ratio equals to 0.5 in the model. Once the tension field is redeveloped at point D, the load in the panel keeps increasing to the yield point A', which is the yield point if the panel is monotonically loaded in this direction. The panel is unloaded at an arbitrary point E through point F' to point F when elastic buckling occurs in the panel, and then to the point G when the tension field is redeveloped. The model assumes the panel reaches the unloading point B in the previous cycle from the point G linearly and then follows BH. A series of small-scale, simply-supported plate girders were tested under a small number of load cycles by Mimura and Akiyama (1977). Reasonable agreement was shown between the predictive model and the tests, but no conclusions were drawn for the resistance of the panel under cyclic loading.

2.3.2 Thorburn et al. (1983)

The so-called "strip model" was developed by Thorburn et al. (1983) for the analysis of steel plate shear walls, in which negligible strength was assumed in the panel prior to buckling and the storey shear is resisted by the diagonal tension field. As shown in Figure 2-2, discrete pin-ended diagonal tension strips with a inclined angle identical to the tension field are used to represent the tension field in the panel. Thorburn et al. (1983) suggested ten strips are adequate for each panel. The beams are modelled infinitely stiff flexurally, instead of using the actual stiffness, except the beams at the top and bottom of the shear walls, to reflect the offset of the opposite tension fields in the panels above and below each beam. The ends of the beam can be modelled as simple connections, as shown in Figure 2-2, or moment connections. Actual stiffness is used for the columns in any storey. The inclined angle of the strips from the vertical, α , was derived by Thorburn et al. (1983) as given in the equation:

$$\tan \alpha = \sqrt[4]{\frac{1 + \frac{Lt}{2A_c}}{1 + \frac{ht}{A_b}}} \quad (2.19)$$

where t is the thickness of the panel, A_b and A_c are the cross-sectional areas of the beam and column, respectively, and L and h are shown in Figure 2-2. The use of the strip model is specified in the Canadian steel design standard (Clause 20.3, CSA S16-09).

To simplify the analysis of multi-storey steel plate shear walls, Thorburn et al. (1983) developed an equivalent brace model, in which a single diagonal tension-only brace intersecting the working points of the frame was used instead of strips, as shown in Figure 2-3. As the angle of the single diagonal brace is ϕ , the area of the brace, A , is calculated as:

$$A = \frac{tL \sin^2 2\alpha}{2 \sin \phi \sin 2\phi} \quad (2.20)$$

A parametric study to assess the effect of the thickness, height and width of the panel and the column stiffness on the stiffness and strength of the panel showed that the parameters were closely interdependent with complex interaction.

2.3.3 Timler and Kulak (1983)

To verify the analytical method developed by Thorburn et al. (1983), Timler and Kulak (1983) tested a pair of single storey steel plate shear walls. The test specimen is shown in Figure 2-4, in which the columns are oriented horizontally and the beams oriented vertically due to the testing procedure.

The equation for determining α , originally developed by Thorburn et al. (1983), was modified as follows:

$$\tan \alpha = \sqrt[4]{\frac{1 + \frac{Lt}{2A_c}}{1 + ht \left(\frac{1}{A_b} + \frac{h^3}{360I_c L} \right)}} \quad (2.21)$$

where I_c is the moment of inertia of the column about an axis perpendicular to the panel. Another equation was also given to calculate α for the panel at the top of the steel plate shear walls considering the effect of the stiffness of the top beam, which has an infill panel at one side only and is free to bend.

$$\tan \alpha = \sqrt{\frac{1 + Lt \left(\frac{1}{2A_c} + \frac{L^3}{120I_b h} \right)}{1 + ht \left(\frac{1}{2A_b} + \frac{h^3}{320I_c L} \right)}} \quad (2.22)$$

where I_b is the moment of inertia of the beam about an axis perpendicular to the panel.

Timler and Kulak (1983) used the strip model to model the test specimen and good correlation was found between the predicted and test values. The research recommended that Equation (2.21) should be used for more accuracy and the Canadian steel design standard (Clause 20.4.1, CSA S16-09) permits the use of Equation (2.21) for the calculation of the angle of the tension field.

2.3.4 Tromposch and Kulak (1987)

Tromposch and Kulak (1987) tested a two-panel shear wall to examine the hysteretic behaviour of the specimen and to verify the strip model developed by Thorburn et al. (1983). The response of the test specimen to the cyclic loading indicates ductile behaviour with severely pinched hysteresis curves due to the thin infill panel and flexible boundary frame. As shown in Figure 2-5, a hysteresis model was developed by Tromposch and Kulak (1987) based on the previous hysteresis model (Figure 2-1) by Mimura and Akiyama (1977). Based on the test result, two modifications on the previous hysteresis model were suggested. First, the line C'C in Figure 2-1 has zero length since the strength prior to buckling of a very thin panel is neglected. Second, the line CD in Figure 2-1 has the stiffness of the boundary frame since the load is sustained by the boundary frame during the redevelopment of the tension field. The strip model was determined to be

conservative for both initial stiffness and ultimate capacity of steel plate shear walls. The research also found a negligible effect of the eccentricity of the fish plate on the behaviour of the steel plate shear wall specimen.

2.3.5 Driver et al. (1997; 1998a,b)

Driver et al. (1997; 1998a) conducted a cyclic test on a large-scale four-storey steel plate shear wall, as shown in Figure 2-6, to evaluate the overall in-plane performance of steel plate shear walls under extreme cyclic loading. Moment-resisting beam-to-column connections were used in the specimen and the panels were connected to the boundary elements through fish plates. Gravity loads were applied to the tops of the columns while the lateral loads were designed according to ATC-24 (Applied Technology Council 1992) and applied at each floor level. Great ductility was observed in the test and even the post-ultimate degradation was slow and controlled. The moment-resisting beam-to-column connections used in the specimen led to significantly larger energy dissipation capacity than similar specimens with simple shear beam-to-column connections. The research shows the steel plate shear wall system to be an excellent system to resist lateral loads if properly designed.

To predict the behaviour of the specimen, Driver et al. (1997; 1998b) developed a finite element model, in which the boundary elements were modelled by beam elements and the panels were modelled by shell elements. In the model, the ultimate capacity was predicted well, but with a slight overestimation of the initial stiffness when the model was subjected to monotonic loading. When cyclic loading was applied to the model, as was done in the test, the load vs. displacement response showed good agreement with the test data without capturing the pinching of the hysteresis curves due to buckling and redevelopment of the tension field. To analyse the test specimen using structural analysis software, Driver et al. (1997) extended the strip model developed by Thorburn et al. (1987) to include inelastic behaviour. The strip model gave a good prediction of the ultimate

strength with a slight underestimation of the elastic stiffness of the specimen. Varying the angle of the tension field from 42° to 50° was studied and determined to have little effect on the prediction of the storey shear vs. storey drift curve. The research also showed the use of ten strips for the panel provided enough accuracy and the use of more than ten strips did not improve the prediction of the overall response.

2.3.6 Behbahanifard et al. (2003)

Behbahanifard et al. (2003) conducted a test on a steel plate shear wall specimen, which was taken directly from the one tested by Driver et al. (1998a) with the bottom panel removed. Again, excellent ductility, high energy dissipation capacity, stable hysteresis loops and a high degree of redundancy were observed in the test specimen. To further study the behaviour of steel plate shear walls, a finite element model was developed for both monotonic and cyclic response. The model result was compared with the test results from both Behbahanifard et al. (2003) and Driver et al. (1998a) and good agreement was found, with a slight underestimation of the predicted capacity. A parametric study was conducted after the validation of the finite element model. Negligible effect was found of varying the aspect ratio of the panel from 1.0 to 2.0 on the behaviour of the panel. The inward displacement of the column was found to be induced by the tension field and then resulted in a non-uniform tension field. It was also found that the imperfections in the panel could have a significant influence on the stiffness of the panel with little effect on the capacity of the panel.

2.3.7 Choi, I and Park, H. (2008)

Choi, I and Park, H. (2008) conducted tests on three steel plate shear walls, one moment-resisting frame (MRF) and one centrally braced frame (CBF) to investigate the ductility and energy dissipation capacities of steel plate shear walls with thin infill plates. Ductile details were used in the specimen to maximize the potential ductility, including full penetration welded connections at beam-to-column joints, ductile fish plate details, and

seismic compact column sections. Columns with only 60% of the shear strength for resisting tension field action of the infill panel were used in one of three steel plate shear walls to study the effect of the shear capacity of the columns on the ductility of the steel plate walls, while the MRF and CBF were tested to be compared with the steel plate shear walls. Excellent ductility and great energy dissipation capacity were exhibited in the steel plate shear walls when ductile details were used. The test showed that columns with adequate shear capacity must be designed to resist the tension field action of the infill panel. The research recommended that an idealized tension strip model can be used to estimate the energy dissipation capacity of the steel plate walls.

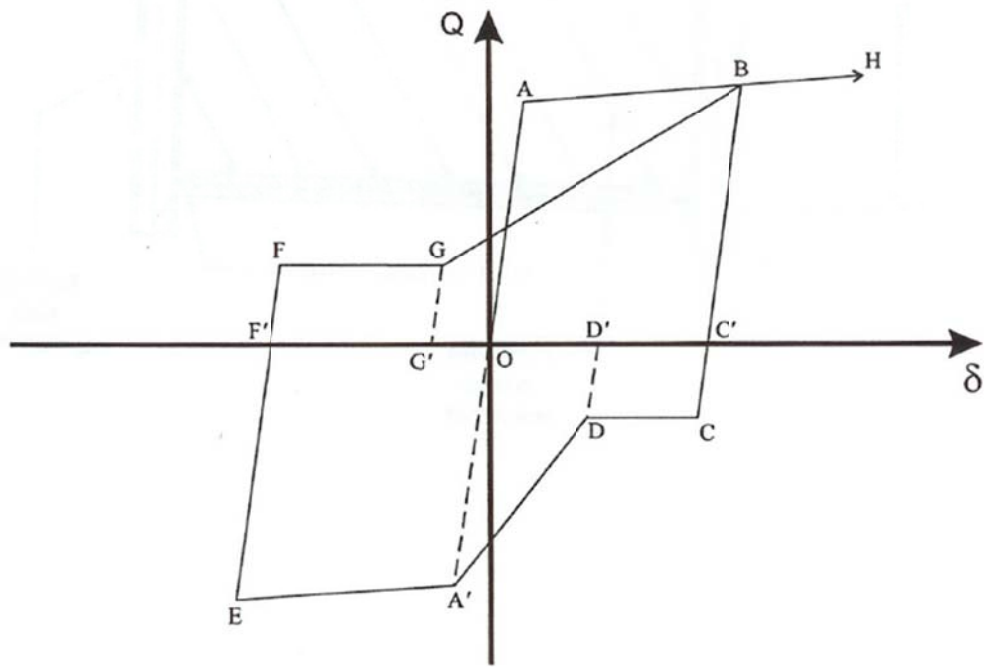


Figure 2-1: Hysteresis Model (Mimura and Akiyama 1977)

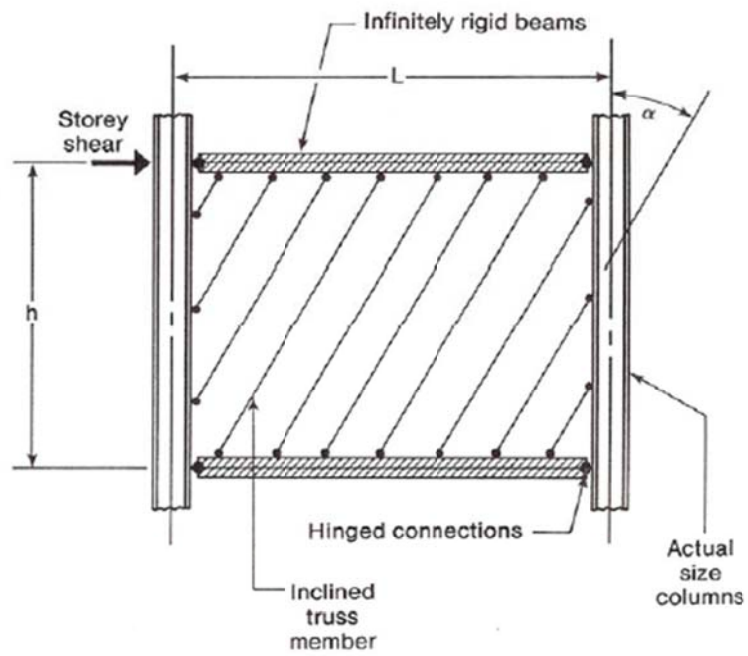


Figure 2-2: Strip Model (Thorburn et al. 1983)

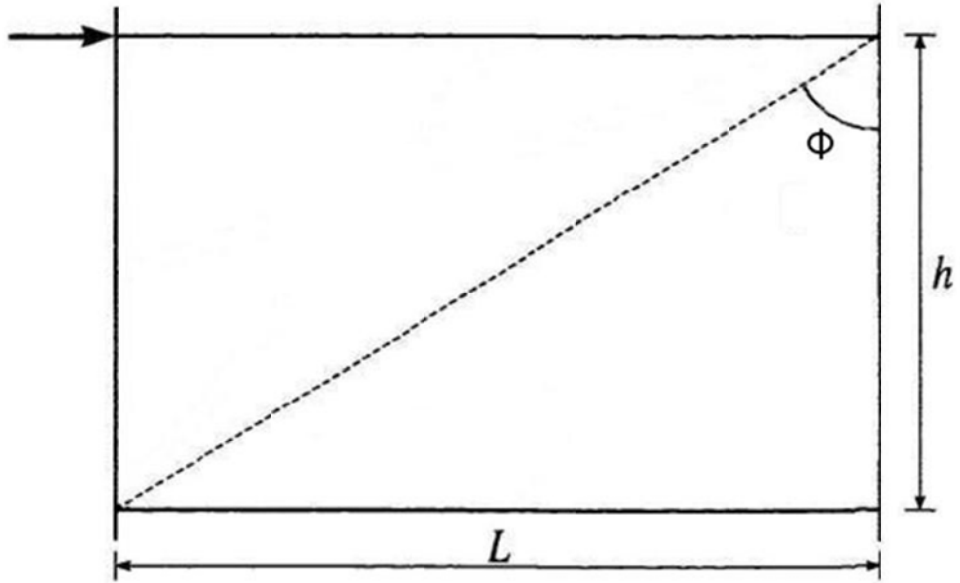


Figure 2-3: Equivalent Brace Model (Thorburn et al. 1983)

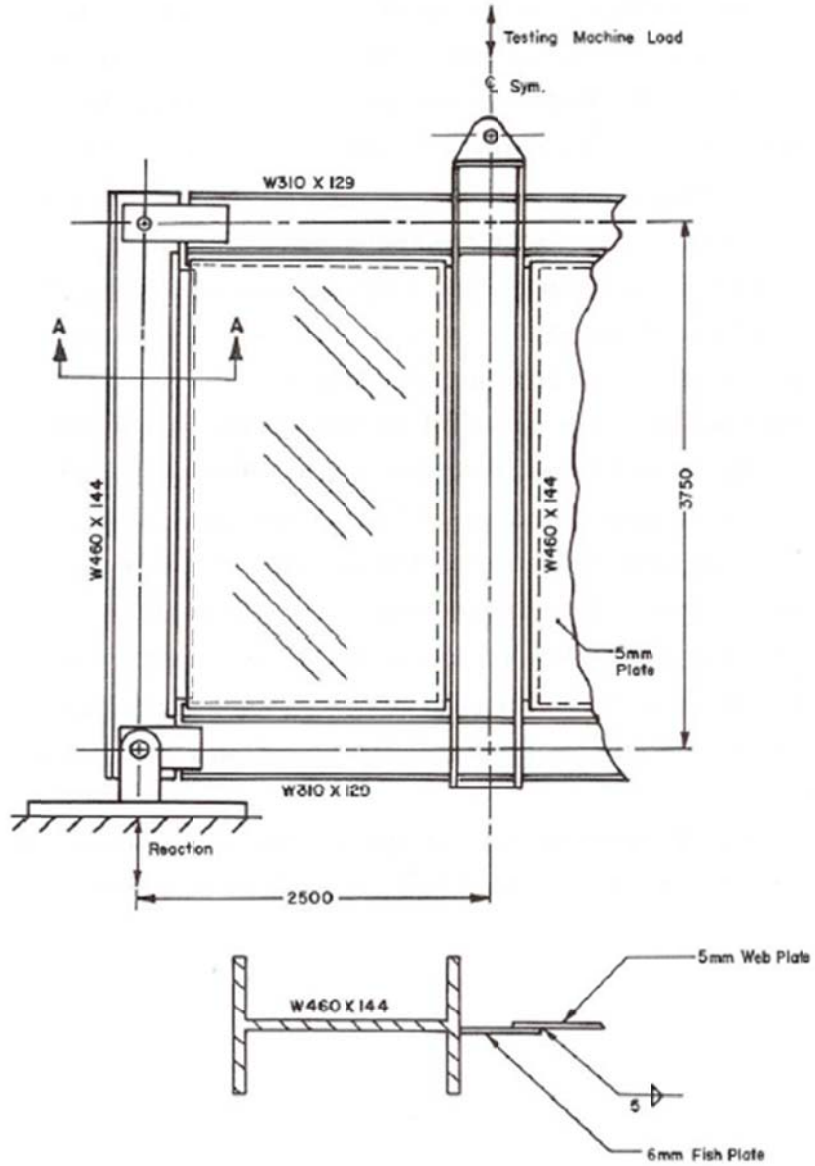


Figure 2-4: One-storey Test Specimen (Timler and Kulak 1983)

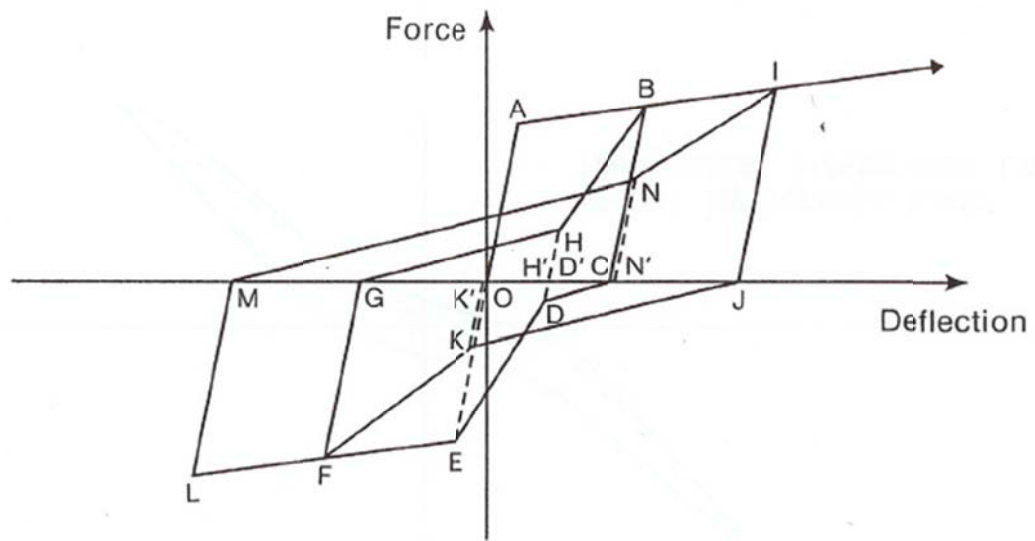


Figure 2-5: Hysteresis Model (Tromposch and Kulak 1987)

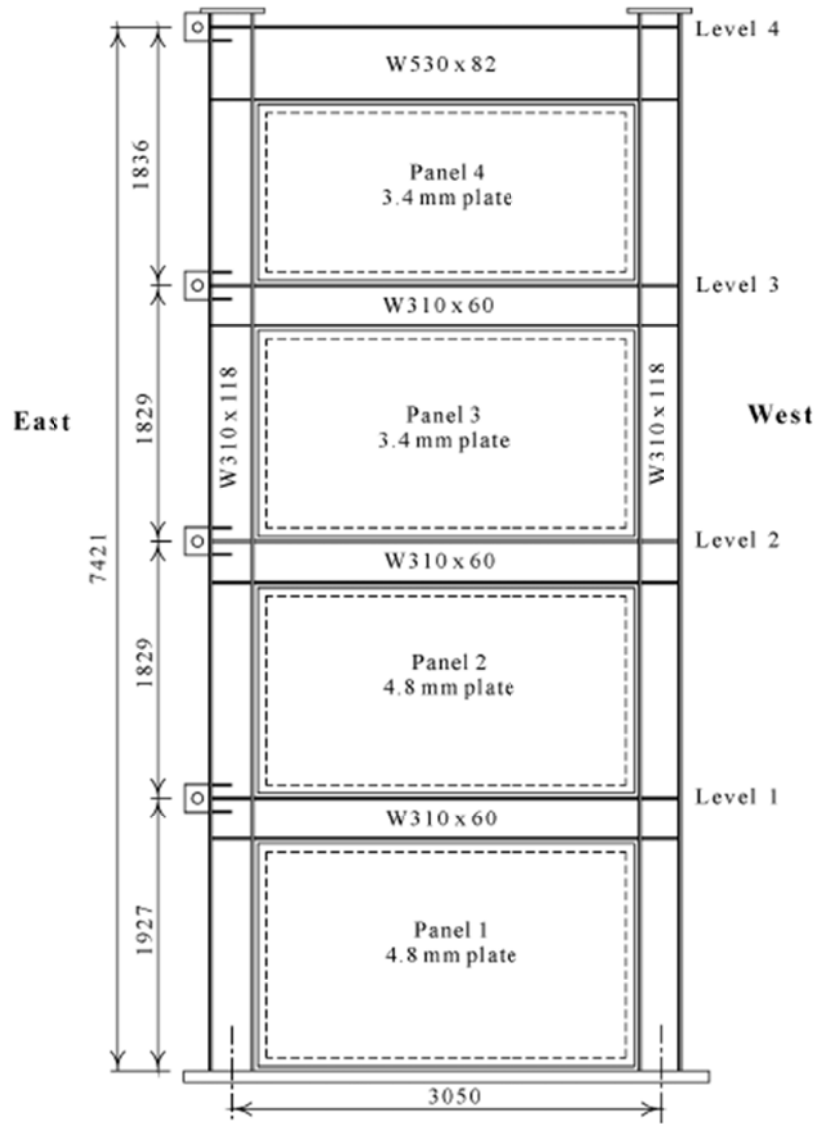


Figure 2-6: Four-storey Test Specimen (Driver et al. 1997; 1998a)

3. DESCRIPTION OF TEST SPECIMEN

3.1 Objectives

A half-scale two-storey steel plate shear wall with PEC columns was designed and tested to study the behaviour of the system under cyclic loading. The prime interest of the experiment is the column behaviour, including tension field anchorage capability, ductility and failure mode, while other interests pertain to the system behaviour, such as the ultimate capacity, the post-ultimate strength, and ductility of the system as a whole. The research also aims at characterising the distribution of the tension field in the infill panel, the anchoring stress near the top beam, and the force developed in the beam. Moreover, the test results are used as the reference for the design of specimens for further research, and also to validate the finite element model developed in this research. Design recommendations are provided based on the test results.

Material curves were determined by ancillary tests for interpreting the test results and developing the finite element model. Tension coupons were taken to represent the steel section in the PEC columns, the top and bottom infill panels, the links inside of the PEC columns and the lower beam, while cylinders were taken to represent the concrete in both the south and north columns in the first and second storeys.

3.2 Specimen Design Details and Considerations

The specimen was designed so that not only the research goals would be fulfilled, but also the specimen would be able to be tested successfully considering the restrictions of the test facilities in the I.F. Morrison Structural Engineering Laboratory at the University of Alberta. Copies of the shop drawings are provided in Appendix A for reference.

3.2.1 Overall Design

A two-storey steel shear wall with PEC columns was designed and tested, which is about half the size of a typical building. As shown in Figure 3-1, the specimen had an overall height of 4.196 m and an overall width of 3.24 m, including the base plate. Each storey was 1.9 m high and the column centreline spacing was 2.44 m. Plates of 3 mm thickness were used for the infill panels and the beams framed into the PEC columns, oriented so that they would bend about the strong axis, through moment connections.

The specimen was selected as two-storey, so the first storey could be observed as a typical critical storey with the most damage occurring, while the second storey could be used to study the tension anchorage stress from the infill panel to the top beam.

3.2.2 PEC Columns

The overall size of the PEC columns is 250 mm x 250 mm, with the same dimensions for the flange width and the column depth, which was chosen to provide enough column stiffness for anchoring the tension field in the infill panels. The details of the PEC columns are shown in Figure 3-2.

As mentioned before, compared with PEC columns under axial compression only, more stiffness and ductility are required for the PEC columns with steel plate shear walls due to the tension force arising in the infill panels. Furthermore, welding in the moment connections also requires steel plates in the PEC columns that are not too thin, to ensure weld quality. Therefore, the thickness of the PEC columns was chosen as 6.35 mm (1/4") and the corresponding flange width-to-thickness ratio was 19.7, which is relatively small compared with the upper limit of 32 in CSA S16-09 for PEC column steel sections.

For attachment of perpendicular beams framing into the PEC columns, which would be necessary in a real building, side plates were welded between the flange tips at each floor level. Besides these side plates, extra side plates were added at the bases of the columns

to help transfer the forces from the columns to the base plate, to improve the sudden stiffness change at the base of the columns and to prevent weld fracture at the column base. The thickness of the side plates was 12.7 mm (1/2") and the height of the side plates was designed to simulate real construction so the forms used in the first storey could be re-used in the second storey. The design of the side plates was also affected by the full plastic moment beam-to-column joint, which is discussed in the next section.

Round bars with a diameter of 10 mm were used as links welded near the PEC column flange tips to delay local buckling of the column flanges and to provide some confinement for the encased concrete. Since less confinement and flange bracing is required for the PEC columns under small bending moments, a relatively large link spacing of 160 mm was used in the middle portion of the columns, which had a link-spacing-to-flange-width ratio of 0.64, approaching the limit of two-thirds specified by CSA S16-09 (CSA 2009) for PEC columns. However, a spacing of 160 mm was used between side plates in the second storey, which were under a severe combination of frame action demand and tension anchorage force from the infill panel. A link spacing of 80 mm was used inside the column panel zones, while a spacing of 50 mm was used inside the bottom side plates to provide extra stiffness at the locations where specimen stiffness changed rapidly.

To meet the requirement in CSA S16-09 (CSA 2009) for PEC columns and for consistency with the previous experiments, CSA-G40.21-350W grade steel was used in the PEC columns, including the steel section, the links, and the side plates. Moreover, it was required that all column plate material be cut from one piece and an extra plate was cut from the same piece for material tests.

3.2.3 Fully Plastic Moment Beam-to-Column Connections

Fully plastic moment beam-to-column connections were used to facilitate comparisons of the behaviour of the specimen with previous research (Driver et al, 1997) on shear walls

with conventional steel columns, in which moment beam-to-column connections were also used.

A typical moment connection for a steel-only frame is shown in Figure 3-3, in which stiffeners are welded between the column flanges adjacent to the beam flanges to help transfer force and to prevent local failure due to the large axial force transferred from the beam flange. However, conventional stiffeners cannot be used inside a PEC column because of the need to pour concrete between the flanges. Moreover, the relatively thin plate used for the steel section of a PEC column is susceptible to local buckling, which is the biggest challenge in transferring the plastic beam moment without causing local failure in the column. A beam-to-column connection capable of transferring the plastic moment capacity of the beam was designed specifically for the test specimen (shown in Figure 3-4).

Beam flanges were connected to the adjacent column flange with complete penetration groove welds, so part of the force would be transferred directly from the beam flanges to the column flange. However, to avoid local failure, additional routes to transfer force needed to be provided. As shown in Figure 3-4, flange extension plates were added between the beam flange tips and the side plates (see Figures 3-4a and 3-4c) so that part of the beam flange force could be transferred through the side plates via longitudinally-oriented fillet welds. Stiffener plates with a thickness of 12.7 mm were welded to the column on the opposite side of the floor beams (see Figure 3-4b and 3-4d), at the level of each beam flange. These extra stiffener plates were used to help transfer the force from the side plates to the columns and would not be needed if a beam framed into the column from each side. To transfer shear simultaneously with moment, "shear tab" web plates (see Figures 3-4b and 3-4c) with a thickness of 10 mm were welded to the column flanges using complete penetration groove welds and to the web of the beam with fillet welds.

3.2.4 Infill Panels and Beams

Steel plates with a thickness of 3.0 mm and a relatively low yield strength of about 250 MPa were chosen as the infill panels to limit the demand on the columns and the overall ultimate strength of the specimen. To obtain ductile material with a low yield strength, ASTM A1011 CS Type B steel was used and the appropriate mechanical properties were confirmed through tension tests before the wall was fabricated. The size of the first floor panel was 2190 mm x 1648 mm, with the height-to-width ratio of 0.75, and the size of the second floor panel was 2190 mm x 1446 mm, with the height-to-width ratio of 0.66. The infill panels were welded to the columns and beams continuously, except at the corners to relieve the demand in the highest stress areas.

Since the tension anchorage force from the panels below and above the first floor beam tend to offset each other, the effect of the infill panels on the first floor beam is negligible. On the contrary, a large stiffness was required for the second floor beam due to the tension anchorage force from the infill panel below. Furthermore, a class 1 cross-section was required to delay local buckling of the beams during the test. W250x58 and W460x67 sections, with a nominal yield strength of 350 MPa, were chosen as the first and second floor beams, respectively.

3.2.5 Column Cap Plates and Base Plate

To avoid local failure due to the small thickness of the steel section elements in the PEC columns, vertical loads were applied uniformly on the whole section of the PEC columns, including the steel section and concrete portion. Hence, cap plates with a thickness of 32 mm were welded to the steel section of the columns at the top and non-shrink grout was cast before the experiment into the gap left intentionally during the concrete pour to ensure proper engagement of the concrete at this location. Holes of 89 mm (3.5 in.) diameter were drilled in the top plates, with one at each side of the column web, to facilitate the casting of the concrete and grout at the tops of the columns.

At the bottom of the specimen, a base plate with a thickness of 76 mm was designed to prevent potential lifting of the columns under frame action. The base plate was connected to the strong floor by 12 pretensioned anchor bolts, each with a diameter of 38 mm (1.5 in.).

3.3 Fabrication Procedures

The steel portion of the test specimen (shown in Figure 3-5) was fabricated and sponsored by the Canam Group Inc., while concrete was mixed and cast in the I.F. Morrison Structural Engineering Laboratory at the University of Alberta (shown in Figure 3-6).

Due to the capacity limitation of the concrete mixer in the lab, one batch of concrete was cast for each column at each floor on two consecutive days. The forms, which were used in the first storey on the first day, were removed and reused in the second storey on the second day, and then removed on the third day. After the forms were removed, the columns were wrapped in plastic sheet with some water injected inside within the following several days for moisture curing.

As mentioned before, vertical loads must be applied to the whole section of the columns, including the concrete portion, which means that the gap between the encased concrete and the top plate due to the concrete shrinkage should be eliminated. Hence, two inch gaps were left on purpose at the top of the columns without concrete (shown in Figure 3-7) and the gaps were grouted through the holes in the top plates before testing. MASTERFLOW 928 was chosen as the grout for its non-shrink properties and high workability.

Because of the existence of the infill panels, the forms used for the PEC columns had to be clamped from the outside of the column only. Since suitable standard C-clamps were not available due to the large column dimension, clamps (shown in Figure 3-8) were designed for this purpose. A mock column, with a cross section of 250x250 mm and link

spaces as in the first floor column in the test specimen, was made in the lab before the concrete was cast in the specimen to test the workability of the concrete, as well as the forms, clamps, and casting protocols (shown in Figure 3-9).

3.4 As-built Measurements

After the whole steel portion of the specimen was fabricated and delivered into the I.F. Morrison Structural Engineering Laboratory, the dimensions and the imperfections were measured.

The specimen and all the extra pieces for the tension coupons were painted because of a misunderstanding with the fabricator, since weather-proofing was required for shipping but “NO PAINT” was overlooked in the general drawing notes. The thickness of the paint was measured and deduced from the dimensions measured directly from the specimen to get the real structural dimensions excluding the paint. One of the extra pieces for the tension coupons was measured at several locations before and after the paint was removed by a hand grinder with great care.

The cross-sectional dimensions of each beam and each column were measured at eight locations either from the specimen directly, if it was convenient, or otherwise from the extra pieces for tension coupons (cut from the same piece as those used in the test specimen), while the thickness of each infill panel was measured at eight locations from the extra pieces. The column cross-sectional dimensions and the thicknesses of the infill panels varied in the most extreme cases by 2.0% and 2.8%, respectively. The thicknesses of the first and second floor infill panels, excluding the paint thickness, were 3.04 mm and 2.97 mm, respectively.

Beam cross-sectional dimensions were measured at the east side and west side of each beam at the ends and at the centreline, while each column height was measured at the east side, west side, and outside at the centerline. The overall widths of the specimen

were measured at five locations along the height in the first floor and at one location in the second floor, since the major interest was focused on the first floor.

The first and second storey heights were 1899 mm and 1896 mm, while the column centre-to-centre spacing was 2437 mm. The thickness of the steel section in the columns was 6.28 mm, while the column depth and flange width were 249.4 mm and 251.8 mm, respectively. The first floor beam depth and flange width were 256.6 mm and 203.0 mm, while the thickness of the flange and the web were 13.67 mm and 8.01 mm. The second floor beam depth and flange width were 455.6 mm and 191.5 mm, while the thickness of the flange and the web were 12.69 mm and 8.60 mm. As such, the measured specimen dimensions in general were very close to the nominal ones.

3.5 Imperfections

In previous research on PEC columns under axial compression only, initial imperfections were found normally to occur as a tendency of the column flanges to bend inward between links due to the fabrication procedure and weld shrinkage. Since the flange deformation is toward the concrete infill between links, these imperfections are treated as negligibly beneficial to column capacity. Similar imperfections were observed in the test specimen and were also neglected, since the initial imperfections in the column flanges had less effect on the column under bending and axial force than a column under axial compression only. However, there was a large inward bending of the south flange between the ninth and tenth links from the south column base (shown in Figure 3-10), apparently from shop damage. This was considered to be a deficiency and was corrected to some degree by use of a hand hammer with great care. Figure 3-10 also shows the defective column portion after the manual correction. The effect of the deficiency was considered minor, since it was located at the middle portion of the column, which was not the most critical location. Other than that, local imperfections, such as superficial

abrasions, were detected at various locations at the flange tips in both columns and were polished before the concrete was cast to avoid fracture due to sharp-shaped abrasions.

For consistency with the scaled size of the column, 10 mm diameter round bar stock was used for the links, which was susceptible to damage during fabrication and delivery. Obvious imperfections were found mainly at the east side of the south column, where the third, sixth and seventh links from the column base bent inward and the tenth link bent downward, as shown in Figure 3-11. Although bending downward enlarged the link spacing above, the tenth link was not located at a critical position and had no discernible effect on the overall column behaviour.

The south column base was offset 3.5 mm to the east on the base plate, while the location of the north column base was identical to the original design. The camber and sweep of the columns were measured and considered negligible. The out-of-plumb measurements of the columns were taken in the two principal axis directions using a plumb-line after the concrete was cast and cured. The final out-of-plumb of the north column was 25.9 mm (L/157) to the west, which is relatively large compared with the limit allowed by Canadian standard CAN/CSA-S16-09.

The out-of-plane imperfection of the infill panels was measured at 63 and 54 locations in the first and second storey infill panels, respectively, and the maximum out-of-plane imperfections were about 11 mm and 10 mm correspondingly.

3.6 Summary

A two-storey test specimen was designed to study the behaviour of steel plate shear walls fabricated with PEC columns, and especially the behaviour of the PEC columns when the whole system is subjected to cyclic lateral loading.

The overall size of the specimen, as well as the thicknesses and the material strengths of the infill panels, were chosen mainly to achieve good overall performance of the wall and simulate realistic proportions in a building, but also to suit the testing capabilities in the I.F. Morrison Structural Engineering Laboratory at University of Alberta. The PEC columns and the frame beams were designed for adequate strength and to provide the stiffness required to resist the tension field stresses of yielding infill panels. To study the behaviour of the PEC columns subjected to both frame action forces and forces due to tension field in the panel, fully plastic moment connections were used at all the beam-to-column joints. The design and fabrication of the specimen were aimed to be consistent with conventional practice in real construction, except the moment connection, where there was no real construction practice to be compared.

The steel portion of the specimen was fabricated in the sponsor's shop according to the design drawings shown in Appendix A. The finished steel portion of the specimen was then delivered to the I.F. Morrison Structural Engineering Laboratory at the University of Alberta, where the concrete was cast and cured. Before the test, the dimensions of the specimen were measured in detail, as well as the initial imperfections. One local deficiency was partially corrected prior to the test.

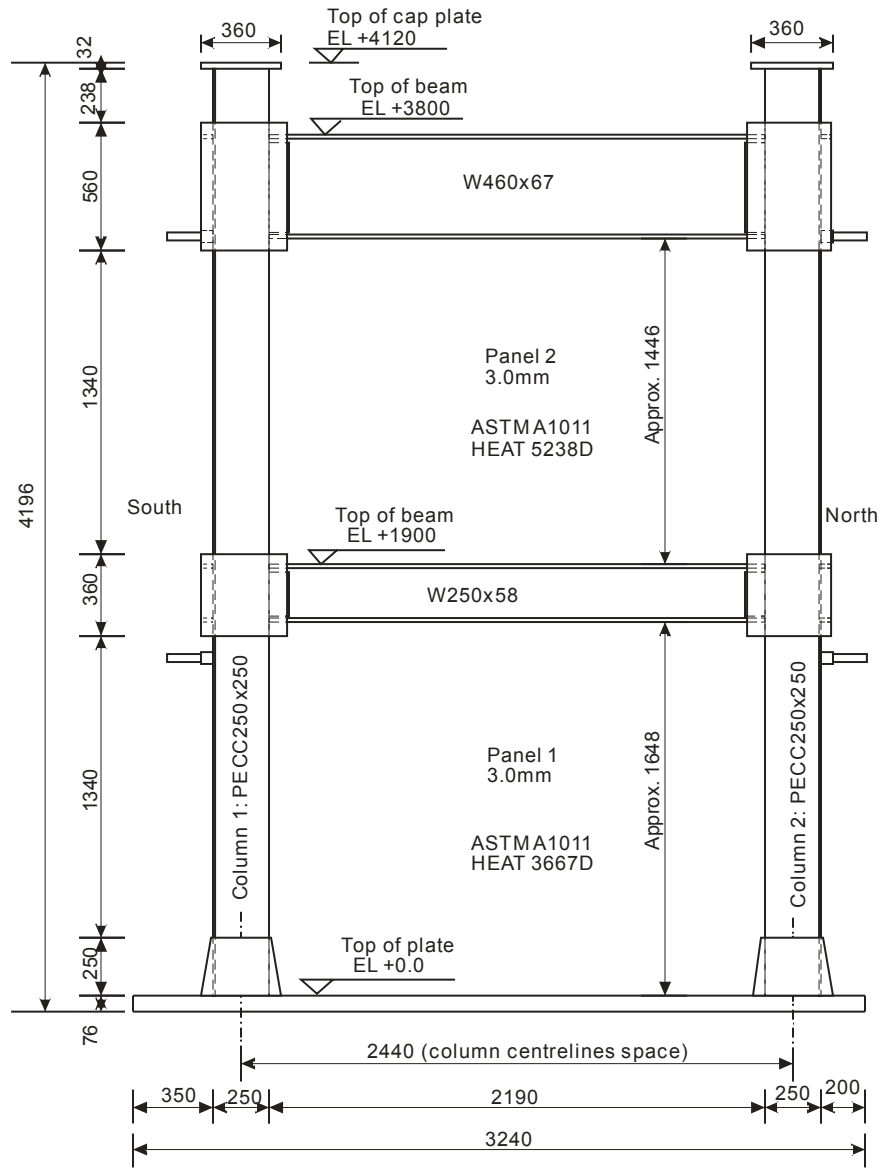


Figure 3-1: Overall Test Specimen (East Elevation)

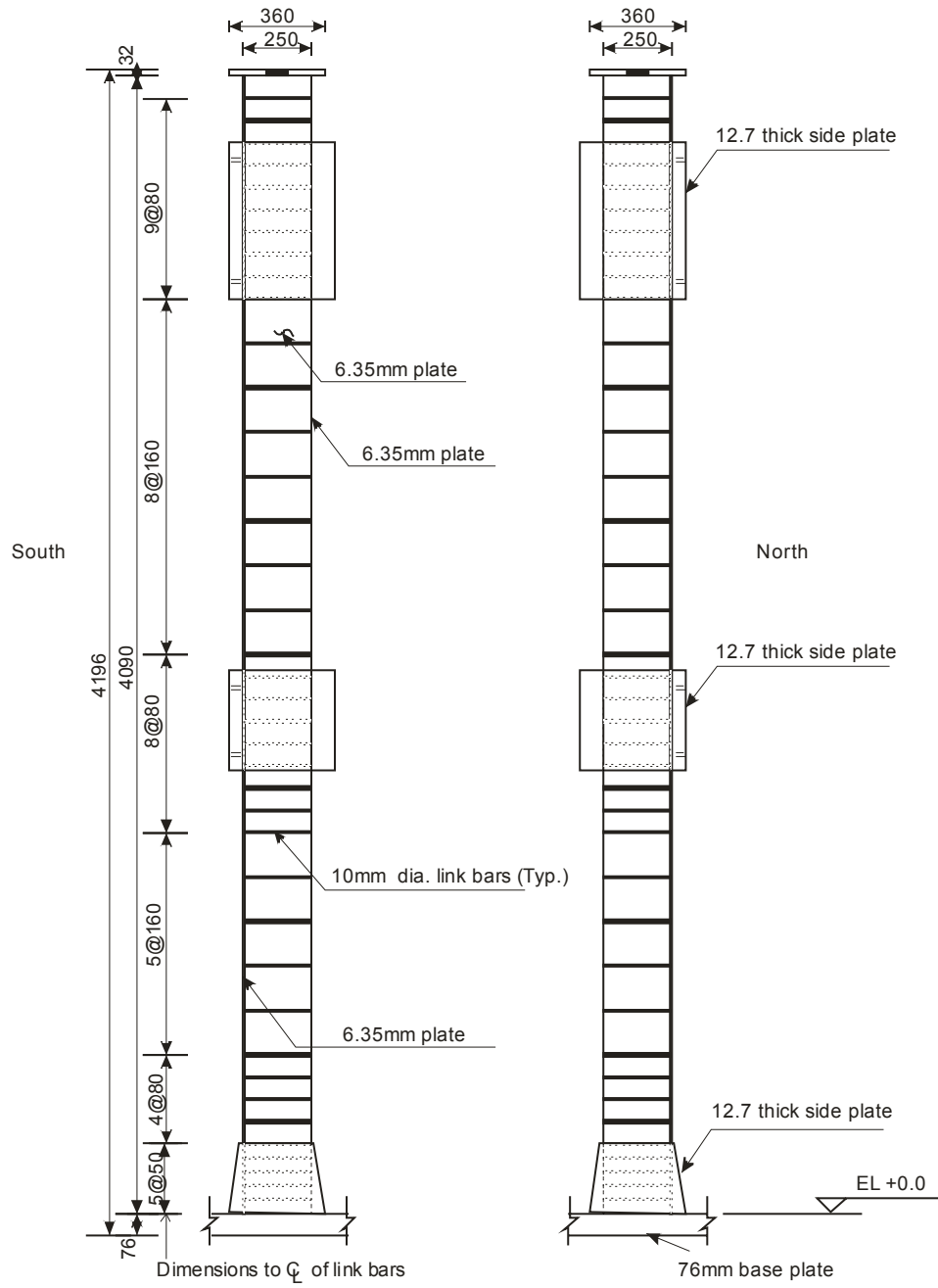


Figure 3-2: Partially Encased Composite Columns (East Elevation)

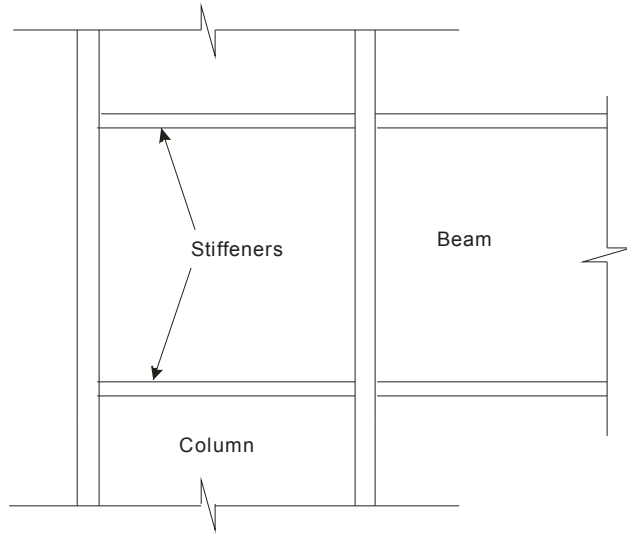


Figure 3-3: Typical Moment Connection for Steel Frame

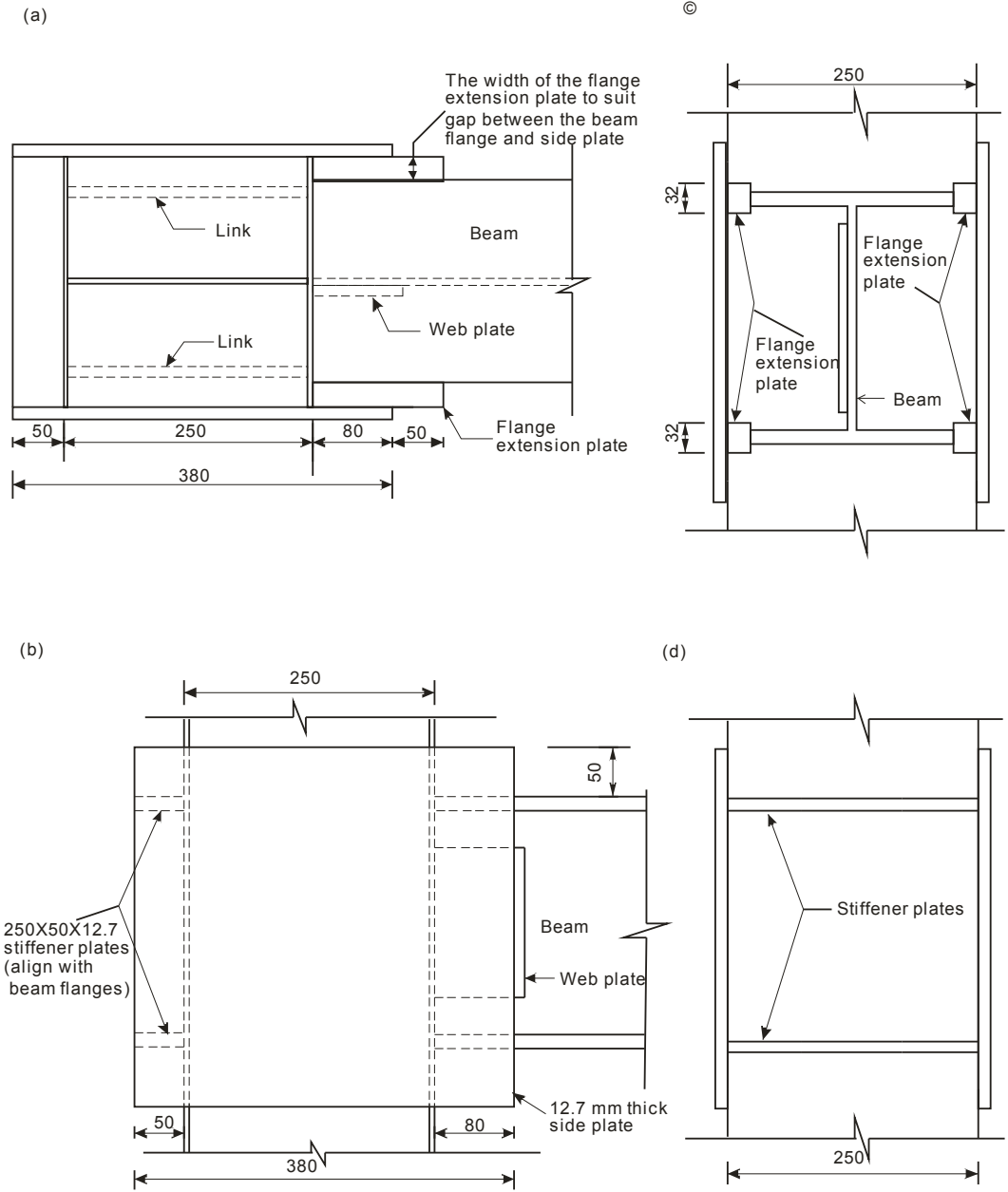


Figure 3-4: Moment Connection for PEC Column
 (a) Plan View; (b) Side View; (c) Inside View; (d) Outside View

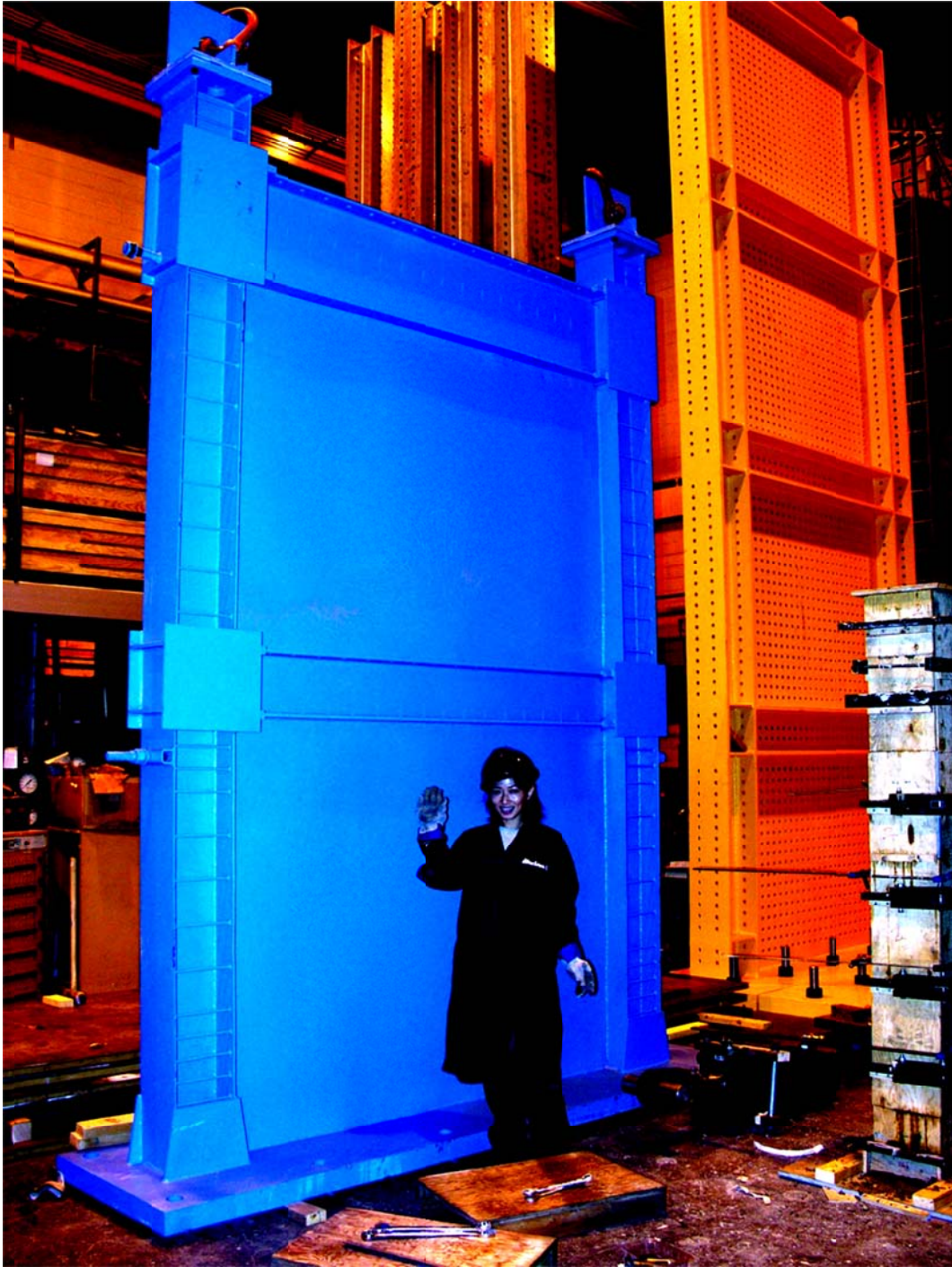


Figure 3-5: Steel Portion of Specimen

(a)

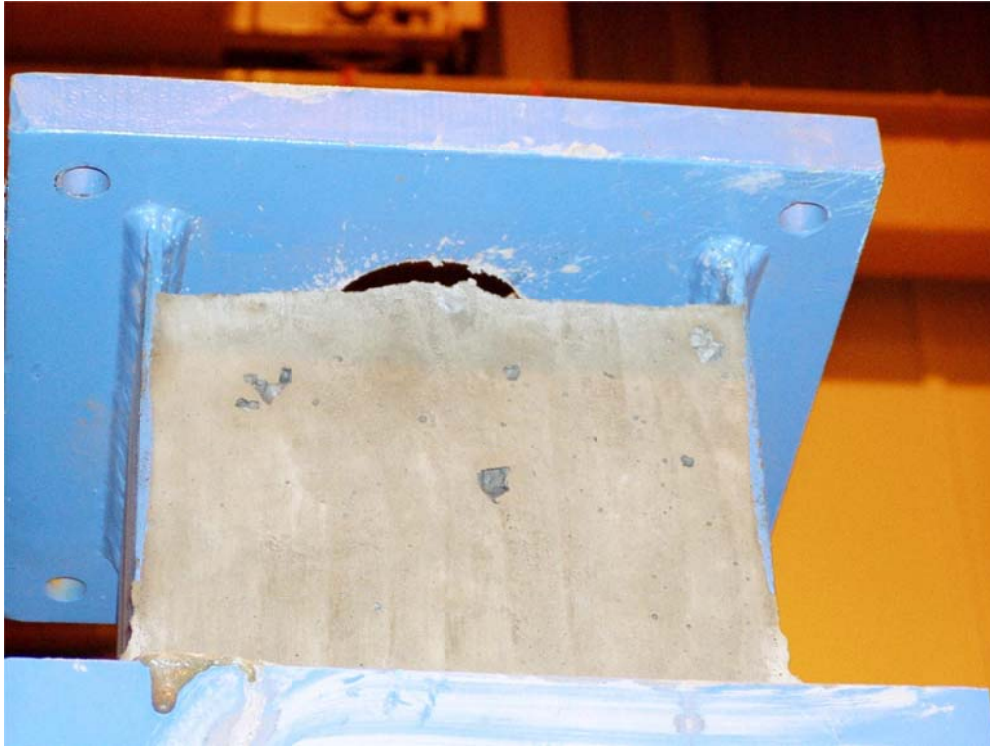


(b)



Figure 3-6: Concrete Casting and Formwork Arrangement
(a) Concrete Casting; (b) Formwork Arrangement

(a)



(b)



Figure 3-7: Gap Left at Top of Columns for Grouting
(a) Gap; (b) Holes in the Cap Plates

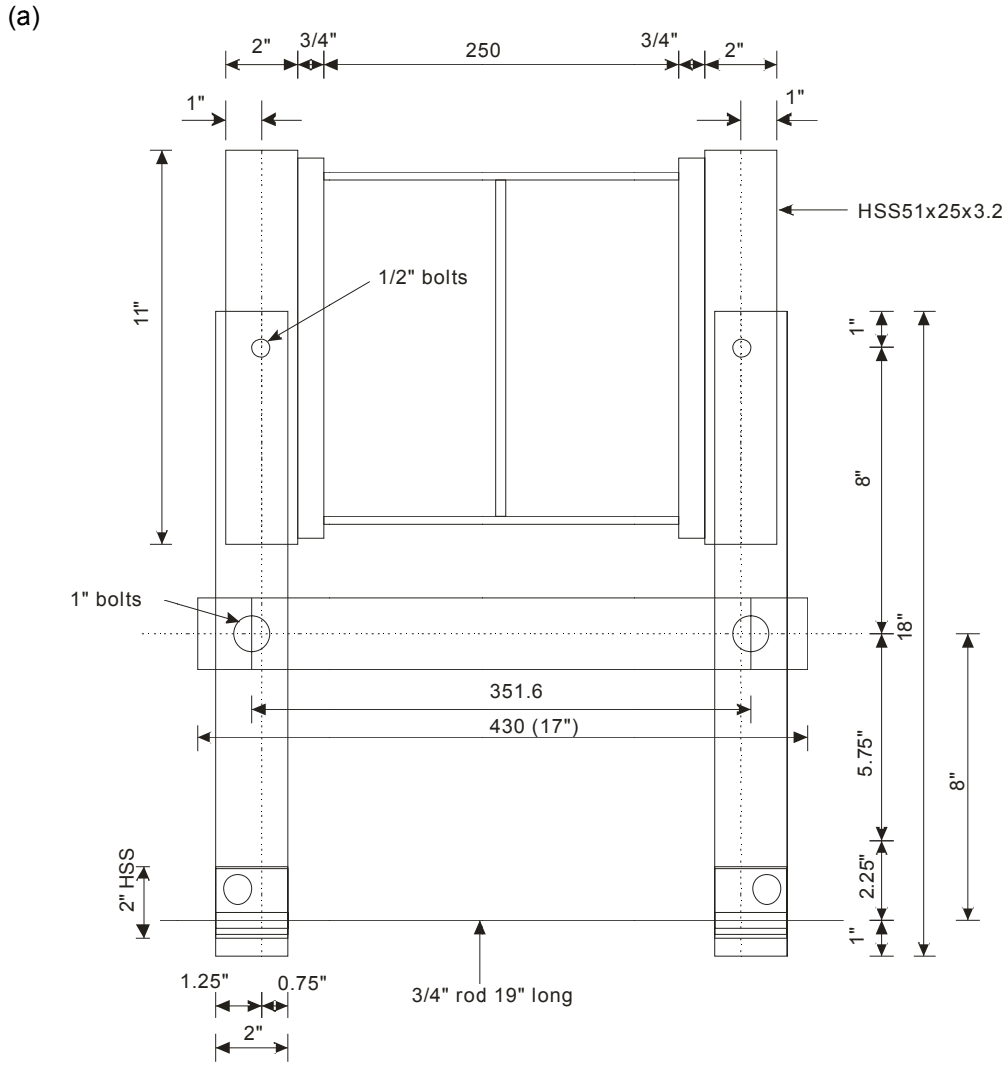


Figure 3-8: Formwork Clamp
 (a) Plan View; (b) Photograph

(b)

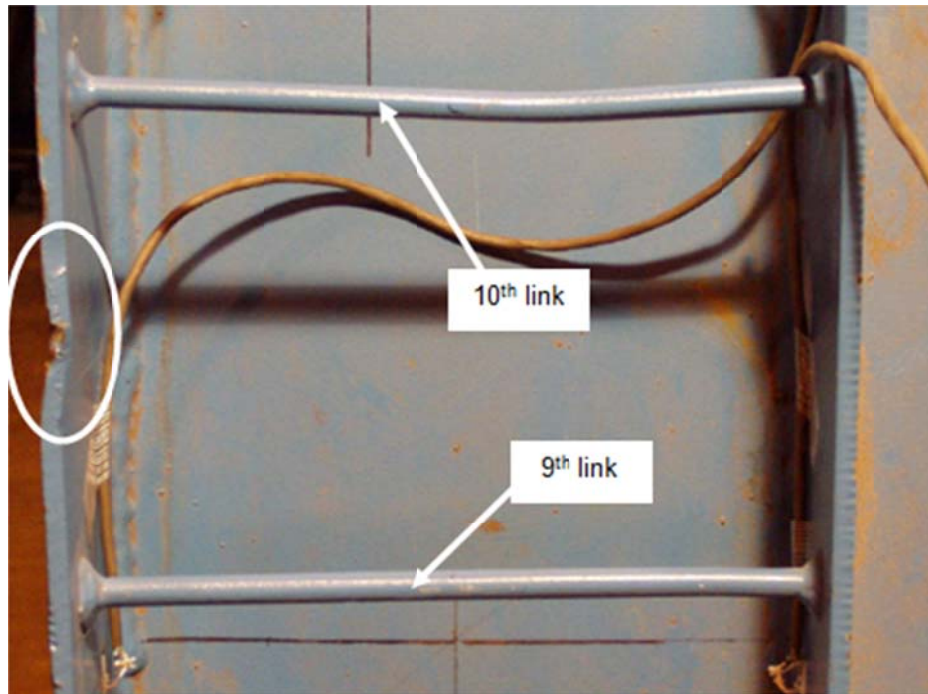


(a)



Figure 3-9: Mock Column
(a) Concrete Casting; (b) After Forms Removed

(a)



(b)

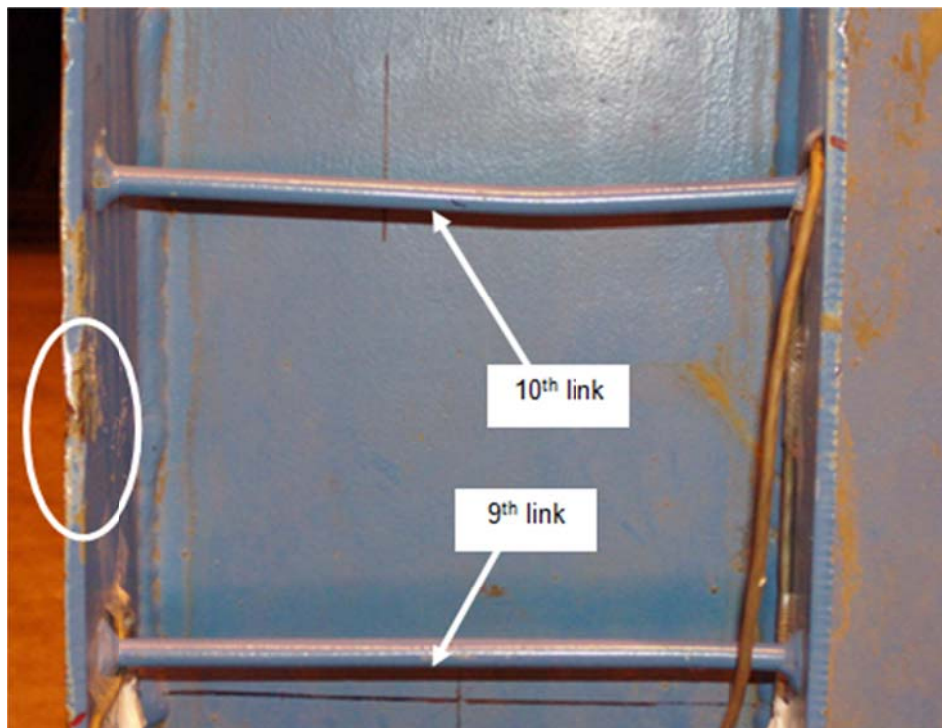
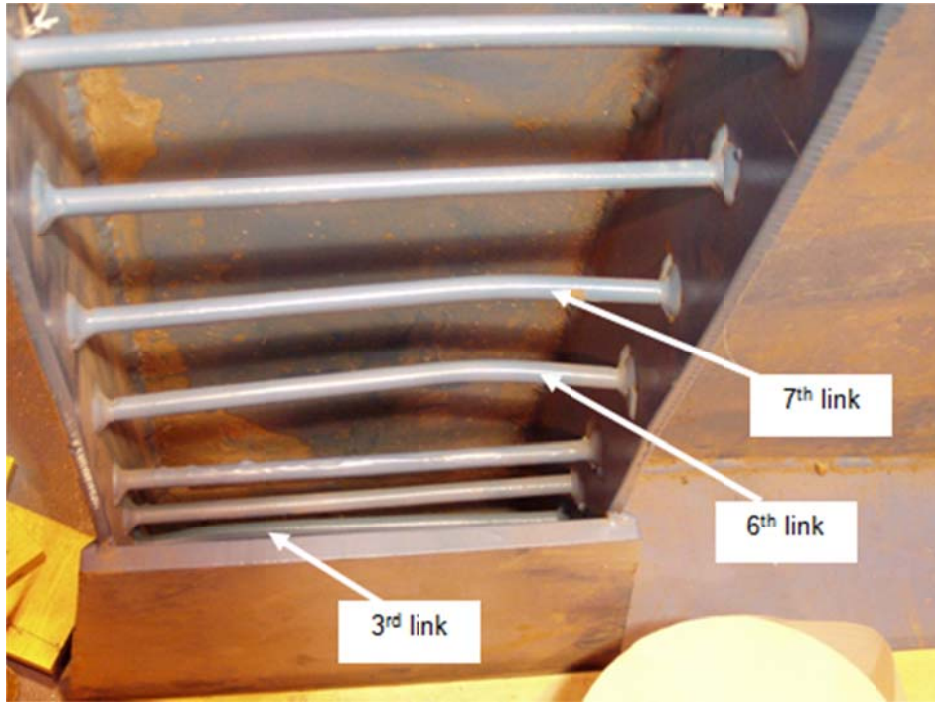


Figure 3-10: Local Imperfection in South Flange of South Column (East Side)
(a) Before Correction; (b) After Correction

(a)



(b)



Figure 3-11: Link Initial Imperfections in South Column (East Side)
(a) Bending Inward; (b) Bending Downward

4. TEST PROCEDURES AND SPECIMEN BEHAVIOUR

4.1 Introduction

A half-scale two-storey steel plate shear wall with partially encased composite columns was tested in the I.F. Morrison Structural Engineering Laboratory at the University of Alberta to determine its performance under simulated earthquake loading. The test set-up and experimental procedures used, as well as the general behaviour of the specimen during testing, are described in this chapter.

4.2 Test Set-up

As depicted in Figure 4-1, Figure 4-2 and Figure 4-3, all the facilities for the test were put in the right position to apply vertical and lateral loads and also to prevent the out-of-plane displacement of the specimen and the sliding of the base plate. The specimen sat on a 3 mm thick grout layer on the strong floor, and the 76 mm thick base plate was connected to the strong floor through twelve high strength anchor rods with a diameter of 38 mm (1.5 in.) after the concrete was cast.

4.2.1 Vertical Loading

Gravity load simulators were used to help apply vertical loads on the tops of the columns, in which a pin-jointed mechanism keeps the loads vertical, or close to the vertical, under large lateral displacements (Yarimci et al. 1966).

In the vertical loading system (shown in Figure 4-2), vertical loads were applied by four hydraulic jacks, each with a capacity of 420 kN, two at each side of the specimen. At one end, hydraulic jacks were attached to the gravity load simulators, which were connected to the strong floor by long rods with a diameter of 38 mm (1.5 in.). At the other end, the hydraulic jacks were attached to the tension rods, which were connected to the

cross-shaped distribution beam above the specimen. Through the distribution beam, vertical loads were distributed to the top of the columns equally.

Considering the test would last days with no operation and no monitoring during the night, the vertical loads were applied before the cyclic loads every day and then unloaded after the loading cycles were finished.

4.2.2 Lateral Loading

In previous steel plate shear wall research, cyclic lateral loads were applied to the steel column flange directly at each floor to represent the action of an idealized earthquake for simplicity. Different from hot-rolled steel columns, PEC columns have steel sections with thin plates, which are susceptible to local damage. If lateral loads were applied to the column flange directly, it is likely that local failure would occur due to the small thickness of the steel section in the column. Therefore, the lateral loads were applied to the top flanges of the beams at each floor level instead of directly to the PEC column. Besides, in reality, inertial forces at each floor height are induced by large floor masses and transferred to the lateral force resisting system through the beams during seismic loading.

At each floor, lateral loads were applied by two hydraulic jacks, each with a capacity of 889 kN and with strokes of 250 mm (10 in.) and 400 mm (16 in.) at the first and second floors, respectively. As shown in Figure 4-1, hydraulic jacks were connected to the reaction walls through clevises at one end, and to the load cells through yokes at the other end. The load cells were then connected to the lateral load transition systems, which were designed to transfer the lateral loads to the top flange of the frame beam at each floor (Figure 4-4).

As shown in Figure 4-5 and Figure 4-6, the lateral load transition systems included a connection tab, channels, T-sections and a W-shape brace. To avoid stability problems within the lateral loading facilities due to the pin connections, the distance between the

reaction wall and the specimen was kept as small as possible, which led to the shallow shape of the connection tabs (shown in Figure 4-7). The connection tabs were connected to the load cells and through the bearing plates to the channels, so the lateral loads applied by hydraulic jacks were able to be transferred to the channels at both sides of the specimen. To further transfer the lateral loads in the channels to the frame beams, the T sections were connected to the channels at the flanges and to the top flanges of the beams at the stem. Slip-critical connections were used between the channels and the T-sections and also between the T-sections and the top flanges of the frame beams to avoid slippage during lateral loading. W-shapes (W200x15) were used at the far end between the channels to improve the integrity of the lateral load transition systems.

4.2.3 Sliding and Out-of-Plane Bracing

It was possible that the specimen would slide under the large lateral loads to be applied, even though the specimen was connected to the strong floor by 12 pre-stressed anchor rods. To prevent this, additional steel base plates were added at the south and north ends of the shear wall base plate to help prevent sliding (shown in Figure 4-8). Steel wedge plates were installed between the additional base plates and the base plate of the specimen to avoid any gap, which could lead to potential sliding of the specimen. The north base plate was connected to the strong floor by six pre-stressed anchor rods to help prevent sliding when the specimen was pushed towards the north. The south base plate was located at the south of the specimen and fitted the gap between the base plate of the specimen and the base plate of the reaction walls to prevent sliding when the specimen was pulled towards the south.

Watt braces (Yarimci et al. 1966), based on the principle of the Watt mechanism, were used so large in-plane displacements of the shear wall would be accommodated with no restraint, while out-of-plane displacements would be prevented. As shown in Figure 4-9, the specimen was braced out-of-plane at the outside flanges of the columns at each floor

using Watt braces. The brace points on the test specimen were located on the columns 410 mm below the beam top flange at each floor level so the Watt-braces would not interfere with the lateral load transition systems. At both ends, the Watt-braces were supported on beams connected to the reaction walls and the columns at the north side of the test set-up (shown in Figure 4-9).

4.3 Instrumentation and Data Acquisition

The overall data acquisition scheme is depicted in Figure 4-10, including all the load cells, LVDTs, strain gauges, strain rosettes, clinometers and dial gauges, used either for measurement or monitoring.

Vertical loads were measured through flat load cells at the tops of the columns. Home-made load cells calibrated from strain gauges mounted on the tension rods in the vertical loading system were used as a redundant measurement. Lateral loads were measured by load cells fitted between the yokes and the lateral loading systems at both the first and second floors and capable of measuring both tension and compressive loads.

Hydraulic jacks used to apply lateral loads shared the same manifold to make sure the lateral loads in the first and second floor were equal, while jacks used to apply vertical loads at the east and west side of the specimen did not share the same manifold. To avoid possible unequal vertical displacements of the jacks at the two sides of the specimen, and out-of-plane bending of the specimen as a consequence, an electronic clinometer was placed on the web of the cross-shaped distribution beam and positioned in the direction perpendicular to the specimen. The clinometer was used to monitor any rotation of the distribution beam so that corrective action could be taken if needed. An additional clinometer was affixed to the web of the distribution beam and positioned in the longitudinal direction of the specimen to monitor in-plane rotation of the specimen at the top.

Two cable transducers with stroke ranges of ± 254 and ± 406 mm (± 10 and ± 16 inches), respectively, were used to measure the first and second floor in-plane deflections and were located 127 mm (5 inches) below the tops of the floor beams to clear the lateral loading systems shown in Figure 4-10.

The out-of-plane displacements of the two columns at mid-height of the beams were monitored by four LVDTs located at the east side of the specimen, as shown in Figure 4-10. The potential movement of the base plate was also monitored by five dial gauges, of which two were located near the columns for possible lifting up of the columns, two were located at the west side of the base plate near the two ends for out-of-plane displacement and rotation of the base plate, and the other one was located at the north end of the base plate for in-plane sliding of the base plate.

Since most of the interest was concentrated on the PEC columns and most of the behaviour occurred in the first floor, internal forces in the columns, especially in the first storey, were obtained by the strain gauges to study the column behaviour, as shown in Figure 4-10. Considering the nonlinear distribution of the internal forces in the column, measurement was taken at three height levels in the first storey. The locations of those three height levels were chosen to be away from the expected plastic hinge zones. To account for the effect of the initial imperfection and local buckling due to the small thickness of the column steel section, strain gauges were mounted to the east and west side and to the inside and outside of the column flanges in pairs. Strain gauges were mounted to the middle of the column webs only at one side since local buckling in the web was prevented by the encased concrete. A total of 54 strain gauges were used in the first floor columns, with nine at each column cross section, while 6 strain gauges were used in the second floor columns with three at each column cross section. All the strain gauges in the second floor columns were mounted to the outside of the column flanges because of the negligible possibility of local buckling due to the low load level in the second floor

columns. The strain gauges in the columns were positioned to measure the strains in the direction along the column height, so the internal forces in the steel could be estimated.

Strain rosettes were mounted on the first floor infill panel at three points at the middle height to study the tension field development, while strain rosettes in the second floor were located close to the top beam to study the anchorage force transferred from the second floor infill panel to the top beam. Strain rosettes were mounted to both sides of the infill panels since plate buckling was expected. To study the tension field in more detail, a digital two-camera system was used to measure full-field strains at the west surface in the north-bottom corner of the first floor infill panel.

For the distribution of internal forces in the bottom beam, measurements were taken along the beam length at three locations away from the beam-to-column joints. Strain gauges were mounted on the bottom of the bottom flange and also the top flange because of the existence of the T-sections, which were part of the lateral loading system and sitting on the top of the top flange. Strain gauges were also mounted to one side of the web at the mid-height at the locations near the beam ends to get a better estimation of the strain gradient near the plastic hinges. All the strain gauges in the beam were positioned to measure the strains in the direction along the beam length.

4.4 Ancillary Tests

Stress–strain curves for the steel and concrete in the specimen were obtained through ancillary tests for analyzing the steel plate shear wall test results and developing the finite element model.

4.4.1 Steel Tension Coupon Tests

A total of 18 coupons for the steel in the specimen were tested in uniaxial tension to obtain the material curves. All coupon tests were conducted by a universal testing machine with a

capacity of 1000 kN, while the elongations were measured by an extensometer with a gauge length of 50 mm.

Three extra steel plates with a size of 500 mm x 500 mm and cut from the same pieces as the infill panels and columns, as well as an extra one-meter W250x58 length cut from the same piece as the first-storey beam, were used for tension coupons. To simulate the fabrication of PEC columns in real construction, steel with the same thickness and heat was used for the flanges and web in the specimen, which required only one extra piece of plate for the columns, while another two were required with one for each infill panel. Tension coupons were cut from the extra pieces (as shown in Appendices B and C) in both principal directions. Tension coupons were also cut from the flanges of the extra one-meter W250x58 length to identify the material behaviour of the first-storey beam. A summary of steel yield strength and elastic modulus is shown in Table 4-1, while the detailed tension coupon test results are shown in Appendix D.

4.4.2 Concrete Cylinder Tests

As mentioned before, one mix of concrete was used for each column in each floor due to the capacity limitation of the concrete mixer used. Six standard cylinders (height of 300 mm and diameter of 150 mm) for each mix were cast when the concrete was cast in the columns to determine the material properties of the concrete, and they were cured in the same way as the columns.

Two collars were connected to the cylinder near the top and bottom with pointed clamping screws to form a gauge length of 200 mm, and the deformation within the gauge length was measured by a dial gauge fixed between two collars. To avoid potential damage to the collars and the dial gauge upon failure, the cylinders were loaded up to about half of the cylinder capacity, after which the collars were removed and the cylinder was loaded to failure. Hence, only about half of the stress–strain curves plus the ultimate stresses were recorded. All the cylinders were tested in a compression testing machine with a capacity of

1350 kN in the concrete lab at the University of Alberta and the loads applied were measured directly from the integral scaled loading ring. A total of 24 cylinders were tested, with six cylinders for each mix, and a summary of concrete strength and elastic modulus is shown in Table 4-2, while the detailed results are shown in Appendix E.

4.5 Load and Deflection History

4.5.1 Gravity load

Vertical loads were applied to the tops of the columns to simulate reasonable service gravity loads on the columns in a real structure. Originally, 720 kN was chosen as the vertical load on each PEC column (Deng and Driver 2007), which is about 26.9% of the factored axial compressive capacity of the composite column, or about 19.5% of the unfactored axial compressive capacity. However, the value was re-assessed to avoid possible concrete cracks in the north PEC column under weak axis moment that would arise due to the combination of the vertical loads and the initial out-of-plumb imperfection of the north column. Based on the strain gauge readings during vertical loading on the first day of the test, the value of 600 kN was finally chosen, which is about 22.5% of the factored axial compressive capacity of the column, or about 16.2% of the unfactored axial compressive capacity.

4.5.2 Lateral load

Quasi-static, cyclic lateral loading was utilized as the testing technique to conduct the experiment, which means cyclic loads or deformations would be applied on the specimen in a slow, controlled and predetermined manner. Although the dynamic effect was not considered in the test, basic information can be obtained through slow cyclic experimentation, including strength, stiffness, deformation capacities, cyclic hardening and softening as well as deterioration behaviour. As steel plate shear walls with partially encased composite columns constitutes a new seismic system, it is important to

investigate those basic characteristics to help characterize the seismic performance of the system.

To assist in preparing, executing and documenting the experiments so that experimental results can be interpreted in a consistent way, ATC-24 (Applied Technology Council 1992) provides standardized procedures for seismic testing of components of steel structures. Hence, the loading method outlined in ATC-24 was adopted for the load and deflection history used in the test.

According to ATC-24, a “deformation control parameter” and a “force control parameter” should be chosen to control the execution procedure of experiments. Since most of the interest was concentrated on the first floor behaviour, the in-plane deformation and the shear force in the first storey were selected. Therefore, the first storey drift was chosen as the “deformation control parameter”, while the base shear was chosen as the “force control parameter”. Correspondingly, yield values were defined as the first storey yield deformation, δ_y^* , and the base shear yield force, Q_y^* .

To estimate yield values for the deformation and force control parameters, a finite element model was developed, which is described in detail in Chapter 6. From the analysis results, the yield deformation was determined initially and adjusted later based on the first six cycles of the test due to the difference observed in the stiffness. The revised estimated yield values, 1264 kN and 7 mm, were used for test control as Q_y^* and δ_y^* , respectively, while the “true” yield values, Q_y and δ_y , were determined after the test based on the complete test results and corresponding updated model.

As shown in Table 4-3, the loading procedure was predetermined based on the requirements of ATC-24. The first nine cycles were performed under force control, with every three cycles carried out using force control values of $0.25Q_y^*$, $0.5Q_y^*$ and $0.75Q_y^*$.

individually. Starting with cycle 10, in which the yield deformation, δ_y^* , was reached, all the remaining cycles were performed under deformation control.

4.6 Specimen Behaviour During Test

Due to the higher storey shear and overturning moment, most of the deterioration was expected to occur within the first storey. Therefore, the first storey was of primary interest for the observations and is the subject of the following descriptions, except for those explicitly specified for the second storey.

Initial hairline cracks due to concrete shrinkage were observed before the test began at the top and middle of the columns, with another initial crack at the bottom of the west side of the north column.

4.6.1 Gravity Load Application

Before the lateral loads were applied, there was no local buckling, concrete cracking (besides the hairline shrinkage cracks) or other obvious deformation or deterioration in the columns. However, there was a sound from the infill panel while the gravity loads were being applied that indicated the deformation of the infill panel due to shortening of the columns under gravity loads.

4.6.2 Lateral Load Application

4.6.2.1 Force Control Cycles

The infill panel buckled into one wave (i.e., one full wavelength) in the first three cycles (cycles to reach a base shear of 316 kN), and buckled into two waves during cycles 4 to 6 (cycles to reach a base shear of 632 kN). The panel then buckled into three waves starting from cycle 7 (first cycle to reach a base shear of 948 kN) until the last cycle in the test (shown in Figure 4-11). The direction of the buckled shapes indicated the diagonal

compression direction of the infill panel under lateral loads. No local buckling was observed in the column flanges during the force control cycles (the first 9 cycles).

There was only one concrete crack detected during the first seven cycles, which crossed almost the whole column depth horizontally and was located at the east side of the north column about 400 mm above the bottom side plate. This crack occurred in cycle 4 (the first cycle to reach a base shear of 632 kN), likely caused primarily by the initial out-of-plumb imperfection of the north column towards the west. During cycle 8 and cycle 9 (the second and third cycles to reach a base shear of 948 kN), there were a small number of partial-depth cracks detected at the bottom of the columns near the bottom side plates, initiating from the outside flanges. All the cracks in the first nine cycles were diagonal cracks with a very short length, except two horizontal cracks with a crack length close to the column depth, which were located at the east side of the columns and about 400 mm above the bottom side plates. The locations of the two horizontal cracks were between the two links with the first link spacing of 160 mm (instead of 50 mm or 80 mm) from the column bases.

Because of the low level of the lateral loads in the first 9 cycles, cracks only arose at the bottom of the columns and only in the column that was under tension force due to the overturning moment. In another words, cracks arose only in the south column when the specimen was pushed towards north, while they opened in the north column when the specimen was pulled towards the south.

4.6.2.2 Deflection Control Cycles before Ultimate

In cycle 10 (the first cycle to reach $\delta = 7$ mm), cracks initiated at the middle of the columns from the inside column flanges. Besides a gradual propagation of the existing cracks, there were a small number of new horizontal cracks initiating with a crack length of more than half the column depth during cycle 10 to cycle 12 (cycles to reach $\delta = 7$ mm).

Starting at cycle 13 (the first cycle to reach $\delta = 14$ mm), concrete cracks developed in the columns much more rapidly than before. Besides propagation of existing cracks, new horizontal cracks initiated at the middle and bottom of the columns, while new diagonal cracks initiated from the outside column flanges at the bottom of the columns in cycle 13. In cycle 14 (the second cycle to reach $\delta = 14$ mm), horizontal cracks started to initiate at the tops of the columns. All the initiation of the new cracks and the propagation of the existing cracks only showed in the column that was in tension. This meant that the tensile force arising from the bending moment in the column was not large enough to conquer the compressive force due to overturning. Moreover, all the concrete cracks that developed in the columns showed a pattern identical to the moment pattern along the height of the columns. In another words, concrete cracks only initiated from the column flange that was in tension under the effect of the bending moment.

In the second floor, the first crack was detected initiating horizontally from the inside column flange at the top of the north column when the specimen was pulled towards the south in cycle 13 (the first cycle to reach $\delta = 14$ mm). Cracks also showed at the top of the south column when the specimen was pushed towards the north in cycle 14 and at the bottom of the south column in cycle 15.

In cycle 16 (the first cycle to reach $\delta = 21$ mm), one concrete crack initiated at the top of the south column from the outside column flange when the specimen was pulled towards the south. This identified that the tension force arising from the bending moment in the column was already large enough to offset the compressive force from overturning under large lateral loads. Thereafter, more and more cracks initiated and propagated in the column that was in compression due to the overturning moment. Also as a result of large lateral loads, small areas of concrete started to spall at the top and the bottom of the columns, accompanied by the development of additional short-length cracks and the propagation of the existing cracks during cycle 16 to cycle 18 (cycles to reach $\delta = 21$ mm). At the end of cycle 18, a kink was found in the infill panel near the north column due to

inelastic stretching of the infill panel in the two perpendicular directions under cyclic loading, which caused a stress concentration and finally led to tearing and opening in the panel.

With the increase of the lateral loads, the compressive force in the outside column flange due to frame action in the column under compression from overturning increased to a level that local buckling finally occurred, which was precipitated by the weakened concrete due to cracking and spalling. As shown in Figure 4-12, the first clear sign of local buckling occurred at the east side of the outside column flange at the base of the south column when the specimen was pulled towards south in cycle 19 (first cycle to reach $\delta = 28$ mm). Due to the bending moment in the columns, local buckling only occurred at one column flange. In cycle 20, local buckling occurred at both east and west sides of the outside column flange at the north column base when the specimen was pushed towards the north. Up to this point, local buckling was detected only in the column under compression and only at the outside flange at the column base where the largest compressive stresses existed. Precisely, local buckling occurred between the top of the bottom side plates and the nearest link above. Besides inelastic local buckling, a large number of new cracks as well as the propagation of existing cracks were detected in the cycles 19 and 20. Starting at cycle 19, the deformation of the beam was clearly visible and the deformed shape was identical to the deformed shape of the beam in a moment frame under lateral loads.

During cycles 21 and 22 (cycles to reach $\delta = 35$ mm), local buckling was detected at the inside column flange at the column top, while more crack initiation, crack propagation and concrete spalling were detected along the whole height of the columns. Moreover, concrete started to bulge outwards near the locations with buckled steel flanges due to the concrete expansion under compression and lack of confinement from the buckled steel flanges. In the infill panel, there was a diagonal tear detected, initiating at the south top corner where the plate was clipped to clear the frame connection weld. The column outside flanges at the bottom of the columns started to tear right at the top of the bottom

side plates during cycle 21 (shown in Figure 4-13). Also, deep concrete cracks right above the bottom side plates opened along the column depth from the outside column flange towards the infill panel. The initiation of the column flange tears coincided with the full development of plastic hinges at the bottom of the columns and the ultimate strength of the specimen was reached.

4.6.2.3 Deflection Control Cycles after Ultimate

After the ultimate capacity of the specimen was reached, more deterioration was detected in the columns during cycles 23 and 24 (cycles to reach $\delta = 42$ mm), such as more severe local buckling of the steel flanges, increased concrete crushing and spalling, and the tear at the outside column flanges propagated from the flange tips towards the web, while the concrete at the same location opened more along the column depth due to the loss of the steel section. The link closest to the top of the bottom side plate at the west side of the north column was exposed as a result of serious crushing and loss of concrete at the bottom of the column (shown in Figure 4-14). The concrete loss and the steel tearing in the column flanges during the cycles to reach $\delta = 42$ mm ($6\delta_y$) caused the first drop in the specimen strength.

During cycle 25 (first cycle to reach $\delta = 49$ mm), the tear at the outside column flange at the south column base finally opened through the entire column flange (shown in Figure 4-15). During cycle 26, a new tear was detected in the outside column flange at the north column base, which initiated from the flange tip at the crest of the local buckle above the bottom side plate rather than right at the top of the bottom side plate (shown in Figure 4-16). Due to further concrete loss at the bottom of the columns, the links closest to the top of the bottom side plate at the east side of the south column and right at the top of the bottom side plate at the west side of the north column were exposed in cycle 25, with the latter displaying clear necking at the end farther from the infill panel. In cycle 26, two links right at the top of the bottom side plates—with one in each column—finally tore from the

flange (shown in Figure 4-17). In the infill panel, besides tears developing at the clipped top corners due to the associated stress concentration and notch effect, one “S” shaped tear was also detected in cycle 25 that developed due to low cycle fatigue failure from a localized kink (shown in Figure 4-18). Cracks were detected in cycle 26 along the toe of the reinforcing fillet weld between the column flange and the backing bar for the beam bottom flange full-penetration weld at both ends of the beam (shown in Figure 4-19).

During cycle 27 (first cycle to reach $\delta = 56$ mm), the tear at the outside column flange at the north column base opened through the entire column flange, while more links were exposed with tears at the end farther from the infill panel due to further concrete loss at the bottom of the columns. Moreover, large shear deformations (shown in Figure 4-20) were observed at the bottom of the columns towards the infill panel caused by the tension field in the infill panel and the reduced stiffness of the columns. In the infill panel, another kink near the north bottom corner due to reversed inelastic stretching under cyclic loading was detected during cycle 27 and propagated during cycle 28.

After pin connections were effectively developed at the bottoms of the columns due to the initiation and propagation of the tears in the outer column flanges, the moments at the tops of the columns kept increasing and finally tore the column flange tips at the bottom of the top side plates during cycles 29 and 30 (cycles to reach $\delta = 63$ mm), as shown in Figure 4-21. Tears in the vertical fillet welds between the inside column flange tips and the bottom side plates were detected after large shear deformations were observed due to the sectional area loss of the columns, while the tears initiating in cycle 26 along the weld between the beam bottom flange and the inside column flanges propagated along the width and the depth of the columns. The test was terminated when the flange tears at the bottoms of the columns propagated significantly into the web (shown in Figure 4-22).

Table 4-1: Steel Strength and Elastic Modulus

	Elastic Modulus (MPa)	Static σ_y (MPa)
1 st Storey Panel	204373	236
2 nd Storey Panel	205655	252
Column Steel	192473	427
1 st Storey Beam	212960	386
Link	224697	400

Table 4-2: Concrete Strength and Elastic Modulus

	Elastic Modulus (MPa)	Strength (MPa)
1 st Storey South Column	23483	52.6
1 st Storey North Column	23548	56.4
2 nd Storey South Column	23448	55.7
2 nd Storey North Column	25132	56.9

Table 4-3: Load and Deflection History

	Force Control Parameter Base shear (kN)	Deformation Control Parameter First storey deflection (mm)
Cycles 1-3	±316	–
Cycles 4-6	± 632	–
Cycles 7-9	± 948	–
Cycles 10-12	–	± 7 (δ_y^*)
Cycles 13-15	–	± 14 ($2\delta_y^*$)
Cycles 16-18	–	± 21 ($3\delta_y^*$)
Cycles 19-20	–	± 28 ($4\delta_y^*$)
Cycles 21-22	–	± 35 ($5\delta_y^*$)
Cycles 23-24	–	± 42 ($6\delta_y^*$)
Cycles 25-26	–	± 49 ($7\delta_y^*$)
Cycles 27-28	–	± 56 ($8\delta_y^*$)
Cycles 29-30	–	± 63 ($9\delta_y^*$)

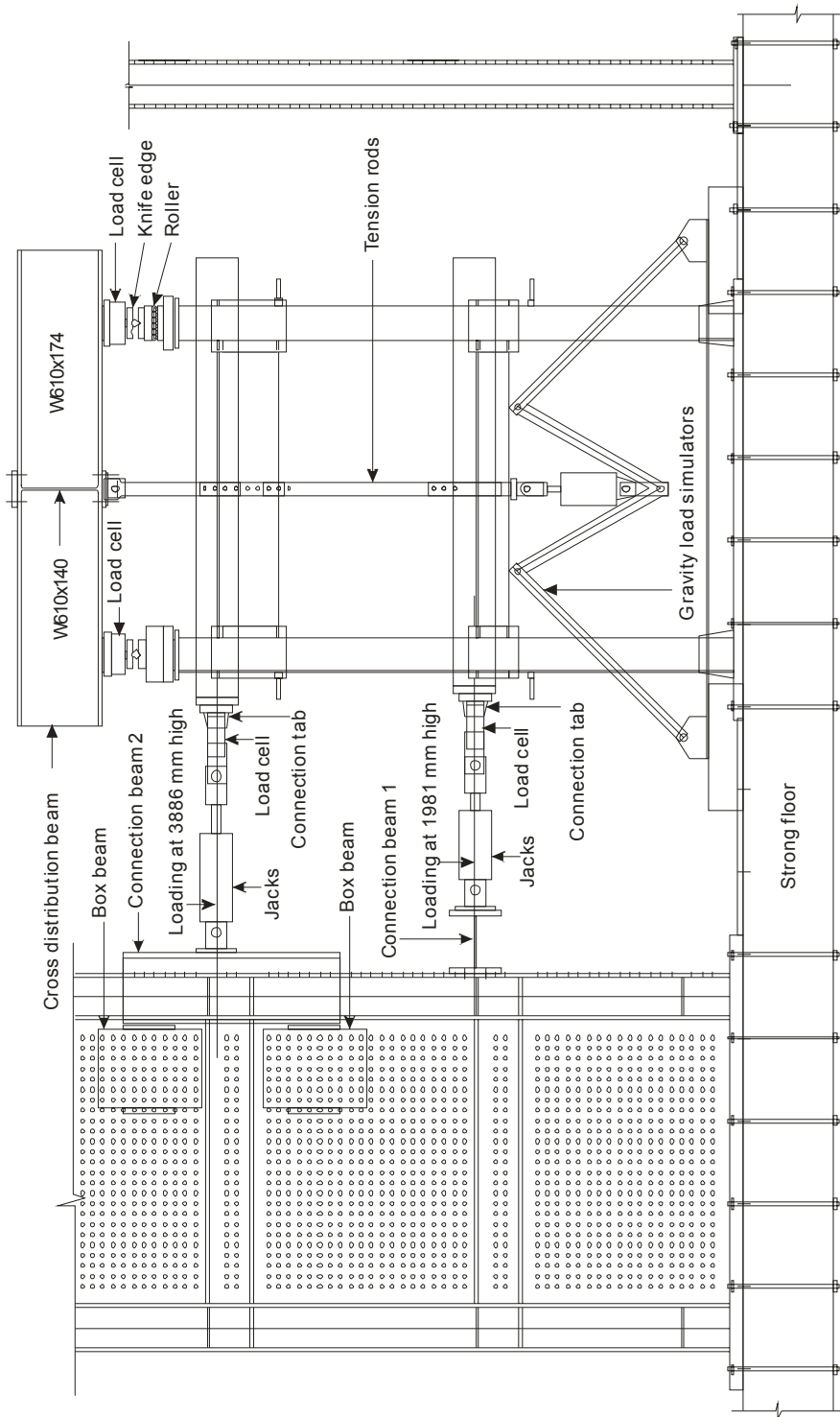


Figure 4-1: Test Set-up (East Elevation)

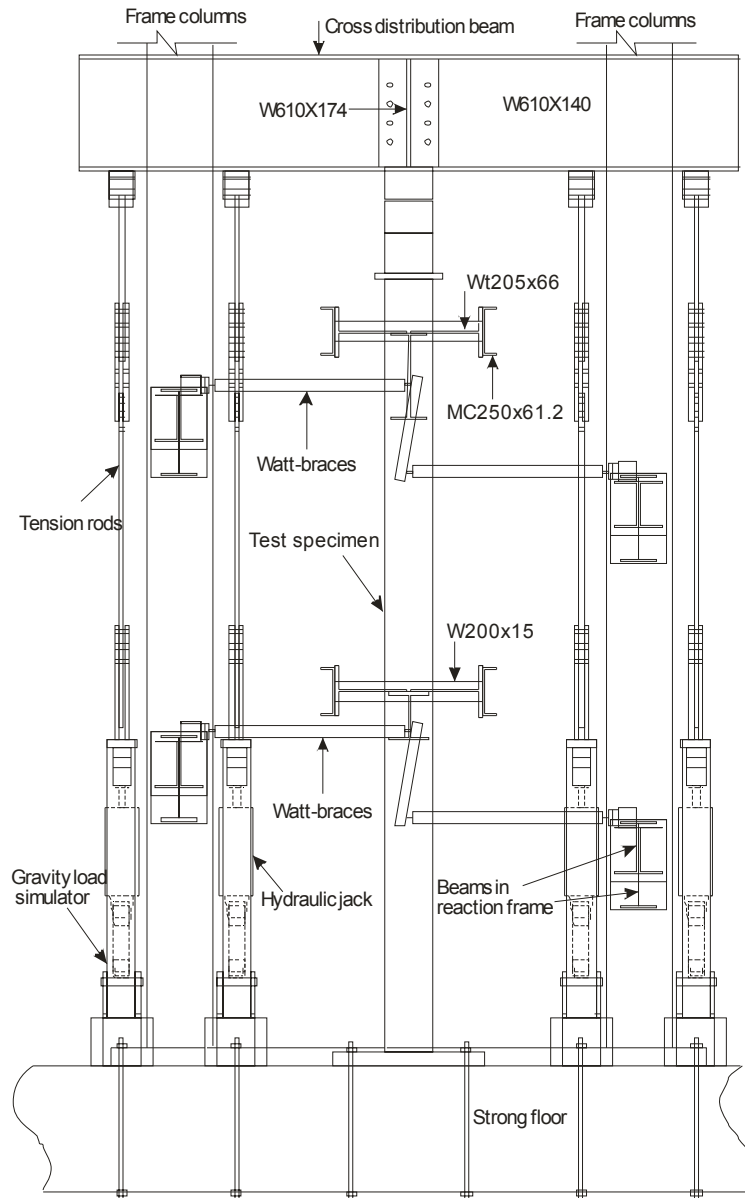


Figure 4-2: Test Set-up (North Elevation)



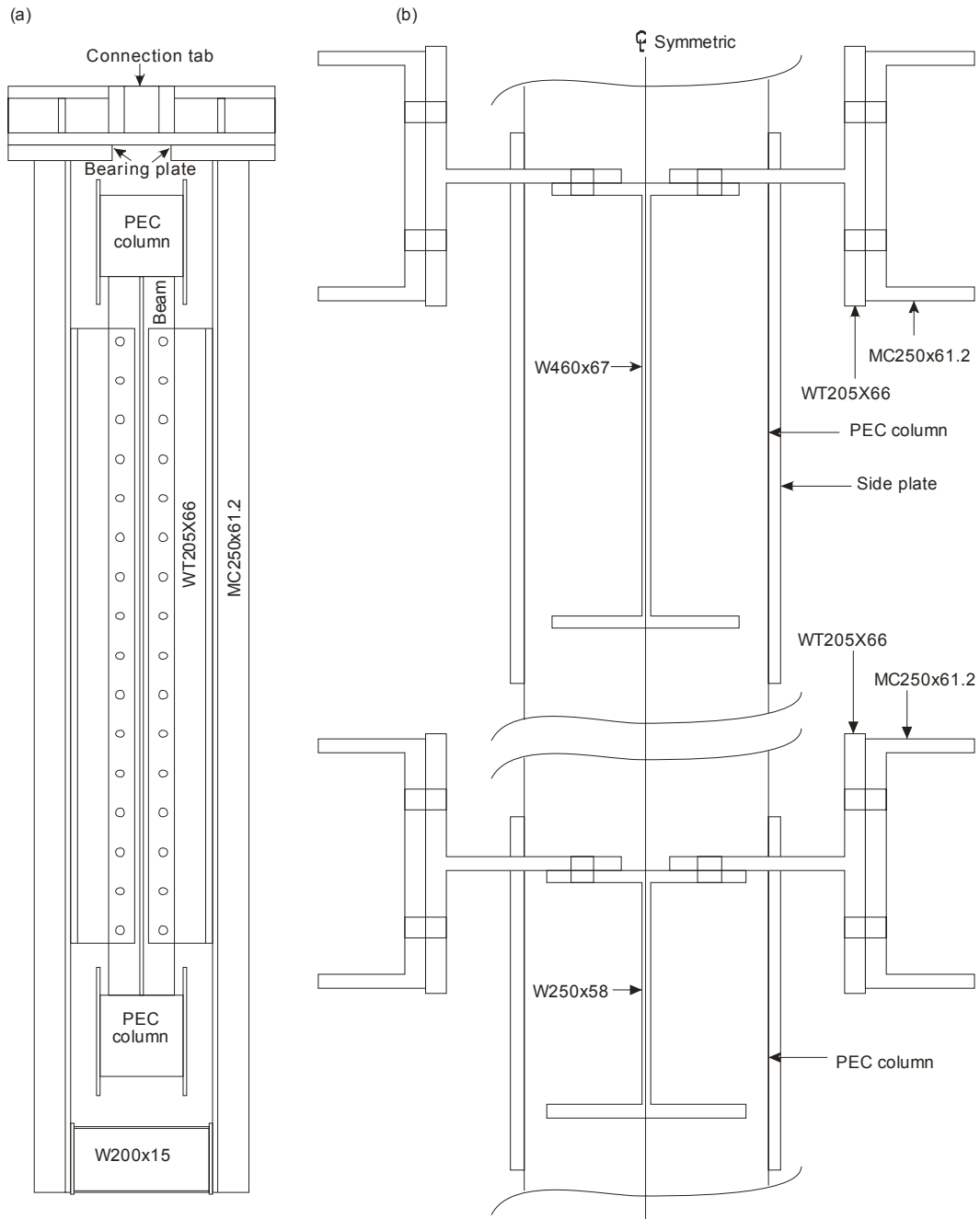
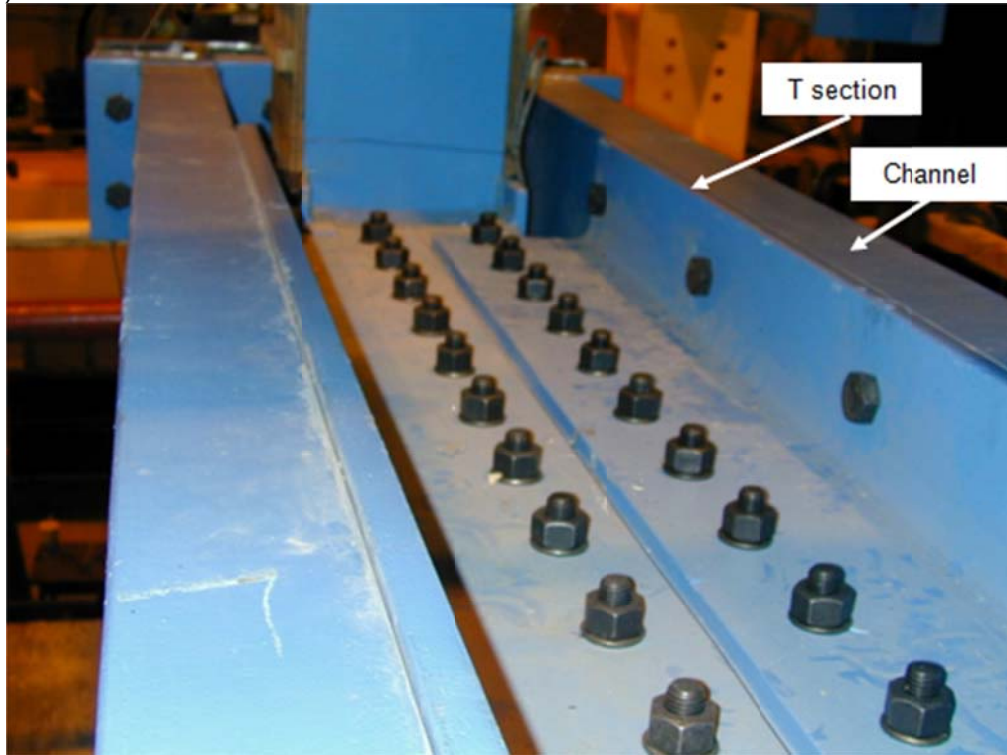


Figure 4-4: Lateral Load Transition System (Schematic)
 (a) Plan View; (b) Elevation View

(a)



(b)

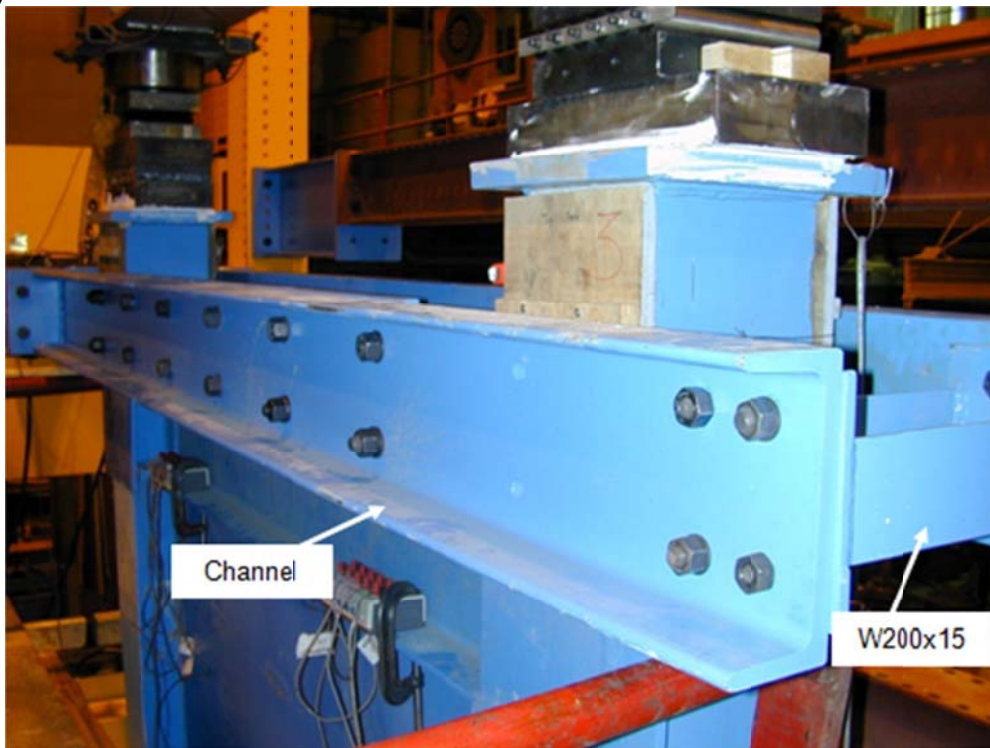


Figure 4-5: Lateral Load Transition System (Photos)
(a) Plan View; (b) Elevation View

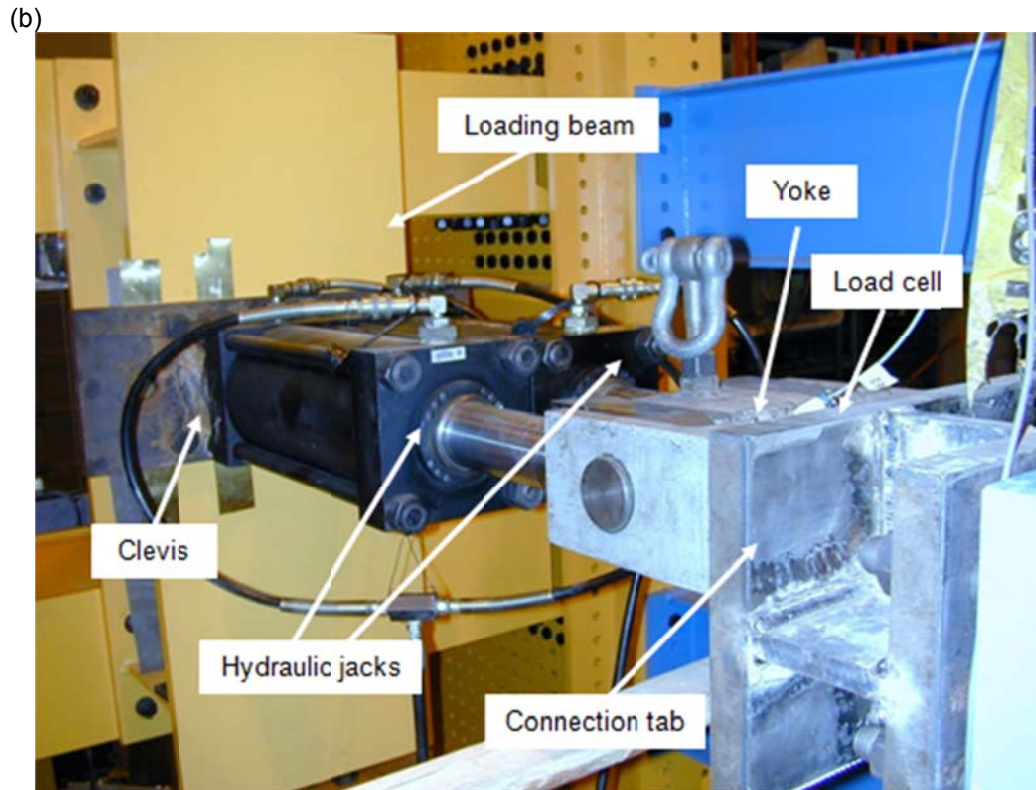
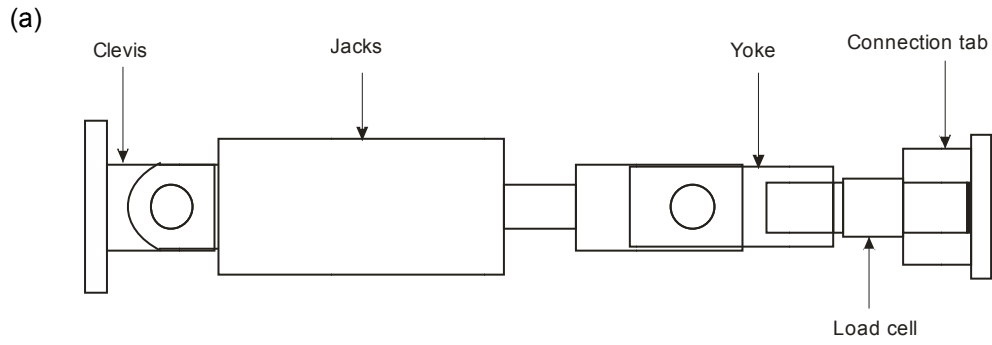


Figure 4-6: Lateral Loading Facilities
 (a) Elevation View Drawing; (b) Photo

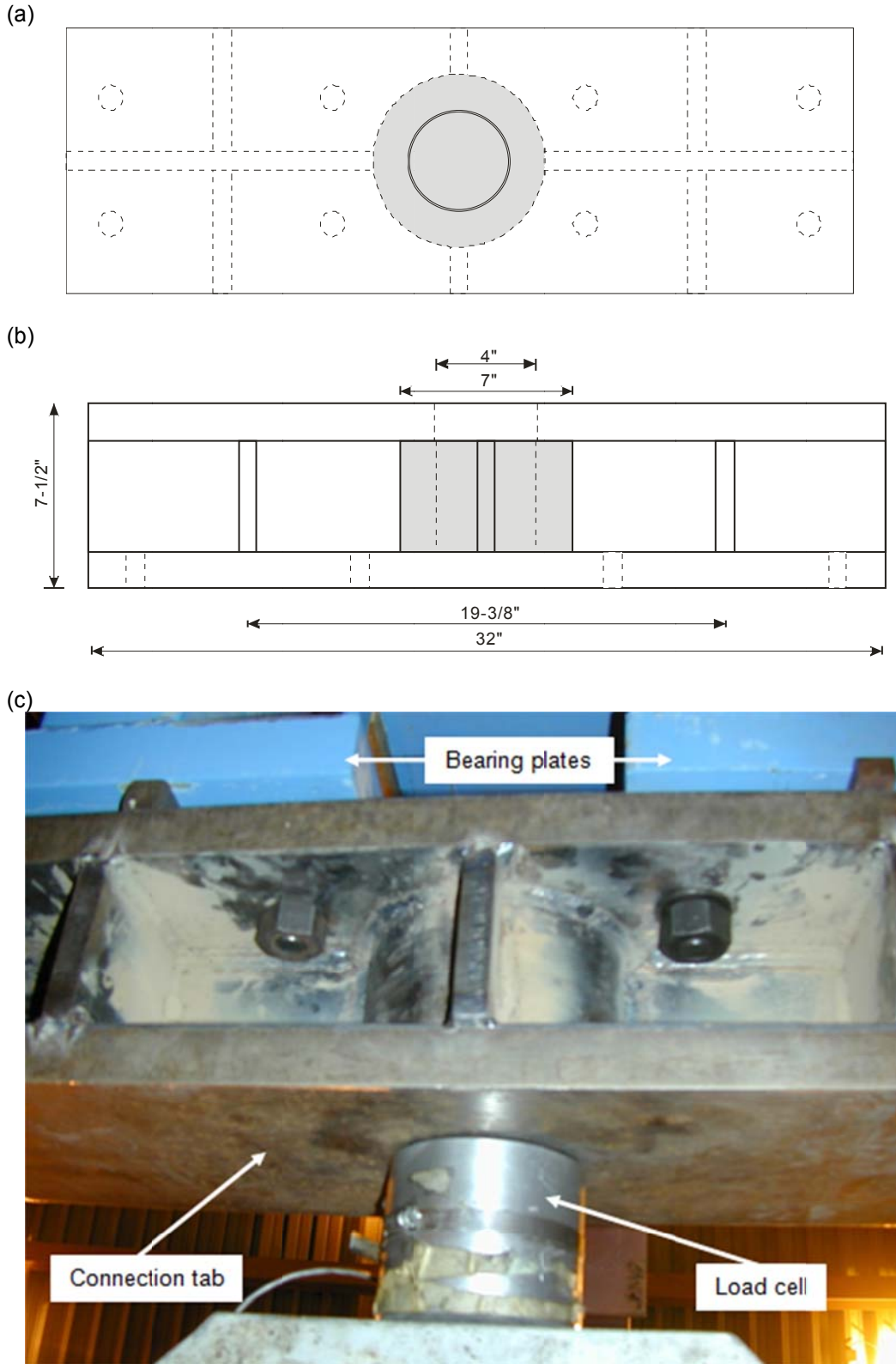


Figure 4-7: Connection Tab
 (a) Plan View; (b) Elevation View; (c) Plan View Photo

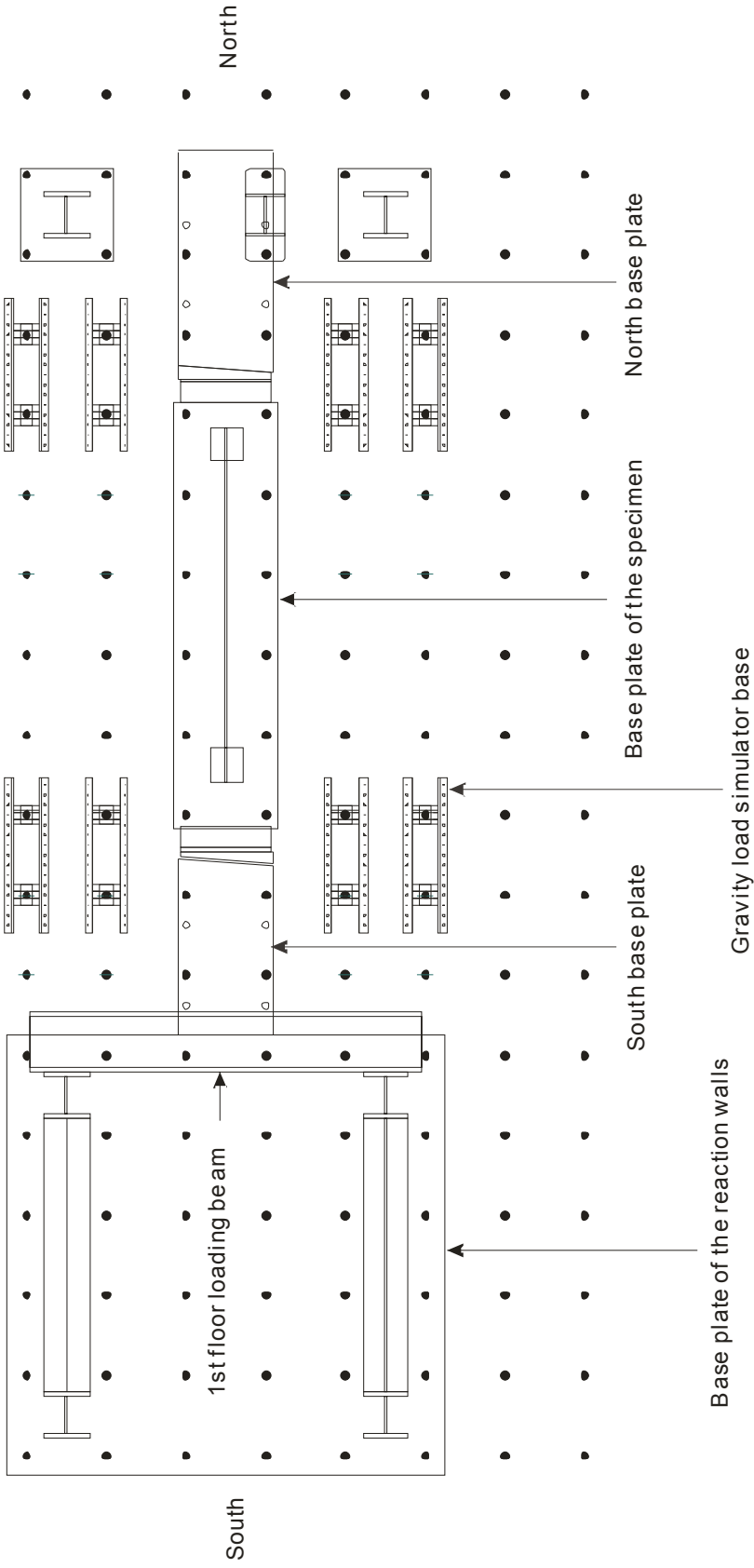
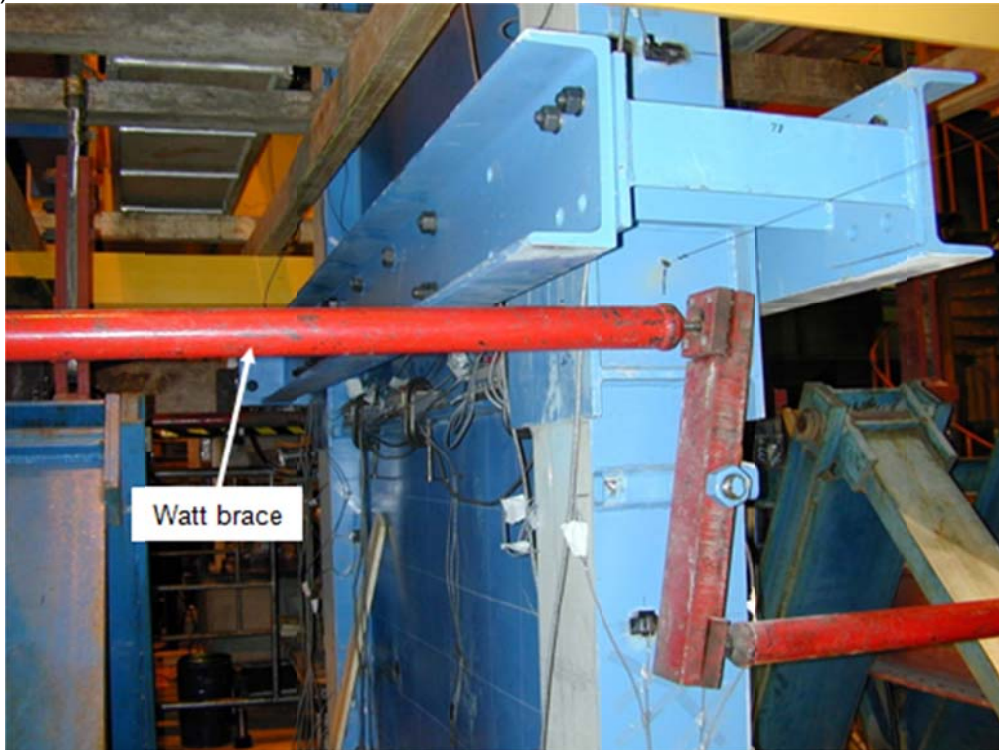


Figure 4-8: Test Set-up at Base (Plan View)

(a)



(b)

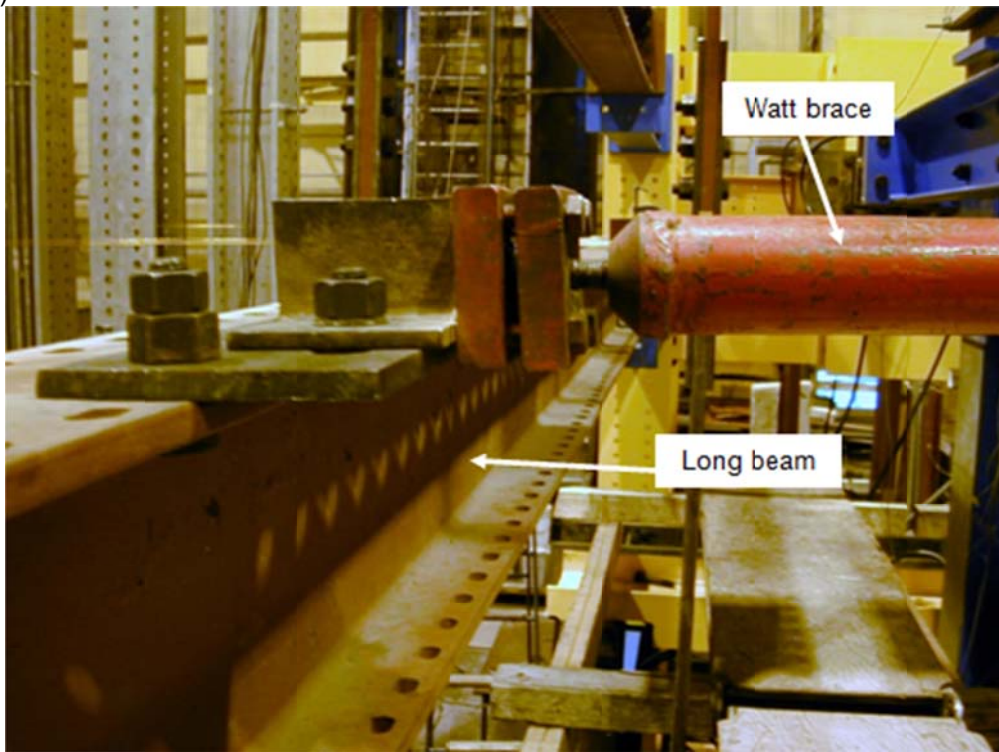
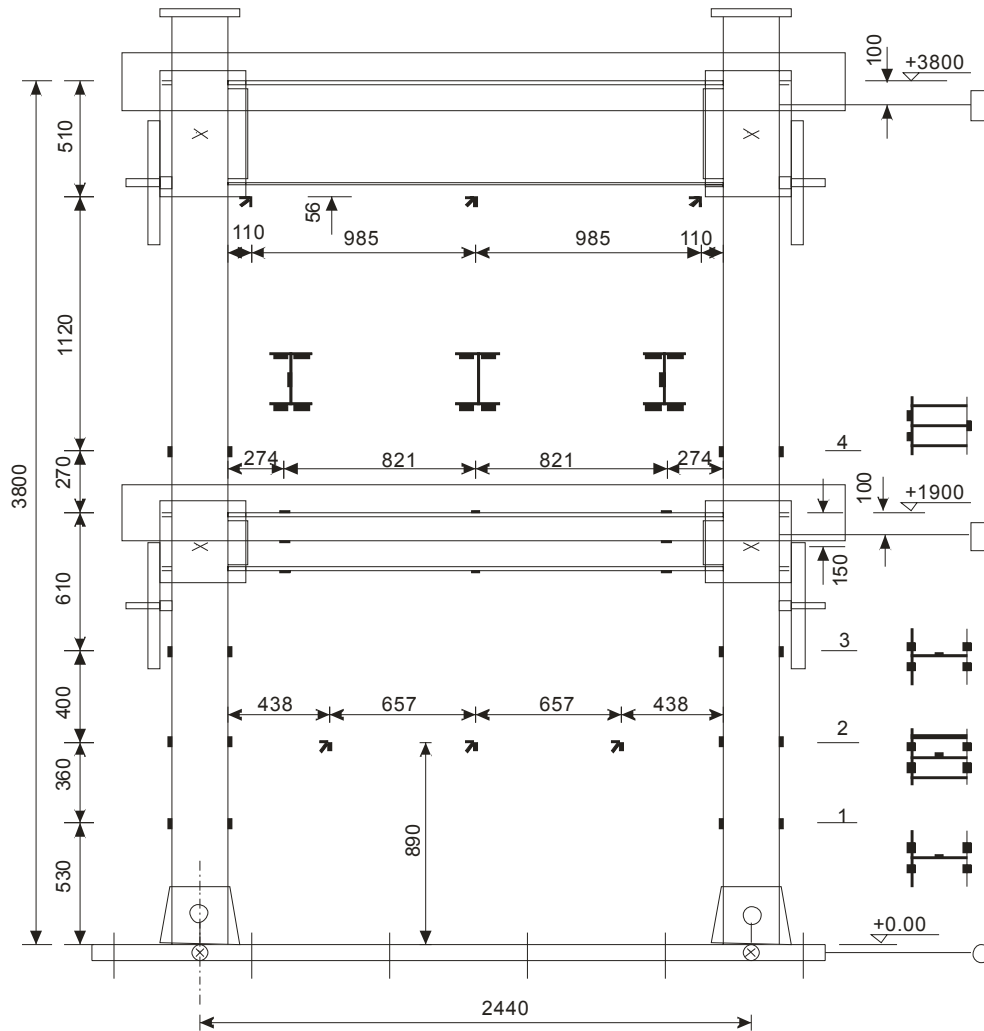


Figure 4-9: Watt Brace
(a) Elevation View; (b) Support



Legend

- | | | | |
|---|------------------------------------|---|-------------------------------|
| × | 4 Cable transducers (out-of-plane) | 4 | Load cells on tension rods |
| □ | 2 Cable transducers (in-plane) | 2 | Load cells for lateral loads |
| ▬ | 74 Strain gauges | 2 | Load cells for vertical loads |
| ↗ | 12 Strain rosettes | ⊗ | 2 Dial gauges (Out-of-plane) |
| ○ | 3 Dial gauges (In-plane) | 2 | Clinometers |

Figure 4-10: Data Acquisition Devices (East Elevation)

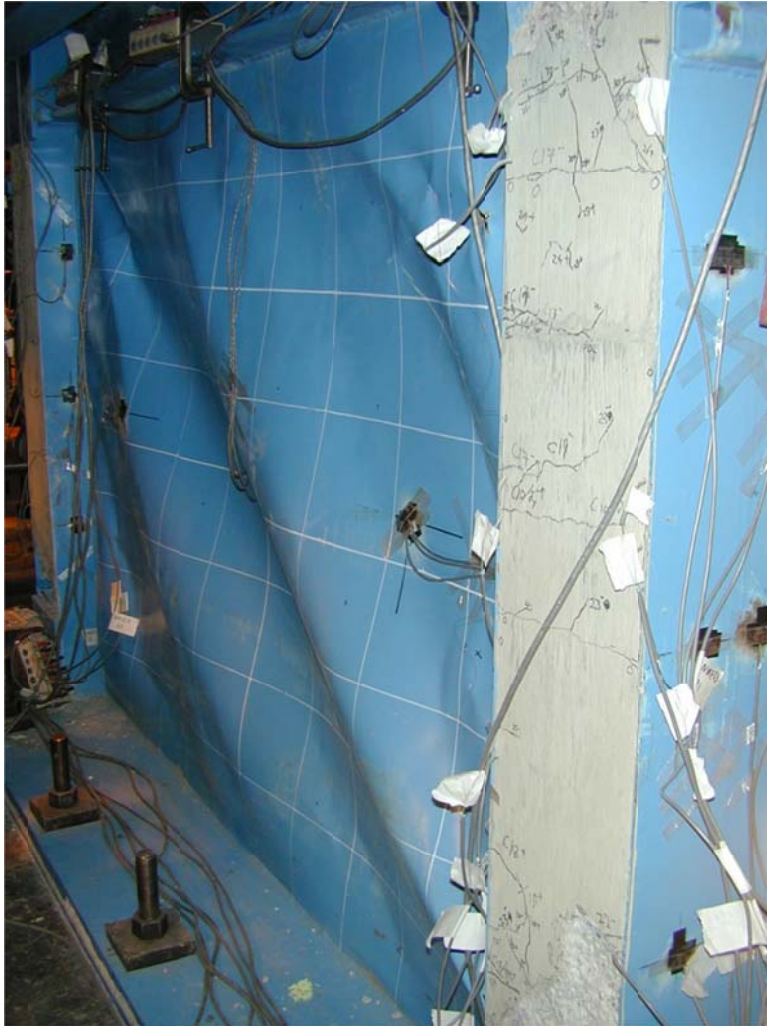


Figure 4-11: Buckled Panel in Cycle 30 (East View)

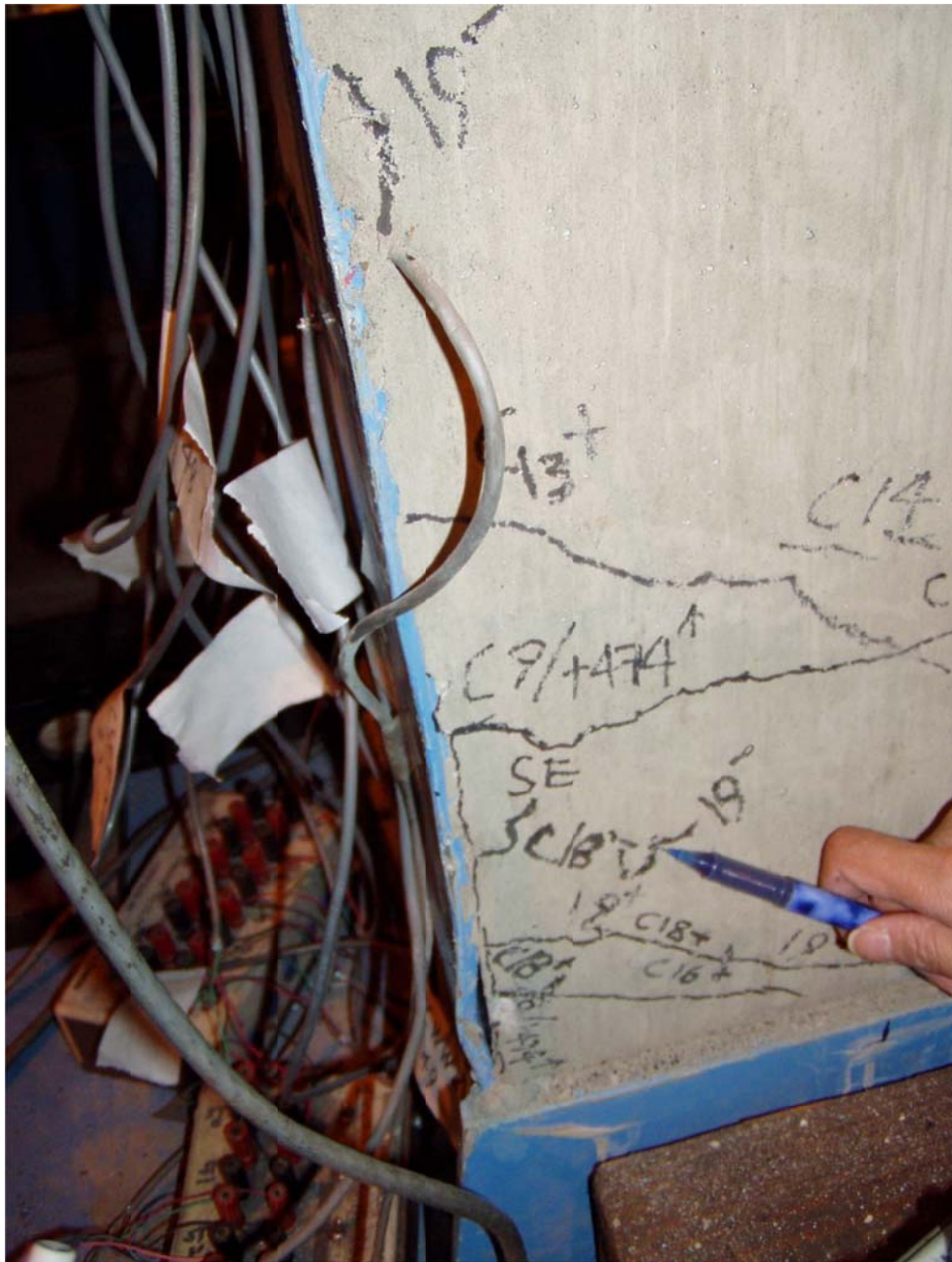


Figure 4-12: Buckled South-East Flange of South Column in Cycle 19



Figure 4-13: Torn South Flange of South Column in Cycle 21



Figure 4-14: Link Exposed in West Side of North Column in Cycle 24



Figure 4-15: Opening in South Flange of South Column in Cycle 25



Figure 4-16: Tear at Crest of Buckled North Flange in North Column in Cycle 26

(a)

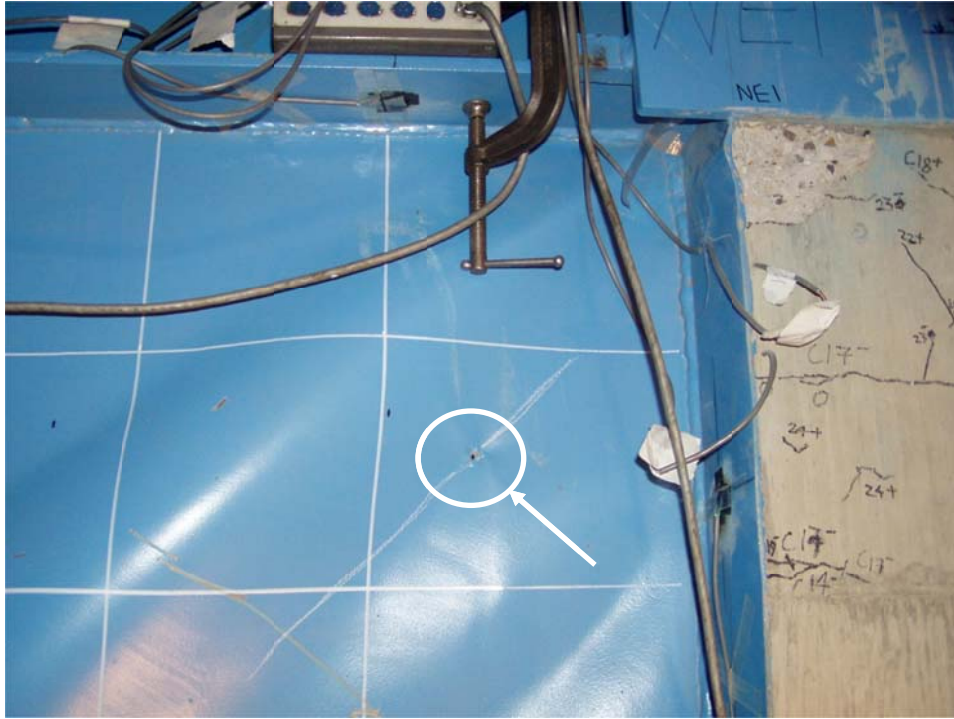


(b)



Figure 4-17: Link Torn from Column Flanges in Cycle 26
(a) South Column; (b) North Column

(a)

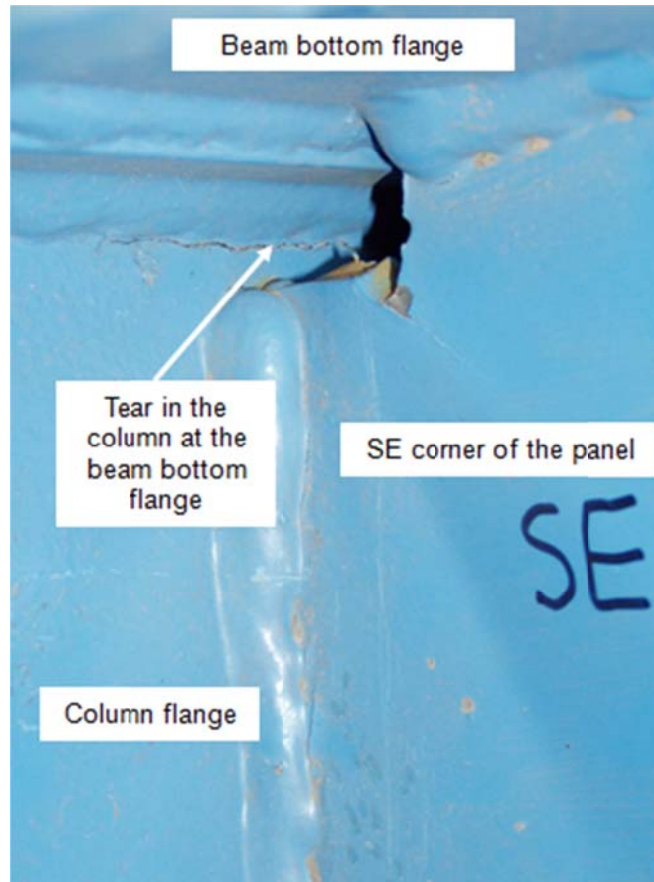


(b)



Figure 4-18: "S" Shaped Tear in Infill Panel in Cycle 25
(a) North East Top Corner of Infill Panel; (b) "S" Shaped Tear

(a)



(b)

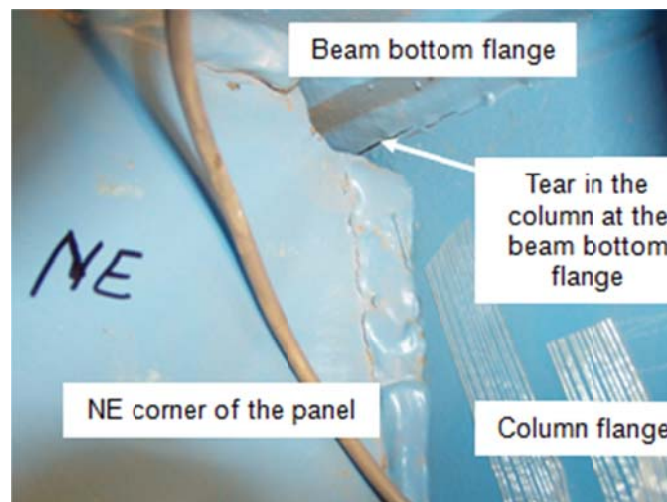
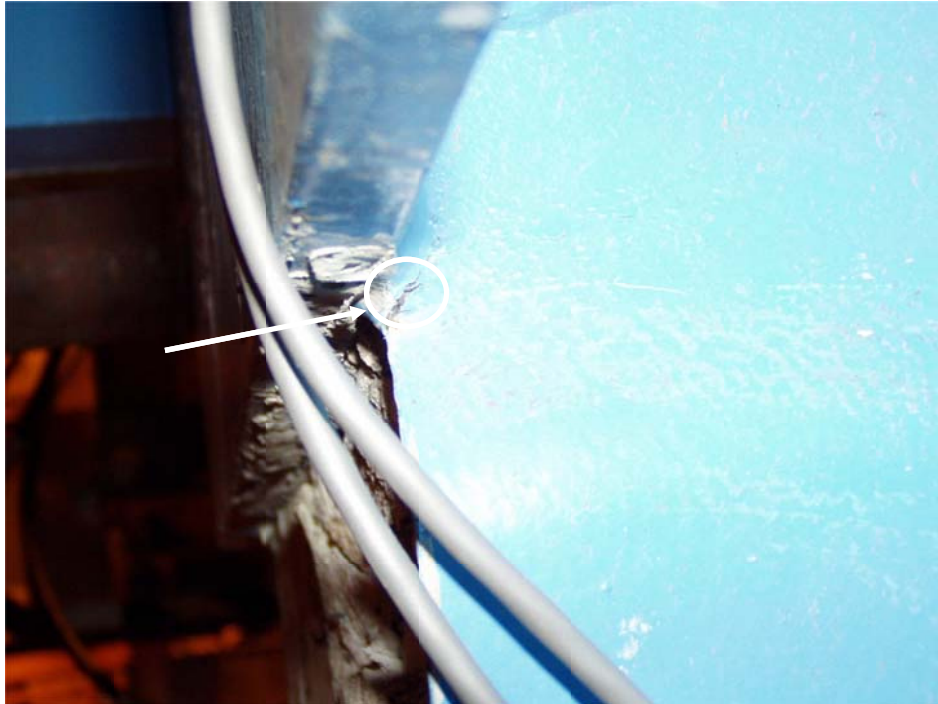


Figure 4-19: Weld Tear in Column at Beam Bottom Flange in Cycle 26
(a) South End; (b) North End



Figure 4-20: South Column Base in Cycle 27

(a)



(b)



Figure 4-21: Flange Tear at Top of Columns in Cycle 29
(a) North Flange of South Column; (b) South Flange of North Column

(a)



(b)



Figure 4-22: Flange Tear in Columns in Cycle 30
(a) South Column; (b) North Column

5. TEST RESULTS

5.1 Introduction

The specimen of a two-storey steel plate shear wall with partially encased concrete columns was tested under cyclic lateral loading. The failure mode and other features shown in the test met the expectations. After local buckling occurred in the steel column flange accompanied by concrete spalling and crushing in the region, column cross section loss caused a stress concentration and finally led to tearing of the outside column flanges at the bottom of the columns. Further cross section loss led to the failure of the columns and prevented further capacity development in the specimen. Hence, the specimen reached the ultimate capacity of 1817 kN, with plastic hinges forming at the top and bottom of the columns near the side plates at a first storey deflection of 35 mm. During the rest of the test, the tear in the column flanges kept propagating until the whole column flanges, as well as most of the web were torn when the test was terminated at a first storey deflection of 63 mm.

Compared with a conventional all-steel steel plate shear wall (Driver et al. 1997), the wall with partially encased composite columns showed less ductility and post-ultimate capacity, but more non-linear behaviour was exhibited in the test due to the concrete in the PEC columns. However, the specimen still failed in a gradual mode after the ultimate capacity was reached and was proved to be suitable for resisting cyclic loading representative of seismic actions based on corresponding ductility and post-ultimate capacity.

5.2 Hysteretic Behaviour

The hysteretic curves of the base shear vs. the first storey deflection are shown in Figure 5-1, where the deflection is given in absolute value as well as deflection to storey height

ratio (drift ratio), δ/h_s . In total, there were 30 loading cycles applied to the specimen, including nine elastic loading cycles and 21 inelastic loading cycles.

Similar characteristics are presented in the hysteresis curves of this steel plate shear wall system with PEC columns and those with steel columns (Driver et al. 1997). The specimen behaved in a stiff and linear manner in the early cycles and then more and more non-linear behaviour was shown in the hysteretic curves, with increasing strength, until the ultimate capacity was reached. After ultimate, the strength decreased gradually.

Compared with a previous all-steel test (Driver et al. 1997), non-linear behaviour showed up at an earlier stage and over a larger range in the hysteretic curves, which means more non-linear behaviour was present in the system with PEC columns. The hysteretic curves also show that the strength of the system with PEC columns dropped faster after ultimate capacity was reached than the system with steel columns (Driver et al. 1997). In another words, the envelope of the hysteretic curves of the previous test is closer to the bi-linear simulation curve, while the envelope of the hysteretic curves herein is more curved.

To further study the behaviour of the hysteretic curves, the curve for cycle 20 was chosen and modified to form a closed loop to represent the typical hysteretic behaviour of the specimen under cyclic loading just prior to the peak load. As depicted in Figure 5-2, cycle 20 includes curve a-b (unloading curve), curve b-c (loading reverse curve), curve c-d (reloading curve), and curves d-e-f-a, which were subsequent curves, repeating the phenomena described for curves a-b-c-d in the opposite direction.

Curve a-b is the portion where the specimen was unloaded laterally. High stiffness and linearity are the typical characteristic and the stiffness decreases gradually when the peak deflection was exceeded, especially after the ultimate capacity was reached.

After unloading, the specimen was loaded in the reversed direction, which was represented by the loading reverse curve b-c, in which a long uneven curve with very low

stiffness is the main characteristic. Due to inelastic stretching of the infill panel as the tension field was developed when the specimen was loaded in the opposite direction in the previous loading, there was still a large amount of residual storey deflection even at zero lateral loads. Significant out-of-plane buckling of infill panel remained, which was stretched back into the neutral position and stretched further so the tension field in the direction perpendicular to the previous one was redeveloped during the loading reverse period (curve b-c). The residual deformation and deterioration in the specimen was increased as the storey deflection was increased, which led to a flatter and longer curve b-c.

The reloading curve c-d is the curve following the loading reverse curve b-c, in which the stiffness was regained because the redeveloped tension field acted as diagonal braces to strengthen the specimen to resist lateral loads. As the storey deflection was increased, the stiffness of curve c-d decreased due to the increased deterioration in the specimen.

There is a flat curve following reloading curve c-d that represents the yielding of the steel plate shear wall with steel columns in the previous test (Driver et al. 1997), which is not observed herein. The lack of a flat yielding portion of the hysteretic curves in the steel plate shear walls with PEC columns is mainly caused by the participation of the encased concrete in the columns and the strain hardening in the infill panel, which is discussed in detail later. Concrete cracking and crushing, as well as local buckling in the column flanges, also enhanced the non-linear behaviour of the specimen and contributed to eliminating the flat yielding portion in the hysteretic curves.

Regardless of the magnitude, the behaviour shown in the hysteretic curves for cycle 20 is also shown in the hysteretic curves for other cycles in the inelastic range. The magnitude of the stiffness, storey deflection and base shear in each portion of the hysteretic curves differs in the cycles with a different peak storey deflection. Even for the cycles with the same storey deflection, there is a minor difference in the stiffness due to the increased

deterioration. The instances of buckling and stretching of the infill panel are identified by the kinks in the hysteretic curves.

As shown in Figure 5-3, the hysteretic curves of the base shear vs. the second storey deflection display similar characteristics to those shown in the hysteretic curves of the base shear vs. the first storey deflection.

5.3 Energy Dissipation

The capacity of the system to dissipate energy is a major factor related to its suitability for use in seismic applications. The energy dissipated by the system in each cycle is represented by the area enclosed in the hysteretic curves for each cycle. Figure 5-4 is a histogram showing how much energy was dissipated during each first cycle (the cycle with the increased storey deflection) within the inelastic range at different displacement ductility ratios, δ/δ_y^* , in which δ_y^* has a value of 7 mm and is the estimated yield deflection used for test control.

In the previous test (Driver et al. 1997), the amount of energy dissipated for each first cycle kept increasing until the end of the test. Differently, the amount of energy dissipated for each first cycle at different values of δ/δ_y^* increased steadily from $\delta/\delta_y^* = 1$ to $\delta/\delta_y^* = 7$ and decreased at $\delta/\delta_y^* = 8$ and $\delta/\delta_y^* = 9$ herein. However, the amount of dissipated energy after cycle 21 ($\delta/\delta_y^* = 5$) is still larger than the energy dissipated at $\delta/\delta_y^* = 5$, at which time the ultimate capacity of the specimen was reached. The increased dissipated energy after cycle 21 ($\delta/\delta_y^* = 5$) was caused by the higher storey deflection, which compensated for the capacity reduction and the stiffness drop caused by the deterioration in the specimen after the ultimate capacity was reached.

The energy dissipated in every cycle within the inelastic range at different displacement ductility ratios, δ/δ_y^* , is shown in Figure 5-5. The histogram shows that the dissipated

energy dropped in each second and third cycles when the storey deflection remained the same and the dissipated energy in every cycle from $\delta/\delta_y^* = 6$ was larger than the energy dissipated at cycle 21 ($\delta/\delta_y^* = 5$).

5.4 Failure Mode

Tearing initiated from the outside flange tips at the bottom of the columns due to the combination of frame action and anchorage force from the infill panel. Repeated local buckling of the column flanges and loss of concrete in the region hastened the propagation of the tear through the flange tips towards the web and eventually the tear opened through the entire outside flanges. As the specimen was further loaded, the opening in the column outside flanges tore into the column webs towards the infill panel until the test was terminated. At the end of the test, the width of the opening at the outside flanges was approximately 20 mm for both columns.

The bottom side plates were added in the specimen design primarily to move the maximum demand in the column away from the column base welds, where the failure of the steel plate shear wall system with the steel frame was initiated (Driver et al. 1997). As a consequence, the tops of the bottom side plates were now the most critical locations in the columns, caused by the frame action and the anchorage force from the infill panel, as well as the welds between the column flange tips and the bottom side plates. The initiation of the tear at the outside column flange tips was located right at the top of the bottom side plates, where the stiffness and the strength of the columns suddenly changed due to the existence of the bottom side plates. Besides the tear at the top of the bottom side plates, one additional tear initiated at the crest of the flange local buckle above the bottom side plate at the north-west side of the north column, where the flange plate curvature was severe due to extensive localized loss of concrete.

The test was terminated without a sudden capacity drop in cycle 30, as the base shear capacity of the specimen had decreased to 72.7% of the peak load achieved in the test. Since the failure initiated at the bottom of the columns, improving the design and detailing at corresponding locations to improve the specimen behaviour is desirable and is discussed later.

As boundary elements for the steel plate shear walls under cyclic loading, the PEC columns were under combinations of axial force, bending moment and shear force. The behaviour of the PEC columns with the steel plate shear walls was quite different from the behaviour of PEC columns under axial compression only (Prickett and Driver 2006), especially for the failure mode. Under axial compression only, the PEC column failed when both flanges buckled and the encased concrete crushed almost simultaneously. In the steel plate shear wall system, local buckling occurred only at one column flange in the PEC column, which was under compression due to frame action. However, the final failure initiated in the PEC column, when the same flange was under tension due to frame action. The tear at the column flange tips rather than the local buckling triggered the final failure of the PEC columns in the steel plate shear wall system.

5.5 Discussion

5.5.1 Infill Panels

5.5.1.1 General Observations

Steel plate shear wall systems with steel frames have been proved to be very ductile and stable at resisting severe cyclic loading in previous research. In the steel plate shear wall system with PEC columns, the infill panels behaved well as the main mechanism to dissipate energy under cyclic lateral loads. Before the specimen reached the ultimate capacity, there was no obvious deterioration in the infill panel except a kink due to inelastic stretches of the infill panel in the perpendicular directions under cyclic loading. After the specimen reached the ultimate capacity, tearing at the kink position occurred in the infill

panel due to the resulting stress concentration, while another kink occurred and propagated into new tear. Moreover, tearing was also seen at the top corners where the plate was clipped to clear the frame connection weld. During the test, the deterioration in the infill panel occurred gradually, despite the presence of the tear and in general local deterioration did not affect the capacity and behaviour of the steel plate shear wall because of the stress redistribution around the tear in the continuous infill plate.

5.5.1.2 Stress Results

Strains were measured at three points at the same height of the first storey infill panel through strain rosettes at both the east and west sides. The corresponding stresses were calculated, through an analysis worksheet, based on plane stress principles and the material curve for isotropic hardening. To show the stresses clearly, the envelope of the stress history at different first storey deflections based on the strain rosette results is shown in Figure 5-6. Data of two out of the six rosettes (North and South points on the east face of the plate) was terminated at a relatively low load level, while the rest reached the yield value and strain hardening.

As mentioned before, strains at the north-west corner of the infill panel were recorded through a dual-camera system. To represent the stress distribution within the camera region, strains at 5x5 points were chosen and transferred into stresses by the same analysis worksheet used for the strain rosette data. To better interpret the stress results, maximum, minimum and average values of stresses at those 25 points, as well as 25 individual stress curves, are shown in Figure 5-7 and Figure 5-8. Since the camera data were taken only at one side of the infill panel, these results were used only as a reference. The results show that the stresses in the first floor infill panel were developed non-uniformly and strain hardening did occur, which is identical to the test results from the strain rosettes.

5.5.2 Partially Encased Composite Columns

5.5.2.1 General Observations

Partially encased composite columns have been proved efficient in resisting axial compression in previous research. As boundary elements for the infill panel in the steel plate shear wall test, the PEC columns behaved quite differently due to the bending moments and also the reversed axial forces under cyclic lateral loading.

Nonlinear behaviour, like concrete cracks, started to show up in the PEC columns at a very early stage. As the lateral loads were increased, more and more concrete cracks formed, while existing concrete cracks propagated. Moreover, the concrete cracks at first only initiated in the column that was in tension due to overturning. When the specimen was approaching the ultimate capacity, cracks initiated in both columns no matter whether in tension or compression, which indicated that the tension force arising from the bending moment was large enough to conquer the axial compressive force due to overturning.

As another nonlinear behaviour in the PEC columns, local buckling only developed at one column flange instead of both column flanges, as would be the case for PEC columns in axial compression only. Local buckling was detected in the outside flange at the column base at first, and then in the inside flange at the column top when the specimen was approaching the ultimate capacity. Accompanied by local buckling, concrete crushed near the buckled column flange after losing the confinement from the steel flange. Since the local buckling and concrete crushing nearby only occurred at one side of the column, the specimen continued to gain strength, while in PEC columns under axial compression only, no further strength was developed after local buckling occurred at both column flanges and concrete crushed through the whole cross section simultaneously.

The most critical location was at the outside of the column base, where the column flange was in the largest tension when the specimen was laterally loaded in one direction and in

the largest compression when the lateral loads reversed. After the local buckling and concrete crushing were developed, concrete loss kept increasing at the outside corner of the column base. Finally, the reduced column section was not large enough to resist the tensile force when the lateral loads reversed and as a result, a tear was finally developed in the outside flange at the bottom of the column, which was in tension due to overturning.

As a result of severe concrete loss at the column base, links at the top of the bottom side plates and above the bottom side plates started to be exposed. Weld tears then initiated in the links at the end close to the outside column flange, eventually rupturing. As another result of the reduced column cross section, the capacity of the columns to anchor the tension field in the infill panel was decreased correspondingly and the deformation of the columns shifted towards the infill panel and became large, especially at the bottom of the columns no matter whether the specimen was pushed towards the north or pulled towards the south. Under large shear at the bottom of the columns, tears occurred along the welds between the column inside flange tips and the bottom side plates.

Due to the thin thickness of the steel section and the encased concrete, the PEC columns behaved quite differently from a steel column. Concrete cracking, steel flange buckling and concrete crushing nearby, as well as flange tip tearing, all contributed to non-linear behaviour of the PEC columns. Hence, there was more nonlinear behaviour and more severe deterioration in the PEC columns than has been observed in steel columns in steel plate shear walls (Driver et al. 1997). However, the development and propagation of all the deterioration in the PEC columns was relatively gradual, although less ductility was shown in the PEC columns than steel columns.

5.5.2.2 Concrete Shrinkage

The volume of concrete decreases during hardening and drying after it is poured due to concrete shrinkage by losing of a layer of absorbed water from the surface. There are many factors affecting the volume change of concrete due to drying shrinkage, such as

temperature, composition of the concrete, aggregate modulus, water/cement ratio, ratio of volume to surface area, etc. Shrinkage strains vary with the environmental humidity and reach the largest values for relative humidities of 40 percent or less. A larger portion of aggregate, higher elastic modulus of aggregate and lower water/cement ratio mean more restraint for the shrinkage from the aggregate and lead to less shrinkage. Since the absorbed water is diffused from the surface, a larger ratio of volume to surface area results in slower and less shrinkage.

The ultimate drying free (unrestrained) shrinkage strain for a cylinder of 6 inch x 12 inch at a relative humidity of 40 percent ranges from approximately 400×10^{-6} to 1100×10^{-6} , with an average of about 800×10^{-6} . Compared with the shrinkage strain of a cylinder, concrete in a structure tends to have smaller shrinkage strains because of the larger ratio of volume to surface area, more restraint for the shrinkage development from reinforcement, and compensation for dissipated shrinkage from adjacent stages of concrete.

If details are known, shrinkage strains can be estimated according to the procedures published by the Euro-International Concrete Committee (CEB 1993) or the American Concrete Institute (ACI Committee 209 1982). Although the CEB method accounts for the effect of the member size, research shows that it underestimates the shrinkage of North American concrete.

Since the concrete in the PEC columns was cast in October, 2006 and the test was conducted in September, 2007, concrete shrinkage was not negligible. In previous research on PEC columns (Chicoine et al. 2003), sustained axial compressive loads were applied to study the long term behaviour of PEC columns. When the concrete between the links shrank prior to applying the external load, tension arose in the concrete due to the restraint from the steel section and links, which was released by the applied compressive force. However, there were no sustained loads applied on the specimen described herein until the test started. Therefore, the concrete was in tension and micro-cracks occurred

between the links due to the restraint from the links. This shrinkage was taken into consideration and values of 246×10^{-6} and 230×10^{-6} were used for the north and south columns, respectively, based on the strain gauge data for the columns.

5.5.2.3 Internal Force Distribution

At both columns in the first storey, strains at several points in each cross section at three different elevations were recorded by strain gauges and the strains in the whole cross section were calculated based on the assumption that the strains at the same point in the column were equal, no matter for steel or concrete. Then, corresponding axial forces and bending moments were obtained by an analysis worksheet developed based on column dimensions and material curves. The steel material curve was determined based on the isotropic strain hardening theory, while concrete material curves were determined based on the concrete model by Otter and Naaman (1989), since the model is simple and suitable for any curve for the uniaxial response of concrete.

To better exhibit the test results, Figure 5-9 and Figure 5-10 show the internal force distributions in the first storey along the column height at the peak load when the specimen was pushed towards the north in cycle 1, cycle 4, cycle 7 and cycle 10.

It is shown in Figure 5-9 that the compressive axial forces decreased from the top to the bottom in the south column, but increased from the top to the bottom in the north column, which reflects the fact that the vertical component of the tension field in the infill panel contributed tension to the south column and compression to the north column when the specimen was pushed towards the north. The nonlinear curves of the axial forces in the columns also indicate the non-uniformly distributed tension fields in the infill panel. Moreover, the differences between the top and the bottom of the columns increased as the lateral loads increased, indicating an increase in the tension field stresses at larger lateral loads.

It is shown in Figure 5-10 that the north side of the columns was in tension at the top, while the south side of the columns was in tension at the bottom when the specimen was pushed towards the north. Although the sign of the bending moments at the top and bottom of the columns was consistent with what would be expected in frame columns without steel plate shear walls, the bending moment curves were bent towards the infill panel at the middle portion of the columns (instead of being straight lines) due to the tension field, which tended to pull both columns inward. Moreover, it is well known that the thin infill plate has a small capacity in compression compared with that in tension, since it is very sensitive to buckling under compression. When the specimen was pushed towards the north, the infill panel at the bottom south corner tended to be compressed while the panel at the bottom north corner tended to be stretched. Hence, the bottom of the north column got higher restraint from the infill panel, and as a result the curvatures (and resulting moments) above the highly restrained region (at the strain gauges 530 mm above the base) increased to fulfill the compatibility requirement that the two columns deflect the same amount at the top of the storey.

5.5.3 Beam

Based on the size of the infill panel, a W250x58 section was chosen as the first floor beam, and moment connections were designed originally to study the behaviour of the moment-resisting frame with PEC columns. However, tearing of the outside column flanges at the bottom of the columns prevented the specimen strength from further developing and also prevented the full moments from developing in the beam. The welding that was introduced to develop the plastic moment transferred from the frame beam into the columns initiated the tear along the weld between the column flanges and the beam bottom flange after the peak load. Hence, the beam behaviour of absorbing a large amount of energy through inelastic deformations was not able to be studied in the test.

Based on the strain gauge data, the corresponding stresses and internal forces were calculated. Figure 5-11 and Figure 5-12 show the internal force distributions in the bottom beam at the peak load in cycle 1, cycle 4, cycle 7 and cycle 10 when the specimen was pushed towards the north. The axial forces in the first storey beam are shown in Figure 5-11, in which the curves are quite linear, representing the uniform transfer of the lateral loads through the lateral load transfer system discussed in Chapter 4. The bending moments in the bottom beam are shown in Figure 5-12. The bottom flange was in tension at the south end, while the top flange was in tension at the north end. The bent shape of the bending moment curves is caused by the unbalanced forces of the tension fields from the infill panels below and above. Although the vertical components of the tension fields in the first storey and second storey infill panels tended to offset each other, the tension field force in the first storey was larger than the tension field force in the second storey and the difference became larger at larger lateral loads.

The results from the strain rosettes at three points in the second storey infill panel near the top beam showed that the differences between the vertical components of the stresses at the locations of the strain rosettes exceeded 20%, which was set as a limit in CSA standard S16-01 (CSA 2001) and was abandoned in CSA standard S16-09 (CSA 2009).

5.5.4 Ductility-Related Force Modification Factor, R_d (NBCC)

Commonly in seismic design, inelastic behaviour is desirable for a relatively low yielding capacity requirement and high energy dissipation capacity compared with elastic design. For a structure designed for elastic behaviour, the maximum displacement during the earthquake is still in the elastic response, regardless of the natural frequency of the structure. For a structure designed for inelastic behaviour, the elasto-plastic response of the structure to an earthquake excitation is different based on different natural frequency ranges. Known as the equal displacement theory, the maximum displacement for elasto-plastic response is about the same as that for elastic response for low frequencies

(long periods), which is used for typical structures for its reasonable accuracy. For higher frequencies (shorter periods), the deformation energy for elasto-plastic response is about the same as that for elastic response, which leads to a larger displacement for elasto-plastic response. Therefore, to represent the capacity of structural systems to maintain a certain level of load capacity while effectively dissipating seismic energy under large inelastic deformations, a factor, R_d , the ductility-related force modification factor (NBCC 2010), is used to determine the design base shear. R_d is greater than or equal to 1.0, with 1.0 implying little or no ductility, and with larger values implying higher ductility for the structure.

To consider the fact that the capacity of the constructed structure is normally higher than the designed capacity, a factor, R_o , the overstrength-related force modification factor (NBCC 2010), is used to represent the expected overstrength in the structure and also to determine the design base shear. R_o is greater than or equal to 1.0 to consider several reasons leading to overstrength of the constructed structure, such as a higher actual yield strength than the nominal value, strain hardening, larger member size chosen for load cases other than seismic loads, etc.

Three base shear vs. deflection responses, including elastic response, actual structure response and bilinear elasto-plastic approximation for the actual structure, are shown schematically in Figure 5-13. If the structure behaves elastically through the whole seismic excitation, the largest base shear will be developed as V_e . However, generally in seismic design, structures are designed to be capable of undergoing some inelastic deformation to reduce the developed base shear. The reduced base shear, at which the structure reaches its capacity, V_y , can be obtained as:

$$V_y = V_e/R_d \quad (5.1)$$

When overstrength is considered, the base shear can be further reduced to V , the design base shear, which can be obtained as:

$$V = V_e/R_d R_o \quad (5.2)$$

Design provisions for steel plate shear walls are stated in Canadian standard CSA-S16-09. The values of R_d and R_o are also provided in the National Building Code of Canada (NBCC 2010), as well as restrictions on usage and height. There are two types of steel plate shear walls as follows:

Type D (ductile) plate walls, with $R_d = 5.0$ and $R_o = 1.6$, should be provided with moment connections between the beams and columns. They are framed by rigidly connecting beams and columns with Class 1 (compact) sections in accordance with Canadian standard CSA-S16-09. There is no restriction on usage and height for ductile plate walls.

Type LD (limited-ductility) plate walls, with $R_d = 2.0$ and $R_o = 1.5$, with simple or rigid connections of beams to columns and Class 2 beams permitted, have a restriction of 60 m or 15 storeys on height in certain seismic zones according to Canadian standard CSA-S16-09 and the National Building Code of Canada (NBCC 2005).

Although Q_y and δ_y were predicted before the test to determine the loading procedure according to ATC-24, the values of Q_y and δ_y needed to be re-assessed based on the test results. Considering the steel plate shear wall infill panels as the main fuse and the PEC columns at the base as a portion of the fuse, yielding in the PEC columns was chosen as a sign of significant yielding of the whole system, as well as the yielding in the infill panel. Since there was no data recorded inside of the plastic hinge range of the columns and no white wash could be used for observing yield lines because of the painting on the whole specimen, the yielding in the columns could only be identified by the

finite element model, which is described and discussed in Chapter 6. Based on the model, Q_y was determined as 1380 kN, when yielding had been detected in the infill panel and had also initiated in three out of the four plastic hinge zones in the two columns, which was considered as significant yielding in the steel plate shear wall. Correspondingly, $\bar{\delta}_y$ was determined to be 9 mm, as shown in Figure 5-14, based on the effective stiffness of the envelope of the test hysteretic curves, according to ATC-24.

The displacement ductilities, R , at the peak load, 90% peak load, 80% peak load, 75% peak load and yield load (on the descending curve) are shown in Table 5-1. The displacement ductility at the peak load is equal to 3.9, and where the actual curve crosses over the assumed yield plateau it is equal to 6.6. These results indicate that the ductility under severe cyclic loading is very good and the steel plate shear wall system with PEC columns shows promise as a seismic force resisting system. As the main cause of deterioration was the degradation of the PEC columns at the base, improved detailing here could increase the ductility of the system even further.

Table 5-1: Displacement Ductility

	Yield	Peak	After Peak			
			90% Peak	80% Peak	75% Peak	Yield*
δ (mm)	9	35	48	56	60	59
Q (kN)	1050	1817	1636	1454	1363	1380
R	1.0	3.9	5.3	6.2	6.7	6.6

* Intersection point with idealized yield plateau

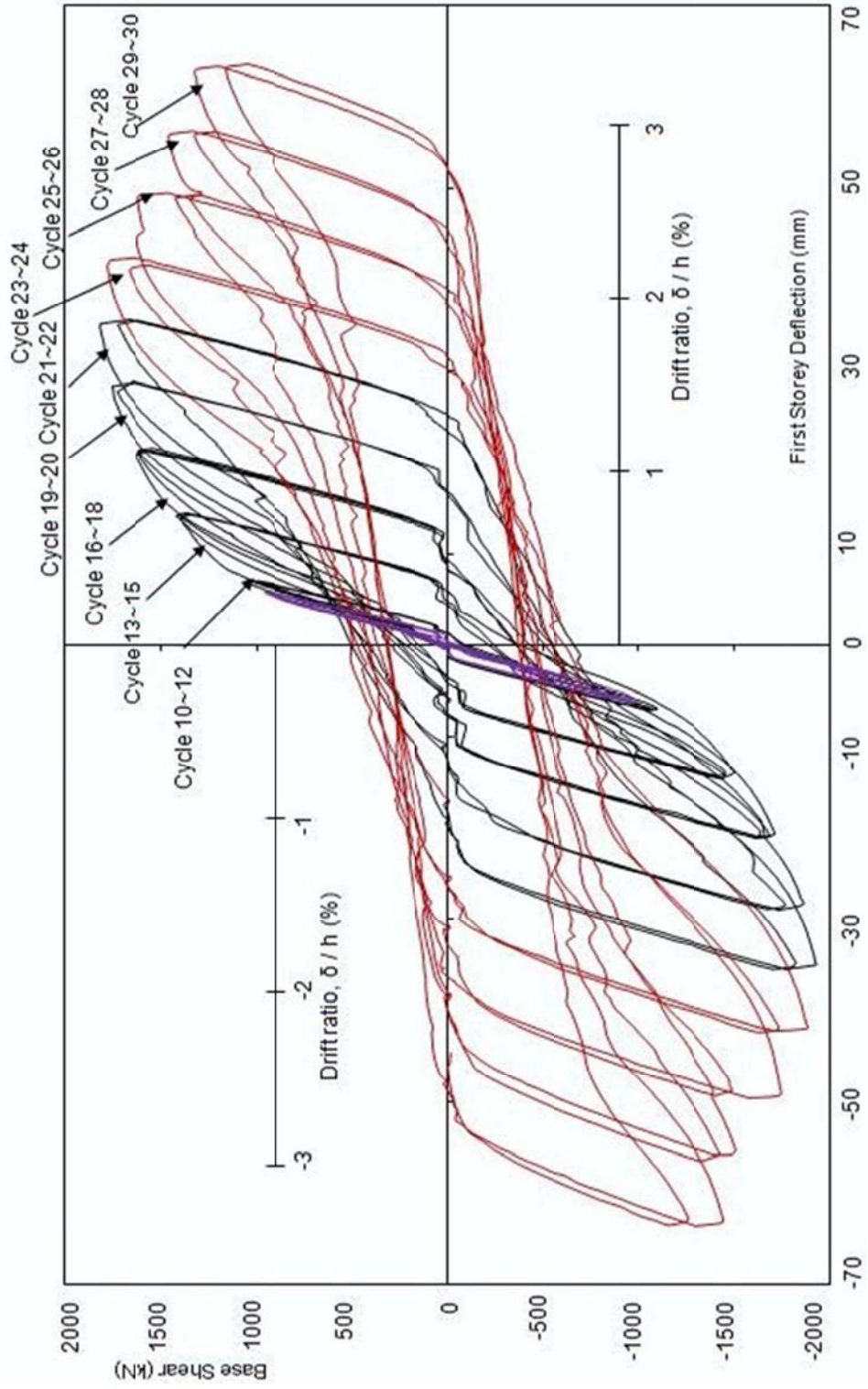


Figure 5-1: First Floor Hysteretic Curves

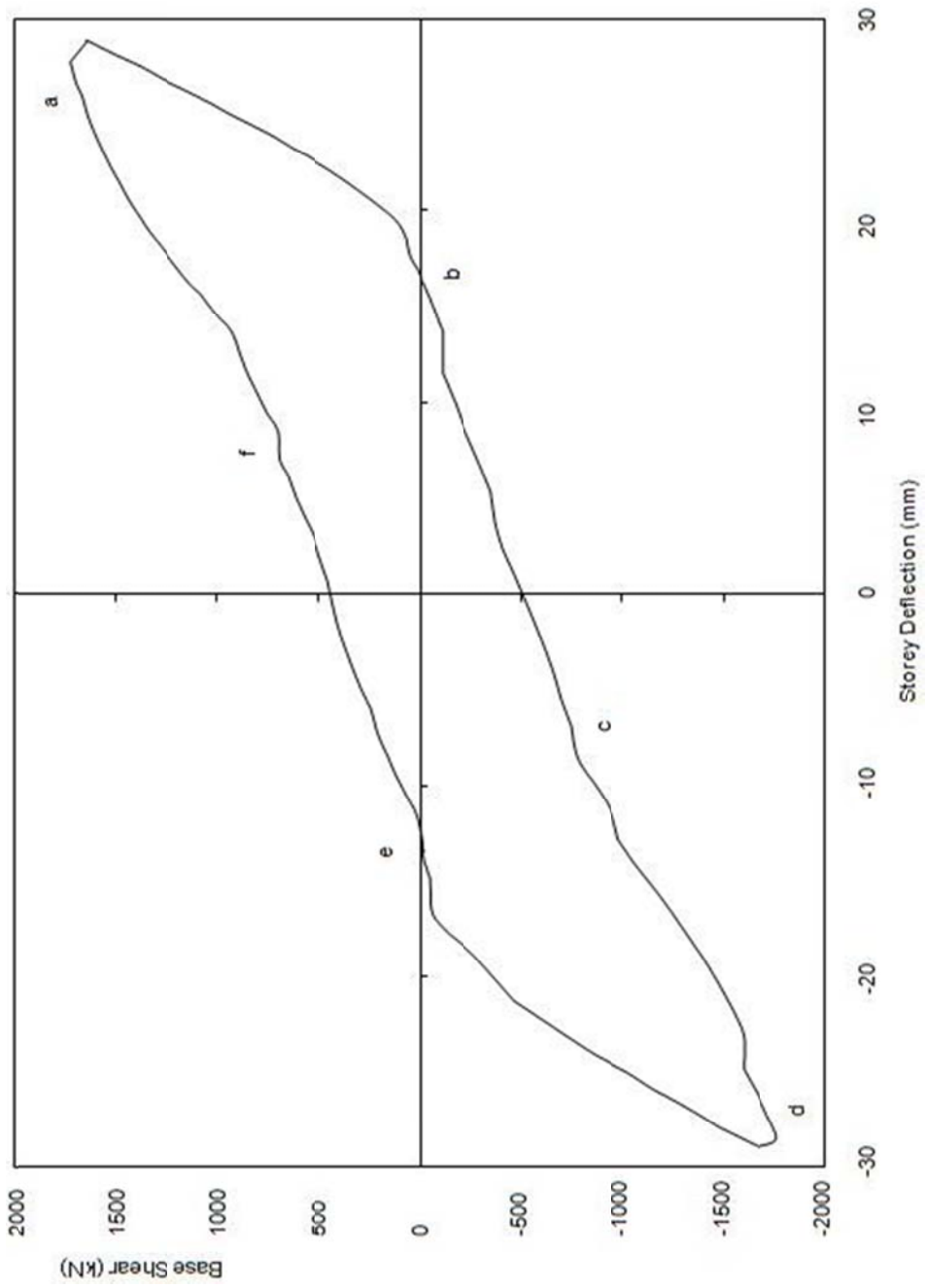


Figure 5-2: First Floor Hysteretic Curve – Cycle 20

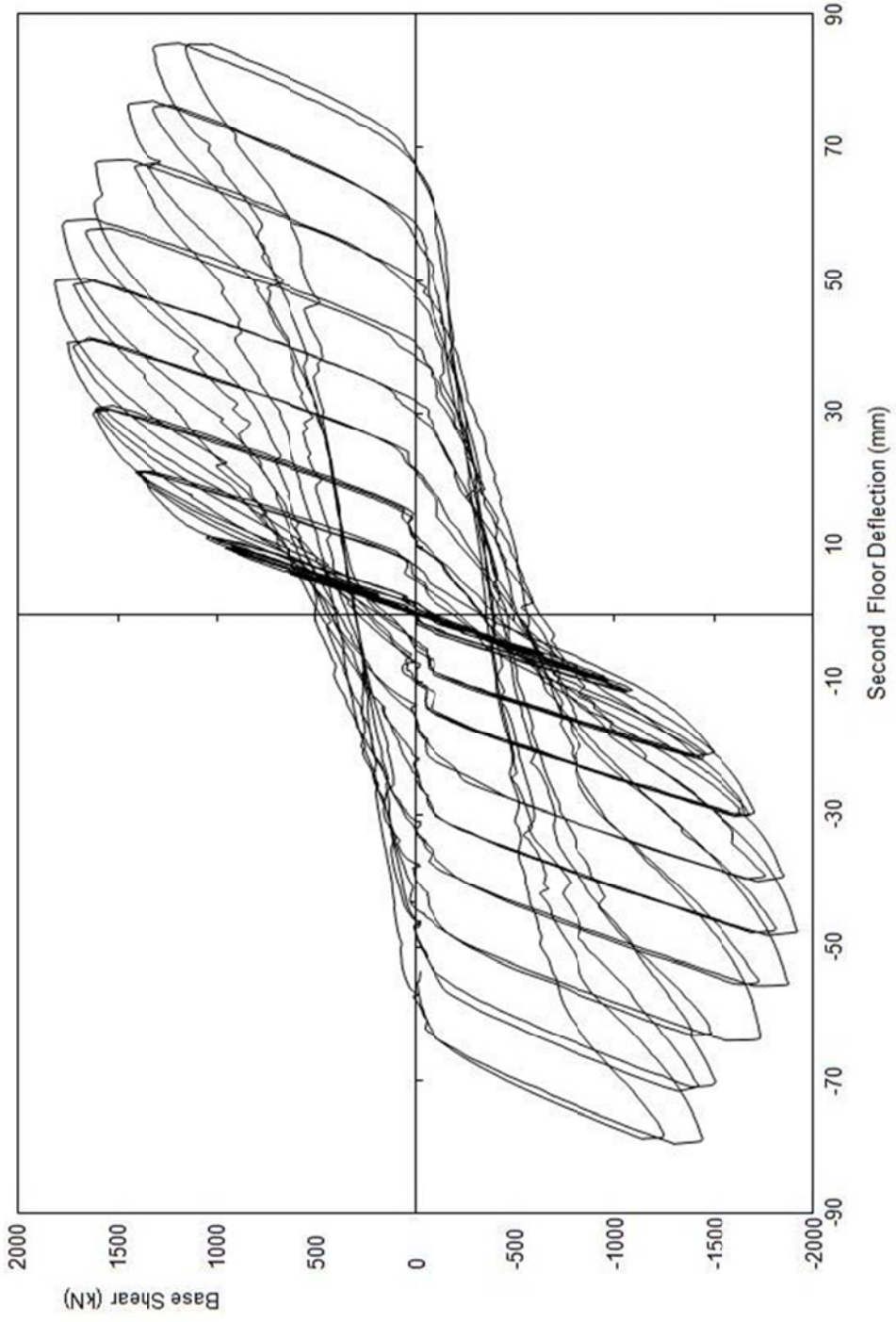


Figure 5-3: Second Floor Hysteretic Curves

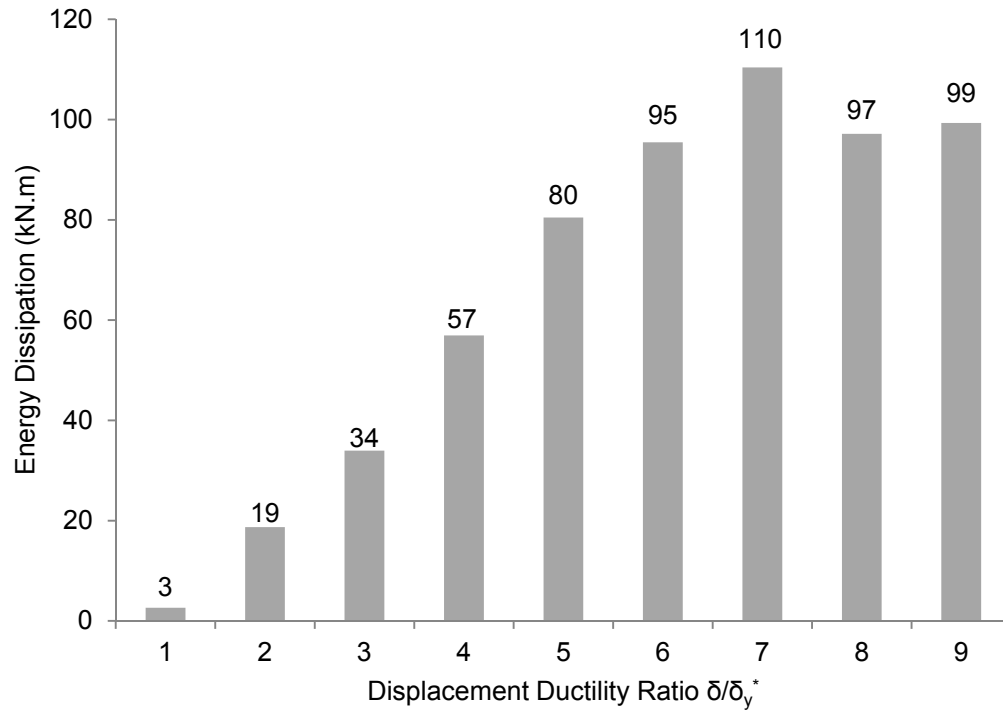


Figure 5-4: Dissipated Energy in First Cycle at Each Ductility Ratio

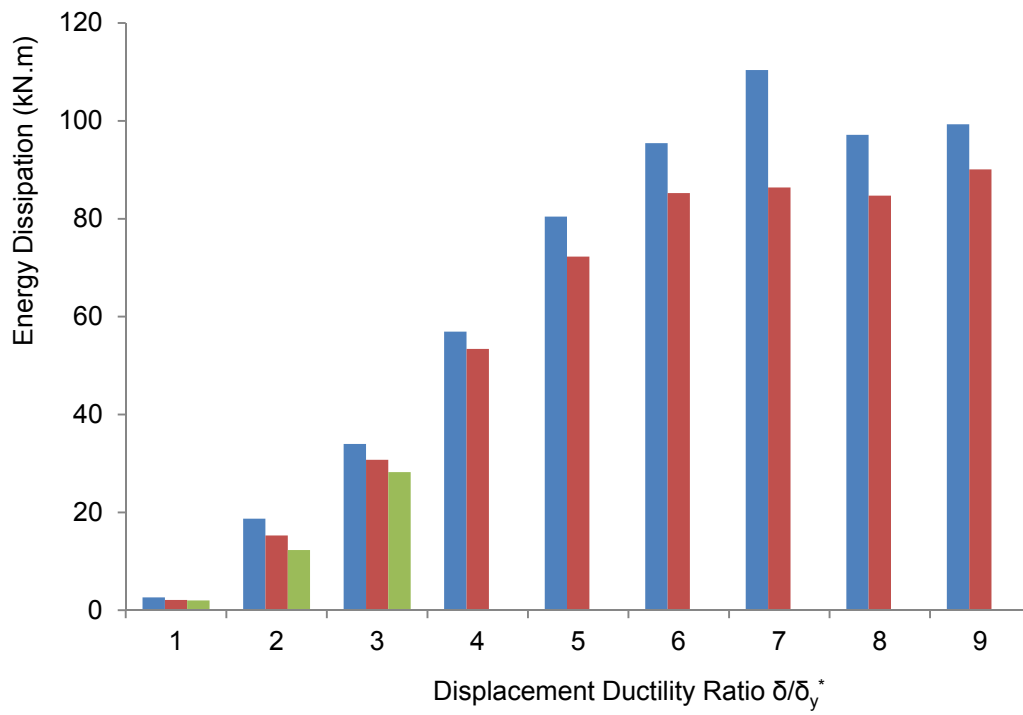


Figure 5-5: Dissipated Energy in Each Cycle

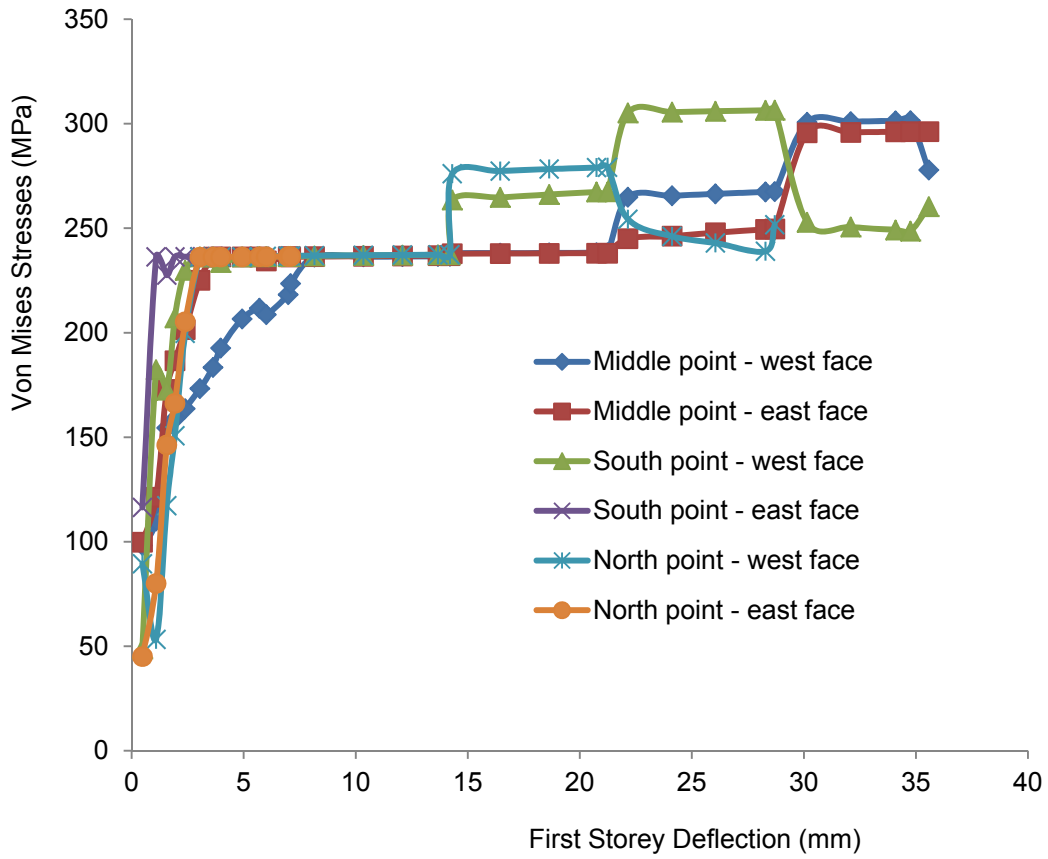


Figure 5-6: Stress Results from Strain Rosettes in Infill Panel

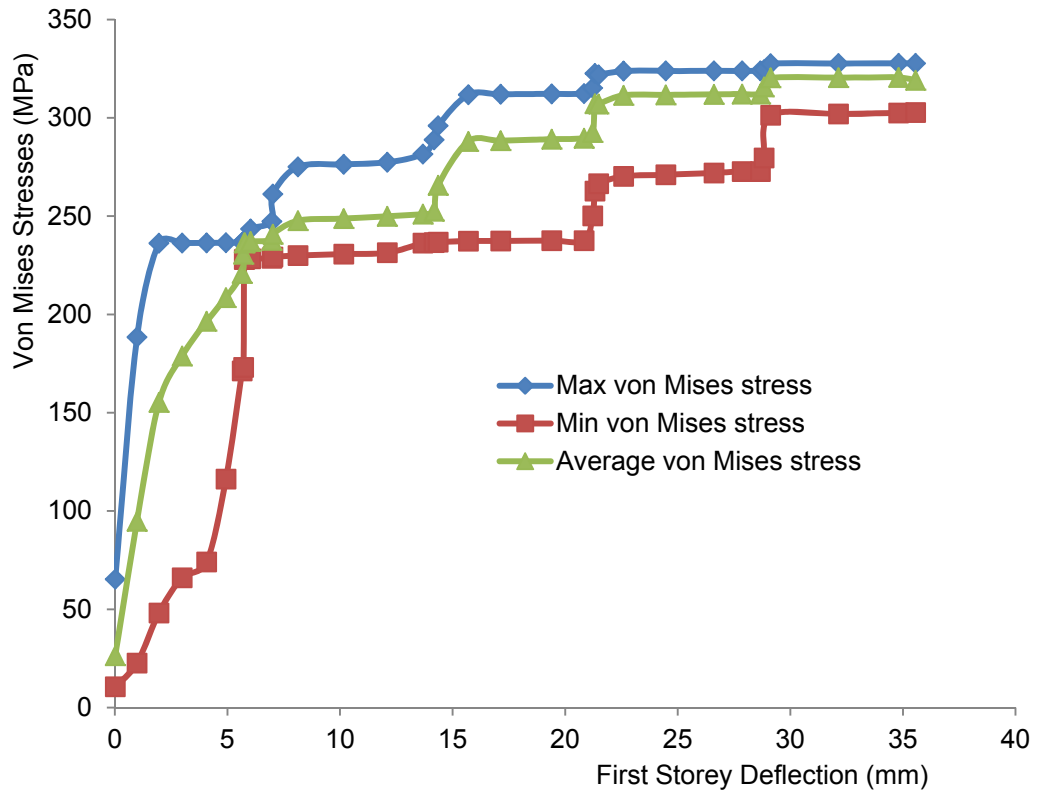


Figure 5-7: Stress Results from Camera System Data for Infill Panel

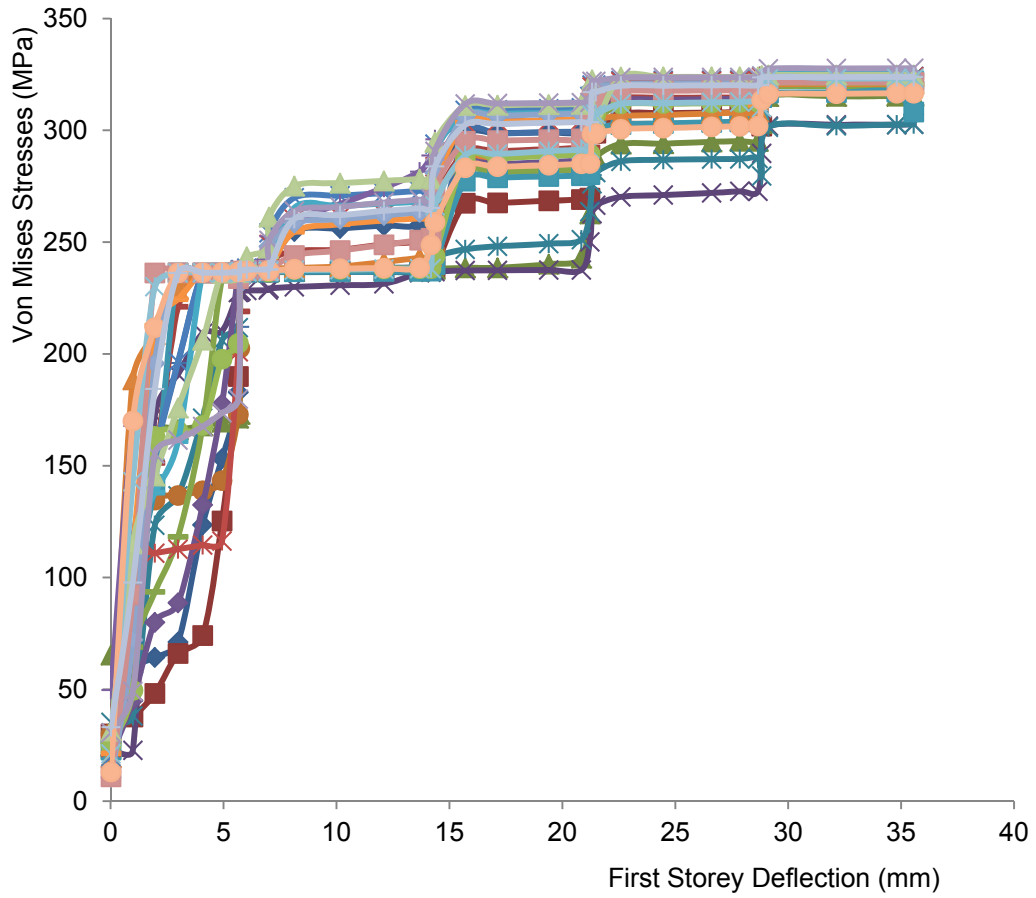


Figure 5-8: Individual Stress Results from Camera System Data for Infill Panel

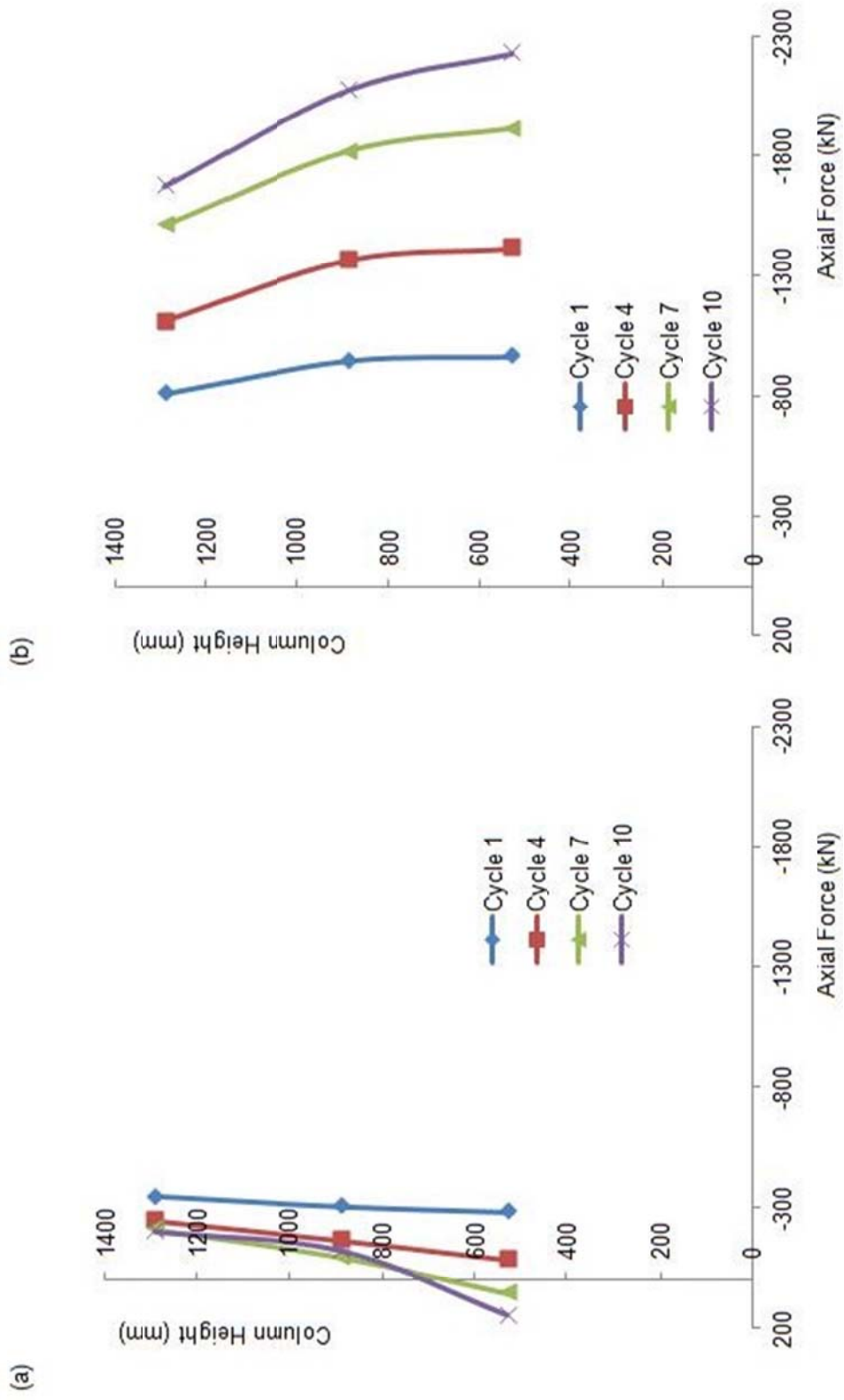


Figure 5-9: Axial Forces in First Storey Columns (Push to North)
 (a) South Column; (b) North Column

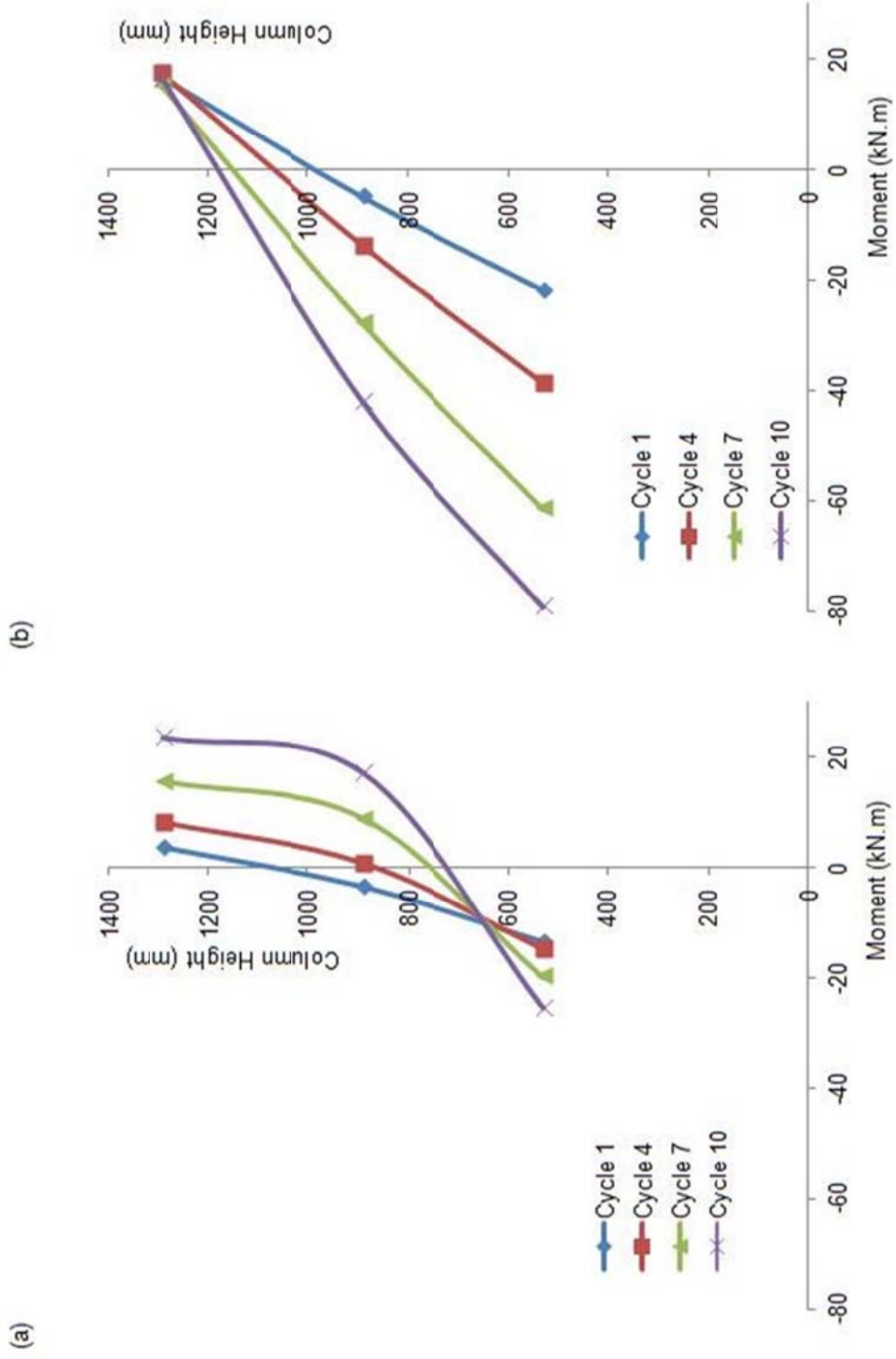


Figure 5-10: Bending Moments in Bottom Columns (Push to North)
 (a) South Column; (b) North Column

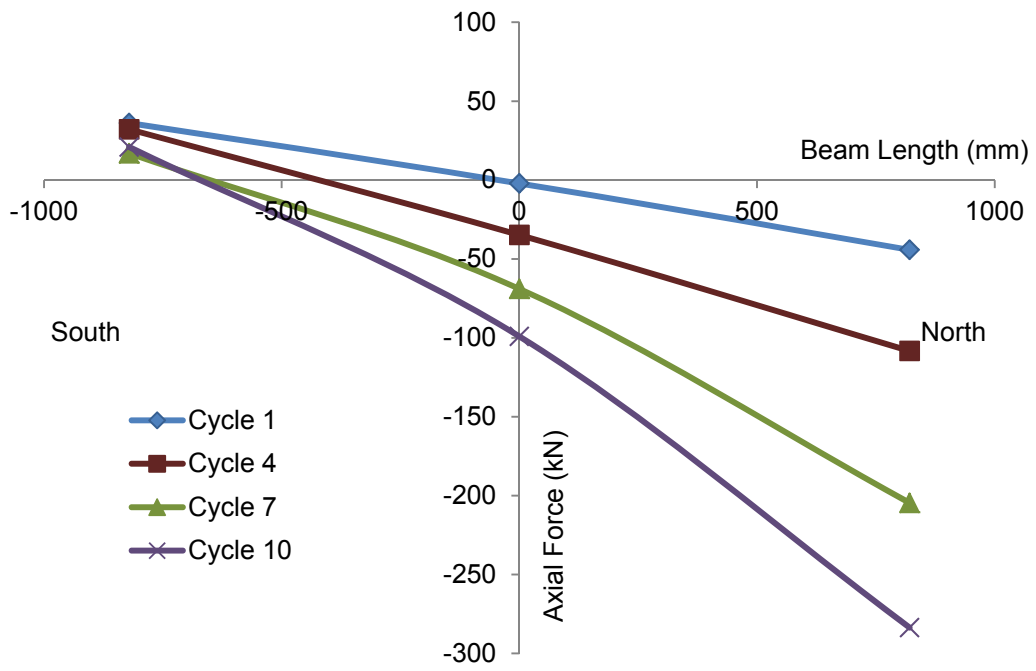


Figure 5-11: Axial Forces in Bottom Beam (Push to North)

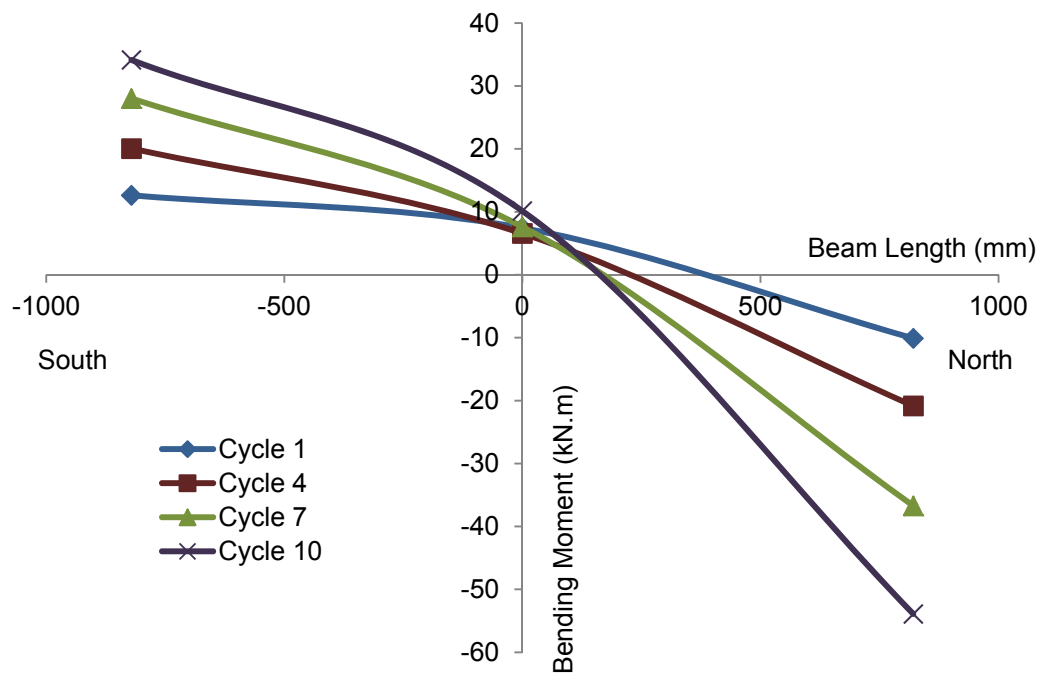


Figure 5-12: Bending Moments in Bottom Beam (Push to North)

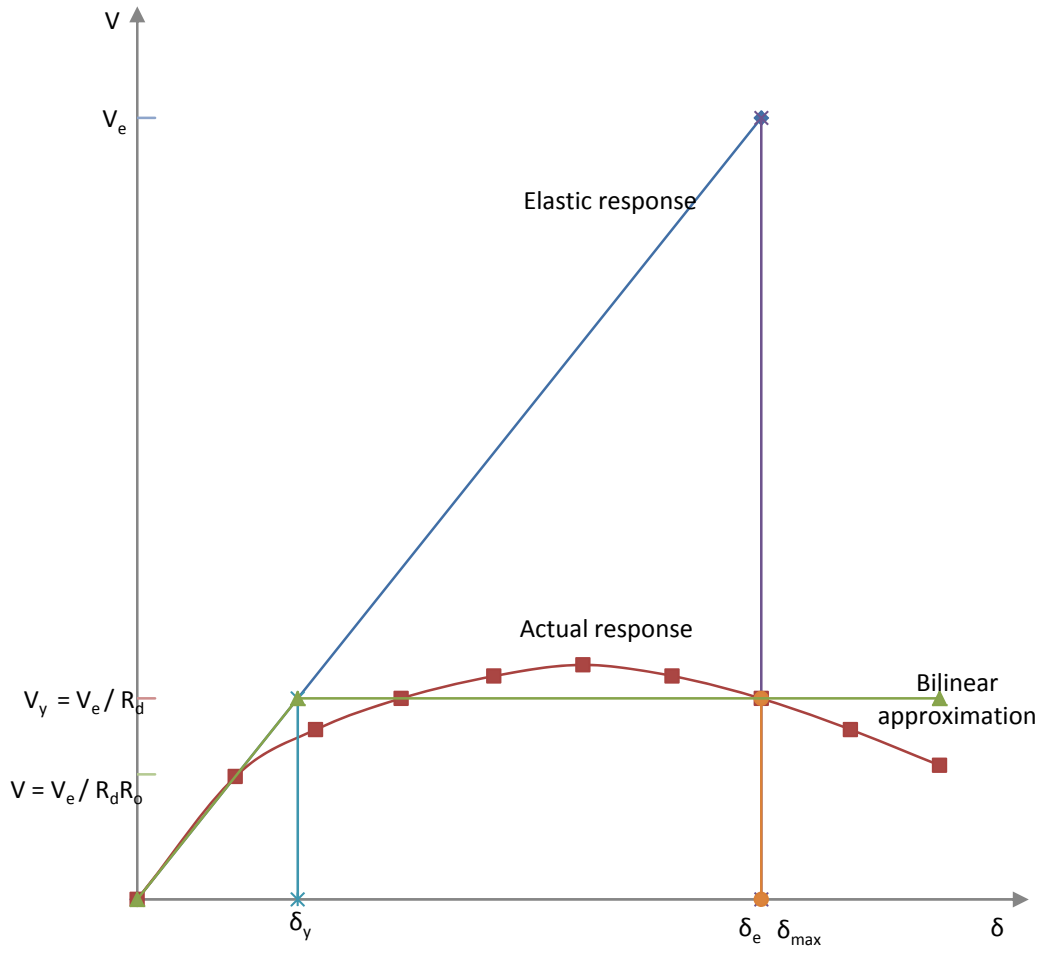


Figure 5-13: Structure Base Shear vs. Deflection Responses

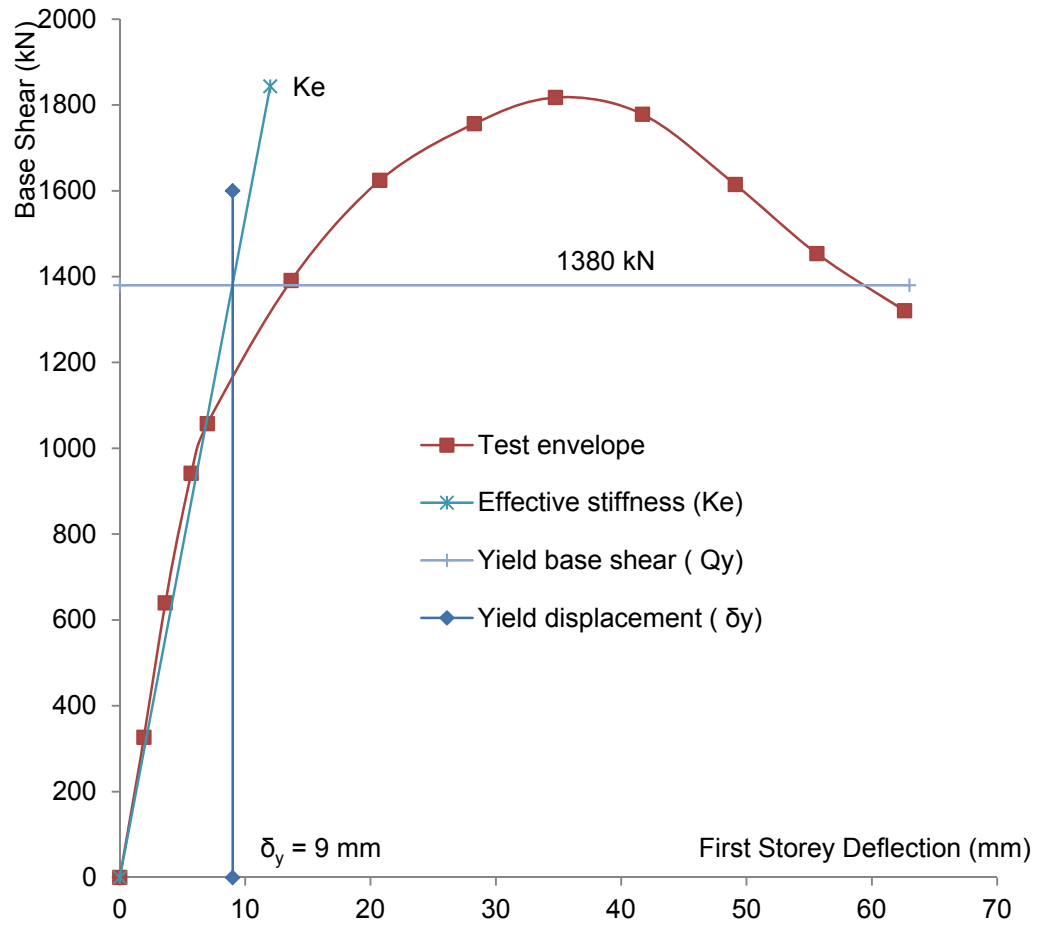


Figure 5-14: Base Shear vs. First Storey Deflection

6. FINITE ELEMENT MODEL

6.1 Introduction

A finite element model was developed before the specimen of the steel plate shear wall with partially encased composite columns was tested to determine the loading procedure of the test and the expected capacity of the specimen. After the test was done, the test data was analyzed and the test results were used to modify the material properties so the model was able to simulate the behaviour of the specimen under monotonic loading instead of cyclic loading. The results of the modified model were then compared with those of the test to verify the validity of the model and to further study the behaviour of the system, and the PEC columns as part of the system.

The specimen was a half-size two-storey steel plate shear wall with PEC columns, which include the steel section, partially-encased concrete, links with different spacing along the column height, and the side plates at the column base and at each floor level. Hence, a huge number of elements arose due to the complicated geometry. Nonlinearities were also present, including nonlinear material behaviour and nonlinear geometry, since the specimen underwent large displacements under lateral loads. Moreover, the contact between the steel section and concrete inside of the columns also contributed to the complexity of the model. To reduce difficulty in achieving numerical convergence caused by model complexity, a dynamic explicit solution strategy in ABAQUS/Explicit was used. A push-over analysis was used in the model, instead of cyclic loading, to simulate the envelope of test results for model efficiency by reducing the running time of the model.

6.2 Model Properties

6.2.1 Element Selection

The thin-walled steel section in PEC columns was adopted to maximize the compression portion resisted by concrete and as a result, local buckling is expected in column flanges

at the ultimate load. Under an axial compressive force, local buckling is expected to occur in both flanges simultaneously, while local buckling is only expected to occur in one flange when bending moment is applied, like for the PEC columns in the specimen. Besides local buckling, axial stretching and out-of-plane bending were the main deformations in the steel flanges, while shear deformation governed the deformations in the steel web. Considering the stresses and large deformations in the steel sections and the thin-walled feature, shell element S4R was chosen for its accurate results with efficient running time. Shell elements S4R were also used to model the side plates, which were welded to the flange tips at each floor level and at the column base. Shell element S4R is a general-purpose 4-node doubly-curved shell element with a large-strain formulation, hourglass control and reduced integration, with both displacement and rotational degrees of freedom. Due to the nonlinear material behaviour in the steel section, the *SHELL SECTION option was used since the *SHELL GENERAL SECTION option is only used for linear elastic response.

The partially encased concrete cracked at the tension side and crushed at the compression side of the columns due to the existence of bending moments, besides axial forces, in the columns. Although second-order elements provide more accurate solutions than first-order elements, first-order solid element C3D8R was used to model the concrete because interaction between the steel section and concrete in the columns was involved, and second-order elements are not suitable if complex contact conditions are present. The lower accuracy of the first-order element was compensated to some degree by the fine mesh in the model. Solid element C3D8R is an 8-node linear brick element with reduced integration, which reduces running time, especially in three dimensions. C3D8R only has displacement degrees of freedom.

The transverse links were welded at the flange tips to provide limited confinement to the concrete and support for the slender column flanges. Under the bending moments, the encased concrete at the compression side of the PEC columns expanded and the steel

flange at the tension side of the columns was stretched. The links tended to bend outwards near the end on the compression side of the column. Bending outwards and upwards simultaneously was observed during the test when the links were exposed after a large loss of the concrete. To simulate the bending of the links in two directions, beam element B31 was used, which is a special beam element using linear interpolation and allowing for transverse shear deformation.

Under lateral loads, the infill plates of the steel plate shear wall buckled in one diagonal direction and stretched in the perpendicular direction. Large shear forces were also expected in the infill plates besides the buckling and stretching, which made shell element S4R suitable for modelling the infill panels. The *SHELL SECTION option was used due to the nonlinear material behaviour in the infill panels.

The beams behaved as boundary members for the infill panels when the specimen sustained lateral loads, more like stiffeners than the frame beams. Hence, shear element S4R was used to model the frame beams instead of a beam element. Under bending, a first-order element with reduced integration, like element S4R, could deform in a way (shown in Figure 6-1) with no deformation in the central point (the integration point), which is called “hourglassing”. In order to prevent hourglassing in each frame beam, at least four elements were used in the depth of the beam web and in the width of the beam flange, which met the minimum recommendation based on previous research (Hibbitt et al. 2001).

Because of difficulties in the performance of the model, use of multi-point constraints (MPCs) was greatly reduced as the model evolved, such as for the welding used to connect the infill panels, beams, and columns, which were originally modelled by MPCs but were replaced by shell element S4R with the same strength as the steel in the columns to make sure failure would not be caused by the rupture in the connections.

The lateral loads were applied by the jacks at each floor level, sharing the same manifold to make sure the floor loads were equal. To apply the lateral loads at each floor equally in the model, a simply-supported vertical distributing beam was used, as shown in Figure 6-2. The ends of the vertical distributing beam were located at each floor level, so the lateral loads applied at its mid-point would be transferred to each floor equally. Moreover, the vertical distributing beam was simply-supported at both ends to transfer lateral loads without producing any moments. A first-order, three-dimensional beam element (B31) with large stiffness was used for the vertical distributing beam to avoid significant axial shortening of the beam because of bending. As mentioned in Chapter 4, the lateral loads were applied to the frame beam top flanges by jacks, and distributed equally to both sides of the beams through connection tabs and channel-and-T-section assemblies. In the model, 2-node, 3-D stress/displacement truss elements (T3D2) with large stiffness were used to model the jacks at the ends of the vertical distributing beam and the connection tabs were simulated by horizontal distributing beams modelled by first order, three-dimensional beam elements (B31) with large stiffness. The channels and T-sections used in the lateral loading system were also modelled by inter-connected first order, three-dimensional beam elements (B31), considering slip-resistant connections were used to connect the channels, T-sections and the top flanges of the beams in the test.

6.2.2 Mesh Description and Imperfections

The mesh configuration for the cross section of the PEC columns is shown in Figure 6-3 for identifying the node arrangement in the column cross section, including the steel section, encased concrete, transverse links and side plates. The model of the whole specimen is shown in Figure 6-4, while the model of the column without concrete is shown in Figure 6-5.

As shown in Figure 6-3(a), there were nine nodes across the steel flange width, dividing it into eight segments of three different lengths. Three nodes were situated across the web

thickness, with two at the outer surfaces and one at the middle surface of the web, one was located at each flange tip, one at each link, and one each between the web and the two links. Correspondingly, there were four nodes (three elements) along the flange width at each side of the web adjacent to the nodes in the concrete component of the model, shown in Figure 6-3(b). There were seven nodes at the middle surface of the steel web along the column depth (Figure 6-3(a)), which divided the web into six segments of equal length. Accordingly, there were six portions with equal length in the concrete along the column depth. The nodes for the links, shown in Figure 6-3(c), coincided with the nodes used for the concrete along the link lines to simplify the mesh. In each side plate, there were eleven nodes along the column depth, shown in Figure 6-3(d), in which the middle nine nodes were located corresponding to the nodes in the steel and concrete sections and the remaining two nodes at the ends were located at the edges of the side plates.

As shown in Figure 6-3, there were 8 elements across each steel flange and web, while the encased concrete had a 6 x 3 mesh at each side of the web. Also in the column cross section, each transverse link had 8 elements and there were 10 elements across each side plate. Although there were shallow shell elements at the points where the flanges and web met and in-plane bending could not be avoided in the shallow shell elements at the ends of the web when the specimen was laterally loaded, it was considered a local effect and was not studied further since the model aimed to simulate the overall behaviour of the PEC columns.

Along the column height, nodes were located at the elevations of the links, the top and bottom of the side plates, the top and bottom of the frame beams, as well as the top and bottom of the column, as shown in the Figure 6-4 and Figure 6-5. Supplementary nodes were placed halfway between the links if the link spacing was 160 mm to reduce the number of slender shear elements.

The dimensions of the columns were measured and input into the model, including the column depth, flange width and the thickness of the steel section. The imperfections in the columns were detected and only out-of-plane plumb in the north column and eccentricity of the south column base were considered in the model. Other imperfections were small and ignored, such as flange bending inwards between the links and imperfections in the links. As a result of the fabrication procedure for PEC columns, imperfections of column flanges by bending inwards between links were observed and studied in previous research (Chicoine et al. 2003; Begum et al. 2007), which suggested that these inward imperfections may be neglected in the numerical model, since they have little influence on the behaviour and capacity of the PEC columns. Hence, the imperfections in the column flanges were not simulated in the model. There were also geometric imperfections detected in a few of the links. The local bending in the third link from the south column base was ignored because it was within the height of the bottom side plates and had a negligible effect on the column behaviour. The local imperfection in the tenth link of the same column was also ignored because the link was located away from the plastic hinge zone and should not have much effect on the overall column behaviour, especially before the specimen reached the ultimate capacity. Although the sixth and seventh links were within the plastic hinge zone, the imperfections were still ignored because the local bending was not severe.

The mesh configurations of the infill panels and frame beams are shown in Figure 6-6 and Figure 6-7. The infill panels and the frame beams were divided horizontally into 24 segments of equal width, which meant the location of the nodes along the edges of the infill panels were identical to those along the centrelines of the beam flanges. To provide hourglass control (Hibbitt et al. 2001), there were four elements across the beam flanges and the bottom beam web (Figure 6-7(a)), while there were seven elements across the top beam web (Figure 6-7(b)). As shown in Figure 6-4, the heights of the nodes in the infill panels and the frame beams were identical to the nodes in the columns to simplify the

model. The out-of-plane imperfections of the infill panels were measured at 63 and 54 locations in the first and second storey infill panels, respectively, and input into the model with maximum out-of-plane imperfections of 11 mm in the first storey panel and 10 mm in the second storey panel, shown in Figure 6-6 with a scale factor of 20 (out-of-plane) for clarity.

6.2.3 Modelling of Steel–Concrete Interactions

The interactions between the encased concrete and the steel section, including steel flanges and web, were simulated in the model, since there was no separation between the concrete and steel section until local buckling occurred in the column flanges.

There are two contact algorithms provided in ABAQUS: a general contact algorithm and a contact pair algorithm. The general contact algorithm is commonly used for its great simplification of contact definitions and less restriction on the contacting surfaces than the contact pair algorithm. However, the contact pair algorithm must be used in some cases because certain interaction behaviours are only available in the contact pair algorithm, such as two-dimensional surfaces, which were involved in the interaction in the columns simulated in the model. Breakable bond is another feature only considered in the contact pair algorithm, which was exhibited in the PEC columns as separation of the steel flanges and concrete in the case of local buckling. Hence, the contact pair algorithm was chosen to model the interactions in the columns.

Contact pairs use either a kinematic predictor/corrector contact algorithm by default or a penalty contact algorithm by definition to enforce contact constraints in an ABAQUS/Explicit simulation. The kinematic constraint method searches for penetrations in a predicted configuration, while the penalty method searches for penetrations in the current configuration. Since the kinematic contact constraint will override other constraints defined by *EQUATION, *MPC, *TIE or kinematic constraints other than contact constraint, only the penalty method can be used when other kinematic constraints are

involved in the contact pairs even though the kinematic constraint contact method is normally chosen for its computational efficiency. Due to MPCs used in the model to connect the top and bottom of the columns to the rigid bodies (discussed in section 6.2.4), the penalty contact algorithm was finally chosen. The basic Coulomb friction model is used in the penalty contact algorithm, in which the tangential forces in the contacted surfaces are modelled as sticking friction, equal to the normal force multiplied by the coefficient of friction. The model result proved to be insensitive to the coefficient of friction, which is usually chosen between 0.1 and 0.3. To maximize the tangential interaction between the steel section and concrete, the coefficient of friction was taken as 0.3.

Finite sliding, small sliding and infinitesimal sliding and rotation are used to account for the relative motion of the contacted surfaces forming a contact pair in ABAQUS/Explicit. Finite sliding allows arbitrary motion of the surfaces and large motion between the surfaces. Small sliding allows large motion of the surfaces with little relative sliding between surfaces. Infinitesimal sliding and rotation assumes both arbitrary and relative motion of the surfaces are small. Although only small relative motion was expected between the steel section and concrete, finite sliding was used since it is the only approach available in the contact pairs using the penalty contact.

A balanced master–slave contact algorithm was used in the model, which means the corrections of the override produced by two contacts were equally weighted, and was chosen by default since the penalty contact algorithm was specified.

6.2.4 Boundary Conditions

The specimen was connected to the base plate through welding, including the first floor infill panel and the steel section of the columns. The base plate of the specimen was then fixed to the strong floor mainly by pre-stressed high-strength rods. To simulate the fixed boundary condition of the specimen, rigid bodies were introduced into the model. Rigid bodies were defined at the base of the specimen at the nodes in the steel section and

concrete in each column, as well as at the nodes along the base of the first storey infill panel. All the rigid bodies were restrained for all the degree of freedom to represent the fact that the base plate of the specimen was very stiff and fixed to the strong floor. Multi-point constraints (MPCs) were used to connect the different portions of the specimen base to the corresponding rigid bodies. At the specimen base, the concrete in each column was connected to the rigid bodies through pin connections, while the steel section in each column and the first storey infill panel were connected to the rigid bodies through tie connections. Hence, all the steel portions were fully restrained and all the concrete portions were restrained for the displacement degrees of freedom at the specimen base.

The same methodology was used for the top of the columns, where the vertical loads were applied. Rigid bodies were defined at the top of the columns at the nodes in the steel section and concrete in each column and the rigid bodies were restrained for all the degrees of freedom except the in-plane displacement and rotation about the column strong axis. At the top of the columns, the concrete in each column was connected to the rigid bodies through pin connections while the steel section in each column was connected to the rigid bodies through tie connections.

The out-of-plane displacement of the specimen was prevented by the Watt-braces located at the outside of the columns and about 410 mm below each floor level (see Chapter 4). Therefore, all the nodes in the outside flange of the columns at the height of the Watt-braces were restrained for out-of-plane displacement to provide the out-of-plane bracing in the model. The vertical distributing beam used for applying lateral loads, shown in Figure 6-2, was restrained at the ends for all the degrees of freedom except the in-plane displacements and rotation about the column strong axis.

6.2.5 Material Properties

Uniaxial tension coupon tests were done to determine material property curves of the steel in the specimen, including the steel section and links in the PEC columns, the bottom

beam, and the first and second storey infill panels. The true stress and logarithmic plastic strain were calculated from the tension coupon test results, except the modified material curve used for the first storey infill panel as discussed in the next paragraph, according to the following equations and then input into the model, in which the formulation is based on the updated Lagrangian description. The stress and strain conversion relationships are:

$$\sigma_{true} = \sigma_{nom}(1 + \varepsilon_{nom}) \quad (6.1)$$

$$\varepsilon_{ln}^{pl} = \ln(1 + \varepsilon_{nom}) - \frac{\sigma_{true}}{E_s} \quad (6.2)$$

where σ_{true} is the true stress, ε_{ln}^{pl} is the logarithmic plastic strain, σ_{nom} is the nominal or engineering stress, ε_{nom} is the nominal or engineering strain, and E_s is the modulus of elasticity of steel.

As mentioned before, a modified material curve was used for the first floor infill panel in the model instead of the material curve obtained directly from the tension coupon test. To simulate the strain hardening occurring in the first storey infill panel, a strain hardening rule was chosen and the material curve was modified accordingly. There are usually three potential rules to determine the hardening properties of a material under a reversed loading condition: isotropic hardening rule, kinematic hardening rule and independent hardening rule. According to the isotropic hardening rule, the yield stresses before and after the stress is reversed are equal, which is illustrated in Figure 6-8(a) as $|\overline{B'C}| = |\overline{BC}|$. If the isotropic hardening rule is used for a material under cyclic loading, the stress at reversed loading will be larger than the stress for unidirectional loading at the same strain. Since an increase in tensile yield strength occurs with no compensation of compressive yield strength, the isotropic hardening rule neglects the Bauschinger effect completely. On the contrary, the kinematic hardening rule considers the Bauschinger effect to its full extent. The total elastic range, including tensile and compressive portions, remains the same during kinematic hardening, which is illustrated in Figure 6-8(b) as $|\overline{BB'}| = |\overline{AA'}|$. If

the kinematic hardening rule is used for material under cycle loading, the stress at reversed loading will be no larger than the stress for unidirectional loading at the same strain. According to both the isotropic and kinematic hardening rules, tensile and compressive yield strengths are related, while tensile and compressive yield strengths are independent according to the independent hardening rule, which is illustrated in Figure 6-8(c) as $|\overline{CB'}| = |\overline{OA'}|$ and $|\overline{BC}| > |\overline{OA}|$. Generally, the strain hardening rule for structural steel is a combination of the isotropic and kinematic hardening rules, which is called a mixed hardening rule. However, the material curve should be determined based on the cyclic loading history, which is not suitable for the situation herein because no cyclic material tests were conducted.

The isotropic hardening rule was chosen for calculating the stress in the infill panel and the steel section in the PEC columns for the test results. As shown in Figure 6-9, the material follows curves o-a-b under unidirectional loading and curves o-a-b-c-d-e-f-g under cyclic loading. The stress of the material reaches strain hardening under cyclic loading according to the isotropic hardening rule, while the stress of the same material at the same strain remains at the yielding level under unidirectional loading. To study the behaviour of the PEC columns and that of the overall steel plate shear wall, and to compare with the test results, the amount of anchorage force applied to the columns from the infill panel in the model should match that in the test. Hence, the material curve of the first storey infill panel was modified for use in the model as shown in Figure 6-10, so the model results (monotonic loading) and the test results (cyclic loading) could be compared. The material properties for the second storey infill plate were not modified since no clear evidence of strain hardening was observed.

As shown in Figure 6-9, the strain hardening occurs earlier under cyclic loading than monotonic loading if the isotropic hardening rule is used, which led to a very short yield plateau in the modified material curve compared with the tension coupon results. Under the effect of the cyclic loading and longer yield plateau, the stresses in the first storey infill

panel in the test were more uniform than in the model. Therefore, the sum of the stresses in the first storey infill panel in the model with the modified material curve would match the test result, but with a different stress distribution from the test, causing some differences between the model and test results regarding the column behaviour.

In ABAQUS, concrete is modelled either using a cracking model or a concrete damaged plasticity model. The brittle cracking model can be used to model concrete and other brittle materials, in which the behaviour is dominated by tensile cracking and the compressive behaviour is always linear elastic. The concrete damaged plasticity model can be used to model concrete and other quasi-brittle materials, in which the two failure mechanisms are considered, including tensile cracking and compressive crushing. The concrete damaged plasticity model is a continuum, plasticity-based, damage model for concrete and is applied for concrete subjected to monotonic, cyclic, and/or dynamic loading under low confining pressure. In PEC columns, concrete is surrounded by the steel section on three sides and partially encased by transverse links on the other side, in which a low level of passive confinement for the concrete is expected. When the specimen was laterally loaded, the PEC columns were under a combination of bending moments and axial forces, which were either tension or compressive forces. At the critical column locations, both concrete cracks and concrete crushing were observed in the test and should be simulated in the model. Hence, the concrete damaged plasticity model was used to predict both tensile and compressive failure of the concrete and expansion of the concrete under low confining pressures.

6.3 Loading application and solution strategy

ABAQUS/Explicit is most suitable for dynamic analyses, while it can also be used to solve static or quasi-static problems. To apply quasi-static loads, smooth application of loading is required to avoid stress waves caused by jerky movements. Smooth application of loading is approached by smooth acceleration changes, which ensure smooth velocity

and displacement. A smooth amplitude displacement loading was used in the model with the initial and final data points given to apply lateral loads without discontinuity in the rate of applied loading. As shown in Figure 6-11, a corresponding smooth step amplitude curve was created in ABAQUS automatically. The histories of different energies varying with the time during lateral loading are shown in Figure 6-12, in which internal and external energies were similar, while the kinetic energy and friction dissipation were negligible. Based on the features shown in Figure 6-11 and Figure 6-12, a quasi-static condition was successfully simulated.

Due to the complexity of the model, including a huge number of elements, complicated geometry, nonlinear material behaviour and inter-surface contact between the steel section and concrete in the columns, the actual time period was very long and the model required a lot of computer time to run in its physical time scale. To save processing time, scaling can be used in the model. One option is load-rate scaling, which reduces processing time through shortening the step time by artificially increasing the punch velocity. The other option is mass scaling, which reduces processing time through increasing the stability limit by artificially increasing the mass density of the elements. Either method can be used to reduce processing time effectively, except a load rate scaling factor of f has the same effect as a mass scaling factor of f^2 . Considering the complexity of the model, a mass scaling factor of 1000 was used to improve the efficiency of the model, while providing an acceptable solution.

For an analysis in ABAQUS, the geometric nonlinearity is ignored if a small displacement formulation is used, but included if a large displacement formulation is used. The geometric nonlinearity of the specimen is considered by defining "NLGEOM=YES" in the model.

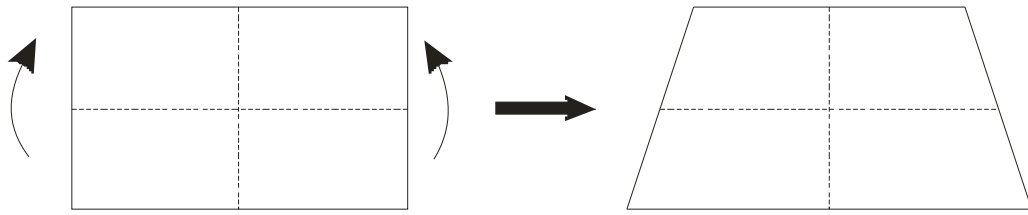


Figure 6-1: Deformation of a First-Order Element with Reduced Integration under Bending

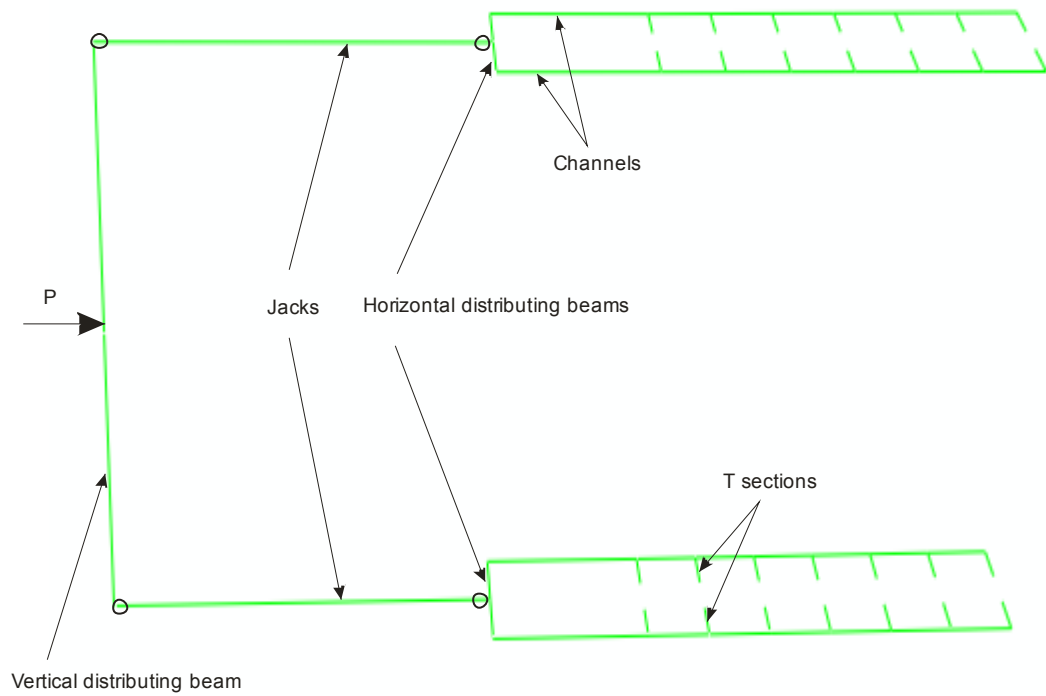
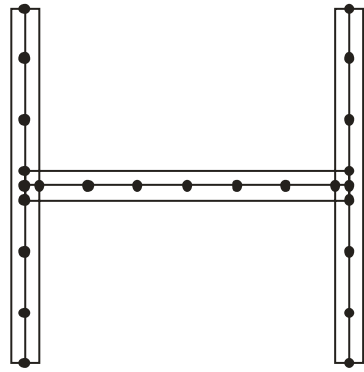
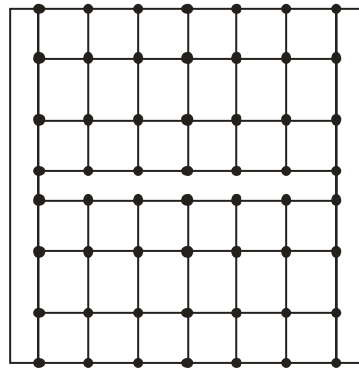


Figure 6-2: Lateral Loading System in Model

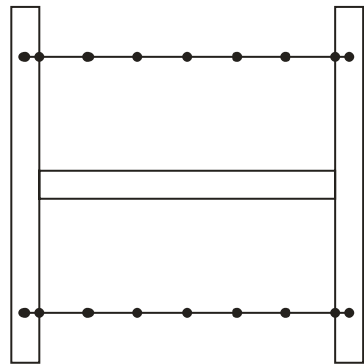
(a)



(b)



(c)



(d)

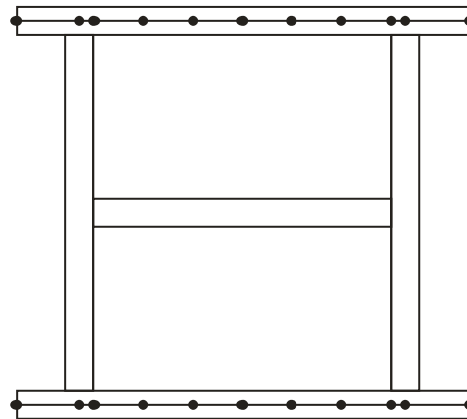


Figure 6-3: Mesh in Columns
a) Steel Section; b) Concrete; c) Links; d) Side Plates

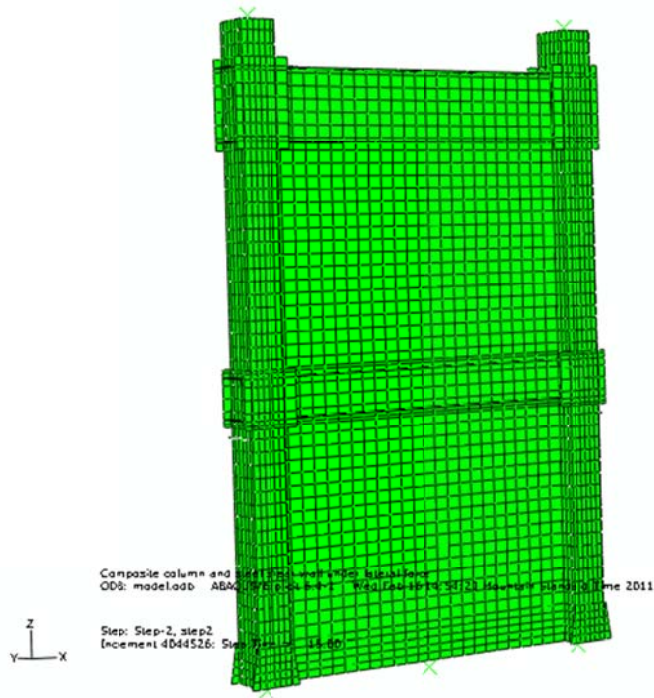


Figure 6-4: Specimen Mesh

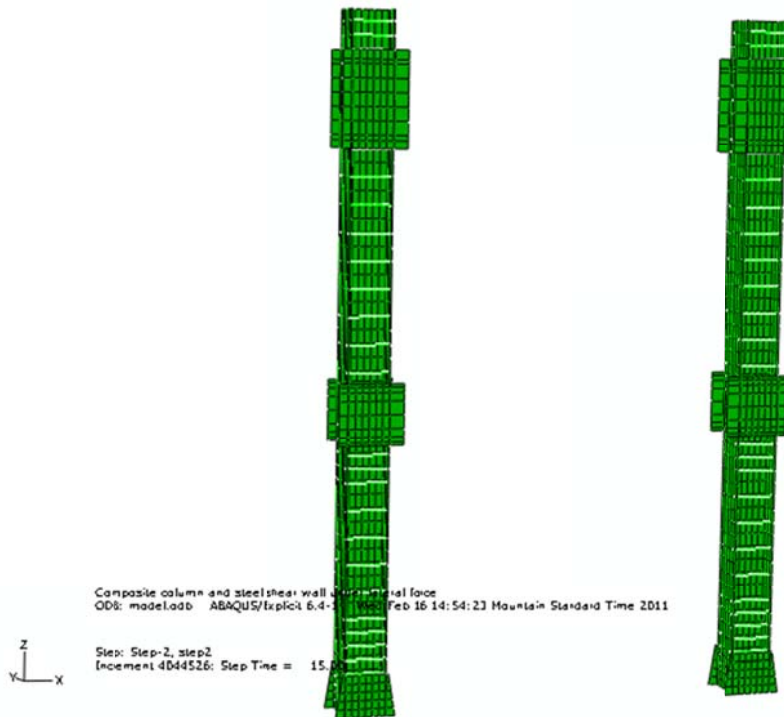
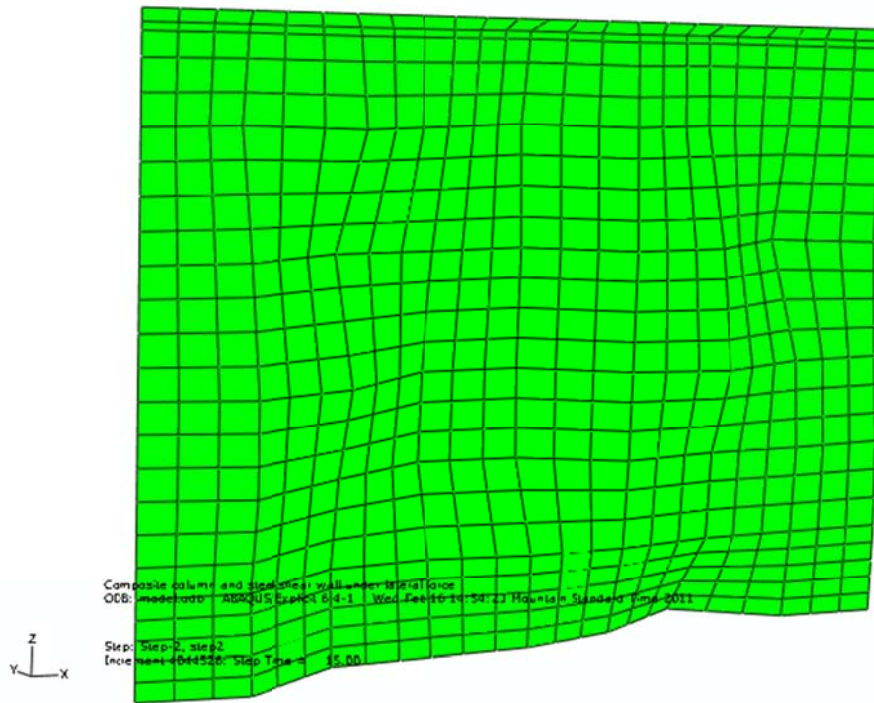


Figure 6-5: Mesh of Columns without Concrete

(a)



(b)

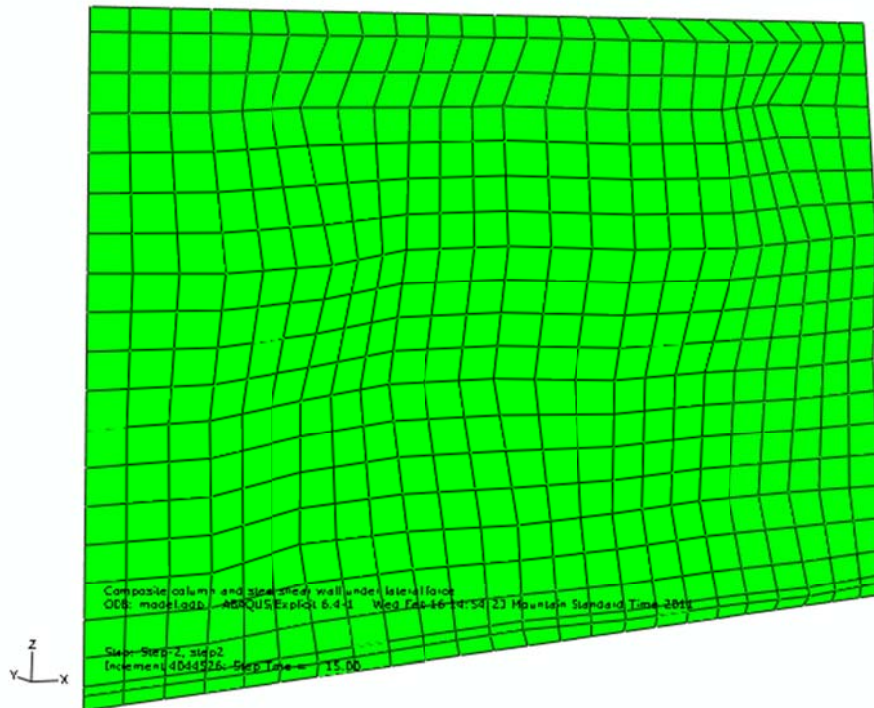
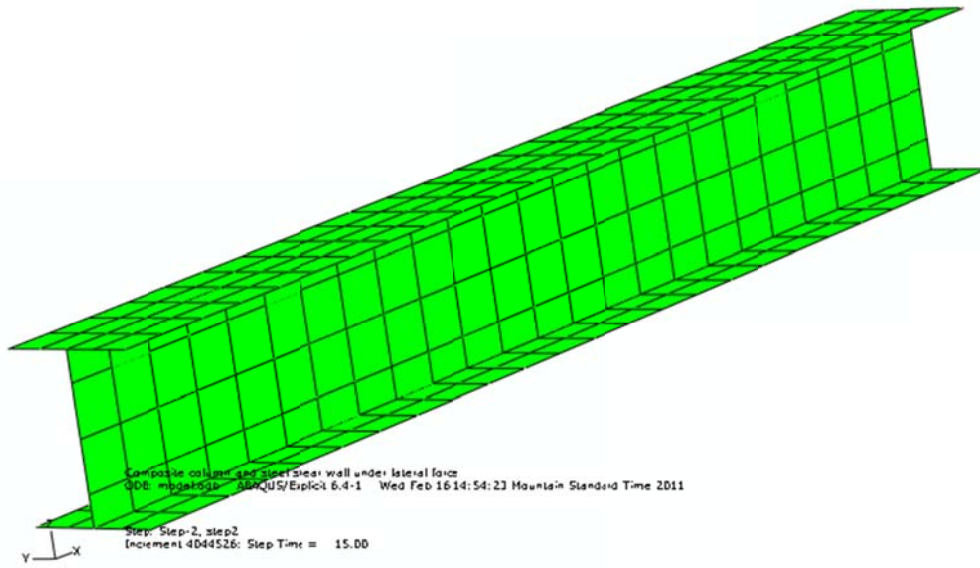


Figure 6-6: Meshes of Infill Panels (Out-of-Plane Scale 20)
(a) First Storey; (b) Second Storey

(a)



(b)

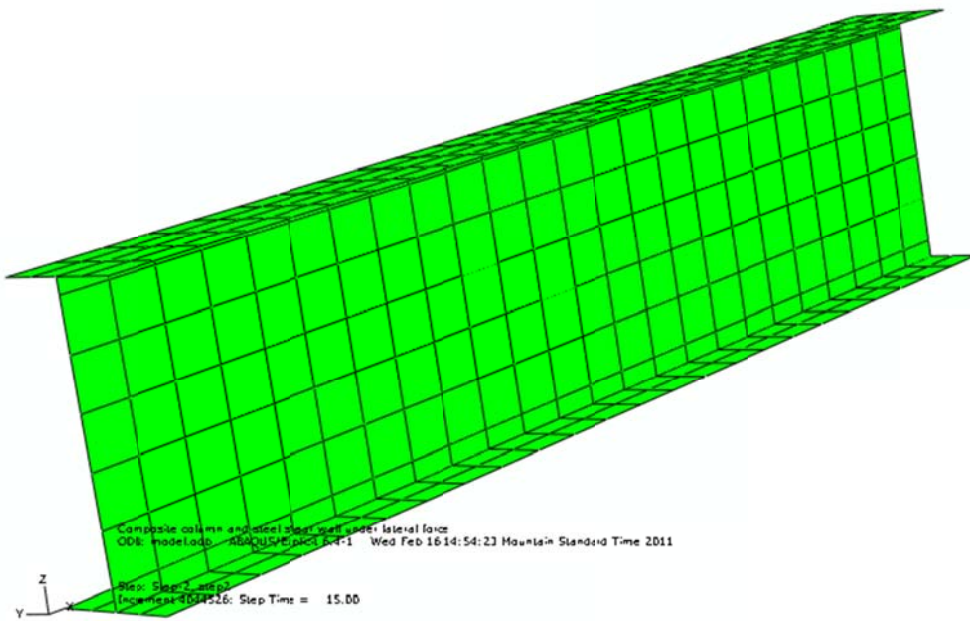


Figure 6-7: Meshes of Frame Beams
(a) First Floor; (b) Second Floor

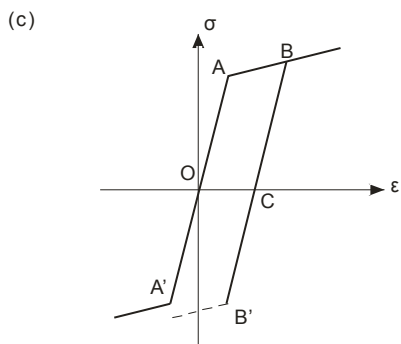
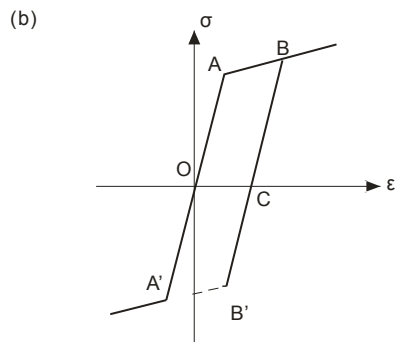
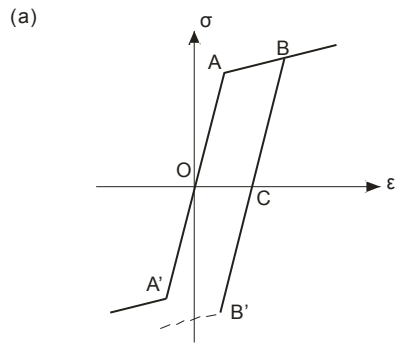


Figure 6-8: Strain Hardening Rules
 (a) Isotropic; (b) Kinematic; (c) Independent

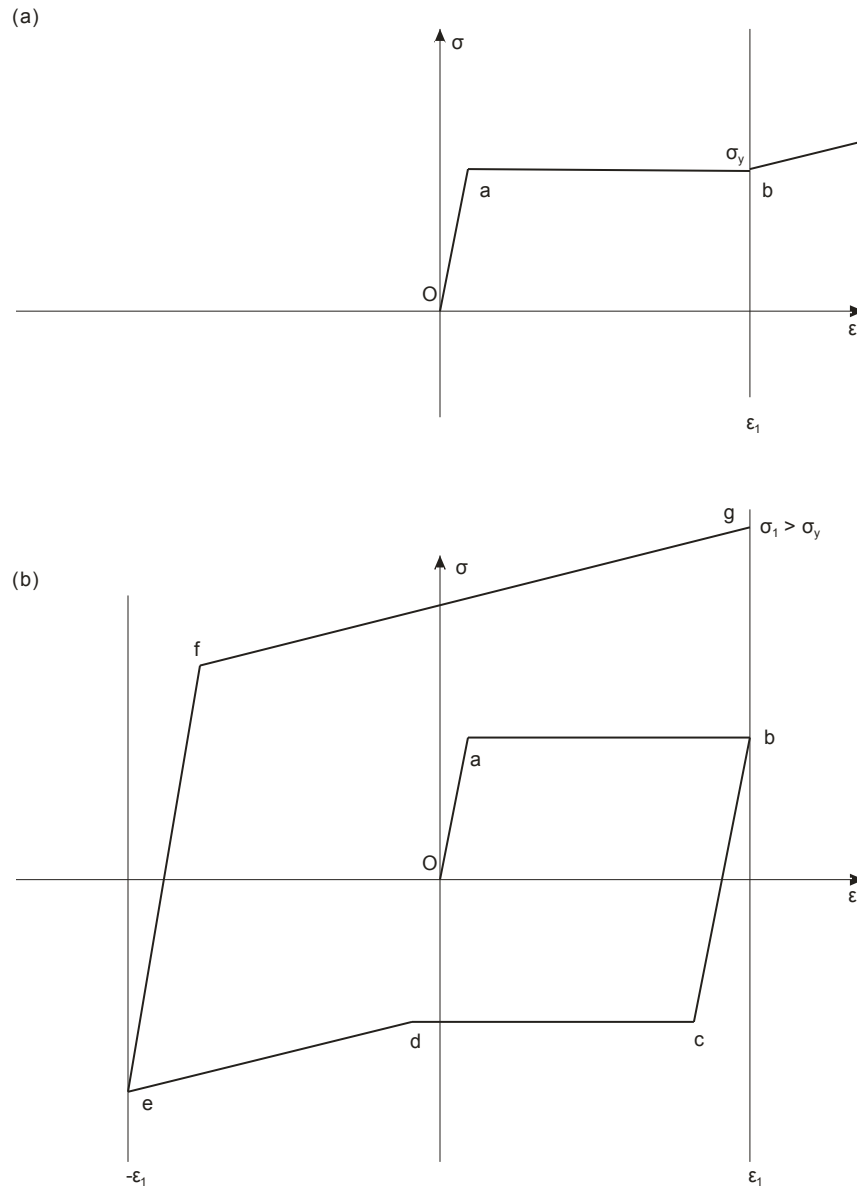


Figure 6-9: Material Curves under Unidirectional and Cyclic Loading
 (a) Unidirectional Loading; (b) Cyclic Loading with Isotropic Hardening

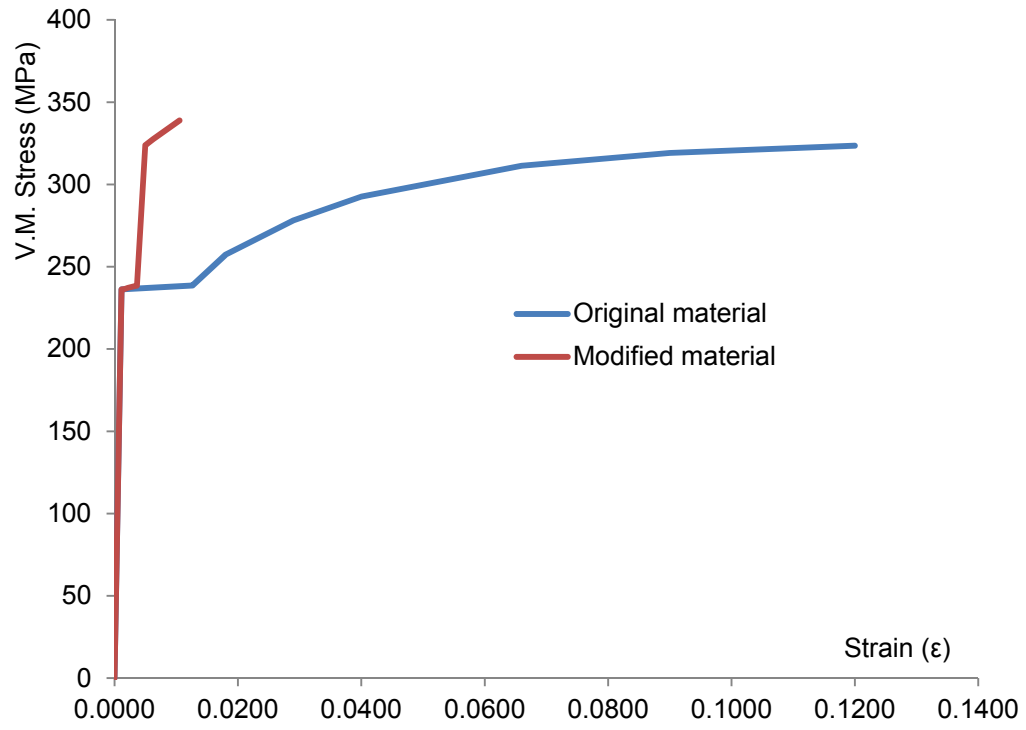


Figure 6-10: Material Curves for First Storey Infill Panel

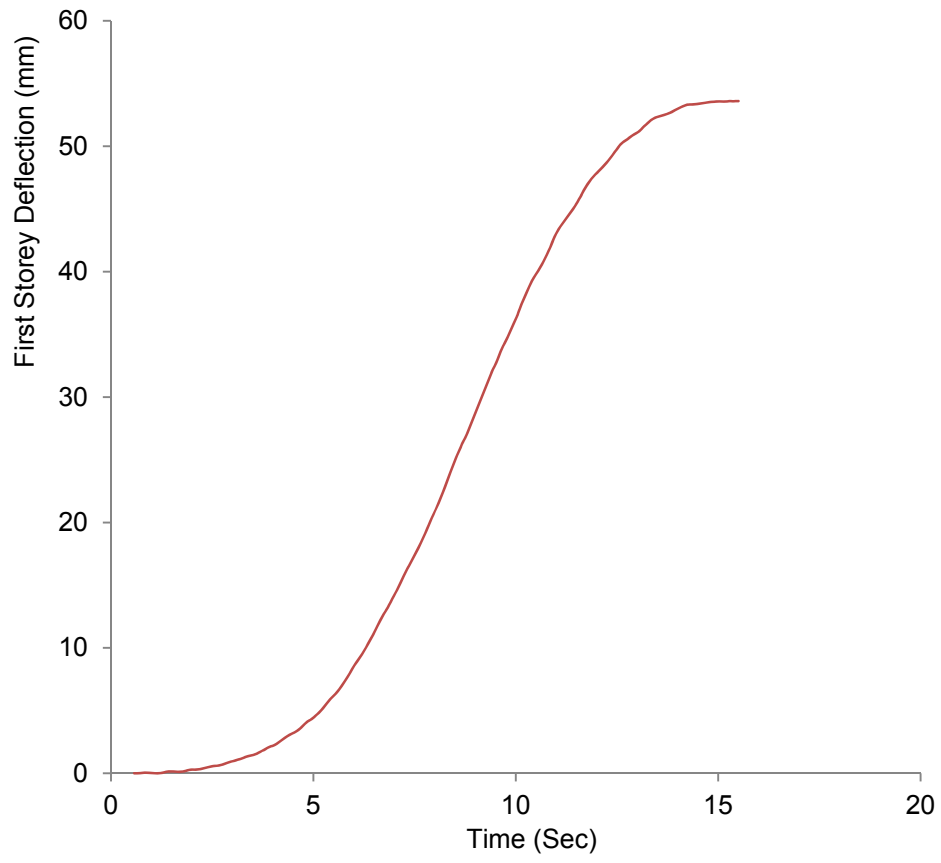


Figure 6-11: History of First Floor Applied Displacement

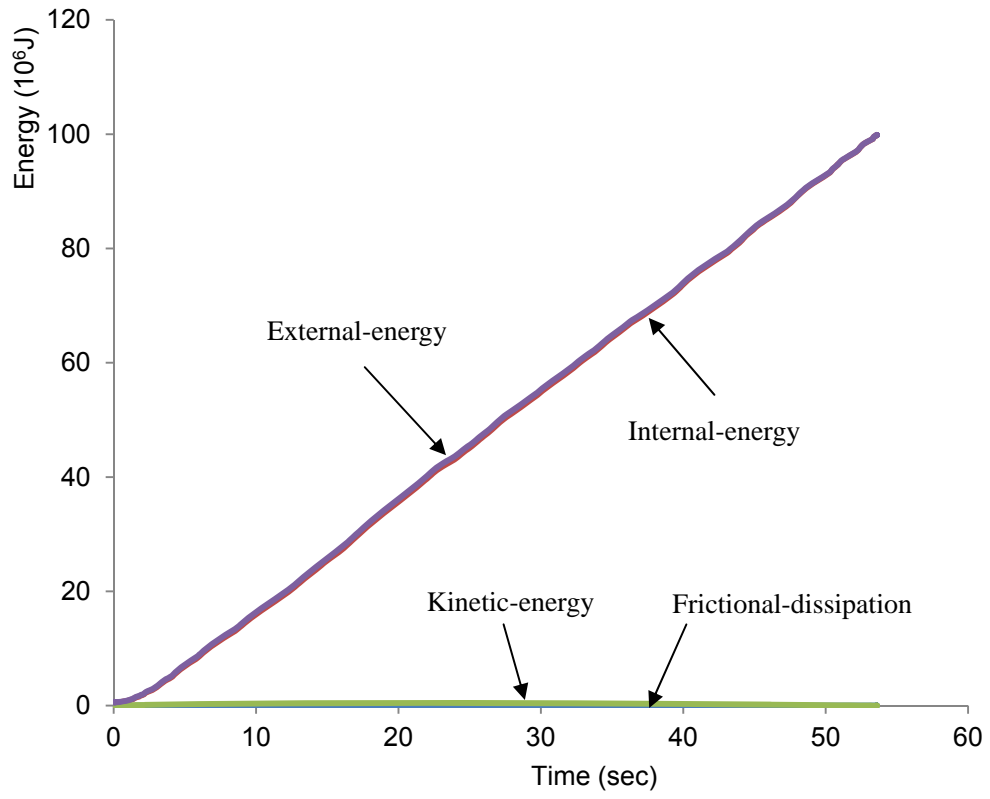


Figure 6-12: Energy History

7. DISCUSSION OF MODEL RESULTS

7.1 Introduction

A finite element model was developed before the specimen was tested and then modified based on observations from the data collected during the test. The model result was compared with the test results, including the behaviour of the infill panel, the PEC columns and the whole specimen, as well as the internal forces in the columns and first storey beam. After the model was verified, it was used to further study the behaviour of the PEC columns.

7.2 Overall Behaviour

The curve of the base shear vs. the first storey deflection in the model using the modified material curves for the bottom infill panel, as discussed in chapter 6, is shown in Figure 7-1, as well as the envelope of the base shear vs. the first storey deflection under cyclic loading in the test. The two curves have similar elastic stiffnesses and similar nonlinear curves until the first storey deflection reached about 21 mm (equivalent to cycle 16). Under cyclic loading, inelastic behaviour occurred in the specimen even at very early stages, such as inelastic buckling in the first storey infill panel and concrete cracking. The inelastic behaviour caused the stiffness to drop slightly in the specimen even at a low load level, which led to the difference in the stiffness between the model and the test. The effective stiffness of the specimen, determined as the slope of the straight line connecting the origin to the point on the curve corresponding to 75% of the yield strength (1380 kN, as discussed in Chapter 5), was 154 kN/mm for the test specimen, while the effective stiffness of the model was 168 kN/mm, which is 9% higher than the test result. As shown in Figure 7-1, the ultimate capacity of the specimen was 1817 kN at a first storey deflection of 35 mm, while the ultimate capacity of the model was 1670 kN, which is 8% lower than the test result.

In the test, the first storey infill panel buckled into one wave (i.e., one full wavelength) in the first three cycles (to reach a base shear of 316 kN), and buckled into two waves during cycles 4 to 6 (to reach a base shear of 632 kN). The plate then buckled into three waves starting from cycle 7 (first cycle to reach a base shear of 948 kN) until the last cycle in the test. Similar to the test, the first floor infill panel buckled into one wave around a base shear of 319 kN, two waves around a base shear of 572 kN, and three waves around a base shear of 848 kN until the end. As shown in Figure 7-2, the specimen was pushed towards the north and the north column was in compression, while the south column was in tension due to overturning. The three-wave buckling of the plate is shown in Figure 7-2, which is the deformed shape of the specimen at the end of the loading in the model ($P = 1690$ kN). The three-wave buckling of the plate is also shown in Figure 7-3, which is the residual deformed shape of the specimen after the test was complete because there was no clear view of the whole specimen during the test due to the existence of the gravity load simulators used at both sides of the specimen. In the model, double curvature was observed in both columns, with the point of contraflexure located at a higher position in the compression column than the tension column (the compression column or the tension column herein means the column in compression or tension due to overturning under lateral loads). A similar characteristic was also shown in the deformed shape of the columns in the test. Compared with the deformation in the first storey infill panel and columns, the bottom beam had minor deformation in both the model and the test.

7.3 Infill Panels

Since the strain rosettes were mounted to the first storey infill panel only at three nodes, the data was not enough to be compared with the stresses distributed in the panel in the model and the camera data was used instead. The camera system was used to record the strains of the first storey infill panel during the test on the west surface in the north bottom corner. A grid of 5 x 5 points inside of the recording region of the camera system were chosen and the stresses at those 25 points were calculated based on the strain history

and isotropic hardening rule. To clearly and simply express the result, the average value of the envelope of von Mises stresses at the 25 points under cyclic loading from the camera data is shown in Figure 7-4. The average value of von Mises stresses in the model at 25 nodes corresponding to those points in the camera data is also shown in Figure 7-4. The stress curve of the camera data exceeds the yield strength, confirming that strain hardening did occur in the first storey infill panel during the test. The stress curve of the model data using the modified material curve was able to simulate the strain hardening in the first storey infill panel. Although the data from the camera system was recorded only at one side of the first floor infill panel, not the middle surface, the average value of the data at 25 points reflected the situation in the middle surface to some degree.

The difference between the maximum and minimum von Mises stresses of the chosen 25 points inside of the camera region in the test and in the model are shown in Figure 7-5. The stresses were non-uniform at the early stage of the test before the tension field was developed completely. The stresses became much more uniform after the panel started to yield and then became less uniform again once strain hardening occurred. The difference between the two curves proves the stresses in the first storey infill panel were more non-uniform in the model than in the test due to the short yield plateau in the modified material curve used in the model, which was discussed in Chapter 6.

To study the anchorage stresses transferred from the first storey infill panel into the columns, the average values of the element stresses in the panel near the south column over the panel height are shown in Figure 7-6 and identified as “south edge”, while the average values of the element stresses in the panel near the north column are identified as “north edge”. The average values of the normal stresses, S_{11} , in both the south and north edges were positive, which means that both columns were pulled towards the infill panel based on the sign definition of S_{11} . The difference between the stresses indicates that the south column was pulled more severely than the north column, which explains why the south column was bent towards the panel more than the north column, as shown

in Figure 7-2. Also shown in Figure 7-6, the average values of the shear stresses, S_{12} , on both the south edge and the north edge were positive, too, which indicates that the south column was pulled up while the north column was pulled down. The positive sign of the shear stresses shows the anchorage stresses contributed tension into the south column and compression into the north column, which caused the compressive force in the south column to decrease from the top to the bottom of the column, but it increased in the north column. Considering the combination of the normal stresses, S_{11} , and shear stresses, S_{12} , the direction of the diagonal anchorage stresses from the panel was identical to the tension field theory of the steel plate shear wall system. Although the shear stresses, S_{12} , in the south edge and north edge were similar, the normal stresses, S_{11} , in the south edge were larger than the north edge, which led to larger principal stresses, SP_1 , in the south edge than the north edge. In the model, the tension field in the panel was not completely uniform.

The test data from the strain rosettes attached to the second storey infill panel were analyzed and the vertical anchorage stresses at the peak of cycle 4 (first cycle to reach a base shear of 632 kN), cycle 7 (first cycle to reach a base shear of 948 kN) and cycle 10 (first cycle to reach a first floor deflection of 7 mm) when the specimen was pushed towards the north are shown in Figure 7-7. The normal stresses of the elements in the second storey infill panel near the top beam in the model at the same first floor deflection are shown in Figure 7-7 as well. Positive stresses at the middle of the top beam and negative stresses at the ends of the top beam indicates that the stresses from the second storey infill panel were pulling the top beam down at the middle, but tended to push the top beam up at the ends, which was considered as a local effect. It is also shown in Figure 7-7 that the top beam was pulled down over a longer range along the beam length when larger lateral loads were applied.

7.4 PEC Columns

7.4.1 Internal Force Distribution

Based on the strain gauge data, the axial forces in the south and north columns at the peak of cycle 4, cycle 7 and cycle 10, when the specimen was pushed towards the north, are shown in Figure 7-8 and Figure 7-9, while the corresponding bending moments in the south and north columns are shown in Figure 7-10 and Figure 7-11, respectively. The model results at the same first floor deflection are also shown in the figures.

It is shown in Figure 7-8 and Figure 7-9 that the axial compressive forces decreased from the top to the bottom of the south column and increased in the north column due to the shear stresses transferred from the panel (shown in Figure 7-6). As the lateral loads increased, the axial compressive forces decreased in the south column and increased in the north column due to the overturning moment. In general, the model predicts the column axial forces well. The moments in the columns are defined as positive when the south flange was in compression and the north flange was in tension. The moments in Figure 7-10 and Figure 7-11 show that the south flange in both columns was in tension at the bottom of the columns, while the north flange in both columns was in tension at the top of the columns, similar to a moment-resisting frame. However, the change in the slope of the curves along the column height indicates that both columns were pulled towards the panel by the tension field. Moreover, the more severe bent shape in the middle portion in the south column represents larger horizontal stresses from the panel into the south column than the north column, which was identical to the result shown in Figure 7-6. The model provides good predictions of the moments in the columns.

Although many features shown in the test data were also shown in the model data, there are some differences caused mainly by the invalidity of some strain gauge readings. In the test, strain gauges were mounted to the outside and inside of the column flanges, so the average value of the strain gauges could be treated as the mid-surface strain in the

flanges. However, some of the strain gauges on the inside of the flanges (on the concreted side) were not working properly and were not used when the stresses of the flanges were calculated, potentially affecting the accuracy of the test values that were compared against the model. This is likely the main reason for the differences between the axial compressive forces in the north column observed in the model and those obtained from the test data. The differences between the internal forces in the columns obtained from the model and the test were also affected by the difference in the stress distribution in the panel between the model and the test due to the difference between the monotonic loading with the modified material curve and the cyclic loading with the original material curve.

When the lateral loads increased, the compressive forces in the north column increased too due to the overturning moment and the diagonal tension forces from the infill panel. As a result, the encased concrete expanded more under larger compression and the column flanges bent outwards between links. The flanges at the link position tended to bend with the outside of the flanges in compression and the inside in tension, as shown in Figure 7-12. The compressive stresses at the middle surface of the column flange calculated based on the remaining strain gauge data would be larger than the real values in the test and the corresponding axial compressive forces in the columns would be larger, too, which led to the differences of the axial forces at the level 2 (890 mm above the column base) of the north column between the model and test. Moreover, as the compressive forces in the north column increased due to overturning at larger lateral loading, the differences of the axial forces between the model and test increased too as shown in Figure 7-9. As mentioned in Chapter 4, strain gauges were mounted to the first storey columns at level 1 (530 mm above the column base), level 2 (890 mm above the column base) and level 3 (1290 mm above the column base).

As mentioned in Chapter 3, the out-of-plumb of the north column was detected as an imperfection and would cause out-of-plane bending under vertical loads. The axial

compression transferred from the panel also increased the bending moments in the north column, which contributed compressive stresses at the west side of the column flange. The discarding of the strain gauge data at the east side of the column flange led to differences between the axial compressive forces in the north column from the model and those from the test. Moreover, larger lateral loads caused larger compressive forces due to overturning, and larger out-of-plane bending due to the out-of-plumb, and then led to larger compressive forces in the north column in the test data than the model results, especially at level 1, as shown in Figure 7-9.

7.4.2 P-M Diagram

To further study the behaviour of the PEC columns in the specimen, the P-M diagram for the columns was derived. The strains in the column were determined according to the assumption that plane sections remain plane under bending, which meant the concrete had the same strain as the steel at the same column depth. The strain at one end of the web was equal to the concrete crushing strain, ϵ_{cu} , while the strain at the other end of the web was equal to $\epsilon_s = k\epsilon_{sy}$, in which ϵ_s is the strain in the steel, ϵ_{sy} is the steel yielding strain and k is a factor with various values leading to different values of axial forces and bending moments. To facilitate the calculation, the steel section was divided into 12 sections, including two flanges and 10 equal web sections along the column depth, as shown in Figure 7-13. The stresses in the column steel section were calculated in each column flange and each section of the web individually. The effective column flange width was used for the flange in compression, considering the slender flange elements. The compressive force in the column concrete portion was calculated according to CSA A23.3-04, while the tensile force of the concrete was taken as zero. The axial forces and bending moments in the column were then calculated as the sum of all 12 steel portions and the concrete compression block. The ultimate compressive capacity of the column was also calculated and treated as an upper limit.

The internal forces in the first storey columns right above the bottom side plate and right below the top side plate during the lateral loading until the first floor deflection reached 35 mm in the model are shown in Figure 7-14, as well as the P-M diagram of the columns. Once the internal forces at the bottom of the north column reached the envelope of the P-M diagram at a first floor deflection of 21 mm, the internal forces at the top and the bottom of the north column, as well as the bottom of the south column, remained relatively constant but the internal forces at the top of the south column kept increasing. When the internal forces at the bottom of the north column reached the envelope of the P-M diagram, the capacity of the specimen stopped increasing.

The internal forces in the columns from the test result, based on the strain gauge data during the lateral loading until the first floor deflection reached 35 mm, are shown in Figure 7-15. The corresponding internal forces in the model are also shown in Figure 7-15, as well as the P-M diagram of the columns. The internal forces in the columns from the model and the test were close until the first floor deflection reached 21 mm, except the internal forces at level 1 (see Figure 7-15) in the north column, in which the test values were always slightly higher than the model values. The reason for the difference between the model and test in the north column were explained in section 7.4.1. In the south column, the internal forces at level 1 remained fairly constant, while the internal forces at level 3 kept increasing in both the model and the test after the first floor deflection reached 21 mm. In the north column, the internal forces in the model diverged from the internal forces at level 1 in the test, with the test values eventually exceeding the envelope of the P-M diagram. This appears to be caused by the presence of strain hardening, which was detected in the calculated stresses at level 1 in the north column flange based on the strain history from the strain gauge data and the isotropic hardening rule. The strain hardening in the north column in the test may also explain why the ultimate capacity of the test specimen was larger than that of the model, in which strain hardening in the panel was simulated, but strain hardening in the column was not.

7.4.3 Yield Deflection

In the system of steel plate shear walls with PEC columns, yielding occurs in the infill plate first and, and then the plastic hinges in the columns start to form. As an important fuse of the system, plastic hinges in the columns should be considered when considering the yielding of the whole system. Hence, the yielding in the columns was treated as a sign of the significant yielding in the system. Since the strain gauges were mounted to the columns at the locations away from the potential plastic hinge zones to avoid early failure of the strain gauges due to yielding, the initiation of the yielding in the columns could not be recorded. Moreover, the paint on the specimen made the direct observation of yielding signs impossible. Since the overall capacity of the model matched that of the test specimen up to the first floor deflection of 21 mm, and the internal forces in the columns in the model were acceptable compared with the test results, the model was used to determine the yield deflection. The maximum stresses in the column flanges at the most critical position inside of each plastic hinge zone are shown in Figure 7-16. Based on the model results, yielding occurred in three out of four potential hinges in the columns at a first floor deflection of about 12.8 mm and the corresponding yield strength of the specimen was about 1380 kN. After the yield strength of the specimen was determined, 75% of the yield strength was then calculated and the effective stiffness was determined based on the straight line from the origin to the point corresponding to 75% of the yield strength. The yield deflection was then determined as 9 mm, which is the intersection point of the effective stiffness line and the yield strength line, as shown in Figure 7-17. This yield deflection based on the refined model and observations from the test is slightly higher than the value of 7 mm used to conduct the test.

7.5 Internal Force Distribution in the Bottom Beam

The internal forces in the first storey beam are shown in Figure 7-18 and Figure 7-19 and there are some differences between the model and test data, especially in the axial forces.

As mentioned before, lateral loads were applied by the lateral loading system to the top flange of the beam at each floor to avoid local failure of the PEC column that could occur if the lateral loads were applied directly to the column. The lateral loading system was connected to the beam through slip-resistant connections and the distance between the first and last bolt in the beam top flange was 1800 mm. The lateral load transfer route was simulated in the model, but with the distance of 1642 mm instead of 1800 mm due to the mesh arrangement in the model, which led to differences between the model and test in the slope of the axial force curves, as shown in Figure 7-18. Moreover, unbalanced shear forces from the infill panels below and above the beam would affect the slope of the axial force curves.

The bending moments in the bottom beam in the model and test are shown in Figure 7-19 and the moments are defined as positive when the bottom flange is in tension. The moments are positive near the south end of the beam and negative at the north end of the beam, both in the model and the test, which is similar to the moment distribution in the beam of a steel frame without infill panels, suggesting that there is significant frame action. The shape of the moment diagram is influenced by the unbalanced normal stresses from the infill panels below and above the beam. The Figure 7-19 shows that the unbalanced normal stresses from the infill panels in the model were more severe than in the test, which might be caused by the use of the modified material curve instead of the original material curve for the first storey infill panel.

7.6 Summary

The model results from a push-over finite element analysis were compared with the test results. The base shear vs. first floor deflection curve from the model matched the curve from the test quite well until the first floor deflection reached around 21 mm. The buckling patterns and internal stresses in the infill panel and the internal forces in the columns observed in the test were simulated well in the model. The modified material curve used in

the model was able to simulate the total stresses in the panel under cyclic loading in the test, but with a less uniform distribution than in the test. The internal forces in the columns and beam in the model were close to those in the test, except the axial forces in the north column due to the early failure of some strain gauges. The internal forces in the columns in the model and test were also shown in the P-M diagram of the columns, which showed the effect of strain hardening that occurred in the north column close to the bottom after the first floor deflection reached 21 mm, while no increase in strength was seen in the model. The strain hardening in the north column partly explains the difference between the ultimate capacity of the model and test specimen.

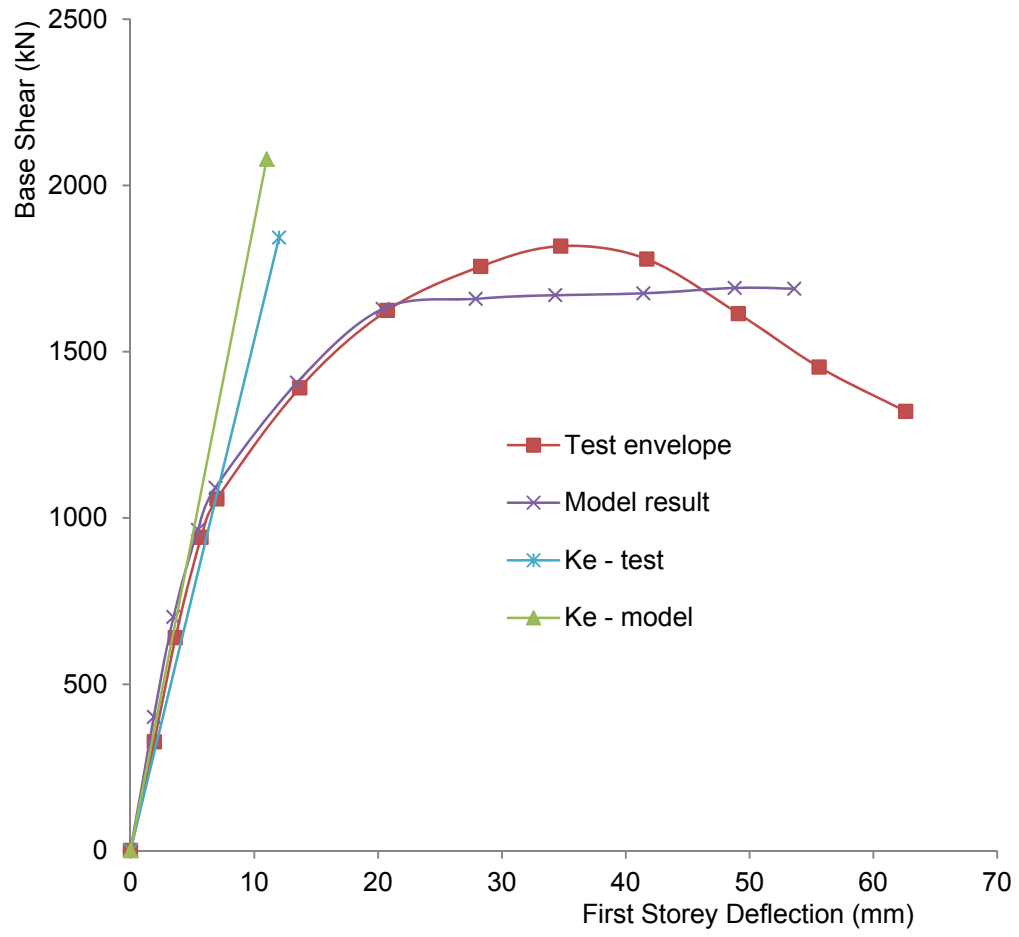


Figure 7-1: Base Shear vs. First Storey Deflection

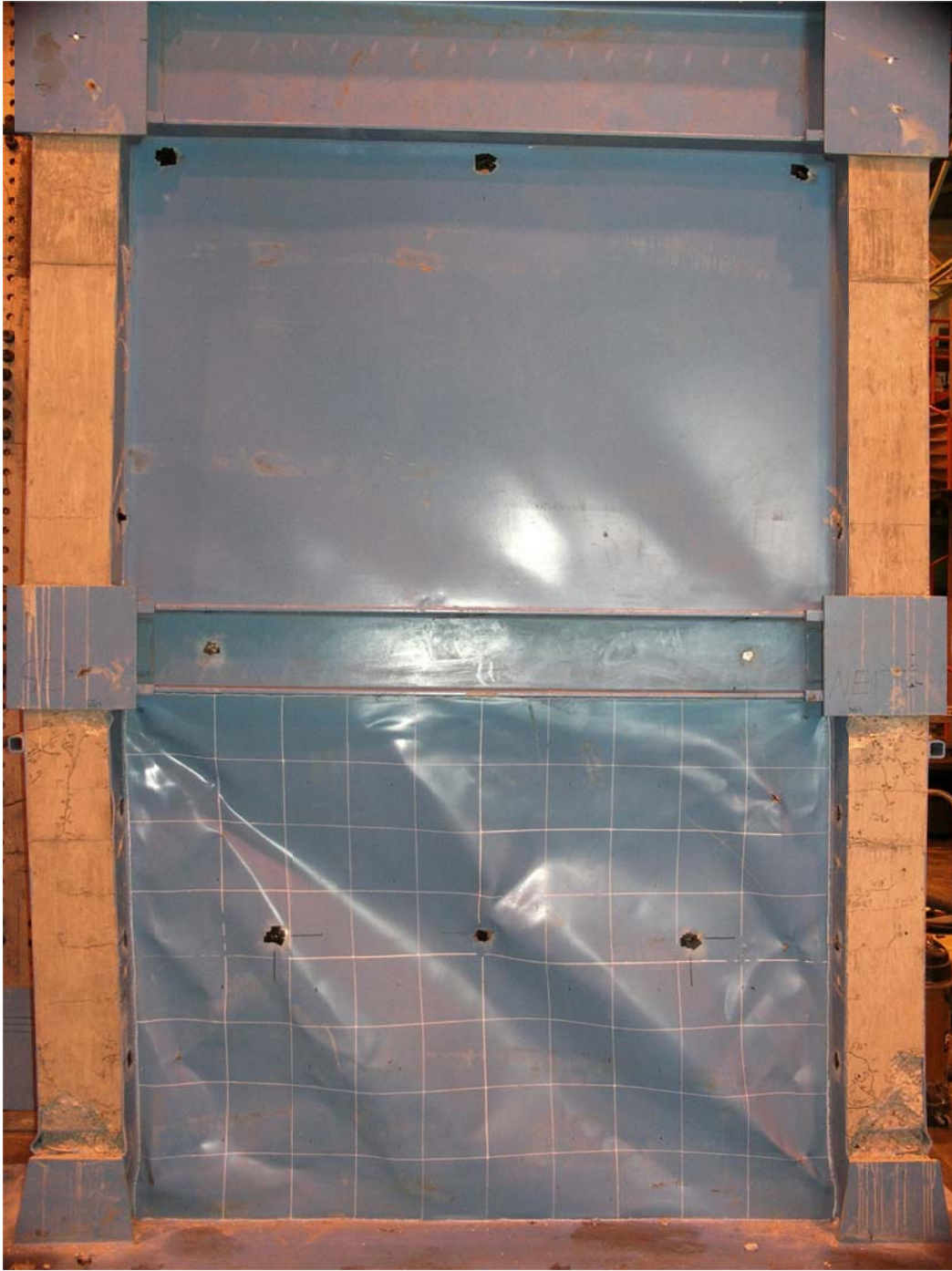


Figure 7-3: Residual Deformed Shape of Test Specimen

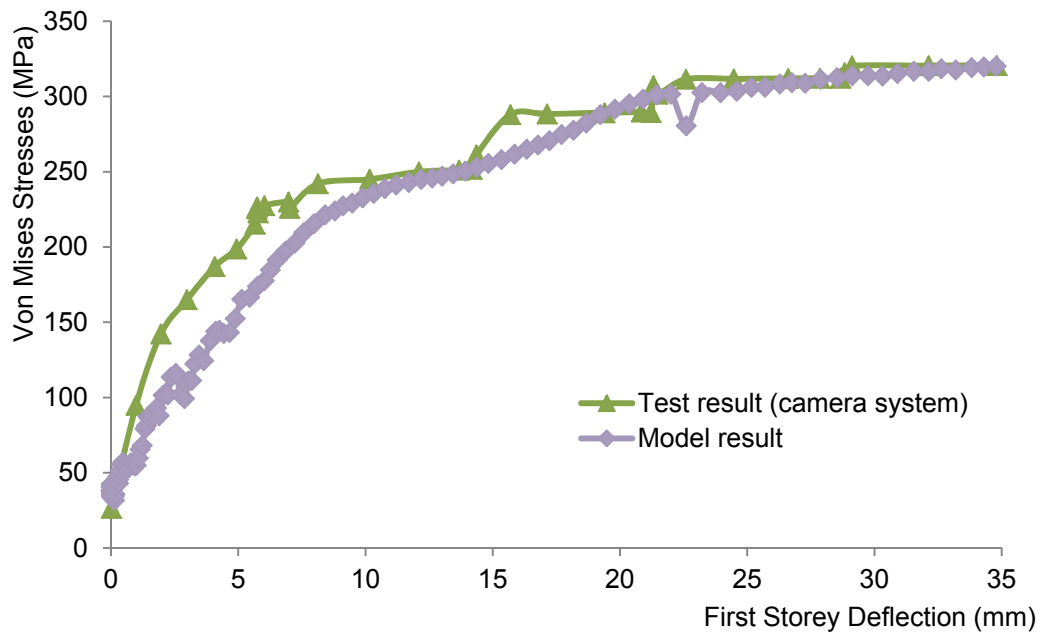


Figure 7-4: Average Value of Von Mises Stresses in North Bottom Corner (West Side) of First Storey Infill Panel

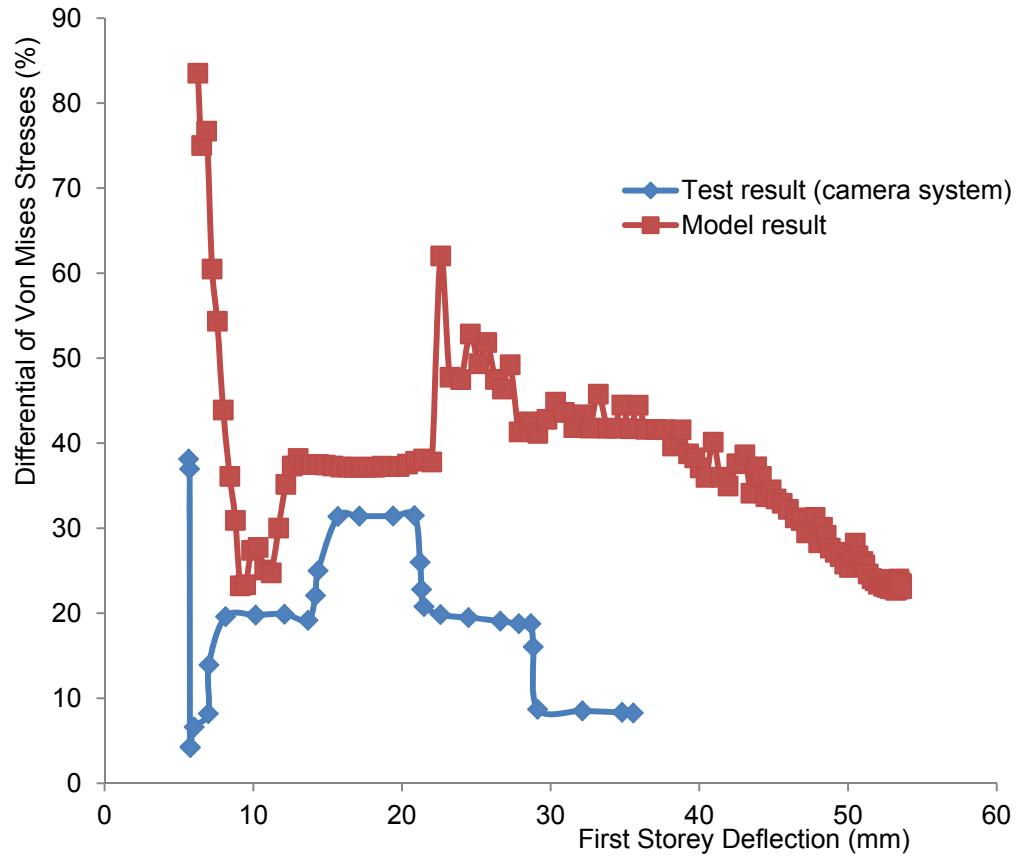


Figure 7-5: Differential of von Mises Stresses in North Bottom Corner (West Side) of First Storey Infill Panel

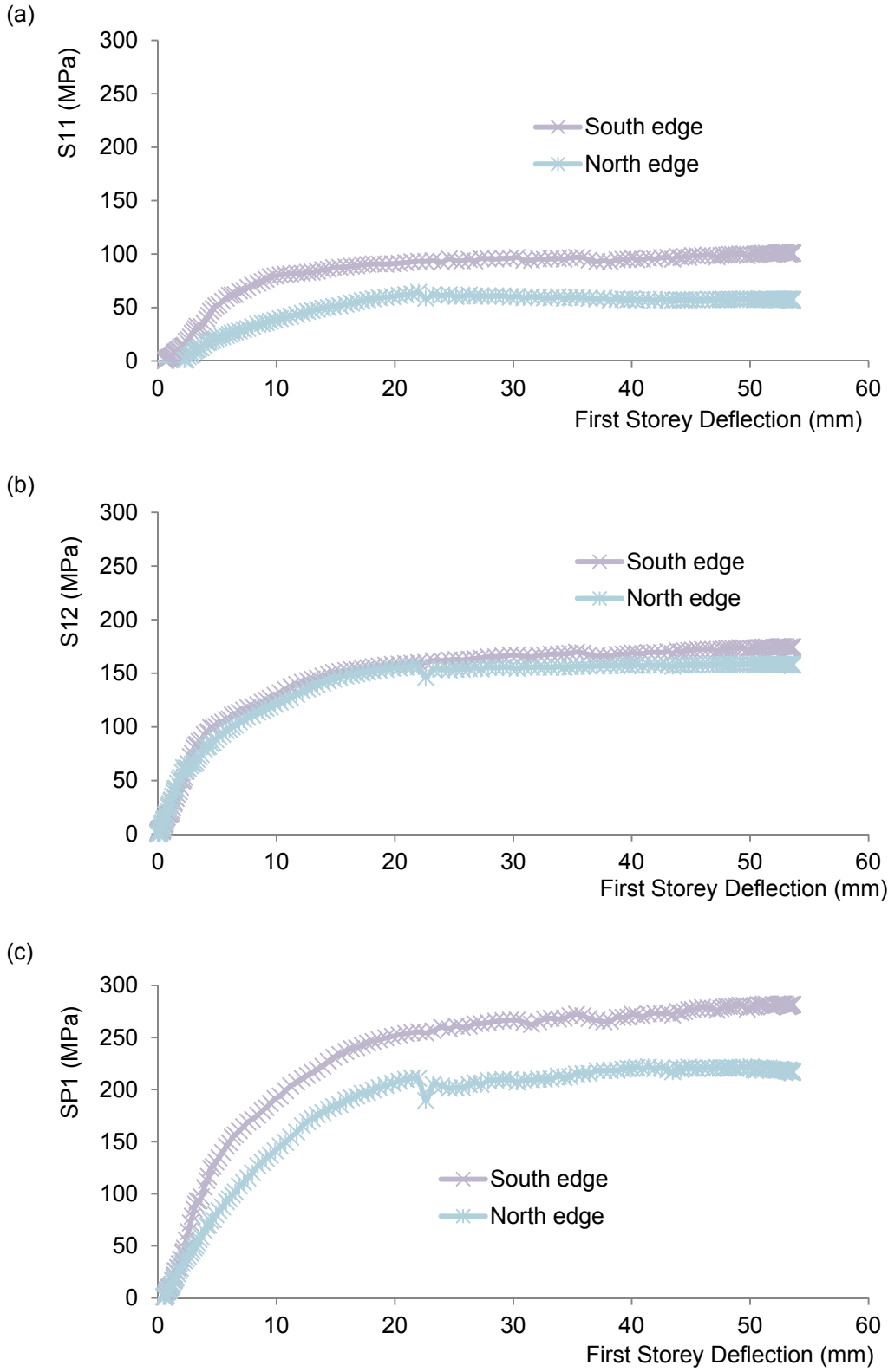


Figure 7-6: Average Stresses in First Storey Infill Panel Near Columns
 (a) S11; (b) S12; (c) SP1

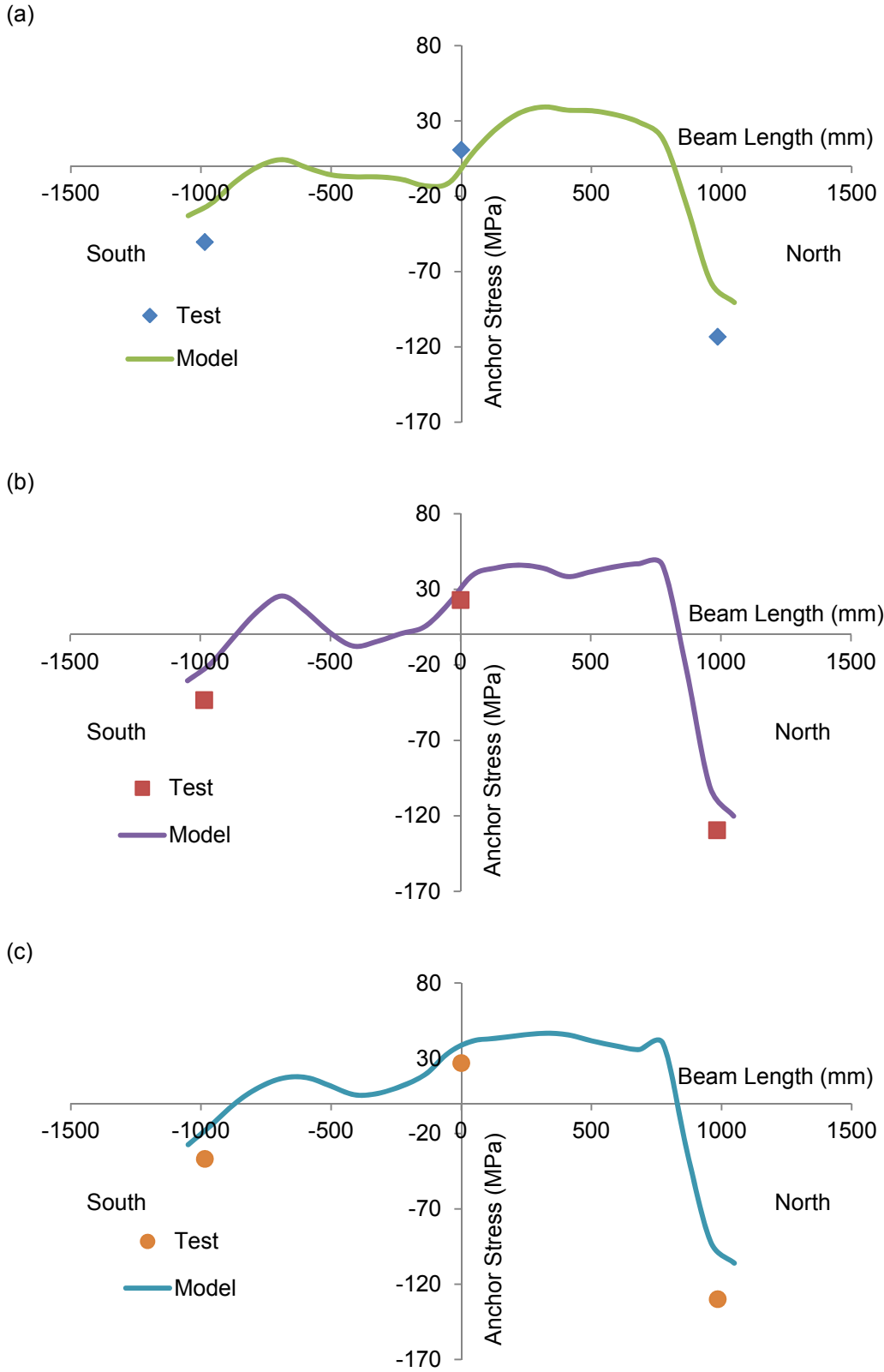


Figure 7-7: Vertical Anchorage Stresses into Top Beam
 (a) Cycle 4; (b) Cycle 7; (c) Cycle 10

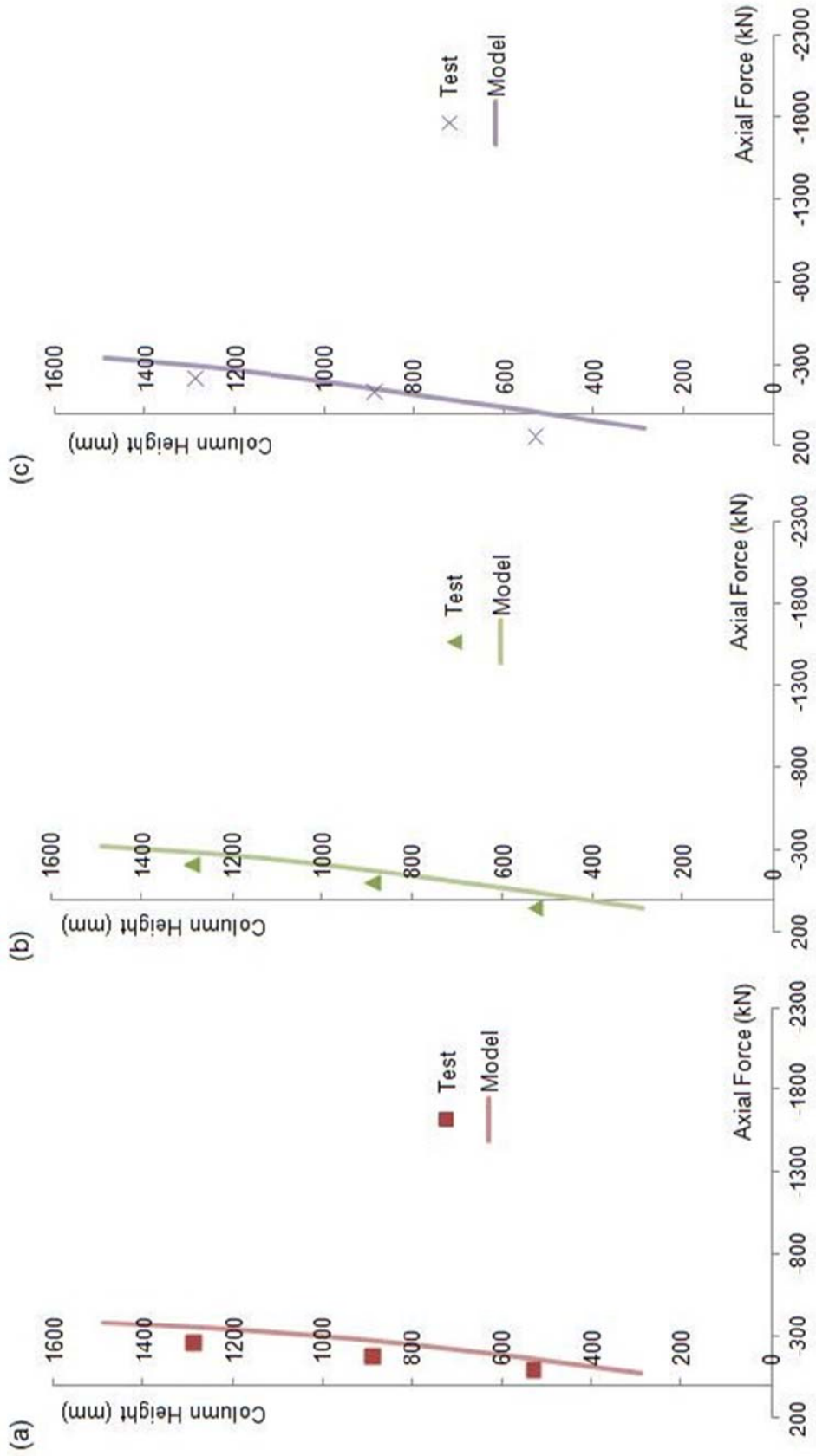


Figure 7-8: Axial Forces in South Column
 (a) Cycle 4; (b) Cycle 7; (c) Cycle 10

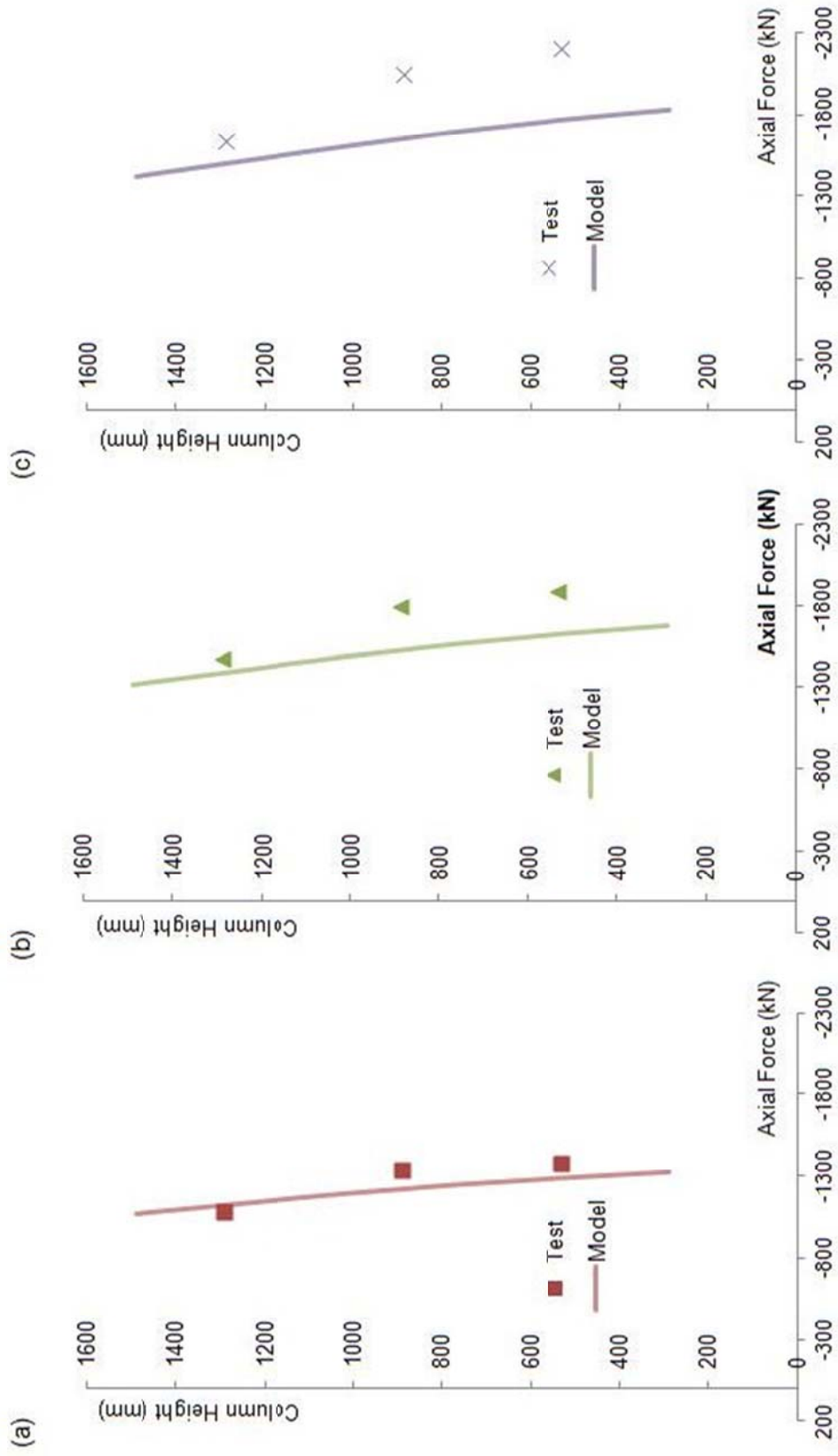


Figure 7-9: Axial Forces in North Column
 (a) Cycle 4; (b) Cycle 7; (c) Cycle 10

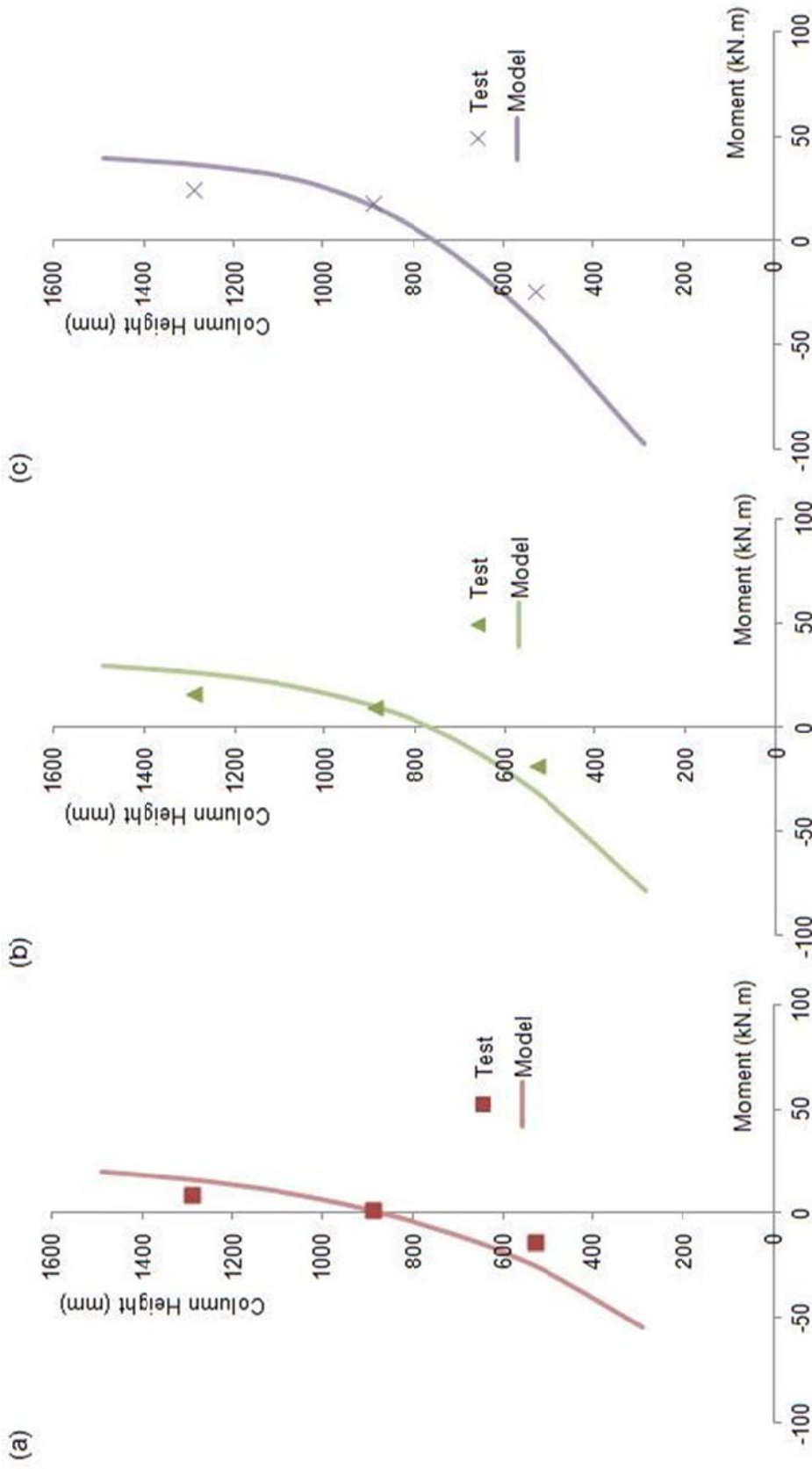


Figure 7-10: Bending Moments in South Column
 (a) Cycle 4; (b) Cycle 7; (c) Cycle 10

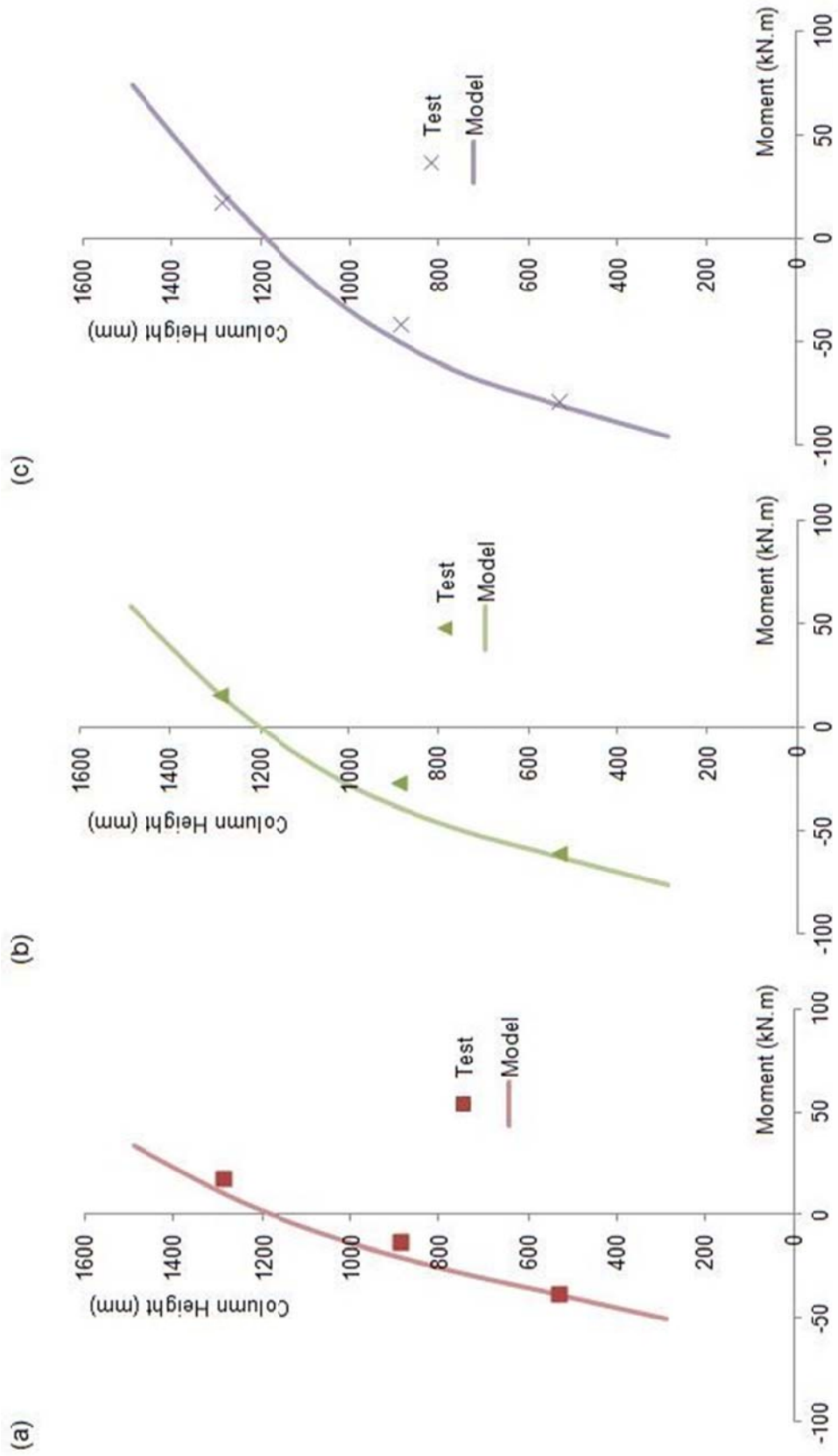


Figure 7-11: Bending Moments in North Column
 (a) Cycle 4; (b) Cycle 7; (c) Cycle 10

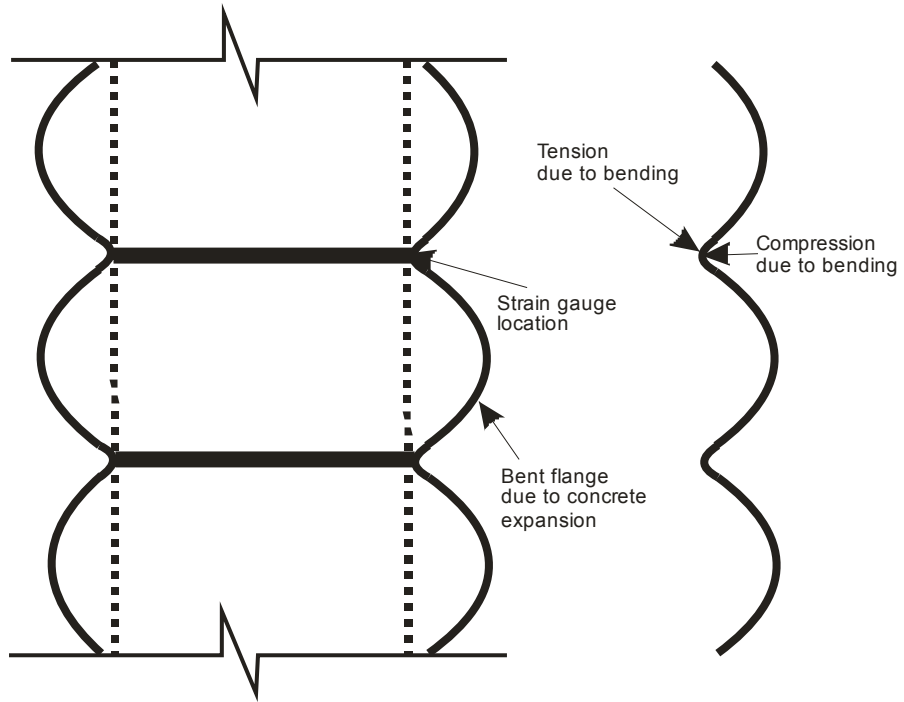


Figure 7-12: Flange Bending between Links due to Concrete Expansion under Compression

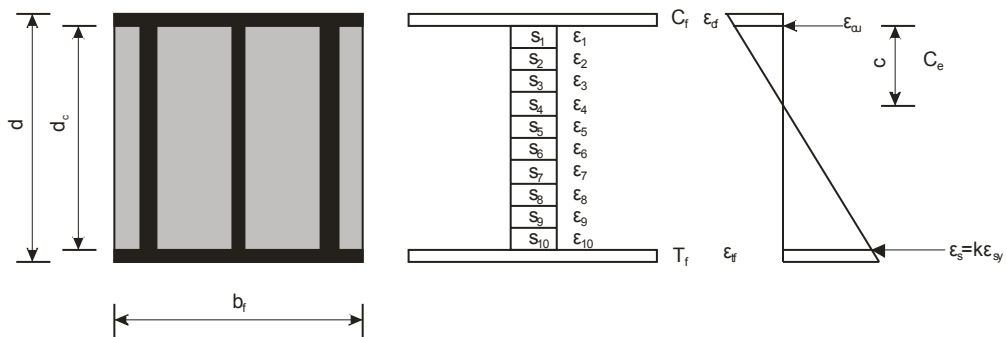


Figure 7-13: Calculation of P-M Diagram of PEC Column

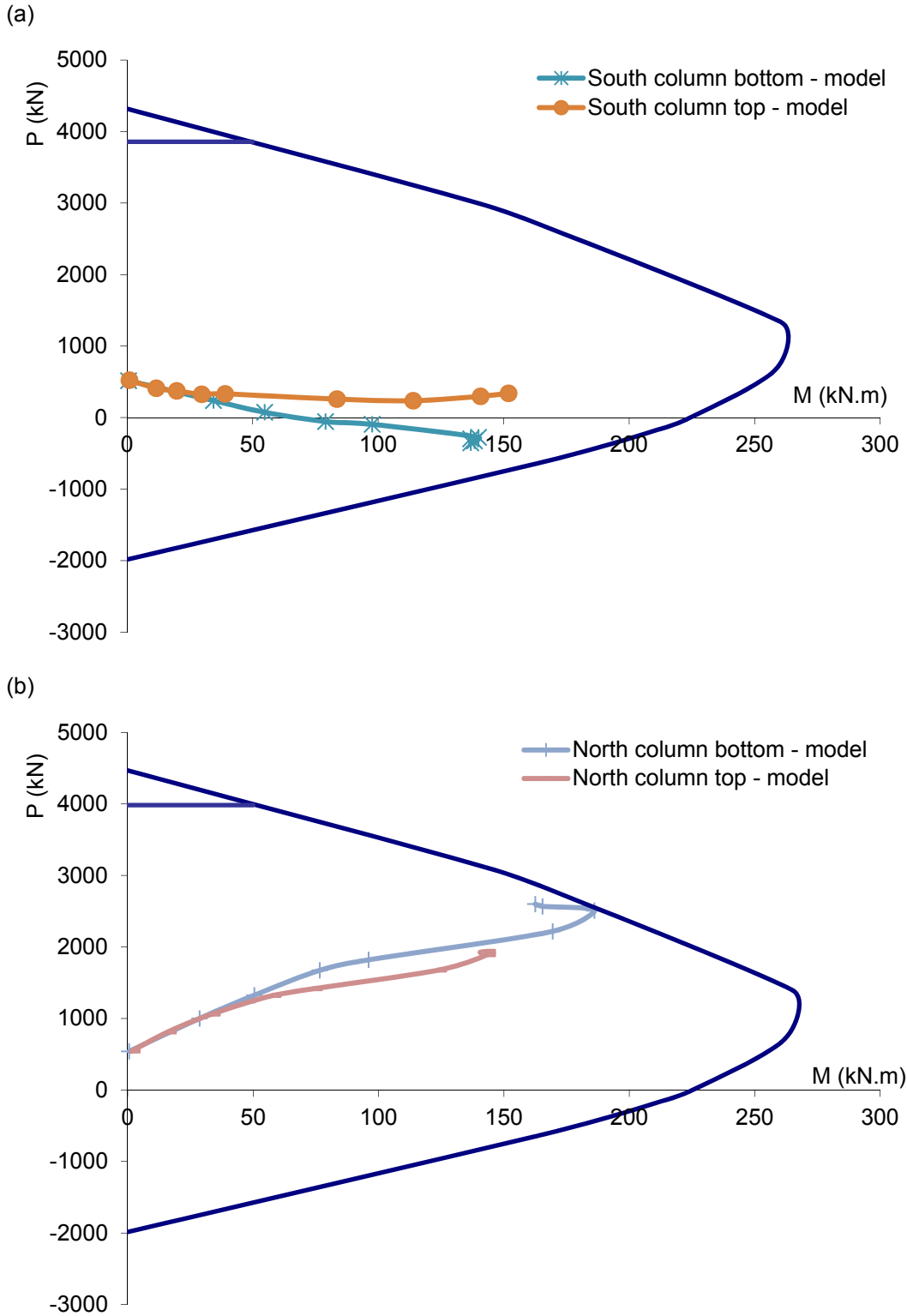


Figure 7-14: Internal Forces at Top and Bottom of Columns in P-M Diagram
(a) South Column; (b) North Column

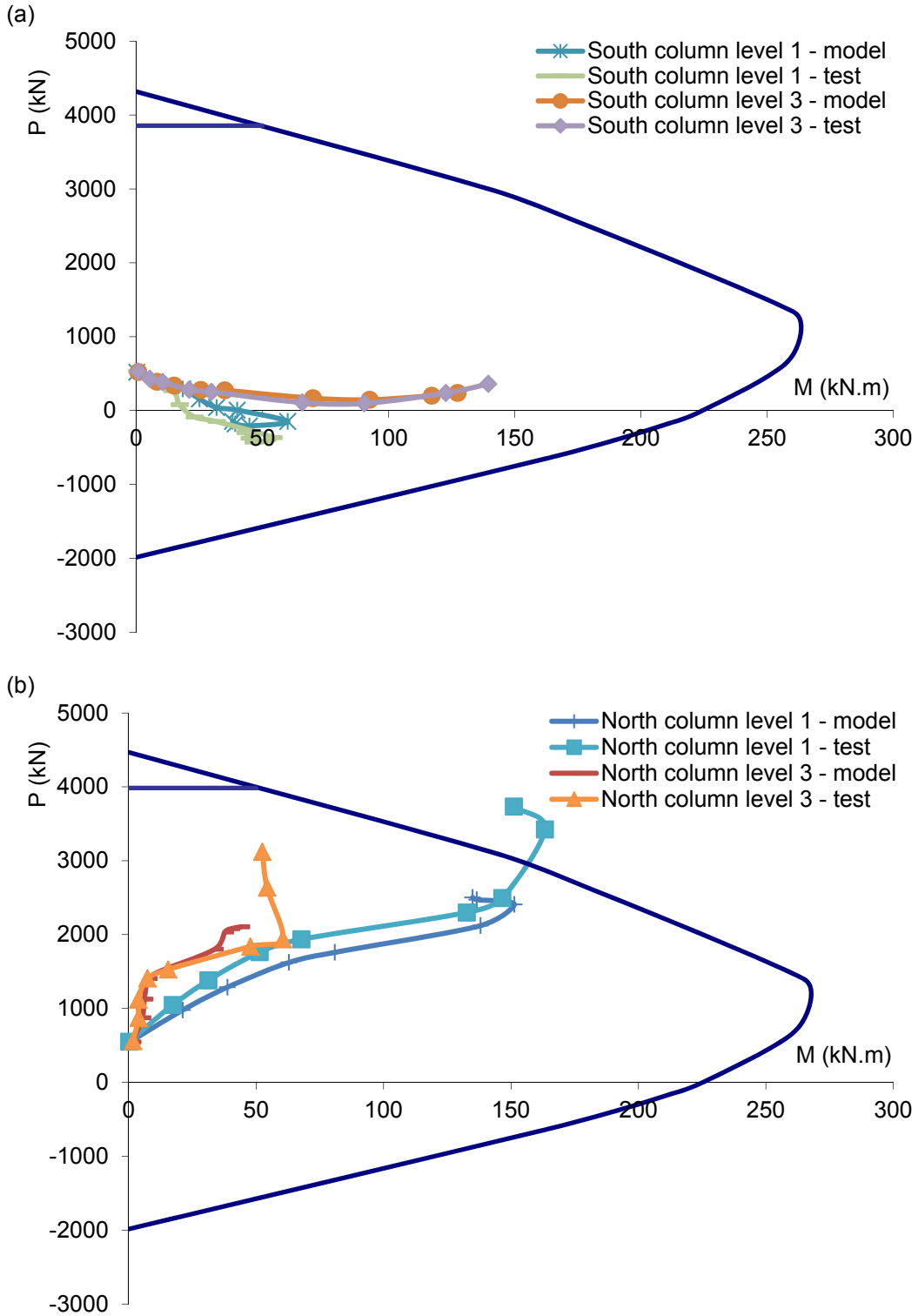


Figure 7-15: Internal Forces at Levels of Strain Gauges in P-M Diagram
 (a) South Column; (b) North Column

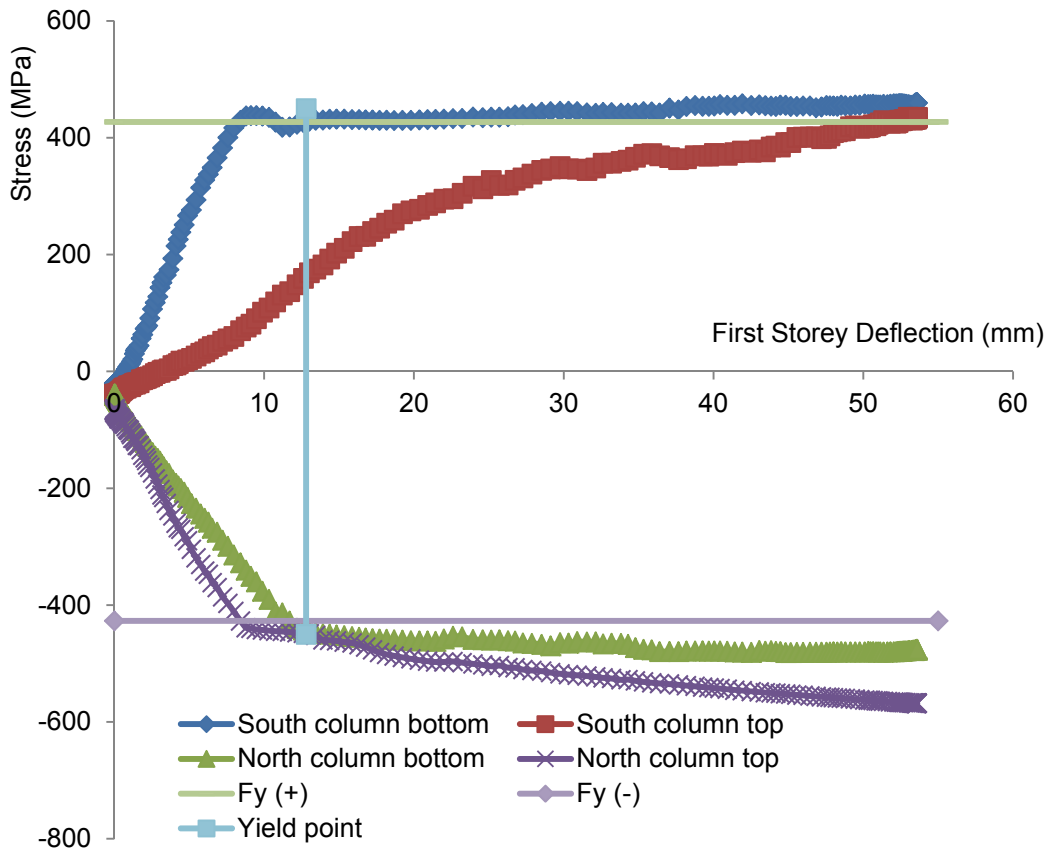


Figure 7-16: Yielding in Critical Column Flanges

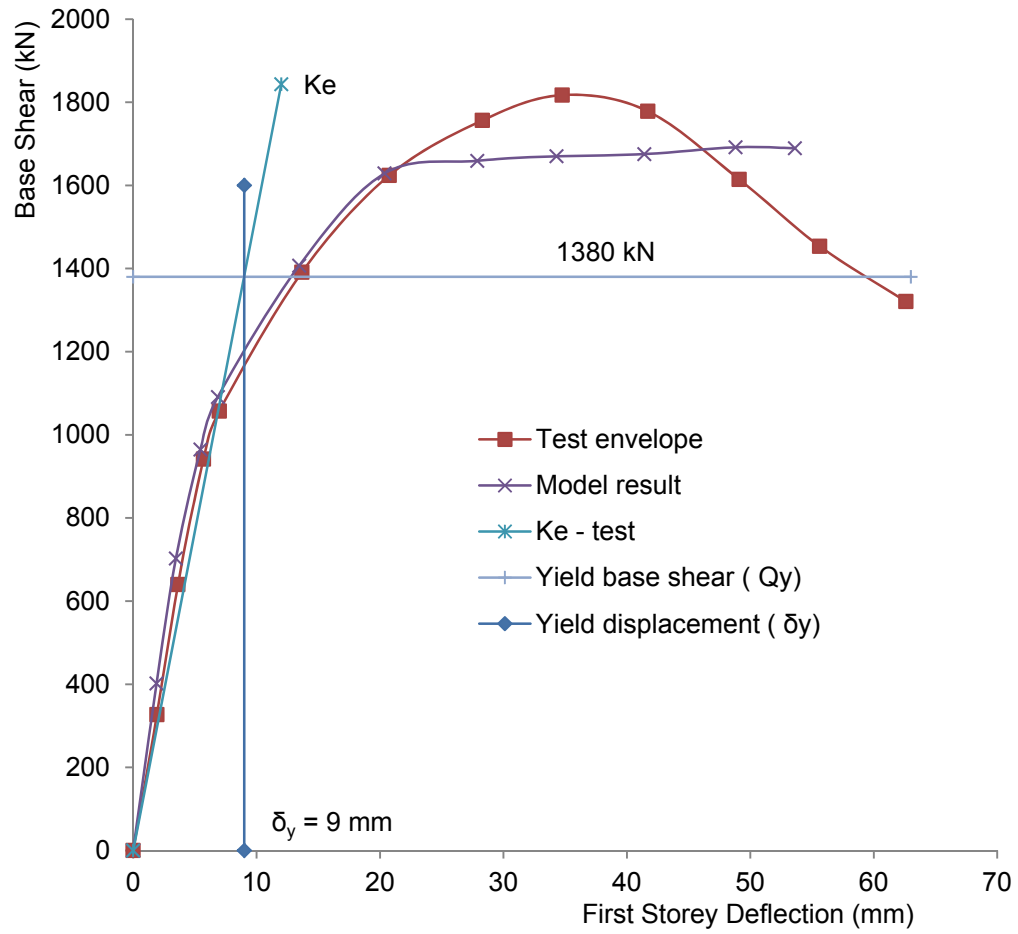


Figure 7-17: Determination of Yield Displacement

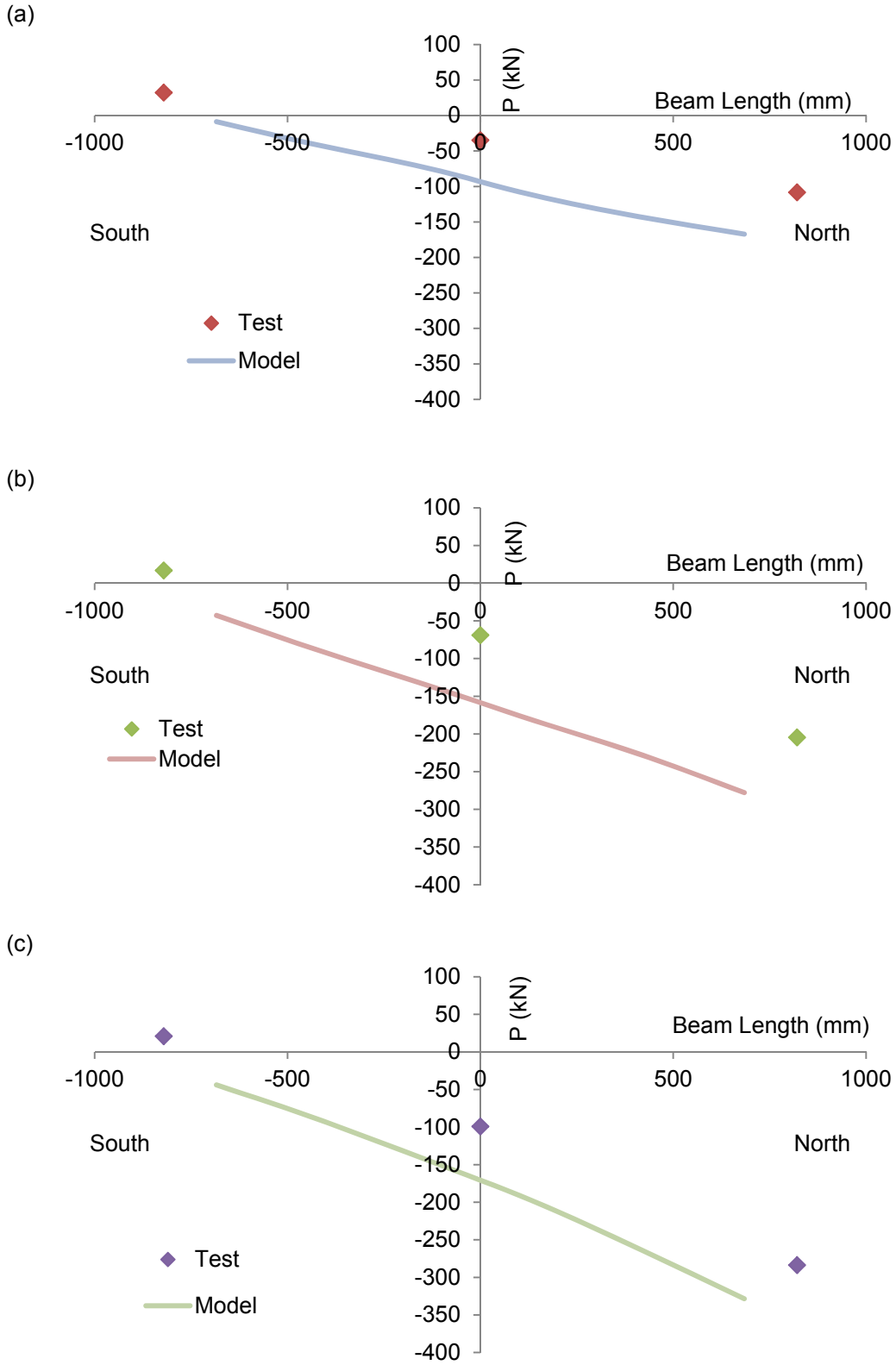


Figure 7-18: Axial Forces in Bottom Beam
(a) Cycle 4; (b) Cycle 7; (c) Cycle 10

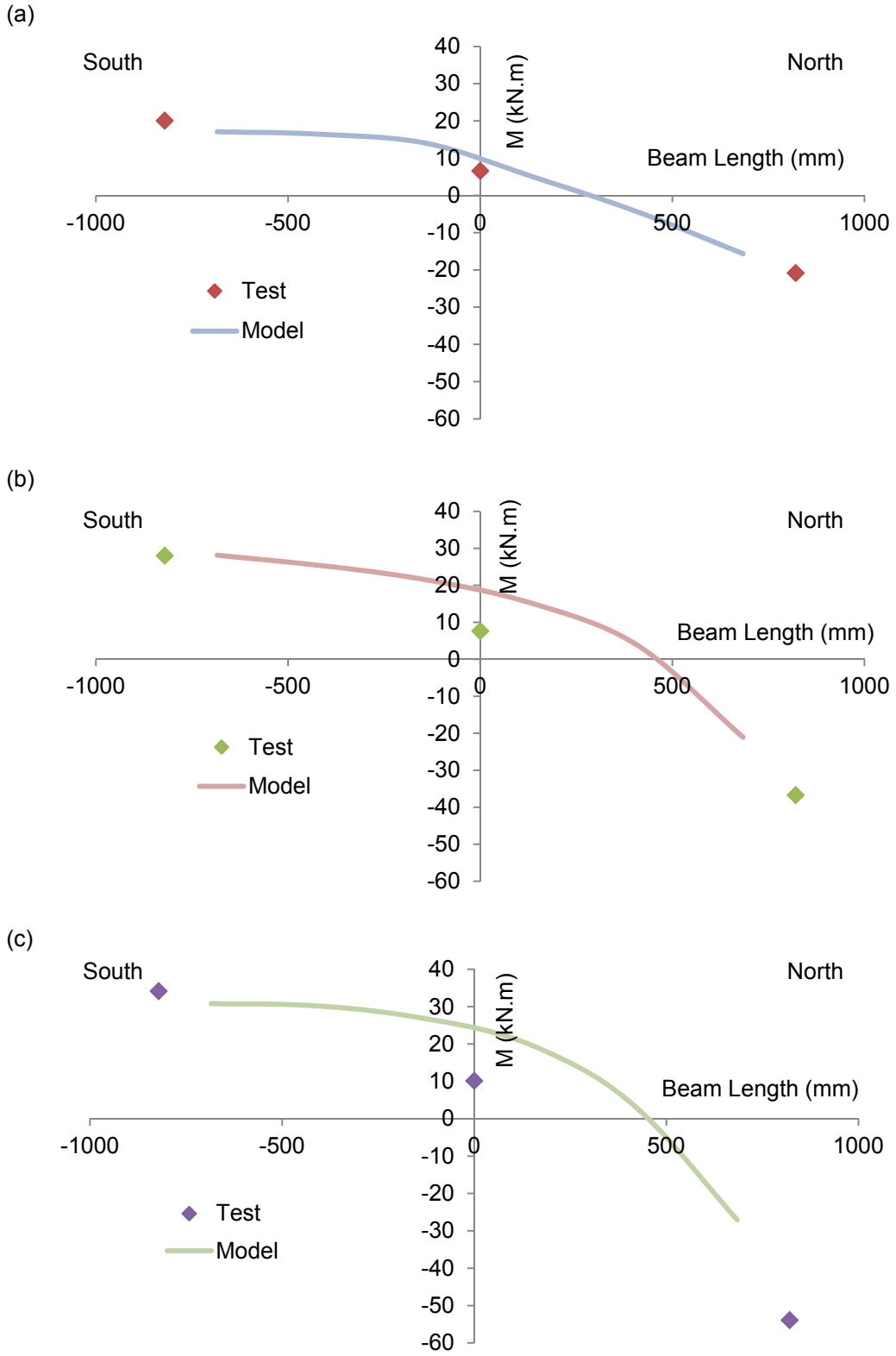


Figure 7-19: Bending Moments in Bottom Beam
 (a) Cycle 4; (b) Cycle 7; (c) Cycle 10

8. SUMMARY AND CONCLUSIONS

8.1 Summary

An exploratory test was performed on a half-scale two-storey specimen to study the behaviour of a steel plate shear wall with PEC columns as a new system under cyclic loading. Correspondingly, a finite element model was developed with the specimen sustaining monotonic loads to help assess the performance of the test and to further study the behaviour of the specimen.

The specimen was a one-bay, two-storey steel plate shear wall with a storey height of 1.9 m and column centreline spacing of 2.44 m. The overall height of the specimen was 4.12 m excluding the 76 mm thick base plate. The infill panels were 3 mm thick and connected to the boundary elements by welding. Standard hot-rolled sections were chosen for the beams and the beams framed into the columns through moment connections with a design specific for the specimen. Both beams and columns were oriented so that they would bend about the strong axis when lateral loads were applied.

PEC columns consist of a thin-walled H-shaped steel section with transverse links welded near the flange tips at intervals and concrete encased between the flanges. The cross section of the PEC columns used in the specimen was 250 mm x 250 mm and a thin plate with a thickness of 6.35 mm (1/4") was used for the steel portion. Side plates were welded at the flange tips at each floor level to simulate real construction, where they are used as connection surfaces for the beams framing into the weak axis of the column. Additional side plates were used at the column bases to prevent weld fracture at the column base. Round bars with a diameter of 10 mm were used as the links and three different link spacings were used along the column height, considering the top and bottom of the columns were more critical than the middle portion of the columns.

The vertical loads were applied to the top of the columns through gravity load simulators, while the lateral loads were applied to the top flanges of the beams through a lateral loading system to avoid local failure due to the thin plate in the columns if lateral loads were applied directly on the columns. The internal forces in the columns were derived using data from strain gauges mounted to both the inside and outside of the column flanges to account for the effect of local buckling and flange bending due to concrete expansion and the thin thickness of the steel section. Strain rosettes were mounted to the panel at three locations at the middle height in the first storey and near the top beam in the second storey. A camera system was used to record the strain history at the bottom north corner on the west side of the first storey infill panel.

A finite element model was developed with a push-over analysis and dynamic explicit solution strategy. In the PEC columns, shell element S4R was used for the steel section and side plates, beam element B31 was used for the links, and solid element C3D8R was used for the concrete. Shell element S4R was also used for the frame beams and infill panels in the specimen. Finite sliding in the contact pair algorithm was used to model the interaction between the steel section and concrete in the columns. A smooth amplitude displacement loading was used in the model to apply lateral loads so the dynamic effect was negligible. The lateral loading system used in the test was also modelled, and additional vertical and horizontal distribution beams were used to apply the lateral loads equally at each floor in the model for consistency with the physical test.

8.2 Conclusions

The failure mode of the test specimen was the initiation of column flange tears coinciding with the full development of plastic hinges at the bottom of the columns. Local buckling occurred at the outside column flanges at the bottom of the columns before the failure. At the failure, local buckling also occurred at the inside column flanges at the top of the columns as well as concrete spalling and crushing near the buckled column flanges. After

the peak load, more deterioration was detected, including a tear in the inside column flanges at the first storey beam bottom flange. Considerable nonlinear behaviour was observed but none led to a rapid drop in the specimen strength. The specimen behaved in a ductile manner, and even the tears in the flanges propagated gradually.

Similar ductile behaviour was observed in the hysteresis curves and the dissipated energy. Compared with a previous test of a steel plate shear wall with steel frame (Driver et al. 1997), more nonlinear behaviour, less ductility, and less energy dissipation capacity were shown in the hysteresis curve of the specimen with PEC columns. However, the dissipated energy kept increasing before the peak load and was stable after the peak load. Moreover, the ductility under severe cyclic loading is very good with the displacement ductility reaching 6.6 where the actual curve crosses over the assumed yield plateau. The displacement ductility at the peak capacity of the specimen was 3.9.

A finite element model was developed with a modified material curve for the first storey infill panel to simulate the isotropic strain hardening occurring during the test based on the strain rosettes and the dual-camera system data. The model and test results were compared, including the base shear vs. first floor deflection curve as well as the internal forces in the first storey columns and beam.

Comparing the envelope of the hysteresis curves in the test with the base shear vs. first floor deflection curve in the model, the effective stiffness in the model was 9% higher than that of the test specimen, while the ultimate capacity in the model was 8% lower than the test. Similar behaviours were observed in the internal forces in the columns and beam in both model and test. When the specimen was pushed towards the north, the compressive axial forces decreased from the top to the bottom in the south column but increased from the top to the bottom in the north column due to the vertical component of the tension field in the panel. The moment distribution in the columns had a sign at the top and bottom of the columns as expected in frame columns without infill panels, but the bending moment

curves were bent towards the infill panel at the middle portion of the columns (instead of being straight lines) due to the horizontal component of the tension field in the panel. The axial forces in the first storey beam were quite linear, representing the uniform lateral loading through the lateral loading system to the top flange of the beam. The curved shape of the moment distribution in the beam was caused by the unbalanced tension field from the panels above and below the beam. However, there are some differences between the test and model data, especially for the compressive axial forces in the north column. The reasons for these differences are mainly the failure of some strain gauges and the out-of-plumb of the north column. Moreover, the more uniform distribution of the tension field in the test than in the model also led to some differences in the column internal forces between the model and test. Both the model and the strain rosettes mounted to the second floor infill panel near the top beam showed non-uniform anchoring stresses from the panel to the beam.

8.3 Recommendations

Based on the results of this research program, recommendations for design and future research on steel plate shear walls with PEC columns are provided below.

8.3.1 Design and Fabrication

As the most critical location, the bottom of the PEC columns should be reinforced, especially on the outside flanges, so the tearing observed in the test would be postponed and the behaviour of the whole system would be improved. The addition of reinforcing bars in the concrete at the column base would be a cost efficient way of increasing the ductility of the hinge location and reducing the demand on the thin flanges.

The bottom side plates were added to prevent failure at the welded column base. As a consequence, the plastic hinges were pushed up to the top of the bottom side plates. Based on plastic design criteria for a steel frame, a small height should be used for the

bottom side plates in PEC columns so the plastic hinges form as close to the column base as possible, reducing the resulting shear demand in the column.

In the test, the moments in the bottom beam were low and no hinges formed at the ends of the beam, even though moment beam-to-column connections were designed. Hence, reduced sections near the beam ends could be used to develop plastic hinges and prevent the development of a soft storey. Moreover, considering the difficulty of transferring the plastic beam moment due to the thin thickness of the steel section in PEC columns, simple shear connections could be used unless a cost-efficient moment connection with minor potential deterioration to the PEC columns is designed.

Since column flange local buckling occurred prior to the peak load and seemed to trigger the failure of the specimen, the use of an effective width is recommended for the column flange in compression when the bending capacity of the PEC column is calculated.

Since the steel section in the PEC column is very thin, the quality of welding could be very influential, especially at critical locations such as the top of the bottom side plates. Caution is required for welding in those locations.

8.3.2 Future Research

Since hinges formed at the top of the first-storey columns rather than at the ends of the beam in this test specimen, behaviour of the moment beam-to-column connections in the system should be studied further by reducing the beam section near the ends. Steel plate shear walls with PEC columns and simple shear connections used at the beam ends should be tested to study the system behaviour.

Different b/t ratios used in PEC columns with different cross-sectional dimensions should be studied to see the effect of these parameters on the behaviour of the columns and the whole system. The maximum b/t ratio of 32 allowed by CSA S16-09 (CSA 2009) needs to be verified for PEC columns used with steel plate shear walls.

The minimum stiffness requirement specified in CSA S16-09 (CSA 2009) for columns as boundary elements of steel plate shear walls needs to be verified for PEC columns by testing the system with PEC columns matching the requirement. A finite element model needs to be developed to study the effect of column stiffness on the behaviour and performance of the system.

Since the tears at the flange tips at the bottom of the columns initiated the failure of the specimen, the provision of reinforcing bars or extra stiffeners at the bottom of the PEC columns should be investigated to study the associated improvement in ductility and robustness of the hinge region. More research is needed for other structural detailing to reduce the stress and strain concentration at the top of the bottom side plates, as well as a finite element study concentrating on the local behaviour at this critical location.

A specimen with fish plates combined with bolted connections between the panel and boundary elements should be tested to develop design and construction options.

Reference List

ACI Committee 209 (1982) "Prediction of Creep, Shrinkage and Temperature Effects in Concrete Structures." Designing for Creep and Shrinkage in Concrete Structures, ACI Publication SP-76, American Concrete Institute, Detroit, 193-300.

Anderson, D. The Stability Provisions of Eurocode 4: Composite Steel-Concrete Building Structures. 1-20

Applied Technology Council (1992) "Guidelines for Cyclic Seismic Testing of Components of Steel Structures." Report No. 24, Applied Technology Council, Redwood City, CA.

ASTM. (2003) A370-03, "Standard test methods and definitions for mechanical testing of steel products." American Society for Testing and Materials, Philadelphia, PA.

Barr, B. and Lee, M.K. (2003) "Modelling the Strain-Softening Behaviour of Plain Concrete Using a Double-Exponential Model." Magazine of Concrete Research, 55(4), 343-353.

Bathe, K. (1975) "Finite Element Formulations for Large Deformation Dynamic Analysis." Internal Journal for Numerical Methods in Engineering, 9, 353-386.

Begum, M., Driver, R.G. and Elwi, A.E. (2007) "Finite Element Modeling of Partially Encased Composite Columns Using the Dynamic Explicit Method." Journal of Structural Engineering, ASCE, 133(3), 326-334.

Begum, M., Driver, R.G., and Elwi, A.E. (2005) "Strength and Stability Simulations of Partially Encased Composite Columns under Axial Loads." Proc., SSRC/NASCC Joint Annual Stability Conference, Montreal, Quebec, Canada, 241-255.

Begum, M., Driver, R.G., and Elwi, A.E. (2007) "Numerical Simulation of the Behaviour of Partially Encased Composite Columns." Structural Engineering Report No. 269, Dept. of Civil and Environmental Engineering, University of Alberta, Edmonton, Canada.

Begum, M., Elwi, A.E., and Driver, R.G. (2004) "Numerical Simulation of the Behaviour of Partially Encased Composite Columns." Proc., 5th Structural Specialty Conference of the Canadian Society for Civil Engineering, Saskatoon, Saskatchewan, Canada, ST-127-1 to 127-10.

Behbahanifard, M.R., Grondin, G.Y., and Elwi, A.E. (2003) "Experimental and Numerical Investigation of Steel Plate Shear Wall." Structural Engineering Report No. 254, Dept. of Civil and Environmental Engineering, University of Alberta, Edmonton, Canada.

Bouchereau, R. and Toupin, J.-D. (2003) "Etude du Comportement en Compression-Flexion des Poteaux Mixtes Partiellement Enrobés." Report EPM/GCS-2003-03, Dept. of Civil, Geological and Mining Engineering, Ecole Polytechnique, Montreal, Canada.

Broderick, B. M. And Elnashai, A. S. (1994) "Seismic Resistance of Composite Beam-Columns in Multi-Storey Structures. Part 2: Analytical Model and Discussion of Results." Journal of Construction Steel Research, 30, 231-258.

Chen, W. and Han, D. (2007) "Plasticity for Structural Engineers." J. Ross Publishing, New York, USA.

Chicoine, T., Massicotte, B., and Tremblay, R. (2003) "Long-Term Behaviour and Strength of Partially Encased Composite Columns Made with Built-up Steel Shapes." Journal of Structural Engineering, ASCE, 129(2), 141-150.

Chicoine, T., Tremblay, R., and Massicotte, B. (2001) "Finite Element Modelling of the Experimental Response of Partially Encased Composite Columns." EPM/GCS No.

2001-06, Dept. of Civil, Geological and Mining Engineering, Ecole Polytechnique, Montreal, Canada.

Chicoine, T., Tremblay, R., and Massicotte, B. (2002b) "Finite Element Modelling and Design of Partially Encased Composite Columns." *Steel and Composite Structures*, 2(3), 171-194.

Chicoine, T., Tremblay, R., Massicotte, B., Yalcin, M., Ricles, J., and Lu, L.-W. (2002a) "Behavior and Strength of Partially Encased Composite Columns with Built-up Shapes." *Journal of Structural Engineering, ASCE*, 128(3), 279-288.

Chicoine, T., Tremblay, R., Massicotte, B., Yalcin, M., Ricles, J., and Lu, L.-W. (2000) "Test Programme on Partially-Encased Built up Three-Plate Composite Columns." Joint Report EPM/GCS No. 00-06, February, Dept. of Civil, Geological and Mining Engineering, Ecole Polytechnique, Montreal, Canada – ATLSS Engineering Research Centre, No. 00-04, Lehigh University, Bethlehem, Pennsylvania, USA.

Choi, I and Park, H. (2008) "Ductility and Energy Dissipation Capacity of Shear-Dominated Steel Plate Walls." *Journal of Structural Engineering, ASCE*, 134(9), 1495-1507.

Comite Euro-International du Beton (1993) "CEB-FIP Model Code 1990." Thomas Telford Services Ltd. London.

CSA. (2001) "CAN/CSA-S16-01: Limit States Design of Steel Structures." Canadian Standards Association, Toronto, ON.

CSA. (2004a) "CSA A23.3-04, Design of Concrete Structures." Canadian Standards Association, Rexdale, ON.

CSA. (2004b) "CSA G40.21-04, Structural Quality Steel." Canadian Standards Association, Rexdale, ON.

CSA. (2009) "CSA S16-09, Limit States Design of Steel Structures." Canadian Standards Association, Toronto, ON.

Dastfan, M., Deng, X., and Driver, R.G. (2008) "Large-scale Tests of Steel Plate Shear Walls with PEC Columns." Proc., North American Steel Construction Conference, April 2-5, Nashville, TN, USA.

Deng, X. and Driver, R., G. (2007) "Steel Plate Shear Walls with Partially Encased Composite Columns." Proc., SSRC/NASCC Joint Annual Stability Conference, New Orleans, United State, 437-453.

Deng, X., Dastfan, M., and Driver, R.G. (2008) "Behaviour of Steel Plate Shear Walls with Composite Columns." Proc., Structures Congress, American Society of Civil Engineers, April 24-26, Vancouver, BC, Canada.

Driver, R.,G., Kulak, G.L., Elwi, A.E., and Kennedy, D.J.L. (1998b) "EF and Simplified Models of Steel Plate Shear Wall." ASCE Journal of Structural Engineering, 124(2), 121-130.

Driver, R.,G., Kulak, G.L., Kennedy, D.J.L., and Elwi, A.E. (1997) "Seismic Behaviour of Steel Plate Shear Walls", Structural Engineering Report No. 215, Dept. of Civil and Environmental Engineering, University of Alberta, Edmonton, Canada.

Driver, R.,G., Kulak, G.L., Kennedy, D.J.L., and Elwi, A.E. (1998a) "Cyclic Test of a Four-Storey Steel Plate Shear Wall." ASCE Journal of Structural Engineering, 124(2), 112-120.

Elghazouli, A.Y. and Elnashai, A.S. (1993) "Performance of Composite Steel/Concrete Members under Earthquake Loading. Part 2: Parametric Studies and Design Considerations." Earthquake Engineering and Structural Dynamics, 22 (4), 347-368.

Elnashai, A.S. and Broderick, B.M. (1994) "Seismic Resistance of Composite Beam-Columns in Multi-Storey Structures. Part 1: Experimental Studies." *Journal of Constructional Steel Research*, 30 (3), 201-229.

Elnashai, A.S. and Elghazouli, A.Y. (1993) "Performance of Composite Steel/Concrete Members under Earthquake Loading. Part 1: Analytical Model." *Earthquake Engineering and Structural Dynamics*, 22(4), 315-345.

Elnashai, A.S., Takanashai, K., Elghazouli, A.Y., and Dowling, P.J. (1991) "Experimental Behaviour of Partially Encased Composite Beam-Columns under Cyclic and Dynamic Loads." *Proc., Institute of Civil Engineers, Part 2: Research and Theory*, 91, 259-272.

FEMA. (2000) "Recommended Seismic Design Criteria for New Steel Moment-Frame Buildings." Publication No. 350, Federal Emergency Management Agency, Washington, DC.

Hibbitt, Karlsson and Sorensen, Inc. (HKS) (2003) *ABAQUS/ Explicit User's Manual*, Version 6.3.

Hillerborg, A., Modeer, A., and Peterson, P.E. (1976) "Analytical of Crack Formation and Crack Growth in Concrete by Means of Fracture Mechanics and Finite Elements." *Cement and Concrete Research*, 6, 773-782.

Konstantinidis, D.K., Kappos, A.J., and Ilauddin, B.A. (2007) "Analytical Stress-Strain Model for High-Strength Concrete Members under Cyclic Loading." *Journal of Structural Engineering*, 133(4), 484-494.

Kulak, G.L. (1991) "Unstiffened Steel Plate Shear Walls." *Structures Subjected to Repeated Loading—Stability and Strength*, Narayanan, R., and Roberts, T.M., Editors, Elsevier Applied Science Publications, London, U.K., 237-276.

Kulak, G.L., Kennedy, D.J.L., and Driver, R. G. (1994) "Discussion of Experimental Study of Thin Steel Plate Shear Walls under Cyclic Load by Caccese, V., Elgaaly, M., and Chen, R." *Journal of Structural Engineering, ASCE*, 120(10), 3072-3073.

Kulak, G.L., Kennedy, D.J.L., Driver, R. G., and Medhekar, M. (1999) "Behaviour and Design of Steel Plate Shear Walls." *Proc., North American Steel Construction Conference, Toronto, Canada, 11-1-11-20.*

Lay, M.G. (1982) "Structural Steel Fundamentals - an Engineering and Metallurgical Primer" Australian Road Research Board.

Lublimer, J., Oliver, J., Oller, S., and Onate, E. (1989) "A Plastic-Damage Model for Concrete." *International Journal of Solids and Structures*, 25 (3), 229-326.

MacGregor, J.G. and Bartlett, F.M. (2000) "Reinforced Concrete Mechanics and Design." Prentice-Hall Canada Inc., Scarborough, Ontario.

Mimura, H. and Akiyama, H. (1977) "Load-Deflection Relationship of Earthquake-Resistant Steel Shear Walls with a Developed Diagonal Tension Field." *Transactions, Architectural Institute of Japan*, 260, October, 109-114 (in Japanese).

NBCC, (2005) "National Building Code of Canada." National Research Council of Canada, Ottawa, ON.

Otter, D. E., and Naaman, A. E. (1989) "Model for response of concrete to random compressive loads." *Journal of Structural Engineering*, 115(11), 2794-2809.

Prickett, B.S. and Driver, R.G. (2006) "Behaviour of Partially Encased Composite Columns Made With High Performance Concrete." *Structural Engineering Report No. 262, Dept. of Civil and Environmental Engineering, University of Alberta, Edmonton, Canada.*

Shishkin, J.J., Driver, R.G., and Grondin, G.Y. (2005) "Analysis of Steel Plate Shear Walls Using the Modified Strip Model." Structural Engineering Report No. 261, Dept. of Civil and Environmental Engineering, University of Alberta, Edmonton, Canada.

Takahashi, Y., Takemoto, Y., Takeda, T., and Takagi, M. (1973) "Experimental Study on Thin Steel Shear Walls and Particular Bracings under Alternative Horizontal Load." Preliminary Report, IABSE Symposium on Resistance and Ultimate Deformability of Structures Acted on by Well-Defined Repeated Loads, Lisbon, Portugal, 185-191.

Thorburn, L.J., Kulak, G.L., and Montgomery, C.J. (1983) "Analysis of Steel Plate Shear Walls." Structural Engineering Report No. 107, Dept. Of Civil and Environmental Engineering, University of Alberta, Edmonton, Canada.

Timler, P.A. (1998) "Design Procedures Development, Analytical Verification, and Cost Evaluation of Steel Plate Shear Wall Structures." Earthquake Engineering Research Facility Technical Report No. 98-01.

Timler, P.A. and Kulak, G.L. (1983) "Experimental Study of Steel Plate Shear Walls." Structural Engineering Report No. 114, Dept. Of Civil and Environmental Engineering, University of Alberta, Edmonton, Canada.

Timler, P.A., Ventura, C.E., Prion, H. and Anjam, R. (1998) "Experimental and Analytical Studies of Steel Plate Shear Walls as Applied to the Design of Tall Buildings." Structural Design of Tall Buildings, 7(3), pp 233-249.

Tremblay, R. (2003) "Flexural Demand on Partially-Encased Composite Columns in Multi-Storey Concentrically Braced Steel Frames." STESSA 2003: Proc., Conference on Behaviour of Steel Structures in Seismic Areas, 9-12 June, Naples, Italy, 479-485.

Tremblay, R., Chicoine, T., and Massicotte, B. (2000b) "Design Equation for the Axial Capacity of Partially-Encased Non-Compact Columns." Proc., Composite Construction in

Steel and Concrete IV, ASCE, ed. By J.F. Hajjar, M. Hosain, W.S.Easterling, and B.M. Sharooz, ASCE, Reston, VA, 506-517.

Tremblay, R., Chicoine, T., Massicotte, B., Ricles, J., and Lu, L.-W. (2000a) "Compressive Strength of Large Scale Partially-Encased Composite Sub Columns." Proc. 2000 SSRC Annual Technical Session & Meeting, Memphis, 262-272.

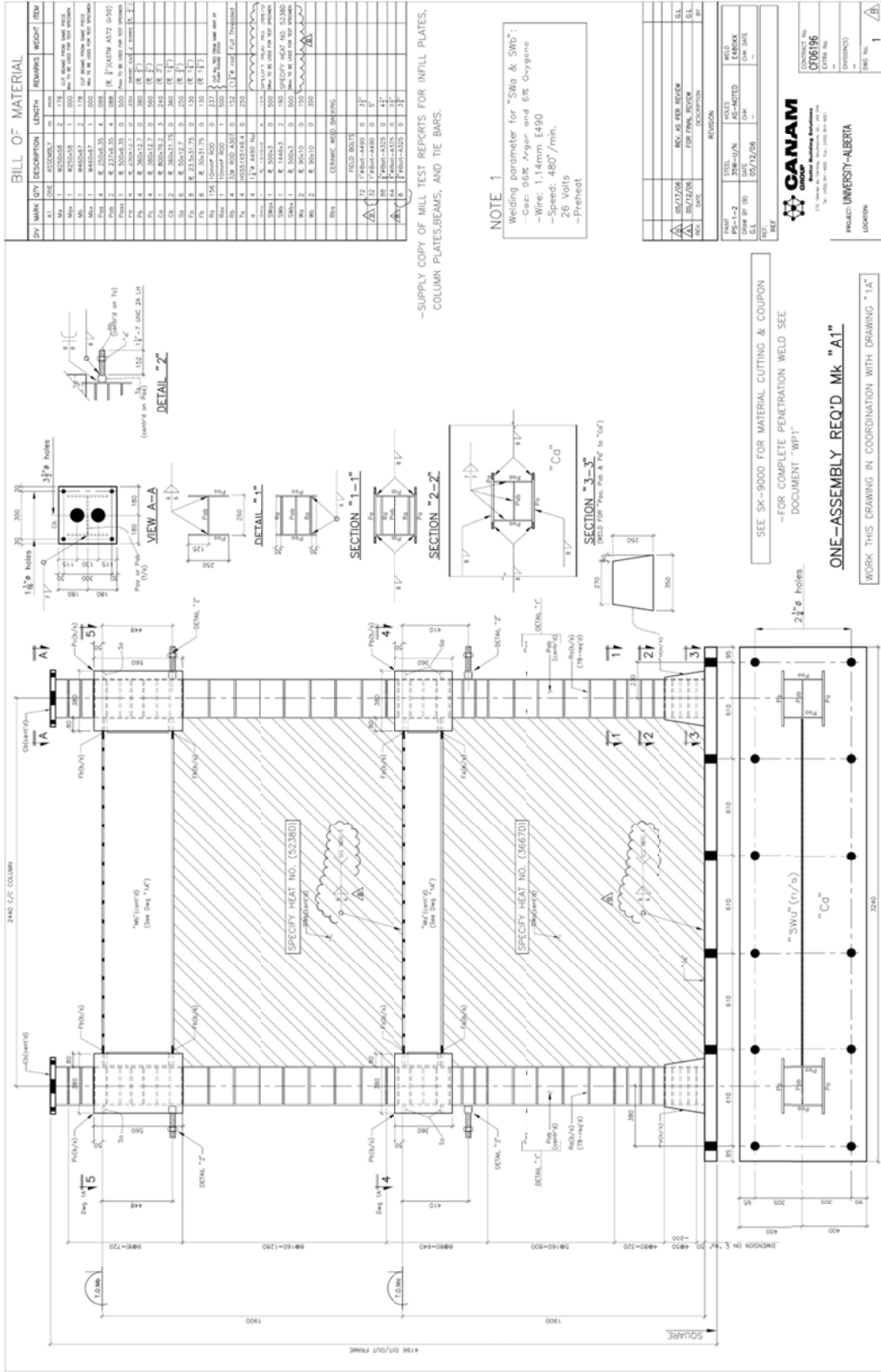
Tremblay, R., Massicotte, B., Fillion, I., and Maranda, R. (1998) "Experimental Study on the Behaviour of Partially Encased Composite Columns Made with Light Welded H Steel Shapes under Compressive Axial Loads. Proc., SSRC Annual Technical Session & Meeting, Atlanta, 195-204.

Tromposch, E.W. and Kulak, G.L. (1987) "Cyclic and Static Behaviour of Thin Panel Steel Plate Shear Walls." Structural Engineering Report No. 145, Dept. Of Civil and Environmental Engineering, University of Alberta, Edmonton, Canada.

Vincent, R. (2000) "Design and Application of Partially Encased Non-Compact Composite Columns for High-Rise Buildings." Proc. Composite Construction in Steel and Concrete IV, 854-864.

Vincent, R. and Tremblay, R. (2001) "An Innovative Partially Encased Composite Column System high-rise Buildings." Proc. North American Conference on Steel Construction Conf., Fort Lauderdale, FL., 30-3 to 30-17.

Appendix A - Shop Drawings



BILL OF MATERIAL

QTY	MARK	QTY DESCRIPTION	LENGTH	REMARKS	WEIGHT (KG)
1	A1	STEEL COLUMN	2400		
1	A2	STEEL BEAM	4000		
1	A3	STEEL PLATE	4000		
1	A4	STEEL PLATE	4000		
1	A5	STEEL PLATE	4000		
1	A6	STEEL PLATE	4000		
1	A7	STEEL PLATE	4000		
1	A8	STEEL PLATE	4000		
1	A9	STEEL PLATE	4000		
1	A10	STEEL PLATE	4000		
1	A11	STEEL PLATE	4000		
1	A12	STEEL PLATE	4000		
1	A13	STEEL PLATE	4000		
1	A14	STEEL PLATE	4000		
1	A15	STEEL PLATE	4000		
1	A16	STEEL PLATE	4000		
1	A17	STEEL PLATE	4000		
1	A18	STEEL PLATE	4000		
1	A19	STEEL PLATE	4000		
1	A20	STEEL PLATE	4000		
1	A21	STEEL PLATE	4000		
1	A22	STEEL PLATE	4000		
1	A23	STEEL PLATE	4000		
1	A24	STEEL PLATE	4000		
1	A25	STEEL PLATE	4000		
1	A26	STEEL PLATE	4000		
1	A27	STEEL PLATE	4000		
1	A28	STEEL PLATE	4000		
1	A29	STEEL PLATE	4000		
1	A30	STEEL PLATE	4000		
1	A31	STEEL PLATE	4000		
1	A32	STEEL PLATE	4000		
1	A33	STEEL PLATE	4000		
1	A34	STEEL PLATE	4000		
1	A35	STEEL PLATE	4000		
1	A36	STEEL PLATE	4000		
1	A37	STEEL PLATE	4000		
1	A38	STEEL PLATE	4000		
1	A39	STEEL PLATE	4000		
1	A40	STEEL PLATE	4000		
1	A41	STEEL PLATE	4000		
1	A42	STEEL PLATE	4000		
1	A43	STEEL PLATE	4000		
1	A44	STEEL PLATE	4000		
1	A45	STEEL PLATE	4000		
1	A46	STEEL PLATE	4000		
1	A47	STEEL PLATE	4000		
1	A48	STEEL PLATE	4000		
1	A49	STEEL PLATE	4000		
1	A50	STEEL PLATE	4000		
1	A51	STEEL PLATE	4000		
1	A52	STEEL PLATE	4000		
1	A53	STEEL PLATE	4000		
1	A54	STEEL PLATE	4000		
1	A55	STEEL PLATE	4000		
1	A56	STEEL PLATE	4000		
1	A57	STEEL PLATE	4000		
1	A58	STEEL PLATE	4000		
1	A59	STEEL PLATE	4000		
1	A60	STEEL PLATE	4000		
1	A61	STEEL PLATE	4000		
1	A62	STEEL PLATE	4000		
1	A63	STEEL PLATE	4000		
1	A64	STEEL PLATE	4000		
1	A65	STEEL PLATE	4000		
1	A66	STEEL PLATE	4000		
1	A67	STEEL PLATE	4000		
1	A68	STEEL PLATE	4000		
1	A69	STEEL PLATE	4000		
1	A70	STEEL PLATE	4000		
1	A71	STEEL PLATE	4000		
1	A72	STEEL PLATE	4000		
1	A73	STEEL PLATE	4000		
1	A74	STEEL PLATE	4000		
1	A75	STEEL PLATE	4000		
1	A76	STEEL PLATE	4000		
1	A77	STEEL PLATE	4000		
1	A78	STEEL PLATE	4000		
1	A79	STEEL PLATE	4000		
1	A80	STEEL PLATE	4000		
1	A81	STEEL PLATE	4000		
1	A82	STEEL PLATE	4000		
1	A83	STEEL PLATE	4000		
1	A84	STEEL PLATE	4000		
1	A85	STEEL PLATE	4000		
1	A86	STEEL PLATE	4000		
1	A87	STEEL PLATE	4000		
1	A88	STEEL PLATE	4000		
1	A89	STEEL PLATE	4000		
1	A90	STEEL PLATE	4000		
1	A91	STEEL PLATE	4000		
1	A92	STEEL PLATE	4000		
1	A93	STEEL PLATE	4000		
1	A94	STEEL PLATE	4000		
1	A95	STEEL PLATE	4000		
1	A96	STEEL PLATE	4000		
1	A97	STEEL PLATE	4000		
1	A98	STEEL PLATE	4000		
1	A99	STEEL PLATE	4000		
1	A100	STEEL PLATE	4000		

—SUPPLY COPY OF MILL TEST REPORTS FOR INFILL PLATES, COLUMN PLATES, BEAMS, AND TIE BARS.

NOTE 1
Welding parameter for "SWa & SWb":
—Gas: 98% Argon and 2% Oxygen
—Elect. 1.4mm E490
—Speed: 400"/min.
—26 Volt
—Preheat

REV.	DATE	DESCRIPTION	BY
1	06/17/2006	REV. AS PER REQUEST FOR FINAL REVIEW	...
2	06/17/2006	REV. AS PER REQUEST FOR FINAL REVIEW	...

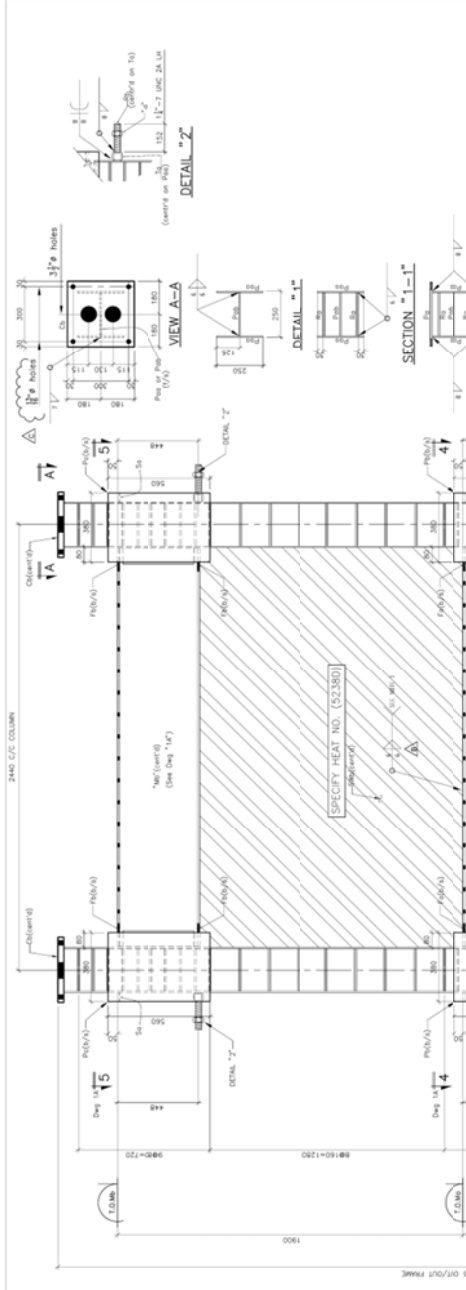
REV.	DATE	DESCRIPTION	BY
1	05/17/2006
2	05/17/2006

REV.	DATE	DESCRIPTION	BY
1	05/17/2006
2	05/17/2006

SEE SK-9000 FOR MATERIAL CUTTING & COUPON
—FOR COMPLETE PENETRATION WELD SEE DOCUMENT "WPI1"
ONE-ASSEMBLY REQ'D. Mk. "A1"
WORK THIS DRAWING IN COORDINATION WITH DRAWING "JA"

GANAM
General Building Solutions
PROJECT: UNIVERSITY-ALBERTA
LOCATION: ...

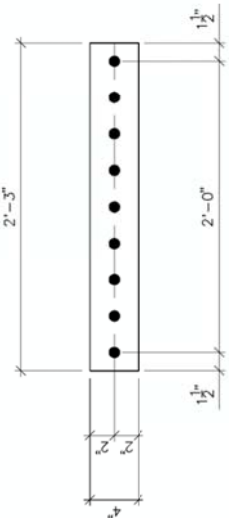
REV	DATE	DESCRIPTION	LENGTH	REMARKS	WEIGHT	REV
A1	05/12/06	ASSEMBLY	2	178	OF 800	
M01	05/12/06		1	1000		
M02	05/12/06		1	1000		
M03	05/12/06		1	1000		
M04	05/12/06		1	1000		
M05	05/12/06		1	1000		
M06	05/12/06		1	1000		
M07	05/12/06		1	1000		
M08	05/12/06		1	1000		
M09	05/12/06		1	1000		
M10	05/12/06		1	1000		
M11	05/12/06		1	1000		
M12	05/12/06		1	1000		
M13	05/12/06		1	1000		
M14	05/12/06		1	1000		
M15	05/12/06		1	1000		
M16	05/12/06		1	1000		
M17	05/12/06		1	1000		
M18	05/12/06		1	1000		
M19	05/12/06		1	1000		
M20	05/12/06		1	1000		
M21	05/12/06		1	1000		
M22	05/12/06		1	1000		
M23	05/12/06		1	1000		
M24	05/12/06		1	1000		
M25	05/12/06		1	1000		
M26	05/12/06		1	1000		
M27	05/12/06		1	1000		
M28	05/12/06		1	1000		
M29	05/12/06		1	1000		
M30	05/12/06		1	1000		
M31	05/12/06		1	1000		
M32	05/12/06		1	1000		
M33	05/12/06		1	1000		
M34	05/12/06		1	1000		
M35	05/12/06		1	1000		
M36	05/12/06		1	1000		
M37	05/12/06		1	1000		
M38	05/12/06		1	1000		
M39	05/12/06		1	1000		
M40	05/12/06		1	1000		
M41	05/12/06		1	1000		
M42	05/12/06		1	1000		
M43	05/12/06		1	1000		
M44	05/12/06		1	1000		
M45	05/12/06		1	1000		
M46	05/12/06		1	1000		
M47	05/12/06		1	1000		
M48	05/12/06		1	1000		
M49	05/12/06		1	1000		
M50	05/12/06		1	1000		
M51	05/12/06		1	1000		
M52	05/12/06		1	1000		
M53	05/12/06		1	1000		
M54	05/12/06		1	1000		
M55	05/12/06		1	1000		
M56	05/12/06		1	1000		
M57	05/12/06		1	1000		
M58	05/12/06		1	1000		
M59	05/12/06		1	1000		
M60	05/12/06		1	1000		
M61	05/12/06		1	1000		
M62	05/12/06		1	1000		
M63	05/12/06		1	1000		
M64	05/12/06		1	1000		
M65	05/12/06		1	1000		
M66	05/12/06		1	1000		
M67	05/12/06		1	1000		
M68	05/12/06		1	1000		
M69	05/12/06		1	1000		
M70	05/12/06		1	1000		
M71	05/12/06		1	1000		
M72	05/12/06		1	1000		
M73	05/12/06		1	1000		
M74	05/12/06		1	1000		
M75	05/12/06		1	1000		
M76	05/12/06		1	1000		
M77	05/12/06		1	1000		
M78	05/12/06		1	1000		
M79	05/12/06		1	1000		
M80	05/12/06		1	1000		
M81	05/12/06		1	1000		
M82	05/12/06		1	1000		
M83	05/12/06		1	1000		
M84	05/12/06		1	1000		
M85	05/12/06		1	1000		
M86	05/12/06		1	1000		
M87	05/12/06		1	1000		
M88	05/12/06		1	1000		
M89	05/12/06		1	1000		
M90	05/12/06		1	1000		
M91	05/12/06		1	1000		
M92	05/12/06		1	1000		
M93	05/12/06		1	1000		
M94	05/12/06		1	1000		
M95	05/12/06		1	1000		
M96	05/12/06		1	1000		
M97	05/12/06		1	1000		
M98	05/12/06		1	1000		
M99	05/12/06		1	1000		
M100	05/12/06		1	1000		



REV	DATE	DESCRIPTION	LENGTH	REMARKS	WEIGHT	REV
A1	05/12/06	ASSEMBLY	2	178	OF 800	
M01	05/12/06		1	1000		
M02	05/12/06		1	1000		
M03	05/12/06		1	1000		
M04	05/12/06		1	1000		
M05	05/12/06		1	1000		
M06	05/12/06		1	1000		
M07	05/12/06		1	1000		
M08	05/12/06		1	1000		
M09	05/12/06		1	1000		
M10	05/12/06		1	1000		
M11	05/12/06		1	1000		
M12	05/12/06		1	1000		
M13	05/12/06		1	1000		
M14	05/12/06		1	1000		
M15	05/12/06		1	1000		
M16	05/12/06		1	1000		
M17	05/12/06		1	1000		
M18	05/12/06		1	1000		
M19	05/12/06		1	1000		
M20	05/12/06		1	1000		
M21	05/12/06		1	1000		
M22	05/12/06		1	1000		
M23	05/12/06		1	1000		
M24	05/12/06		1	1000		
M25	05/12/06		1	1000		
M26	05/12/06		1	1000		
M27	05/12/06		1	1000		
M28	05/12/06		1	1000		
M29	05/12/06		1	1000		
M30	05/12/06		1	1000		
M31	05/12/06		1	1000		
M32	05/12/06		1	1000		
M33	05/12/06		1	1000		
M34	05/12/06		1	1000		
M35	05/12/06		1	1000		
M36	05/12/06		1	1000		
M37	05/12/06		1	1000		
M38	05/12/06		1	1000		
M39	05/12/06		1	1000		
M40	05/12/06		1	1000		
M41	05/12/06		1	1000		
M42	05/12/06		1	1000		
M43	05/12/06		1	1000		
M44	05/12/06		1	1000		
M45	05/12/06		1	1000		
M46	05/12/06		1	1000		
M47	05/12/06		1	1000		
M48	05/12/06		1	1000		
M49	05/12/06		1	1000		
M50	05/12/06		1	1000		
M51	05/12/06		1	1000		
M52	05/12/06		1	1000		
M53	05/12/06		1	1000		
M54	05/12/06		1	1000		
M55	05/12/06		1	1000		
M56	05/12/06		1	1000		
M57	05/12/06		1	1000		
M58	05/12/06		1	1000		
M59	05/12/06		1	1000		
M60	05/12/06		1	1000		
M61	05/12/06		1	1000		
M62	05/12/06		1	1000		
M63	05/12/06		1	1000		
M64	05/12/06		1	1000		
M65	05/12/06		1	1000		
M66	05/12/06		1	1000		
M67	05/12/06		1	1000		
M68	05/12/06		1	1000		
M69	05/12/06		1	1000		
M70	05/12/06		1	1000		
M71	05/12/06		1	1000		
M72	05/12/06		1	1000		
M73	05/12/06		1	1000		
M74	05/12/06		1	1000		
M75	05/12/06		1	1000		
M76	05/12/06		1	1000		
M77	05/12/06		1	1000		
M78	05/12/06		1	1000		
M79	05/12/06		1	1000		
M80	05/12/06		1	1000		
M81	05/12/06		1	1000		
M82	05/12/06		1	1000		
M83	05/12/06		1	1000		
M84	05/12/06		1	1000		
M85	05/12/06		1	1000		
M86	05/12/06		1	1000		
M87	05/12/06		1	1000		
M88	05/12/06		1	1000		
M89	05/12/06		1	1000		
M90	05/12/06		1	1000		
M91	05/12/06		1	1000		
M92	05/12/06		1	1000		
M93	05/12/06		1	1000		
M94	05/1					

DIV	MARK	QTY	DESCRIPTION	LENGTH	REMARKS	WEIGHT	ITEM	DIV	MARK	QTY	DESCRIPTION	LENGTH	REMARKS	WEIGHT	ITEM
	S17	8	PL 4" x 1"	2' 3"											

CONTRACT No.	CF06196	EXTRA No.		DWG. NO	3
PROJECT:	UNIVERSITY ALBERTA	DIVISION			
 Better Building Solutions 270, Grande Prairie, Saskatchewan, S6V 4P8 3A9 Tel.: (403) 641-4000 Fax: (403) 641-0001					
DET. (B)	G.L.	DATE:	21/02/06	CHK.	CHK. DATE
PAIN	PS-2	STEEL	50W	HOLES	15/16φ
WELD	E70XX				
REF		REVISION			
		DATE			
		DESCRIPTION			
		BY			
		G.L.			
		G.L.			



8-PLATES REQ'D Mk "S17"

Appendix B - Steel Tension Coupons

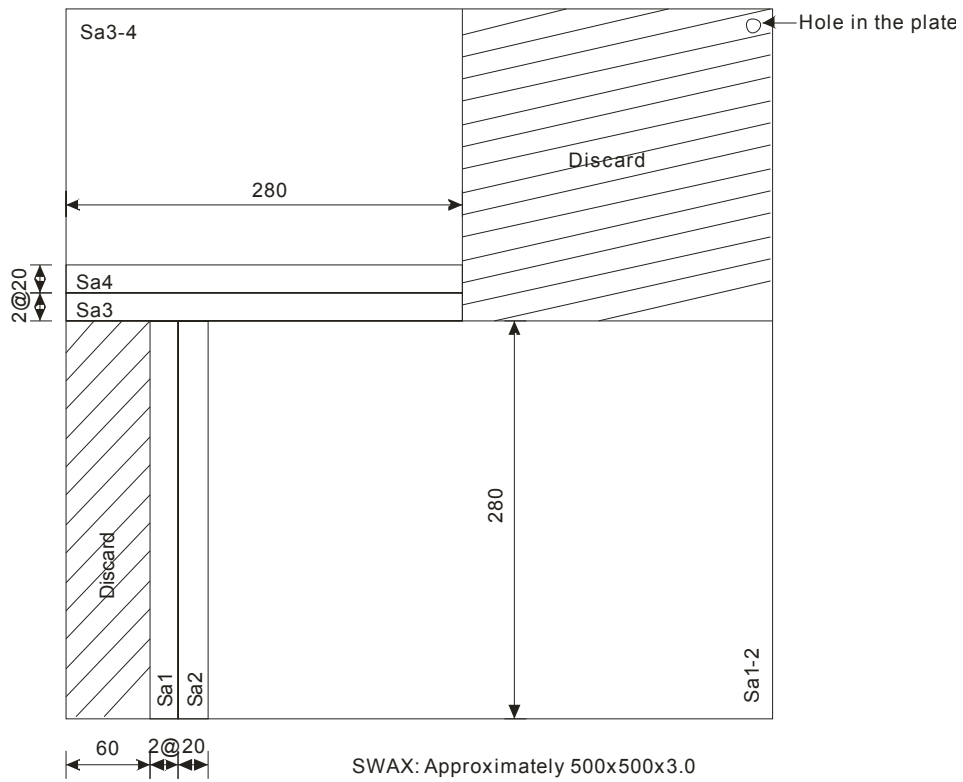


Figure B-1: Tension Coupon Cutting Plan for First Storey Infill Panel

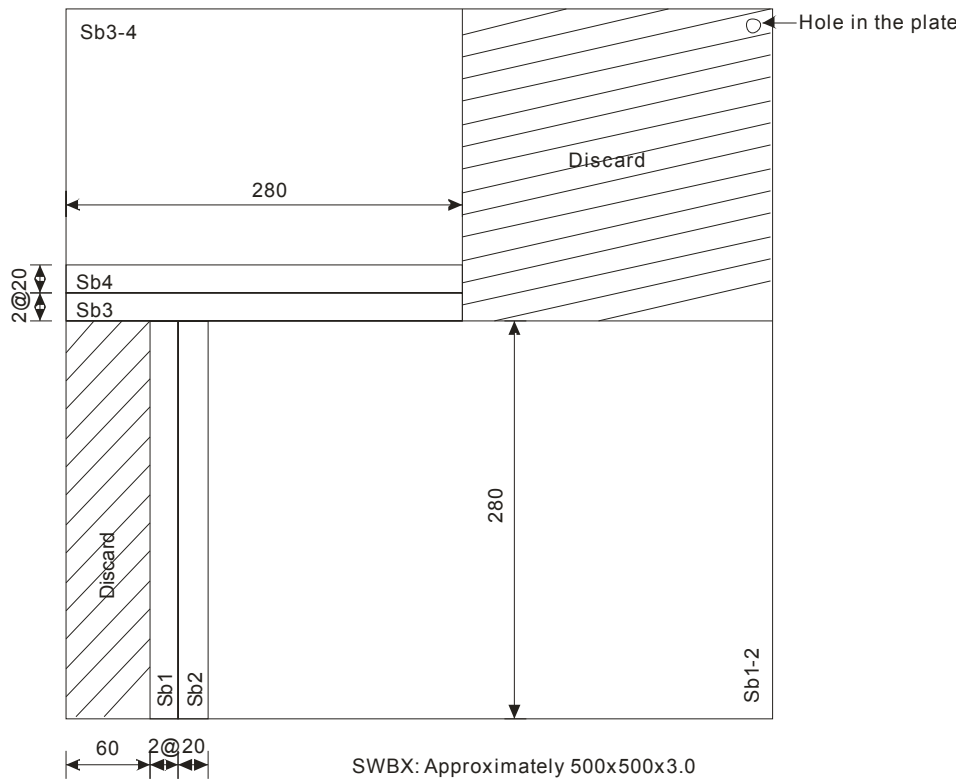


Figure B-2: Tension Coupon Cutting Plan for Second Storey Infill Panel

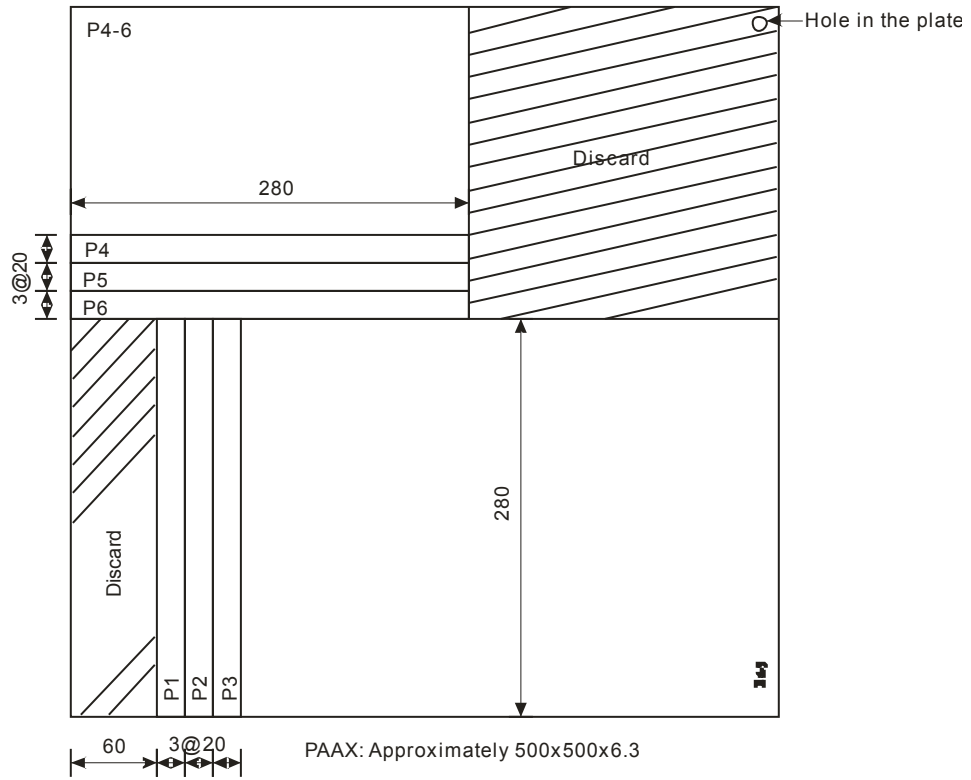
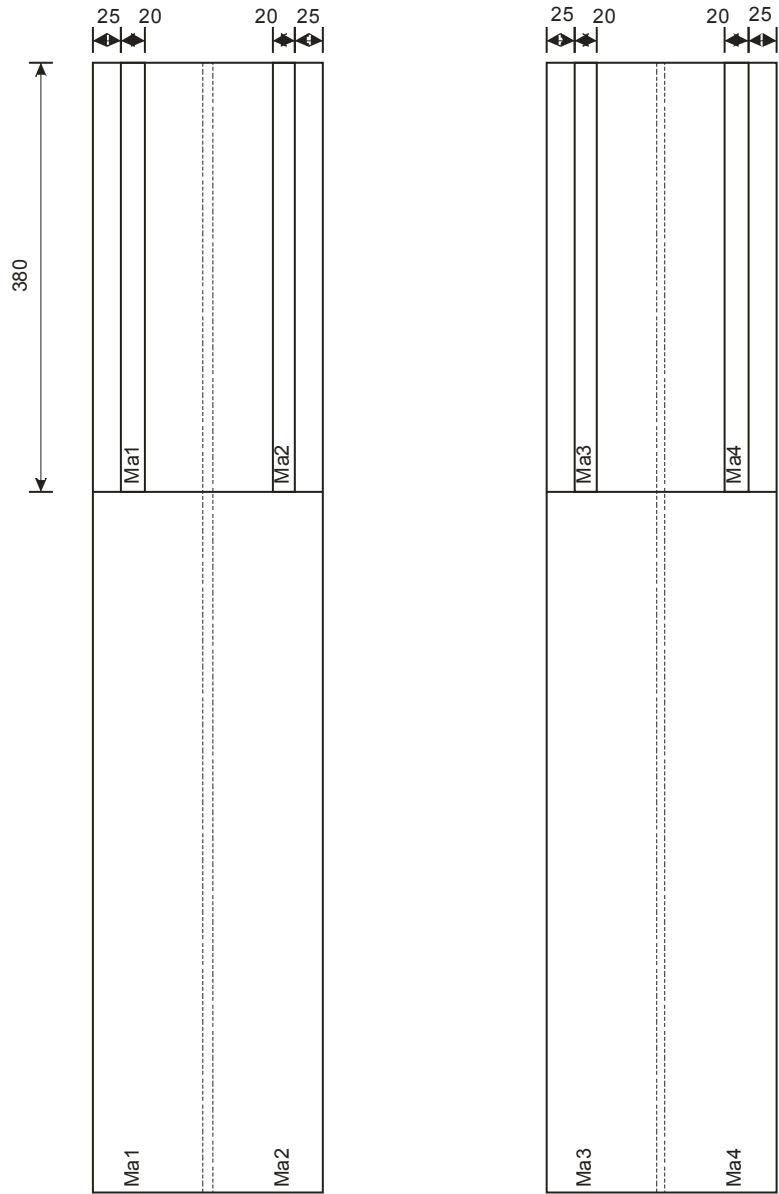


Figure B-3: Tension Coupon Cutting Plan for Steel Section in PEC Columns

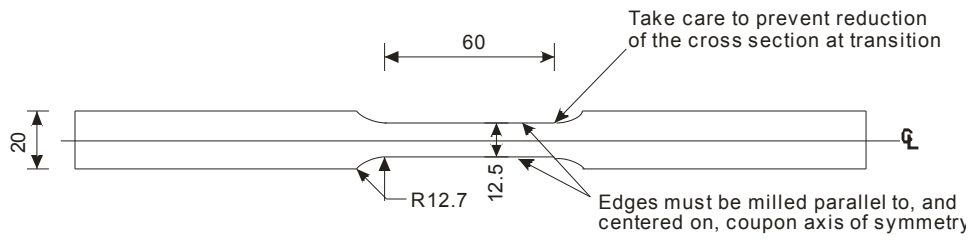


W250x58 (MAX): Approximately 1000 long

Figure B-4: Tension Coupon Cutting Plan for First Storey Beam

Appendix C - Steel Tension Coupon Design

(a) Plan View



(b) Side View

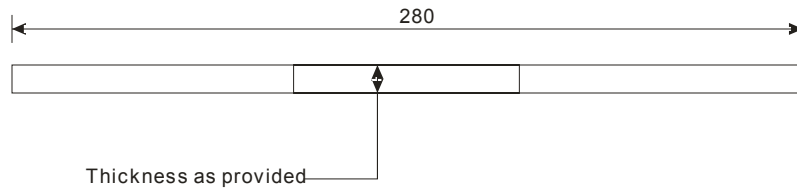
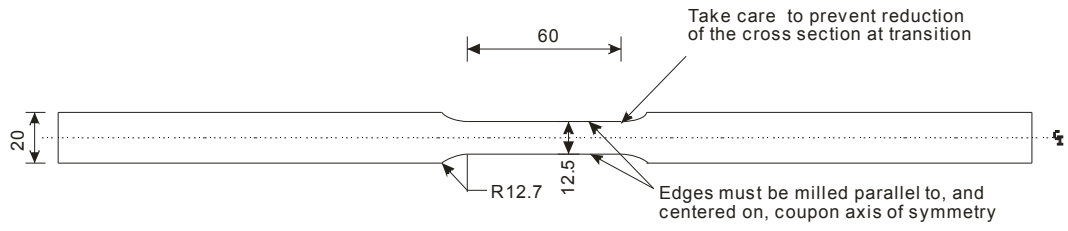


Figure C-1: Tension Coupon Type 1 (Infill Panels and Column Plates)
(a) Plan View; (b) Side View

(a) Plan View



(b) Side View

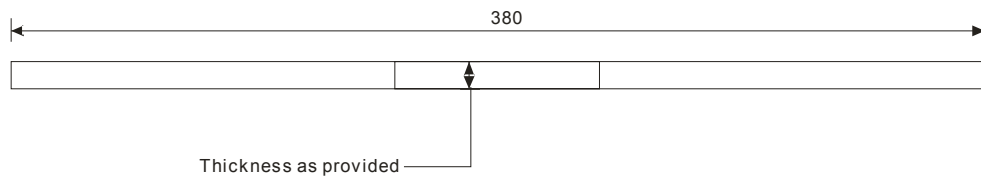


Figure C-2: Tension Coupon Type 2 (First Storey Beam Flanges)
(a) Plan View; (b) Side View

Appendix D - Steel Tension Coupon Test Results

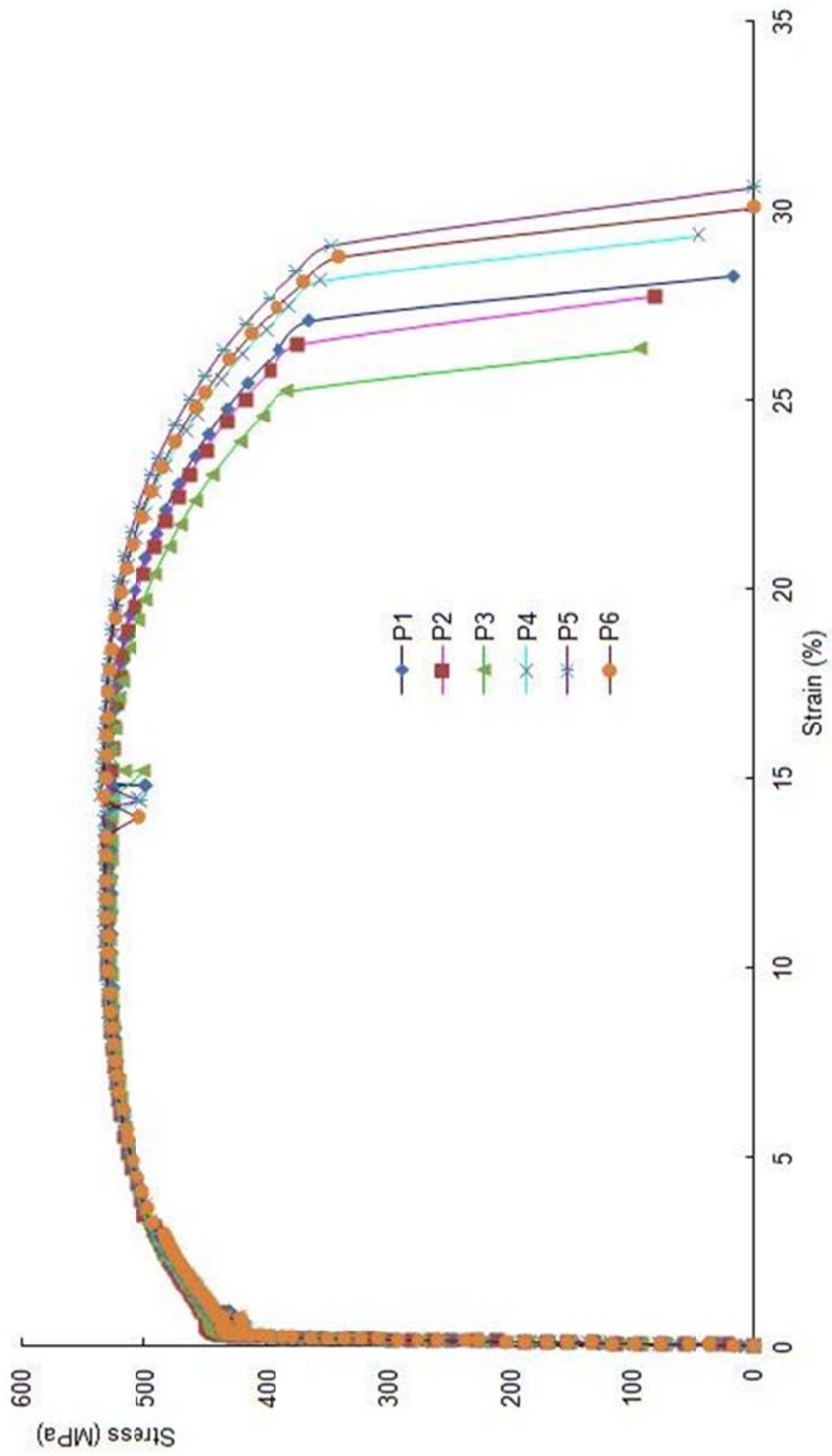


Figure D-1: Stress vs. Strain Curves for Tension Coupon from Column Steel Section

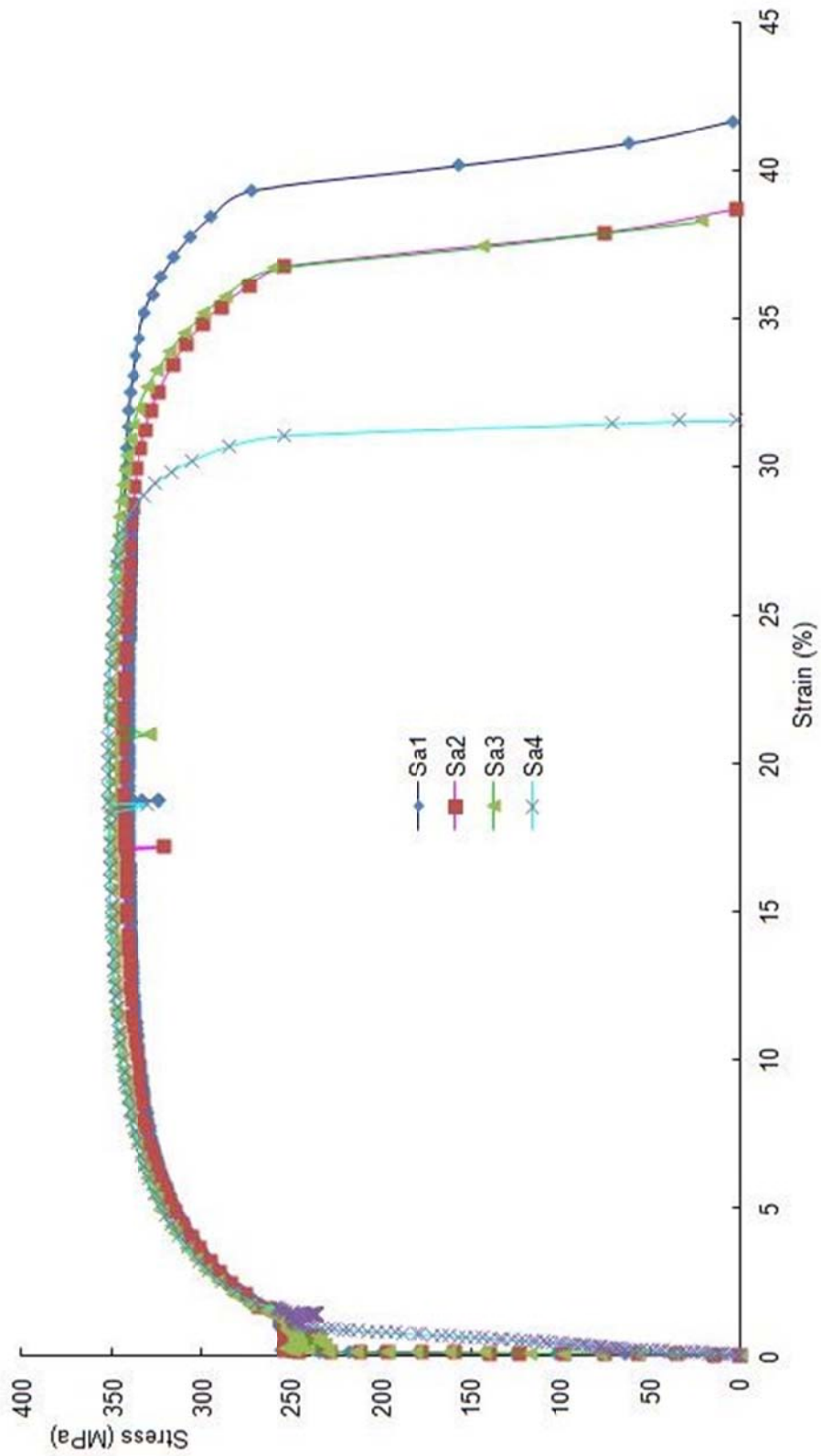


Figure D-2: Stress vs. Strain Curves for Tension Coupon from First Storey Infill Panel

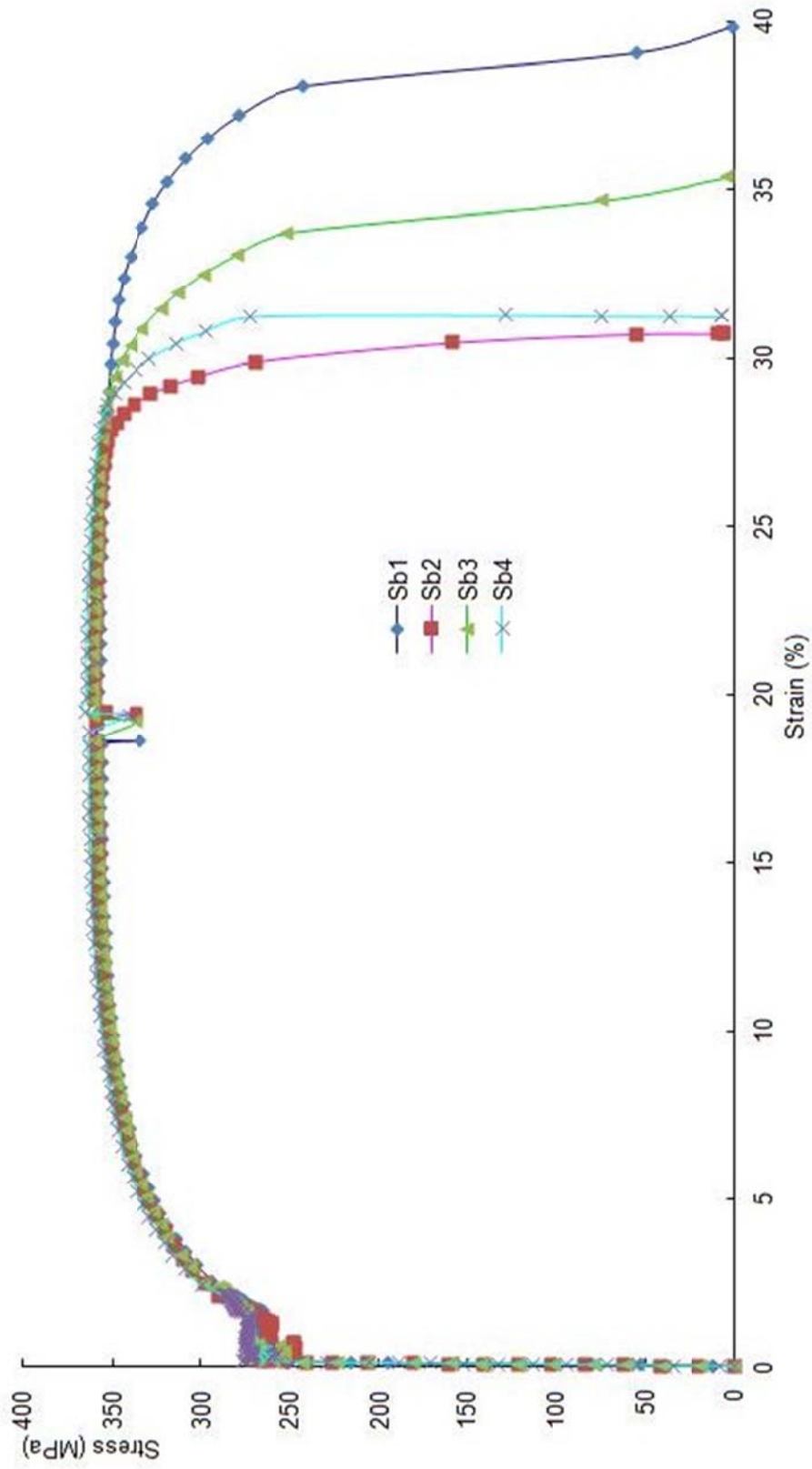


Figure D-3: Stress vs. Strain Curves for Tension Coupon from Second Storey Infill Panel

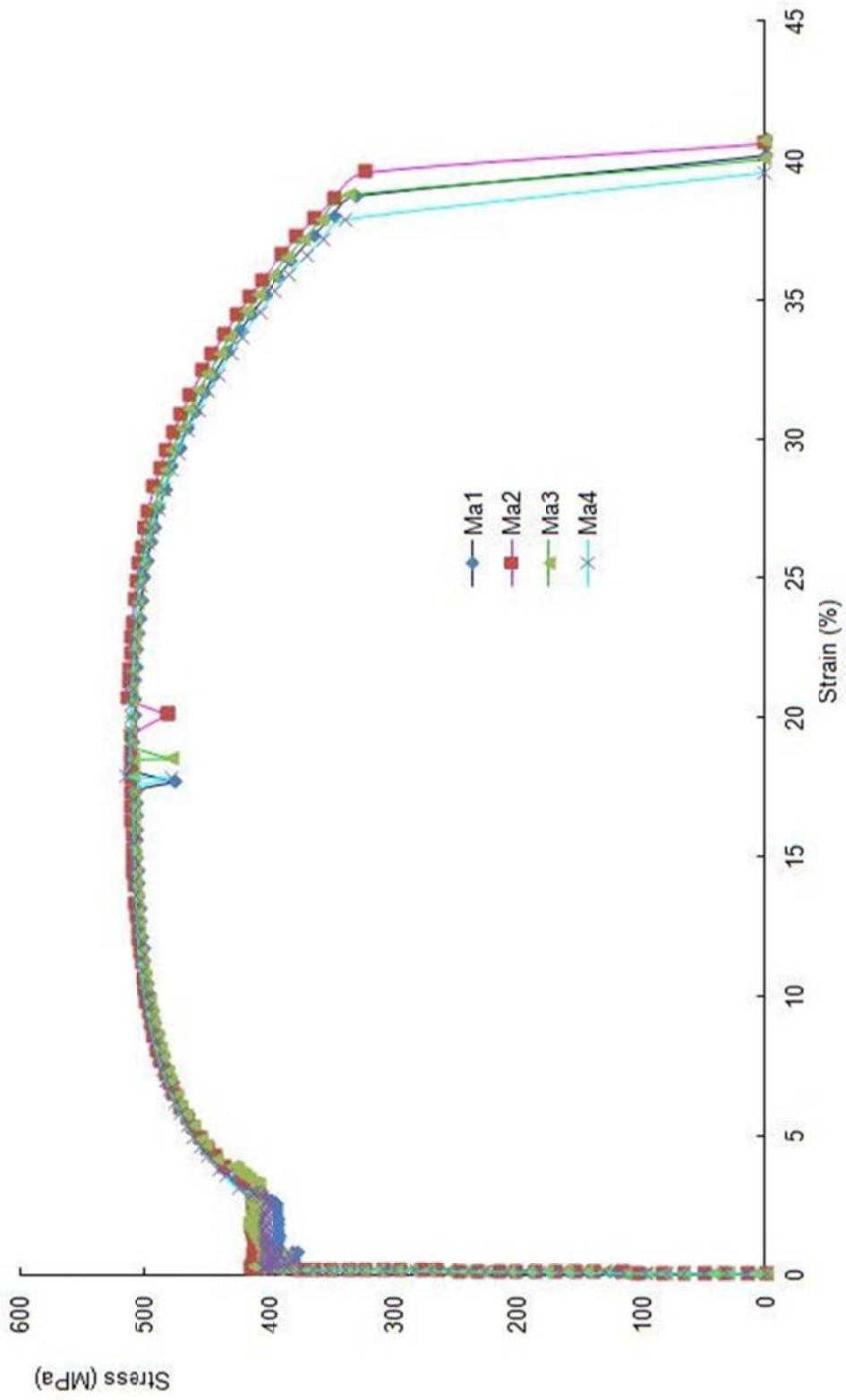


Figure D-4: Stress vs. Strain Curves for Tension Coupon from First Storey Beam

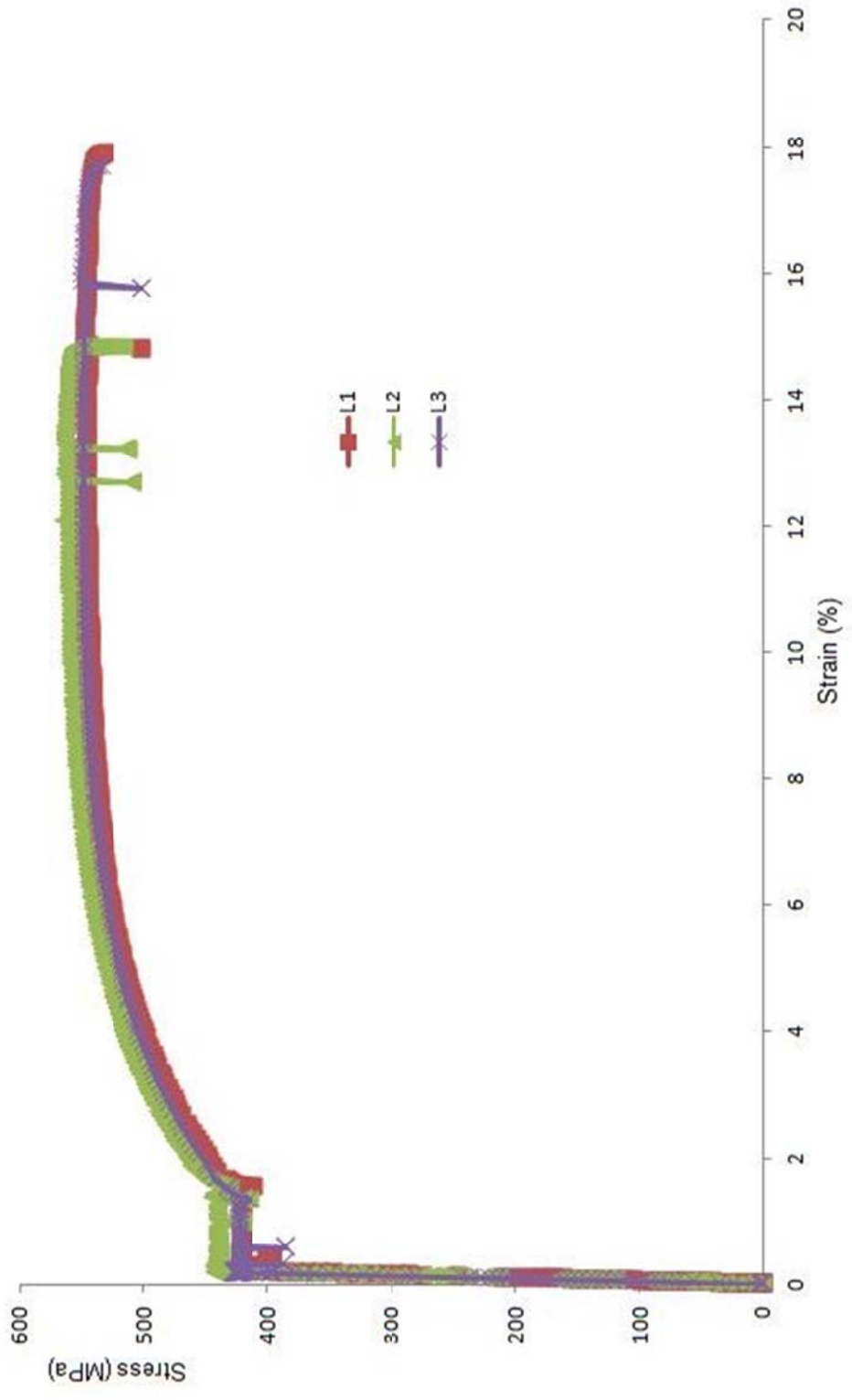


Figure D-5: Stress vs. Strain Curves for Tension Coupon from Column Link

Table D-1: Steel Tension Coupon Test Results

	Coupon Mark	E_s (MPa)	Static σ_v (Mean) (MPa)	Static σ_u (MPa)	Static σ_f (MPa)	ϵ_y (%)	ϵ_{SH} (%)	ϵ_u (%)	ϵ_f (%)
1st Storey Panel	Sa1	209,780	239	324	319	0.11	1.36	18.7	33.7
	Sa2	217,680	236	321	314	0.11	1.22	17.2	29.9
	Sa3	185,660	234	330	321	0.13	1.20	21.0	30.4
	Sa4	N/A	N/A	N/A	N/A	N/A	N/A	N/A	N/A
	Mean	204,373	236	325	318	0.12	1.26	19.0	31.3
2nd Storey Panel	Sb1	215,250	247	335	325	0.11	1.67	18.7	31.1
	Sb2	217,440	247	337	331	0.11	1.40	20.2	27.2
	Sb3	197,250	254	337	330	0.13	0.70	19.3	28.1
	Sb4	192,680	258	341	333	0.13	1.60	19.5	27.8
	Mean	205,655	252	337	330	0.12	1.34	19.4	28.5
Column Steel	P1	195,690	430	500	492	0.22	0.99	14.9	18.0
	P2	194,240	436	N/A	N/A	0.22	0.87	11.7	17.7
	P3	203,500	432	500	493	0.21	0.82	11.3	17.1
	P4	182,190	422	506	499	0.23	0.83	14.5	18.8
	P5	191,500	420	505	497	0.22	0.75	14.9	19.6
	P6	187,720	421	505	497	0.22	0.75	14.5	19.2
	Mean	192,473	427	503	496	0.22	0.83	13.7	18.4
1st Storey Beam	Ma1	205,280	378	476	464	0.18	2.63	18.1	25.6
	Ma2	210,500	396	482	472	0.19	3.20	20.7	26.1
	Ma3	217,500	388	479	466	0.18	3.24	19.0	26.3
	Ma4	218,560	383	479	464	0.18	2.66	17.9	25.3
	Mean	212,960	386	479	467	0.18	2.93	18.9	25.8
Link	L1	207,420	397	503	419	0.19	1.55	14.8	29.4
	L2	235,960	418	513	436	0.18	1.58	13.2	21.6
	L3	230,710	386	503	500	0.17	1.42	15.8	17.2
	Mean	224,697	400	506	452	0.18	1.52	14.6	22.7

Appendix E - Concrete Cylinder Test Results

Table E-1 Concrete Cylinder Test Results

Concrete in the columns		First Floor		Second Floor	
		South Column	North Column	South Column	North Column
Mark		S1	N1	S2	N2
Slump (mm)		160	160	150	145
Air Content (%)		1.9	1.4	1.5	1.7
Density (kg/m ³)		2592	2592	2462	2462
Elastic Modulus (MPa)		23 483	23 548	23 448	25 132
Strength (MPa)		52.6	56.4	55.7	56.9
7 day		32.0	37.8	36.5	35.7
28 day	Cylinder 1	42.3	44.6	45.4	44.5
	Cylinder 2	39.2	47.1	43.7	44.6
	Average	40.7	45.8	44.6	44.6
Test day	Cylinder 1	51.9	59.2	56.6	56.8
	Cylinder 2	51.6	56.8	54.0	56.1
	Cylinder 3	54.5	53.2	56.6	57.8
	Average	52.6	56.4	55.7	56.9